The majestic glory of fjords: Geomorphometry and sedimentology of selected fjords on Cumberland Peninsula and the northeast coast of Baffin Island.

by

© Johnathan Carter

A thesis submitted to the School of Graduate Studies
in partial fulfillment of the requirements for the degree of
Master of Science

Geography Department
Memorial University of Newfoundland

October 2021

St. John's, Newfoundland and Labrador

Up-fjord view of central Akpait Fiord, Baffin Island, Nunavut, Canada. (Photo by Johnathan Carter, 22 October 2015.)

ABSTRACT

This thesis presents a morphometric database of 13 parameters across 29 Baffin Island fjords, and the postglacial sedimentology and chronology of three fjords on Cumberland Peninsula. For the morphometric analysis, the fjords were partitioned into two regional groups (northeast coast and Cumberland Peninsula), and a one-way ANOVA test was conducted for each parameter. Fjords were found to be significantly larger along the northeast coast of Baffin Island than on Cumberland Peninsula, attributable to the Laurentide Ice Sheet supporting larger outlet glaciers than those emanating from the Penny Ice Cap and local alpine glaciation on the peninsula. Sub-bottom acoustic profiles of three Cumberland Peninsula fjords (Boas Fiord, Durban Harbour, and Akpait Fiord) were observed to feature the archetypal postglacial stratigraphy for Canadian east-coast fjords (ice-contact overlain by glaciomarine and marine units), in addition to local facies associated with specific fjord features (deltas, sills, and spillover deposits). Sediment cores from these three fjords contained a total of six lithofacies, which were associated with acoustic facies and sediment sources, and provided new calibrated radiocarbon dates (ranging from 0.9 to 9.6 cal ka BP). One of these new radiocarbon dates from Durban Harbour, when combined with Cowan's (2015) earlier interpretation, associates the postglacial sea-level lowstand with the Preboreal-Cockburn transition (9.5 cal ka BP). Moreover, the sedimentology of these Cumberland Peninsula fjords was found to be comparable to fjords on the northeast coast of Baffin Island in terms of sedimentary sequence and sedimentation rates, but had overall thinner deposits.

GENERAL SUMMARY

This thesis has two distinct components. The first is a database of physical measurements for 29 fjords on Baffin Island. The second is a detailed study of the postglacial sedimentary record of three fjords on Cumberland Peninsula, for which detailed bathymetry, acoustic stratigraphy, and sedimentary core data were obtained. Using the morphometric data, the fjords of two regions of Baffin Island associated with different ice sources, the northeast coast and Cumberland Peninsula, were compared. Overall, the northeast coast fjords, carved by outlet glaciers of the Laurentide Ice Sheet, were larger than Cumberland Peninsula fjords, which were carved by the smaller Penny Ice Cap and local alpine glaciers. Meanwhile, the three Cumberland Peninsula fjords studied were found to show the same sedimentary sequence as other fjords throughout eastern Canada, with the exception of a few local sedimentary features. Sediment cores from these fjords showed six different sediment units, and provided new calibrated radiocarbon dates (ranging from 0.9 to 9.6 cal ka BP). One of these radiocarbon dates places the timing of a period of lower relative sea level at ~9.5 cal ka BP, the transition between the Preboreal ice recession (11.7 – 9.5 cal ka BP, based on ice-core data) and the Cockburn ice readvance (9.5 – 8.5 cal ka BP). In addition, these Cumberland Peninsula fjords were found to feature similar sedimentary sequence and sedimentation rates as fjords on the northeast coast of Baffin Island, but had overall thinner deposits.

ACKNOWLEDGEMENTS

First and foremost, I must thank both of my thesis supervisors, Dr. Trevor Bell and Dr. Donald Forbes, for their acceptance of me as a graduate student, their ongoing guidance and mentorship in the field of Canadian Arctic geography, and, above all, their truly benevolent patience over the course of the writing of this thesis.

Some of the material of this thesis, relating to the timing of the relative sea level lowstand based on a radiocarbon date from Durban Harbour, has been submitted for publication in a paper co-authored with Beth Cowan. Her earlier work, based entirely on acoustic data, provided a foundation for this study.

In addition, I would like to thank the crew members of the 2014 *MV Nuliajuk* cruise and the 2014 and 2015 *CCGS Amundsen* cruises, and my fellow passengers Robbie Bennett and Robert Murphy of the Geological Survey of Canada, for their efforts and assistance in collecting the sediment cores analyzed in this thesis. In the same vein, I would like to thank Kate Jarrett, Jenna Higgins, Owen Brown, and their laboratory assistants for their efforts and guidance in the analysis of the sediment cores. The late Alice Telka (Paleotec Services) assisted with meticulous preparation and identification of mollusc fossil samples from the cores, and John Southon of the University of California, Irvine, supervised the AMS analyses. Special thanks go to my fellow graduate student, Robert Deering, for his participation and support in both the collection and laboratory analysis of the sediment cores and samples.

Significant financial assistance towards the field research conducted for this thesis was provided by the Natural Sciences and Engineering Research Council (NSERC), the Northern Scientific Training Program (NSTP), ArcticNet, the Geological Survey of Canada, the Government of Nunavut, the University of New Brunswick, and Memorial University of Newfoundland.

I suppose I should also thank my parents for *not* throwing me out of their basement and forcing me to get a “real job” before I finished this thesis.

I respectfully acknowledge my time at the Memorial University of Newfoundland as spent on the ancestral homeland of the Beothuk, and the island of Newfoundland as the ancestral homelands of the Mi’kmaq and Beothuk. I also acknowledge that my field research for this thesis, along the northeastern coast of Baffin Island, was conducted within the traditional territory of the Inuit.

TABLE OF CONTENTS

LIST OF TABLES

LIST OF FIGURES

CHAPTER 3: PROBING THE LATE- AND POSTGLACIAL SEDIMENTARY RECORD OF EASTERN CUMBERLAND PENINSULA FJORDS, BAFFIN ISLAND....105

LIST OF ABBREVIATIONS

ANOVA	analysis of variance
asl	above sea level
BP	years before the Present, defined as 1950 when using the radiocarbon timescale
bsl	below sea level
CAA	Canadian Arctic Archipelago
cal	indicates "calibrated years" and that the date is the result of radiocarbon calibration. It can be directly compared to calendar years.
DEM	digital elevation models
GA	billion years ago
HTM	Holocene Thermal Maximum
ka	thousand years ago
LGM	Last Glacial Maximum
LAG	local alpine glaciation
LIA	Little Ice Age
LIS	Laurentide Ice Sheet
MBES	Multibeam echo-sounding
MSR	mean sedimentation rate
MWP	Medieval Warm Period
PIC	Penny Ice Cap
RSL	relative sea level
SAFE	Sedimentology of Arctic Fjords Experiment
YD	Younger Dryas

LIST OF APPENDICES

CO-AUTHORSHIP STATEMENT

I, Johnathan Carter, was the lead author of all chapters of this thesis. However, the long-lasting guidance and assistance of my academic supervisors, Dr. Trevor Bell and Dr. Donald Forbes, was truly invaluable.

I compiled published research into extensive literature reviews that established conceptual frameworks for two topics. I also conducted the collection and statistical analysis of fjord-morphometry data, participated in the collection of sediment-core samples, the initial analyses of acoustic profiles and lithologic datasets, and the calibration of radiocarbon dates. I drafted the thesis chapters and manuscripts.

My supervisors were responsible for initially suggesting the research topics covered in this thesis. They participated in components of the ship-based data collection and laboratory analysis of sediment cores, developed and refined the scope of analyses and discussion, provided numerous edits of the thesis drafts, and secured funding for the fieldwork and sample analysis.

Chapter 3 (Probing the Late- and Postglacial Sedimentary Record of Eastern Cumberland Peninsula Fjords, Baffin Island) was written by me with edits from Dr. Trevor Bell and Dr. Donald Forbes. Calibrated radiocarbon dates and sedimentological interpretations from this chapter have been submitted for publication by Canadian Journal of Earth Sciences in an article co-authored with Beth Cowan, Donald Forbes, and Trevor Bell. Material from Chapter 2 has not yet been submitted for publication in any journal.

CHAPTER 1: INTRODUCTION

Throughout the alpine and polar regions of the world, glaciers have flowed through and eroded valleys, steepening the sidewalls while widening and lowering the valley floors. If the sea floods a glacial valley open to the coast, it becomes a *fjord* (or fiord, the spelling used in Canadian official names). Along the eastern margin of the Canadian Arctic Archipelago (CAA) run the Davis Highlands, a mountain belt spanning the east coasts of Ellesmere Island, Devon Island, Bylot Island, and Baffin Island (Fig. 1.1; Bostock, 2014). Fjords are found throughout these highlands, and more widely on Ellesmere and Axel Heiberg islands, with varying extents of active glaciation. Because most fjords along the coast of Baffin Island are deglaciated, they present an environment conducive to geomorphological and sedimentological research, as has been conducted by the Sedimentology of Arctic Fiords Experiment (Syvitski & Blakeney, 1984; Syvitski, 1984; Syvitski & Praeg, 1987), which includes the work of Gilbert and MacLean (1984, and other researchers (e.g., Gilbert, 1978, 1982a, b, 1985; Dyke, 1979; Dowdeswell & Andrews, 1985; Andrews et al., 1996; Cowan, 2015).

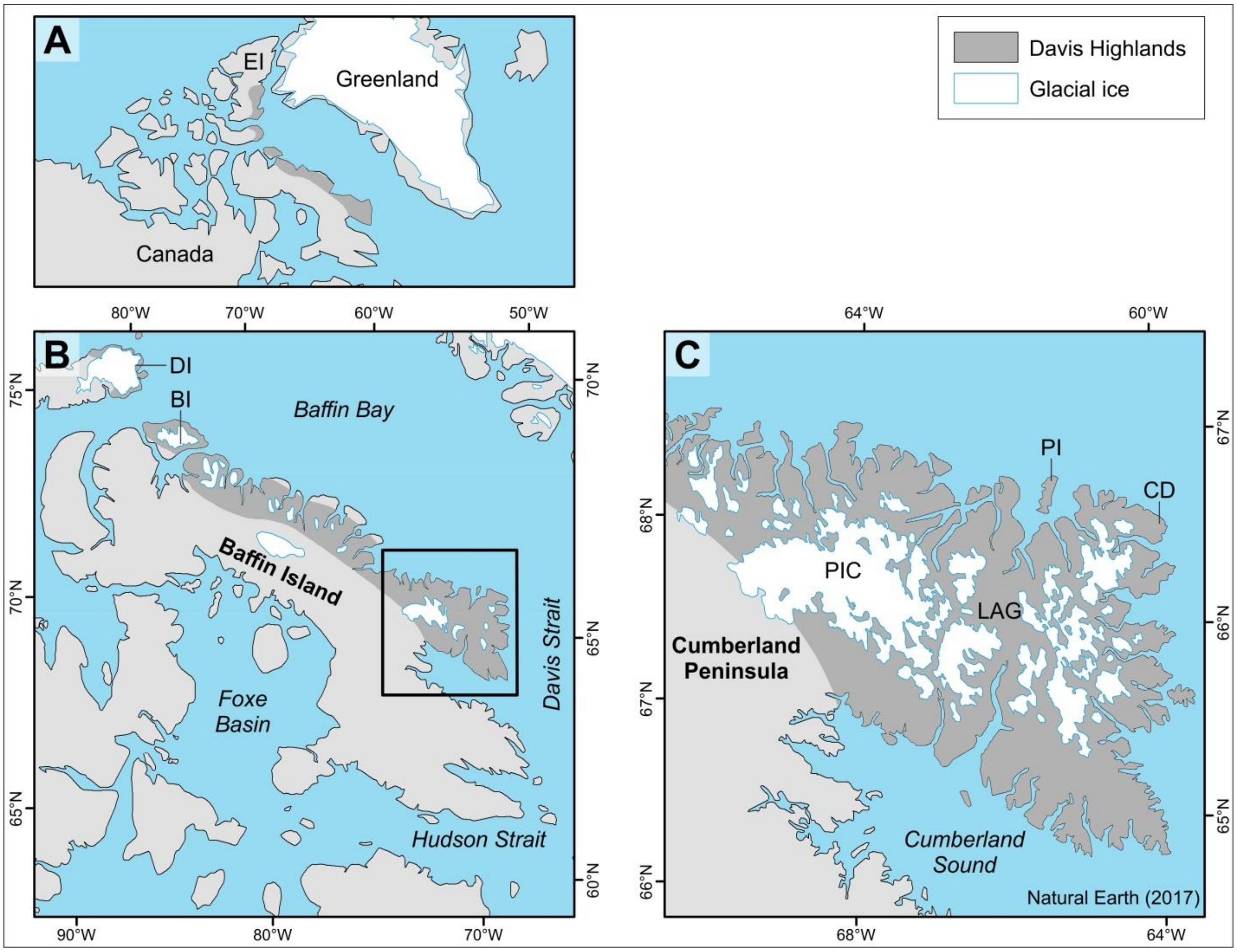

Figure 1.1: Baffin Island and Cumberland Peninsula with surrounding environs. A) The full extent of the Davis Highlands throughout the CAA (Bostock, 2014), EI: Ellesmere Island. B) Baffin Island and the surrounding water bodies; not pictured is the Labrador Sea (Atlantic Ocean) to the southeast; DI: Devon Island, BI: Bylot Island. C) Cumberland Peninsula and its two glacial systems: Penny Ice Cap (PIC) and Local Alpine Glaciation (LAG); PI: Padloping Island, CD: Cape Dyer.

1.1 Fjord geomorphology and sedimentology

A fjord is defined as a segment of a glacially-excavated valley that is open to and partially flooded by the sea. It may contain one or more sills, seafloor ridges composed of either bedrock or sediment (Flint, 1971; Løken & Hodgson, 1971; Dowdeswell & Andrews, 1985; Syvitski et al., 1987; Trenhaile, 2010), and may be fed by smaller tributary fjords or valleys.

Fjord formation is driven by topography and glaciation, occurring where glacial ice-flow accumulates in pre-existing coastal depressions (e.g. a fault line or valley) and excavates it further through basal erosion. A positive feedback loop then forms, where the increasing valley-depth and -steepness accelerates the ice flow, thus increasing glacial erosion which further deepens and steepens the valley (Kessler et al., 2008). Glacial erosion allows the valley to be deepened below sea level, until the water depth reaches 90% of the ice thickness and causes floatation (Flint, 1971). This active submarine erosion does not occur in fluvial valleys.

Each fjord provides one or more natural basins (separated by sills) for the accumulation and storage of sediments from multiple sources (Flint, 1971; Syvitski et al., 1987). Ice-contact sediments are deposited either directly by the glacier or adjacent to it, and include various types of moraines and meltwater outflow deposits. Glaciomarine sediments are released from a tidewater glacier directly into the water column before gradually falling out of suspension. Glaciofluvial sediments are transported from the glacier into the fjord by either subglacial meltwater streams during glaciation or subaerial meltwater streams once the ice has receded from the fjord head, and may accumulate at river mouths to become deltas. Valley deposits upstream from a delta front are typically coarse gravel, forming braided-stream systems referred to as '*sandar*' (Icelandic; singular: *sandur*). Fine material in suspension is carried out into the basin to add to the glaciomarine units. Once meltwater delivery to the fjord ceases, marine hemipelagic muds accumulate more slowly and may incorporate ice-rafted (primarily via icebergs) sediments, as observed in some northern fjords included in this study. If the relative sea level (RSL) rises, or transgresses, following a glacial retreat, then marine muds will likely accumulate on previously subaerial surfaces as a post-submergence unit. In some fjords, aeolian processes also contribute to down-valley sediment transport (Syvitski & Hein, 1991). Changes in the mean sedimentation rate within fjord basins reflect past environmental changes, such as ice extent, rate of ice melt, glacial meltwater discharge, and the position of tidewater ice margins, which affected sediment delivery and redistribution within the fjord (Andrews, 1987; Syvitski et al., 1987).

Some of the fjords discussed throughout this thesis (specifically, Boas, Durban, Akpait, and Sunneshine) still contain alpine ice in their drainage basins, which may raise concerns over the meaning of the term “postglacial sediments”. For the purposes of this thesis, glaciomarine sediments are defined as released from a tidewater glacier directly into the marine water column, and settling within a relatively short timeframe. In contrast, postglacial sediments are defined as those deposited following ice retreat from the fjord. This includes deltaic deposits which accumulated at river mouths, and marine muds (composed of very fine biogenic and mineral sediments) which have been suspended in the marine water column for an extended period.

1.2 Research question and objectives

At least two distinct groups of fjords appear evident along the eastern coast of Baffin Island. Quasi-parallel fjords, including very large composite systems such as Scott Inlet, along the northeast coast are associated with outflow from the Laurentide Ice Sheet at the Last Glacial Maximum (and presumably earlier glaciations). Smaller, radially-oriented fjords around Cumberland Peninsula were formed by ice from the Penny Ice Cap and local alpine glaciation. Are there morphometric differences between these fjord populations and, if so, can they be attributed to differences in the scale and origin of the ice sources, or to geological or other factors? This question is addressed in Chapter 2 of this thesis.

Prior to this study and a companion project (Cowan, 2015), the generally smaller fjords of Cumberland Peninsula had received less attention and exploration than fjords along the northeast coast. The limited previous work included that of Dyke (1979, 2013) and detailed studies on Pangnirtung, Maktak, Coronation, North Pangnirtung, and Sunneshine fjords (Gilbert, 1978, 1982a, 1985; Aitken & Gilbert, 1989; Andrews et al., 1996). As this study concluded, new work had been undertaken in Southwind and nearby fjords (Normandeau et al., 2019a, b, c). However, prior to Cowan (2015), no multibeam bathymetry and only limited acoustic stratigraphic data had been acquired in these fjords (e.g., Gilbert & MacLean, 1984, Gilbert 1985), and the only piston core was HU82-SU5 PC (82031-6221) from Sunneshine Fiord (Cole & Blakeney, 1984; Natural Resources Canada, 2017a), collected in 1982 alongside gravity cores from Maktak, Coronation, and North Pangnirtung fjords (Hein & Longstaffe, 1984).

The timing and style of deglaciation, the resulting post- and paraglacial sedimentation, and the sea-level history of fjords in this region are poorly understood. Therefore, the second objective of this project, addressed in Chapter 3 of the thesis, is to examine the deglacial and postglacial sedimentary record in a sample of relatively small fjord systems associated with alpine ice sources on the northeast coast of Cumberland Peninsula.

This project was enabled by access to vessels equipped with multibeam echo-sounding systems, subbottom profilers, and seabed coring capability. Multibeam bathymetry enables more detailed surveys of the seafloor than previously possible using depth-soundings along a single acoustic profile (see Fig. 1.2). The more complete coverage, and ability to produce submarine digital elevation models (DEMs) when combined with modern mapping software, allow fjord basin bathymetry and seafloor geomorphology to be studied with more comprehensive 3D visualization than previously, adding greater detail (e.g., fjord basin maximum depths, sill morphology) to morphological comparisons between fjords. Combining this technology with subbottom profiling and sediment core analysis provides the means to decipher the deglacial and postglacial evolution of these large estuarine systems.

The sedimentary records that accumulate within fjords can be studied using acoustic imagery and the lithostratigraphy of deposits sampled in cores. Seabed morphology from multibeam bathymetry, combined with acoustic stratigraphy and sediment core lithology, provide the data required to interpret the past environments represented by the fjord basin sedimentary deposits. Radiocarbon dates on organic fossils (primarily marine molluscs) retrieved from sediment cores can be used to determine the ages of sedimentary units, document the changes in mean sedimentation rates over time, and to constrain the timing of the postglacial lowstand identified by Cowan (2015). The latter is achieved by obtaining radiocarbon ages on shells retrieved from bottomset and topset beds of submerged glacial-outwash deltas, in order to establish maximum and minimum age constraints for the timing of delta progradation, and thus the lowstand.

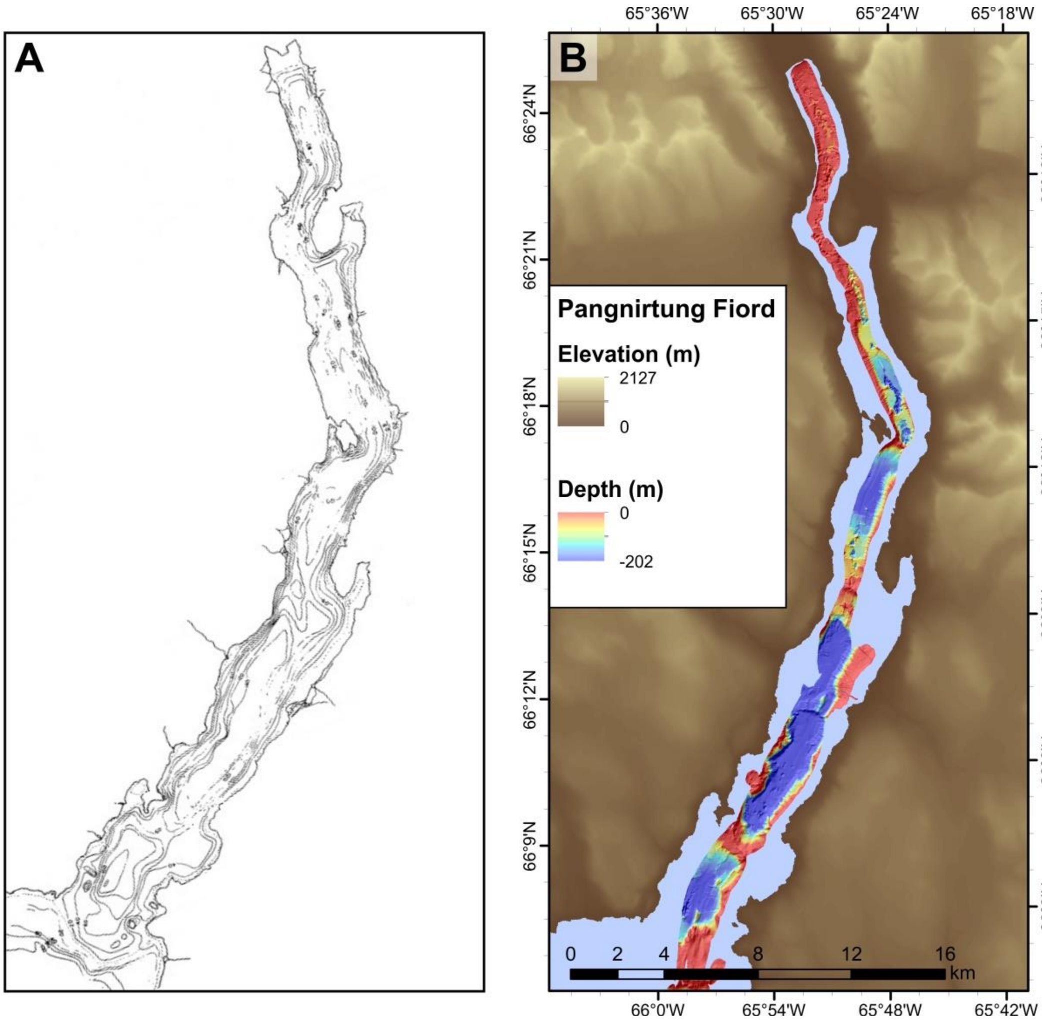

Figure 1.2: Comparison of bathymetry based on single-beam and multibeam technology for Pangnirtung Fiord. Panel A is modified from Gilbert (1978).

1.3 Regional Setting

1.3.1 Baffin Island: the northeast coast and Cumberland Peninsula

Baffin Island is located in the eastern CAA, bordered by Baffin Bay to the northeast, Davis Strait to the east, the Labrador Sea (Atlantic Ocean) to the southeast, and Hudson Strait to the south (Fig. 1.1). The island is roughly crescent-shaped, with mountains (up to ~2100 m asl) along the northeast coast and parts of Cumberland Peninsula, more subdued plateau terrain along the central spine and in the southeast, and extensive lowlands in the west along the coast of Foxe Basin. Cumberland Peninsula, extending to the easternmost point of Baffin Island, is dissected by numerous fjords in a radial pattern, emanating from central mountains that previously supported alpine glaciers, the great majority of which have disappeared. At the present time, the peninsula supports alpine glaciers (total area of >5700 km^2) concentrated in the northeast and the Penny Ice Cap (>6000 km^2; Dyke et al., 1982; Margreth, 2015) in the west, together representing ice cover on ~29% of the peninsula.

The oldest bedrock on Baffin Island is the Archean Rae craton (3.25 to 2.58 Ga), composed of intrusive plutonic rock. Further southeast towards Home Bay and Cumberland Peninsula, the craton is overlain by a sedimentary cover (2.16 to 1.90 Ga) and the Qikiqtarjuaq suite granitic intrusives (1.89 Ga). The bedrock geology of Cumberland Peninsula is predominantly defined by the Rae craton (tonalite-granodiorite plutonic rock) throughout its eastern half, partly overlain by Paleoproterozoic sedimentary cover (semipelite, psammite, quartzite, and siltstone). The western half of the peninsula appears to be dominated by the Qikiqtarjuaq granite suite (Sanborn-Barrie & Young, 2013; Sanborn-Barrie et al., 2013; St-Onge et al., 2015). Small, localized Paleocene basalt flows underlain by impure sandstone have been mapped along the northeastern coast, from the northern end of Padloping Island to the end of Cape Dyer, mainly upon upland summits (Fig. 1.1C; Sanborn-Barrie & Young, 2013; Sanborn-Barrie et al., 2013). Given their scarcity, these basalt-sandstone units might indicate areas of minimal glacial erosion due to either absent or cold-based glacial ice.

The east Baffin uplands were uplifted as Greenland rifted away from North America and opened Baffin Bay (Clarke & Upton, 1971; MacLean & Falconer, 1979; MacLean et al., 1990; Keen & Beaumont, 1990; Hosseinpour et al., 2013), a rifting event assigned to the period of the Early

Jurassic to Paleocene and labelled the Cordilleran orogeny by St-Onge et al. (2015). A horst-and-graben fracture zone developed along the rift margin, wherein linear troughs cross-cut the rift-parallel fault lines to create a trellis drainage-pattern (Manchester & Clarke, 1973; MacLean et al., 1990; Funck et al., 2007, 2012). During the orogeny, Cumberland Sound developed from a subsiding graben, which simultaneously produced Cumberland Peninsula (Hood & Bower, 1975; MacLean & Falconer, 1979; MacLean et al., 1990).

During the Last Glacial Maximum (LGM), which locally terminated ~20.5 cal ka BP (Dalton et al., 2020), the majority of Baffin Island was glaciated by the northeast sector of the Laurentide Ice Sheet (LIS), which fed multiple outlet glaciers along its northeast coast, scouring fjords and extending to the mouths of shelf-crossing troughs. However, an ice stream into Cumberland Sound diverted Laurentide ice around Cumberland Peninsula, allowing the Penny Ice Cap and Local Alpine Glaciation (PIC-LAG) complex to expand over the peninsula as an independent glacial system (Figs. 1.3 and 1.4; Jennings, 1993; Margreth, 2015). The northeast LIS was much larger than the PIC-LAG complex in both area and volume, and thus capable of feeding much larger outlet glaciers.

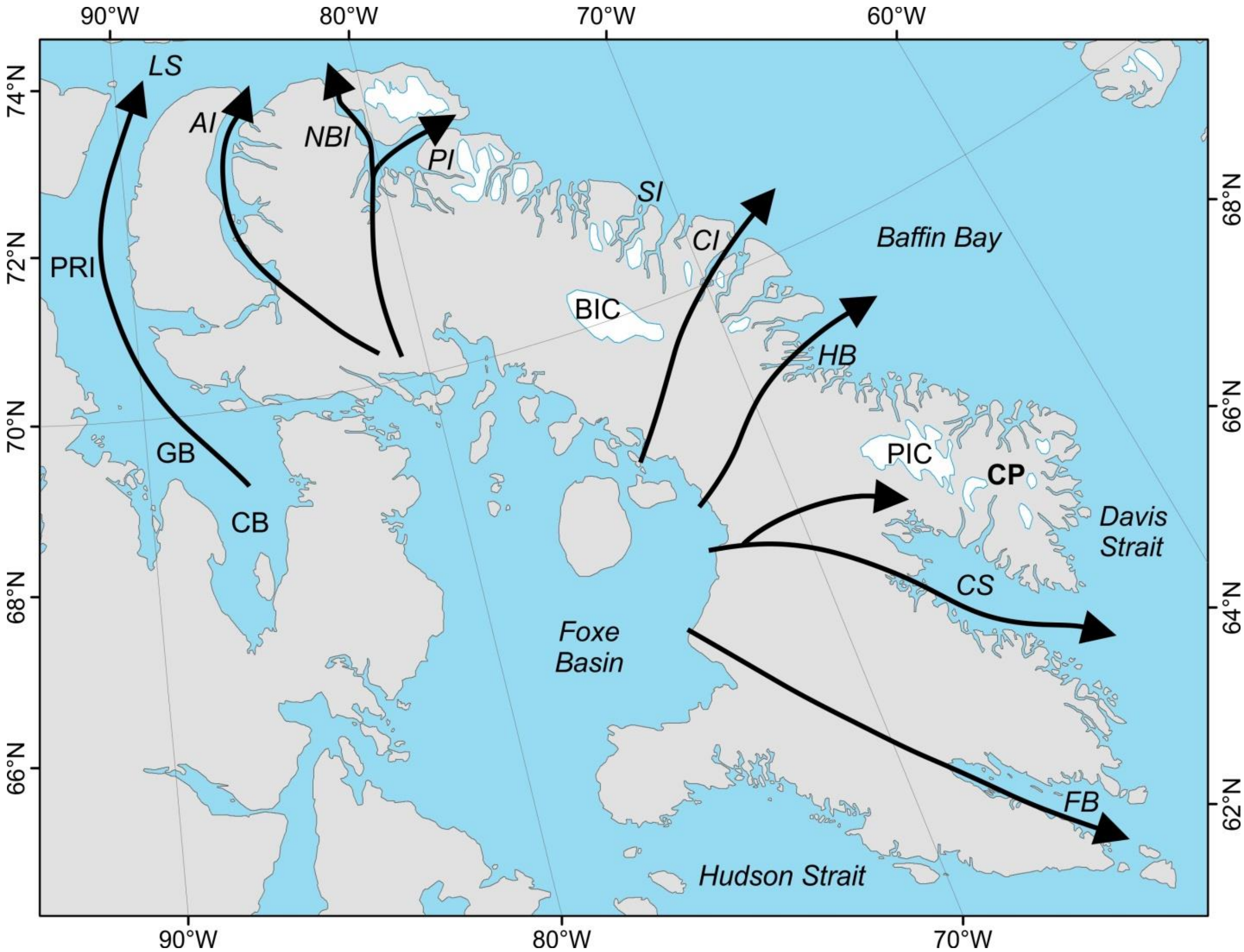

Figure 1.3: Arrows illustrate the major directions of LIS ice flow from the Foxe Dome west of Baffin Island, with ice essentially bifurcating around Cumberland Peninsula (CP) (Margold et al., 2015; Margreth, 2015). BIC: Barnes Ice Cap, PIC: Penny Ice Cap, CB: Committee Bay, GB: Gulf of Boothia, PRI: Prince Regent Inlet, LS: Lancaster Sound, AI: Admiralty Inlet, NBI: Navy Board Inlet, PI: Pond Inlet, SI: Scott Inlet, CI: Clyde Inlet, HB: Home Bay, CS: Cumberland Sound, FB: Frobisher Bay. Glaciers are from Natural Earth (2017), land from Natural Resources Canada (2017b).

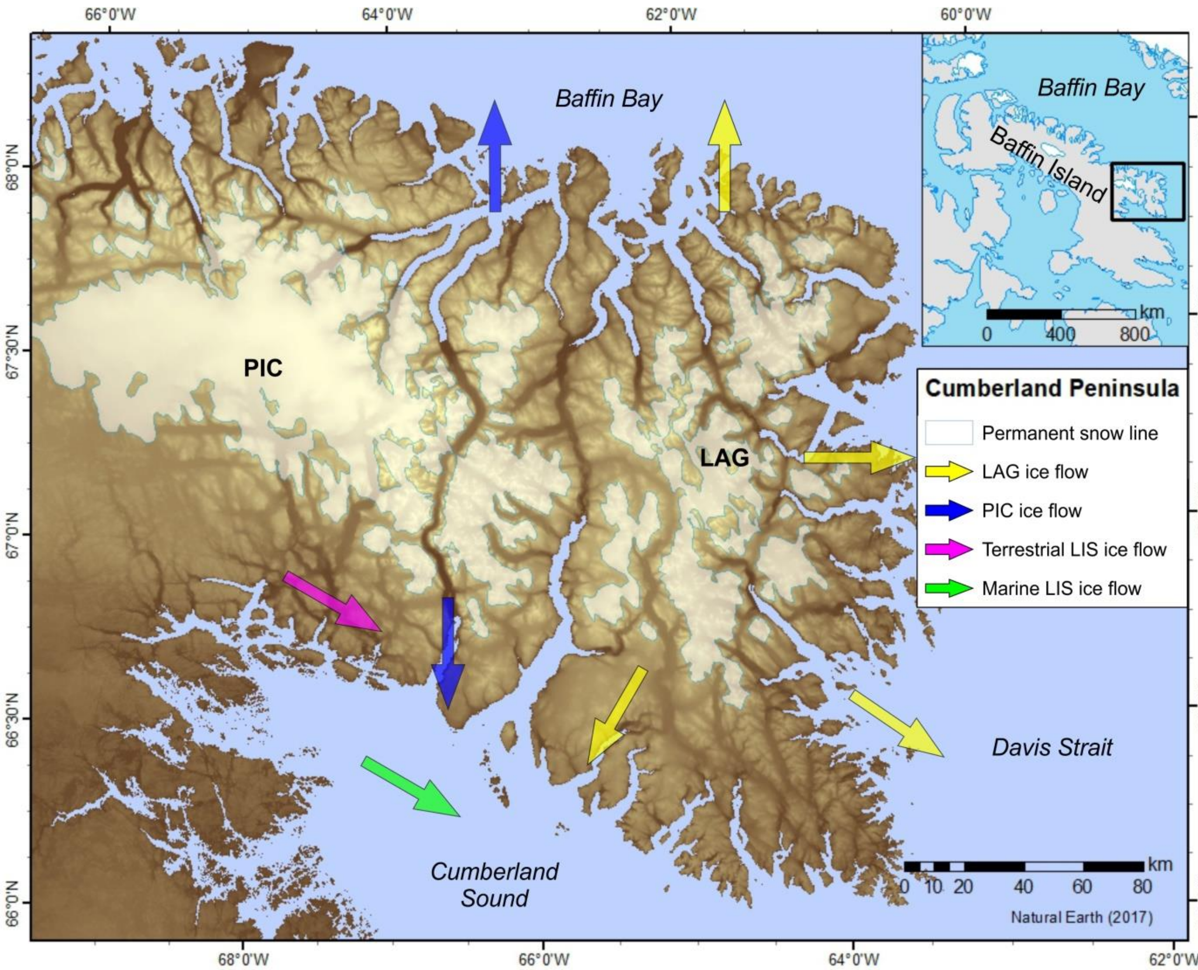

Figure 1.4: Directions of ice flow on and around Cumberland Peninsula, illustrating the general ice-flow of the Penny Ice Cap (PIC) and Local Alpine Glaciation (LAG) compared to the Laurentide Ice Sheet (LIS). Ice-flow directions are further illustrated in Margreth (2015).

1.3.2 Previous glaciations.

Over time, an ice body may alternate between advancing and retreating. As glacial advance and retreat are directly related to temperature, precipitation, and the interplay between mass balance and ice dynamics, long-term climate changes generally drive changes in ice extent. During glacial retreat, the influx of sediment into a fjord increases in response to increased meltwater and/or ice calving, which increases the input of suspended sediment and ice-rafted deposits. Therefore, periods of glacial retreat may be reflected in the sedimentary history by higher sedimentation rates, and glacial advance or withdrawal from the drainage basin (or exposure of intermediate lake accommodation space) by lower rates.

Many studies on the glacial history of Baffin Island have focused on the northeastern Laurentide Ice Sheet margin (e.g., Lamb, 1965; Bradley et al., 2003; Kaufman et al., 2004; Anderson et al., 2008; Briner et al., 2009a, b). During the LGM, LIS outlet glaciers extended across Baffin Island via fjords and onto the continental shelf (Miller et al., 2005; Briner et al., 2009a, b; Margreth, 2015). Following 16–15 cal ka BP (Miller et al., 2005; Margreth, 2015), deglaciation from eastern Baffin Island was underway, although interrupted by multiple glacial readvances. The glacial history of Cumberland Peninsula has been reconstructed using radiocarbon and cosmogenic nuclide dating to determine the timing of ice-margin positions represented by moraines (e.g., Dyke et al., 1982; Margreth, 2015).

In the chronology below, and elsewhere throughout this thesis, ages in *ka* refer to thousands of calendar years (from ice cores or cosmogenic nuclide dating) or calibrated radiocarbon dates (in thousands of years BP). New radiocarbon dates presented in this thesis were calibrated using CALIB 8.20 with a ΔR_R value derived from the MARINE20 database (Chapter 3). The oldest calibrated radiocarbon age included in this study is 13.4 cal ka BP (SU5 852-860 cm), which corresponds to the Bølling-Allerød interstadial (a glacial recession). Glacial readvances are associated with at least three subsequent cooling/precipitation events (Younger Dryas, Cockburn Substage, and Neoglaciation), while glacial recessions are associated with the Preboreal interstadial and the Holocene Thermal Maximum.

- The **Bølling-Allerød interstadial** occurred between 14.6 and 12.8 cal ka BP, based on ice-core analysis by Rasmussen et al. (2006). Associated with this warming was a recession of Laurentide and Penny ice, and local alpine outlet glaciers from the coast (Rasmussen et al., 2006; Margreth, 2015).

- The **Younger Dryas** (YD) was a cold, arid interval between 12.8 and 11.7 cal ka BP (Miller et al., 2005; Rasmussen et al., 2006; Briner et al., 2009b). During this period, glacial readvance approached fjord-mouth positions along the northeast coast of Cumberland Peninsula (e.g., Boas Fiord), but was more limited along the eastern (e.g., Durban Harbour, Akpait Fiord, Sunneshine Fiord) and southwestern coasts (Fig. 1.5; Margreth, 2015).

- The **Preboreal interstadial** occurred between 11.7 and 9.5 cal ka BP, based on the ice-core chronology (Rasmussen et al., 2006, 2007). This period saw significant summer warming (Briner et al., 2009a), but remained cooler than today (Miller et al., 2005). This warming is also associated with the recession of LIS, PIC, and LAG outlet glaciers (Margreth, 2015).

- The **Cockburn Substage** glacial readvance on Baffin Island occurred between 9.5 and 8.5 cal ka BP (Miller et al., 2005; Briner et al., 2009b)[1]. During this period, LAG ice on Cumberland Peninsula readvanced in the interior but was mostly confined to small individual ice masses (Fig. 1.5).

- A separate cooling and readvance event, at 8.2 cal ka BP, is indicated by both Donard Lake sediments and Greenland ice cores (Miller et al., 2005; Rasmussen et al., 2006; 2007; Briner et al., 2009b).

[1] Prior to radiocarbon calibration, the Cockburn Substage was dated by Andrews and Ives (1978) as lasting from 9 to 8 ka BP.

- The **Holocene Thermal Maximum** (HTM)[2] was a warming event that occurred asynchronously, beginning and ending much later in the Atlantic-sector of the Arctic than in the Pacific sector (Kaufman et al., 2004). In eastern Arctic Canada, the highest temperatures occurred between ~8.0 and 5.2 cal ka BP (Gajewski, 2015). Although the Holocene Thermal Maximum was warmer than today, deglaciation in the region was incomplete—the Penny and Barnes ice caps and some alpine ice survived (Briner et al., 2009b).

- The **Neoglacial** refers to a readvance of Arctic and alpine glaciers (Miller et al., 2012). Gajewski (2015) places the onset of cooling from the HTM for eastern Arctic Canada at 5.2 cal ka BP. However, on eastern Cumberland Peninsula, the onset appears to have been as early as ~6 to 5.5 cal ka BP (Moore et al., 2001; Miller et al., 2005), supported by evidence for increased offshore sea ice in Baffin Bay after 6 cal ka BP (de Vernal & Hillaire-Marcel, 2006). Specific to Cumberland Peninsula, Briner et al. (2009b) report subsequent readvances at ~3.5, ~2.3, ~1.5, and ~1.1 cal ka BP, while Margreth (2015) reports three pulses of ice growth at 1.58–1.53, 1.41–1.34, and 1.22–1.16 cal ka BP.

- The Neoglacial also contains two climate phases of lesser duration, the **Medieval Warm Period** (MWP) and the **Little Ice Age** (LIA) (Lamb, 1965). The MWP, originally described by Lamb, is currently defined as a North Atlantic climate event that lasted from 950 to 1250 AD (Bradley et al., 2003; Mann et al., 2009; Miller et al., 2012; Margreth, 2015). This warming interrupted the Neoglacial trend on Cumberland Peninsula with a glacial recession, but was insufficient to fully melt all ice masses (Anderson et al., 2008;

[2] Also known as the Hypsithermal, or the Holocene Climatic Optimum.

Margreth, 2015). The LIA was a cooling event and glacial readvance that followed the MWP and is considered to have lasted until the onset of 20th century warming. The years between 1400 and 1700 AD were the coldest interval, while the central Cumberland Peninsula saw alpine glacial readvances that culminated at: ~1350 AD, ~1600 AD, and ~1900 AD (Bradley et al., 2003; Briner et al., 2009b; Mann et al., 2009).

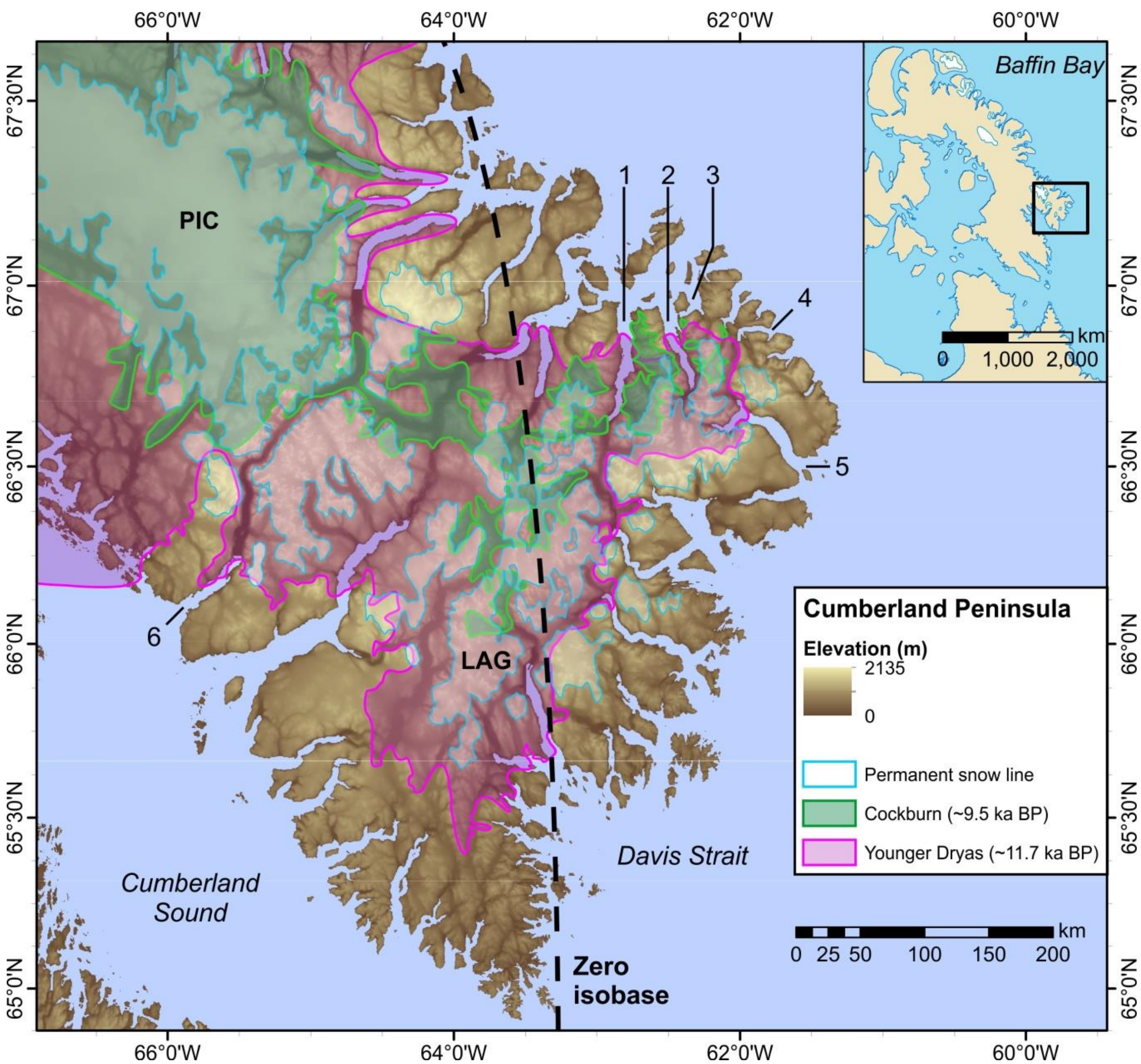

Figure 1.5: Cumberland Peninsula, illustrating the modern snow line (Natural Earth, 2017), ice margins for the Younger Dryas and Cockburn Substage as mapped and interpolated by Margreth (2015) based on moraine deposits, and the zero-isobase (Cowan, 2015). 1) Boas Fiord, 2) Southwind Fiord, 3) Durban Harbour, 4) Akpait Fiord, 5) Sunneshine Fiord, 6) Pangnirtung Fiord.

1.3.3 Lingering effects of glaciation on Baffin Island.

During the LGM, the LIS expanded over much of North America, including Baffin Island. Beneath the mass of an ice sheet, two phenomena occur: the Earth's crust bends like a board (elastic deformation), and the underlying mantle material is displaced outward (viscous deformation). These deformations produce sub- and proglacial depressions, and a peripheral bulge. When the ice-sheet recedes, the weight is removed and the crust rebounds elastically and then more gradually as viscous mantle material returns (see Fig. 1.6). Most of the central CAA was subglacially depressed by the LIS at the LGM, and has been rebounding since deglaciation (James et al., 2014). This has resulted in RSL fall, or regression, along most of the Canadian Arctic coastline in response to crustal uplift. However, eastern Cumberland Peninsula extends beyond this region of uplift, and thus is a rare location in the eastern CAA where the effects of rising RSL and marine transgression may be observed (Pheasant & Andrews, 1973; Clark et al., 1978; Dyke, 1979; Cowan, 2015).

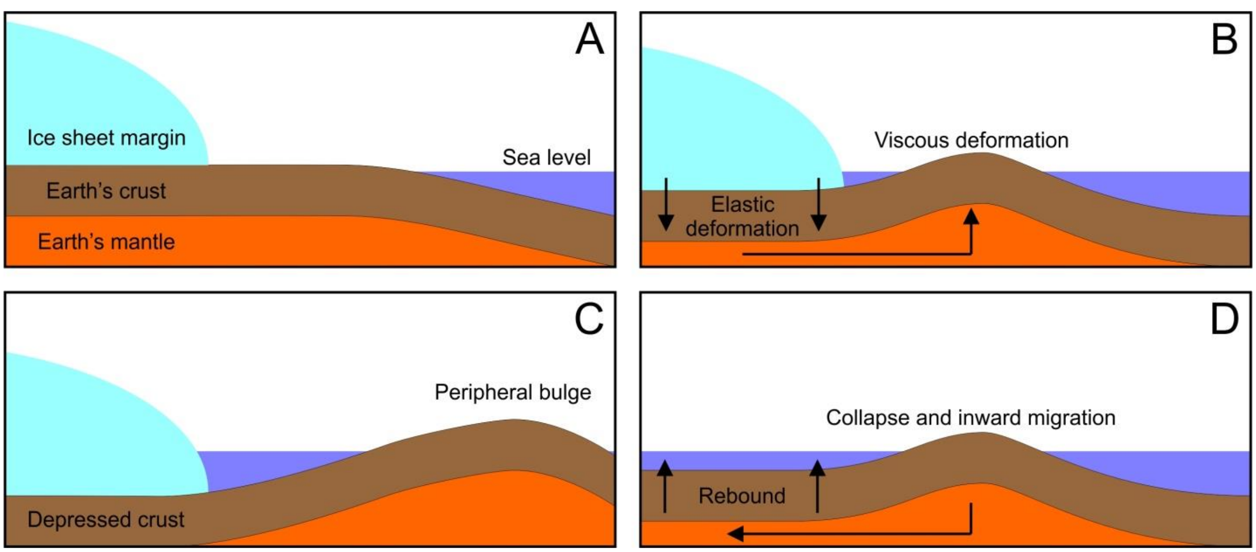

Figure 1.6: Diagrams illustrating glacio-isostasy (the onset of pro- and subglacial depressions and the rebound of crust and mantle following a glacial recession) and the changing elevation of land relative to the sea level. A) Initial ice advancement. B & C) Elastic deformation depresses Earth's crust, creating subglacial and proglacial depressions, while viscous deformation of the mantle creates a peripheral bulge. D) Following ice retreat, the crust rebounds upwards while the peripheral bulge migrates inwards and retreats.

1.4 Research context

The fjords of Baffin Island have previously been studied in multiple respects, best exemplified by the Sedimentology of Arctic Fiords Experiment (SAFE) conducted from 1982 to 1985 (Syvitski & Blakeney, 1984; Syvitski, 1984; Syvitski & Praeg, 1987). Fjord morphometry has been described by Gilbert and MacLean (1984), and statistically analyzed by Dowdeswell and Andrews (1985). Meanwhile, other studies have documented fjord sedimentology (Hein & Longstaffe, 1984; Cole & Blakeney, 1984; Andrews et al., 1984; Andrews et al., 1996) and raised and submerged shoreline deposits (Miller & Dyke, 1974; Dyke, 1979; Cowan, 2015). This thesis updates the morphometric data for selected fjords (highlighting the influence of ice-source size), while investigating the sedimentary history of selected fjords on Cumberland Peninsula.

Morphometrics for ten Baffin Island fjords were described by Gilbert and MacLean (1984) as part of SAFE. These morphometrics added context to the acoustic profiles of fjords, but were not used for making inferences. In contrast, Dowdeswell and Andrews (1985) conducted a thorough statistical analysis of Baffin Island fjords using 29 parameters and a sample of 227 fjords. They used a cluster analysis to identify two fjord groups, which they labelled ‘east coast’ and ‘north/south coast’, and a discriminant analysis to compare the two. However, the groups were not spatially exclusive, showing notable overlap on the east coast of Cumberland Peninsula, and only one parameter (maximum elevation along the fjord) was found to be significantly different. It is interesting that two groups defined by clustering similar attributes could not be found to have many significant differences between them. This thesis compares spatially exclusive fjord groups, and uses modern GIS-based measurements in morphometry datasets, including multibeam bathymetry where available.

Other studies documented raised and submerged coastline features in fjords throughout western and eastern Cumberland Peninsula. A study by Miller and Dyke (1974) discovered submerged terraces interpreted as deltas at tributary valley-mouths within fjords along Cumberland Peninsula's northeast coast. Subsequently, Miller (1975, as cited in Cowan, 2015) described submerged deltas in Boas Fiord at the fjord head and the mouth of a side-entry valley. Later, Dyke (1979) observed that raised shoreline features along the west side of Cumberland Peninsula were tilted at a gradient intersecting the present shoreline. Thus, Dyke hypothesized that the peninsula was undergoing marine regression (falling RSL) in the west and transgression (rising RSL) in the east. Cowan (2015) collected seafloor bathymetry and documented multiple submerged coastal features, including deltas, throughout Cumberland Peninsula. The submerged deltas further indicated that a postglacial lowstand event occurred (Fig. 1.7), but the study lacked age control to constrain its timing.

Following the third SAFE data report (Syvitski & Praeg, 1987), marine-based research on Canadian Arctic fjords experienced a hiatus. Beginning in 2003, marine-based research was renewed by ArcticNet and research cruises by the *CCGS Amundsen*. In 2011, the Government of Nunavut began conducting Arctic coastal waters research using the RV *Nuliajuk*. These programs have enabled the acquisition of the extensive multibeam bathymetry, acoustic subbottom profiles, and gravity and piston cores (providing lithostratigraphic and chronological data) that form the basis of this thesis. Cowan (2015) documented eight submerged deltas in Cumberland Peninsula fjords. These were interpreted to indicate a synchronous relative sea-level lowstand concurrent with high sediment discharge to form proglacial deltas. Using radiocarbon dating of shell samples retrieved from sediment cores, this study establishes maximum and minimum age constraints for the postglacial lowstand, as part of its examination of the sedimentary history for Cumberland Peninsula fjords.

1.5 Methods and materials

This thesis investigates fjord morphology and sedimentology using two main classes of data: geophysical data and sediment cores. In the context of this thesis, ‘geophysical data’ is an umbrella term for topography and digital elevation models (DEMs), multibeam bathymetry, and acoustic subbottom profiles. Complementary ‘geological data’ (primarily from sediment cores) include textural (grain-size) and other physical properties, and fossil material (mollusc shell samples) for radiocarbon dating.

1.5.1 Geophysical data

Topographic maps depict the physical geography of an area, such as elevation, surface terrain, and water bodies. Digital topographic map data were retrieved from the Toporama collection, which is available from the online archive[3]. Multiple map files were required to cover the full areal extent of most fjords in the study. These maps formed the basis of the morphometric analysis of fjords, as they were used in ArcGIS to trace the shoreline of each fjord and thus measure area, length, and width.

Digital elevation models (DEMs) are raster-data representations of the Earth’s surface, in terms of metres above sea level. Subsets of the Canadian Digital Elevation Model (CDEM), representing Baffin Island drainage basins, were retrieved using the Geospatial Data Extraction

[3] https://ftp.maps.canada.ca/pub/nrcan_rncan/raster/toporama/

service[4]. These large-scale DEMs were then clipped into several smaller DEMs localized to specific fjord systems, which provided data on the maximum elevations of fjord sidewalls and the surrounding drainage basins.

Multibeam echo-sounding (MBES) is a tool used for imaging the seafloor (*bathymetry*) at high resolution by means of multiple cone-shaped beams of sound, providing a marine equivalent to aerial photogrammetry used in terrestrial studies (Courtney & Shaw, 2000; Dartnell & Gardner, 2004; Todd & Shaw, 2009). The bathymetry data used in this thesis were originally collected onboard the *CCGS Amundsen* and the *MV Nuliajuk*, and downloaded from the Ocean Mapping Group website at the University of New Brunswick (Hughes-Clarke et al., 2015). Multibeam bathymetry provided maximum basin and sill depth measurements, and was used in selecting the coring sites targeted in Boas Fiord, Durban Harbour, and Akpait Fiord.

Acoustic subbottom profiles image the stratigraphy below the seabed at the coring sites and in the surrounding basin, enabling interpretation of the sedimentary record through the identification of acoustic facies. For Boas Fiord and Durban Harbour, the coverage of the subbottom data corresponds to the bathymetric coverage, roughly extending from mouth to head. However, the acoustic profile coverage for Akpait Fiord is restricted to the proximity of the fjord-mouth sill due to an equipment malfunction (Cowan, 2015).

1.5.2 Sediment cores

Sediment cores were acquired to validate interpretations of the acoustic stratigraphy and collect mollusc shells for radiocarbon dating. The calibrated radiocarbon ages provided data points to constrain the timing of the postglacial lowstand and enable estimates of sedimentation rates.

[4] https://maps.canada.ca/czs/index-en.html

The sediment cores analyzed in this thesis were collected by the *MV Nuliajuk* and *CCGS Amundsen* in 2014 and 2015 from Boas Fiord, Durban Harbour, and Akpait Fiord. The specific coring sites were selected in advance using previously collected multibeam bathymetry and acoustic subbottom profiles, in order to identify target sedimentary features and acoustic facies.

Laboratory analysis of the collected sediment cores was conducted at the Bedford Institute of Oceanography (Geological Survey of Canada – Atlantic), and included: x-radiography, photography, visual description, extraction of grain-size and mollusc-shell samples, and additional physical properties (magnetic susceptibility, p-wave velocity, bulk density, shear strength, and L* a* b* colour values; see Appendix C). The x-radiographs were used in targeting shell samples for extraction, while the grain-size data provided the basis of lithofacies interpretation.

From the extracted shells, preferred specimens were selected based on shell quality and whether they bracketed lithostratigraphic unit boundaries. The samples selected for radiocarbon dating were cleaned, imaged, and identified to species where possible by PALEOTEC Services (Alice Telka) and submitted to the University of California, Irvine for AMS radiocarbon analysis (Telka, 2015, 2016). The reported ^{14}C ages were calibrated using Calib 8.2 (Stuiver et al., 2021) and the MARINE20 data curve (Heaton et al., 2020). The calibrated radiocarbon dates were then used to interpret minimum and maximum constraints on the postglacial lowstand timing, and to estimate mean sedimentation rates.

1.6 Thesis outline

This thesis examines two aspects of Baffin Island fjords, morphology and sedimentology, with a chapter dedicated to each. Chapters 2 and 3 are written as independent journal manuscripts to be submitted to an undetermined journal. They have not been submitted for peer review at this time.

Chapter 2 compares the geomorphology of fjords along the northeast coast and Cumberland Peninsula of Baffin Island. Twenty-one fjords were analyzed using geophysical data and ArcGIS, producing a database of 13 morphometric parameters. Additional data for Sunneshine Fiord and seven other fjords were acquired separately (Gilbert & MacLean, 1984; Syvitski et al., 1986; Andrews et al., 1994), bringing the database up to 29 fjords for some parameters. These parameters were statistically analyzed for the difference of means in order to test whether the two fjord groups represented by Cumberland Peninsula and the northeast coast are significantly different. The chapter also discusses how the differently sized ice-sources (PIC-LAG vs LIS) may have influenced fjord morphology. It appears that the northeast coast fjords, formed by outlet ice-flow from the LIS, as a group are longer, deeper, and wider, in addition to sharing a narrower range of orientation.

Chapter 3 discusses the sedimentary history of selected Cumberland Peninsula fjords, and constrains the timing of a relative sea-level lowstand. Acoustic subbottom imagery and sediment cores were collected for three Cumberland Peninsula fjords, and compared to previous data for Sunneshine Fiord. Acoustic stratigraphy was interpreted from acoustic profiles and correlated with lithological units observed in the sediment cores. Radiocarbon dates provide evidence of mean sedimentation rates over time, as well as maximum and minimum age constraints for the postglacial lowstand.

Chapter 4 summarizes the results and discussion of Chapters 2 and 3. Contributions made to fjord morphology, sedimentology, and chronology are highlighted, and multiple potential avenues for future research are suggested and described.

1.7 References

Aitken, A.E. & Gilbert, R. (1989). Holocene nearshore environments and sea-level history in Pangnirtung Fiord, Baffin Island, N.W.T., Canada. *Arctic and Alpine Research,* 21(1): 34-44.

Anderson, R.K., Miller, G.H., Briner, J.P., Lifton, N.A., & DeVogel, S.B. (2008). A millennial perspective on Arctic warming from ^{14}C in quartz and plants emerging from beneath ice caps. *Geophysical Research Letters*, 35, L01502.

Andrews, J.T. (1987). Late Quaternary marine sediment accumulation in fiord-shelf-deep-sea transects, Baffin Island to Baffin Bay. *Quaternary Science Reviews,* 6: 231-243.

Andrews, J., & Ives, J. (1978). “Cockburn” nomenclature and the Late Quaternary history of the eastern Canadian Arctic. *Arctic and Alpine Research*, 10: 617–633.

Andrews, J.T., Osterman, L., Kravitz, J., Jennings, A., Stravers, J., Williams, K., & Mothersill, J. (1984). Quaternary piston cores. In J.P.M. Syvitski & C.P. Blakeney (Compilers), *Sedimentology of Arctic Fjords Experiment: HU 82-031 Data Report*, *Volume 1*. Geological Survey of Canada, Open File 960. doi: 10.4095/129793

Andrews, J.T., Syvitski, J.P., Osterman, L.E., Williams, K.M., Mode, W.N., Kravitz, J.E. & Locke, W.W. III. (1994). *Quaternary geology of Sunneshine Fiord (Baffin Island).* Geological Survey of Canada, Open File 3004. doi:10.4095/195129

Andrews, J.T., Osterman, L.E., Jennings, A.E., Syvitski, J.P.M., Miller, G.H., & Weiner, N. (1996). Abrupt changes in marine conditions, Sunneshine Fiord, eastern Baffin Island, NWT during the last deglacial transition: Younger Dryas and H-0 events. *Late Quaternary Palaeoceanography of the North Atlantic Margins,* Geological Society Special Publication 111: 11-27.

Bostock, H.S. (2014). *Geology, Physiographic Regions of Canada*; Geological Survey of Canada, Map 1254A (2nd edition), scale 1:5,000,000. doi:10.4095/293408

Bradley, R.S., Hughes, M.K., & Diaz, H.F. (2003). Climate in Medieval time. *Science,* 302: 404–405.

Briner, J.P., Bini, A.C., & Anderson, R.S. (2009a). Rapid early Holocene retreat of a Laurentide outlet glacier through an Arctic fjord. *Nature Geoscience,* 2: 496–499.

Briner, J.P., Davis, P.T., & Miller, G.H. (2009b). Latest Pleistocene and Holocene glaciation of Baffin Island, Arctic Canada: key patterns and chronologies. *Quaternary Science Reviews*, 28: 2075–2087.

Clark, J.A., Farrell, W.E., & Peltier, W.R. (1978). Global changes in postglacial sea level: A numerical calculation. *Journal of Quaternary Research*, 9: 265–287.

Clarke, D. B. & Upton, B.G.J. (1971). Tertiary basalts of Baffin Island: field relations and tectonic setting. *Canadian Journal of Earth Sciences,* 8: 248–258. https://doi.org/10.1139/e71-025

Cole, F. & Blakeney, C.P. (1984). Description and X-radiographs of the Baffin fjord cores. In J.P.M. Syvitski & C.P. Blakeney (Compilers), *Sedimentology of Arctic Fjords Experiment: HU 82-031 Data Report, Volume 1* (GSC Open File 960). doi: 10.4095/129793

Cowan, B. (2015). *Shorelines beneath the sea: Geomorphology and characterization of the postglacial sea-level lowstand, Cumberland Peninsula, Baffin Island, Nunavut*. M.Sc. thesis, Memorial University of Newfoundland, St John's, NL.

Courtney, R., & Shaw, J. (2000). Multibeam bathymetry and backscatter imaging of the Canadian continental shelf. *Geoscience Canada,* 27 (1): 31-42.

Dalton, A.S., Margold, M., Stokes, C.R., Tarasov, L., Dyke, A.S., Adams, R.S., Allard, S., Arends, H.E., Atkinson, N., Attig, J.W., Barnett, P.J., Barnett, R.L., Batterson, M., Bernatchez, P., Borns Jr., H.W., Breckenridge, A., Briner, J.P., Brouard, E., Campbell, J.E., ... Wright Jr., H.E. (2020). An updated radiocarbon-based ice margin chronology for the last deglaciation of the North American Ice Sheet Complex [Supplementary material]. *Quaternary Science Reviews,* 234: 1-27. https://doi.org/10.1016/j.quascirev.2020.106223

Dartnell, P., & Gardner, J.V. (2004). Predicting seafloor facies from multibeam bathymetry and backscatter data. *Photogrammetric Engineering & Remote Sensing,* 70 (9): 1081-1091.

de Vernal, A., & Hillaire-Marcel, C. (2006). Provincialism in trends and high frequency changes in the northwest North Atlantic during the Holocene. *Global and Planetary Change,* 54: 263-290.

Dowdeswell, E.K. & Andrews, J.T. (1985). The fjords of Baffin Island: description and classification. In J.T. Andrews (Ed.), *Quaternary Environments: Eastern Canadian Arctic, Baffin Bay and Western Greenland* (pp. 93–123). London: George Allen & Unwin Publishers.

Dyke, A.S. (1979). Glacial and sea-level history of southwestern Cumberland Peninsula, Baffin Island, N.W.T., Canada. *Arctic and Alpine Research,* 11 (2): 179–202.

Dyke, A.S., Andrews, J.T., & Miller, G.H. (1982). *Quaternary Geology of Cumberland Peninsula, Baffin Island, District of Franklin.* Geological Survey of Canada, Memoir 403. 32 p. https://doi.org/10.4095/116169

Dyke, A.S. (2013a). Surficial geology, Broughton Island–Padloping Island, Baffin Island, Nunavut, NTS 16-M, NTS 16-N, and parts of NTS 26-P. *Geological Survey of Canada, Canadian Geoscience Map 23* (ed. prelim.). doi:10.4095/288968

Dyke, A.S. (2013b). Surficial geology, Cape Dyer North, Baffin Island, Nunavut, NTS 16-L northeast and NTS 16-K northwest. *Geological Survey of Canada, Canadian Geoscience Map 22* (ed. prelim.). doi:10.4095/288967

Flint, R. F. (1971). *Glacial and Quaternary Geology*. John Wiley and Sons: New York.

Funck, T., Jackson, H.R., Louden, K.E., & Klingehofer, F. (2007). Seismic study of the transform-rifted margin in Davis Strait between Baffin Island (Canada) and Greenland: What happens when a plume meets a transform. *Journal of Geophysical Research, 112*, B04402: 1-22. https://doi.org/10.1029/2006JB004308

Funck, T., Gohl, K., Damm, V., & Heyde, I. (2012). Tectonic evolution of southern Baffin Bay and Davis Strait: Results from a seismic refraction transect between Canada and Greenland. *Journal of Geophysical Research, 117*. B04107: 1-24. https://doi.org/10.1029/2011JB009110

Gajewski, K. (2015). Quantitative reconstruction of Holocene temperatures across the Canadian Arctic and Greenland. *Global and Planetary Change*, 128: 14–23.

Gilbert, R. (1978). Observations on oceanography and sedimentation at Pangnirtung Fiord, Baffin Island. *Maritime Sediments*, 14(1): 1-9.

Gilbert, R. (1982a). Contemporary sedimentary environments on Baffin Island, N.W.T., Canada: Glaciomarine processes in fiords of eastern Cumberland Peninsula. *Arctic and Alpine Research*, 14(1): 1-12.

Gilbert, R. (1982b). The Broughton Trough on the continental shelf of eastern Baffin Island, Northwest Territories. *Canadian Journal of Earth Sciences*, 19: 1599-1607.

Gilbert, R. (1985). Quaternary glaciomarine sedimentation interpreted from seismic surveys of fiords on Baffin Island, N.W.T. *Arctic*, 38 (4): 271-280.

Gilbert, R. & MacLean, B. (1984). Geophysical studies based on conventional shallow and Huntec high resolution seismic surveys of fiords on Baffin Island. In J.P.M. Syvitski & C.P. Blakeney (Compilers), *Sedimentology of Arctic Fjords Experiment: HU 82-031 Data Report, Volume 1* (GSC Open File 960). doi: 10.4095/129793

Heaton, T.J., Köhler, P., Butzin, M., Bard, E., Reimer, R.W., Austin, W., Ramsey, C.B., Grootes, P.M., Hughen, K.A., Kromer, B., Adkins, J., Burke, A., Cook, M.S., Olsen, J. & Skinner, L.C. (2020). Marine20—the marine radiocarbon age calibration curve (0 – 55,000 cal BP). *Radiocarbon*, vol. First View. https://doi.org/10.1017/RDC.2020.68

Hein, F.J. & Longstaffe, F.J. (1984). Geotechnical sedimentology and mineralogical investigations in Arctic fjords. In J.P.M. Syvitski & C.P. Blakeney (Compilers), *Sedimentology of Arctic Fjords Experiment: HU 82-031 Data Report, Volume 1* (GSC Open File 960). doi: 10.4095/129793

Hood, P. & Bower, M. (1975). Aeromagnetic reconnaissance of Davis Strait and adjacent areas [Abstract]. *Canada's Continental Margins and Offshore Petroleum Exploration,* 4: 433-451.

Hosseinpour, M., Müller, R.D., Williams, S.E., & Whittaker, J.M. (2013). Full-fit reconstruction of the Labrador Sea and Baffin Bay. *Solid Earth*, 4(2): 461-479. https://doi.org/10.5194/se-4-461-2013

Hughes-Clarke, J.E., Muggah, J., Renoud, W., Bell, T., Forbes, D.L., Cowan, B., & Kennedy, J. (2015). Reconnaissance seabed mapping around Hall and Cumberland peninsulas, Nunavut: opening up southeastern Baffin Island to nearshore geological investigations. *Summary of Activities 2014*. Canada-Nunavut Geoscience Office: 133-144.

James, T.S., Henton, J.A., Leonard, L.J., Darlington, A., Forbes, D.L., & Craymer, M. (2014). Relative sea-level projections in Canada and the adjacent mainland United States. Geological Survey of Canada Open File 7737. doi:10.4095/295574

Jennings, A. (1993). The Quaternary history of Cumberland Sound, southeastern Baffin Island: The marine evidence. *Géographie physique et Quaternaire*, 47(1): 21-42.

Jennings, A.E., Tedesco, K.A., Andrews, J.T., & Kirby, M.E. (1996). Shelf erosion and glacial ice proximity in the Labrador Sea during and after Heinrich events (H-3 or -4 to H-0) as shown by foraminifera. *Late Quaternary Palaeoceanography of the North Atlantic Margins,* Geological Society Special Publications 111: 29–49.

Kaufman, D.S., Ager, T.A., Anderson, N.J., Anderson, P.M., Andrews, J.T., Bartlein, P.J., Brubaker, L.B. & 23 others. (2004). Holocene thermal maximum in the western Arctic (0–180°W). *Quaternary Science Reviews*, 23: 529–560.

Keen, C.E. & Beaumont, C. (1990). Geodynamics of rifted continental margins. In M.J. Keen & G.K. Williams (Eds.), *Geology of the Continental Margin of Eastern Canada* (pp. 391-474). Geological Survey of Canada, *Geology of Canada*, 2. https://doi.org/10.4095/132690

Kessler, M.A., Anderson, R.S., & Briner, J.P. (2008). Fjord insertion into continental margins driven by topographic steering of ice. *Nature Geoscience*, 1: 365-369.

Lamb, H.H. (1965). The early medieval warm epoch and its sequel. *Palaeogeography, Palaeoclimatology*, *Palaeoecology*, 1: 13–37.

Løken, O. H., & Hodgson, D. A. (1971). On the submarine geomorphology along the east coast of Baffin Island. *Canadian Journal of Earth Sciences,* 8(2): 185–195.

MacLean, B. & Falconer, R.K.H. (1979). Geological/geophysical studies in Baffin Bay and Scott Inlet-Buchan Gulf and Cape Dyer-Cumberland Peninsula areas of the Baffin Island Shelf. *Geological Survey of Canada*, Paper 79-1B: 231–244. https://doi.org/10.4095/105432

MacLean, B., Williams, G.L., & Srivasta, S.P. (1990). Geology of the Labrador Shelf, Baffin Bay, and Davis Strait. Part 2: Geology of Baffin Bay and Davis Strait. In M.J. Keen & G.K. Williams (Eds.), *Geology of the Continental Margin of Eastern Canada* (pp. 293-350). Geological Survey of Canada, *Geology of Canada*, 2. https://doi.org/10.4095/132690

Manchester, K.S. & Clarke, D.B. (1973). Geological structure of Baffin Bay and Davis Strait as determined by geophysical techniques. In M.G. Pitcher (Ed.) *Arctic Geology*, American Association of Petroleum Geologists, Memoir 19: 536-541.

Mann, M.E., Zhang, Z., Rutherford, S., Bradley, R.S., Hughes, M.K., Shindell, D., Ammann, C., Faluvegi, G., & Ni, F. (2009). Global signatures and dynamical origins of the Little Ice Age and Medieval Climate Anomaly. *Science*, 326: 1256–1260.

Margold, M., Stokes, C.R., & Clark, C.D. (2015). Ice streams in the Laurentide Ice Sheet: Identification, characteristics and comparison to modern ice sheets. *Earth-Science Reviews*, 143: 117-146.

Margreth, A. (2015). Climate sensitivities of polythermal ice sheet, ice cap, and alpine ice dynamics and related episodic erosion on Cumberland Peninsula, Baffin Island, Nunavut. Ph.D. dissertation, Dalhousie University, Halifax, NS.

Miller, G.H. & Dyke, A.S. (1974). Proposed extent of late Wisconsin Laurentide Ice on Eastern Baffin Island. *Geology*, 2(3): 125–130.

Miller, G.H., Wolfe, A.P., Briner, J.P., Sauer, P.E., & Nesje, A. (2005). Holocene glaciation and climate evolution of Baffin Island, Arctic Canada. *Quaternary Science Reviews*, 24: 1703–1721.

Miller, G.H., Geirsdóttir, Á., Zhong, Y., Larsen, D.J., Otto-Bliesner, B.L., Holland, M.M., Bailey, D.A., & 6 others. (2012). Abrupt onset of the Little Ice Age triggered by volcanism and sustained by sea-ice/ocean feedbacks. *Geophysical Research Letters*, 39, L02708.

Moore, J.J., Hughen, K.A., Miller, G.H., & Overpeck, J.T. (2001). Little Ice Age recorded in summer temperature reconstruction from varved sediments of Donard Lake, Baffin Island, Canada. *Journal of Paleolimnology*, 25: 503-517.

Natural Earth. (2017). *Downloads*. [Shapefiles]. Retrieved October 30, 2017, from https://www.naturalearthdata.com/downloads/

Natural Resources Canada. (2017a). *Expedition 82031*. [Data file]. Available from http://ed.gdr.nrcan.gc.ca/index_e.php

Natural Resources Canada. (2017b). *Geospatial Data Extraction* [CanVec shapefiles]. Retrieved March 4, 2021, from https://maps.canada.ca/czs/index-en.html

Normandeau, A. Dietrich, P., Hughes-Clarke, J., van Wychen, W., Lajeunesse, P., Burgess, D. & Ghienne, J.F. (2019a). Retreat pattern of glaciers controls the occurrence of turbidity currents on high-latitude fjord deltas (eastern Baffin Island). In *The Arctic*, an AGU joint special collection. *Journal of Geophysical Research, Earth Surface*, 124 (6): 1559-1571, https://doi.org/10.1029/2018JF004970

Normandeau, A., Robertson, A.G., Philibert, G., Regular, K. & Sedore, P. (2019b). *R/V Nuliajuk expedition 2019Nuliajuk: marine geohazards near Qikiqtarjuaq, Padle Fiord, Southwind*

Fiord and Pangnirtung, southeast Baffin Island, Nunavut. Geological Survey of Canada, Open File 8641, 62 p., https://doi.org/10.4095/315676

Normandeau, A., Broom, L.M., Carson, T. & Trottier, A.P. (2019c). *CCGS Amundsen 2019804 expedition: marine geohazards and sediment transport processes in Baffin Bay, Nunavut.* Geological Survey of Canada, Open File 8649, 24 p., https://doi.org/10.4095/321054

Pheasant, D.R. & Andrews, J.T. (1973). Wisconsin glacial chronology and relative sea-level movements, Narpaing Fiord Broughton Island area, eastern Baffin Island, N.W.T. *Canadian Journal of Earth Sciences,* 10 (11): 1621–1641.

Rasmussen, S.O., Andersen, K.K., Svensson, A., Steffensen, J.P., Vinther, B.M., Clausen, H.B., Sigaard-Andersen, M.-L., Johnsen, S.J., Larsen, L.B., Dahl-Jensen, D., Bigler, M., Röthlisberger, R., Fischer, H., Goto-Azuma, K., Hansson, M.E., & Ruth, U. (2006). A new Greenland ice core chronology for the last glacial termination. *Journal of Geophysical Research,* 111: 1–16

Rasmussen, S.O., Vinther, B.M., Clausen, H.B., & Andersen, K.K. (2007). Early Holocene climate oscillations recorded in three Greenland ice cores. *Quaternary Science Reviews,* 26: 1907–1914

Sanborn-Barrie, M. & Young, M. (2013). Geology, Durban Harbour, Baffin Island, Nunavut. *Geological Survey of Canada, Canadian Geoscience Map 38* (ed. prelim.). doi:10.4095/292015

Sanborn-Barrie, M., Young, M., Keim, R., & Hamilton, B. (2013). Geology, Sunneshine Fiord, Baffin Island, Nunavut. *Geological Survey of Canada, Canadian Geoscience Map 6* (ed. prelim.). doi:10.4095/288931

St-Onge, M. R., Harrison, J. C., Paul, D., Tella, S., Brent, T. A., Jauer, C. D. & Maclean, B. C. (2015). *Tectonic Map of Arctic Canada*; Geological Survey of Canada, Canadian Geoscience Map 187 (preliminary), scale 1:4,000,000

Stuiver, M., Reimer, P.J, & Reimer, R.W. (2021). *CALIB 8.2*. http://calib.org/calib/

Syvitski, J.P. (Compiler). (1985). *Sedimentology of Arctic Fjords Experiment: HU 83-028 Data Report, Volume 2* (GSC Open File 1122). doi: 10.4095/129977

Syvitski, J.P.M., & Blakeney, C.P. (Compilers). (1984). *Sedimentology of Arctic Fjords Experiment: HU 82-031 Data Report, Volume 1* (GSC Open File 960). doi: 10.4095/129793

Syvitski, J.P.M. & Hein, F.J. (1991). *Sedimentology of an Arctic basin: Itirbilung Fiord, Baffin Island, Northwest Territories*. Geological Survey of Canada, Paper 91-11, 66p. https://doi.org/10.4095/132684

Syvitski, J.P.M., & Praeg, D.B. (Compilers). (1987). *Sedimentology of Arctic Fjords Experiment: Data Report, Volume 3* (GSC Open File 1589). doi: 10.4095/130318

Syvitski, J.P.M., Schafer, C.T., Asprey, K.W., Hein, F.J., Hodge, G.D., & Gilbert, R. (1986). *Sedimentology of Arctic fjords experiment: PA-85-062 expedition report.* (GSC Open File 1234). https://doi.org/10.4095/130052

Syvitski, J.P.M., Burnell, D.C., & Skei, J.M. (1987). *Fjords: Processes and Products*. Springer-Verlag: New York.

Telka, A. (2015). *Expedition 2014805 Baffin Island shell dating report*. Paleotec Services.

Telka, A. (2016). *Expedition 2014805 Baffin Island shell dating report*. Paleotec Services.

Todd, B.J., & Shaw, J. (2009). Applications of seafloor mapping on the Canadian Atlantic continental shelf. *Geoscience Canada*, 36 (2): 81-94.

Trenhaile, A. (2010). *Geomorphology: A Canadian Perspective* (4^{th} ed.). Oxford University Press: Don Mills, ON.

CHAPTER 2: MORPHOMETRIC ANALYSIS OF NORTHEAST COAST AND CUMBERLAND PENINSULA FJORDS, BAFFIN ISLAND, NUNAVUT.

Abstract

This study presents a morphometric database of 13 parameters across 29 Baffin Island fjords, compiled using ArcGIS in conjunction with topographic and geophysical data from Natural Resources Canada and the University of New Brunswick Ocean Mapping Group. The fjord-morphometry database was partitioned into two regional groups, each associated with a separate glacial system: northeast coast (Laurentide Ice Sheet) and Cumberland Peninsula (Penny Ice Cap and local alpine glaciation). A difference-of-means *t* test and Wilcoxon rank sum *W* test were conducted for each morphometric parameter to test if fjord morphology was significantly different between these two regions. Overall, fjords were found to be significantly larger along the northeast coast of Baffin Island than Cumberland Peninsula for the vast majority of parameters (fjord area; length; mean, minimum, and maximum width, maximum basin depth, sill depth, outer depth, and drainage-basin area). The difference is attributed to the Laurentide Ice Sheet having supported significantly larger outlet glaciers, with greater erosive power, than the combined Penny Ice Cap and local alpine glaciation complex on Cumberland Peninsula.

2.1 Introduction

Fjords dominate the landscape of northeastern Baffin Island (Fig. 2.1), which was previously glaciated by the Laurentide Ice Sheet and the Penny Ice Cap – Local Alpine Glaciation complex. Previous geomorphic research on Baffin Island fjords has included 1980s studies on fjord morphometry (Gilbert & MacLean, 1984; Dowdeswell & Andrews, 1985) and more recent surveys on fjord bathymetry (Cowan, 2015), but has not yet examined how the different glacial systems may have affected fjord morphology. The present study aims to provide an updated survey of fjord morphometry that incorporates multibeam bathymetry. The resulting morphometric data provide a basis for analyzing how glacier size controls fjord morphology across two different environments on Baffin Island.

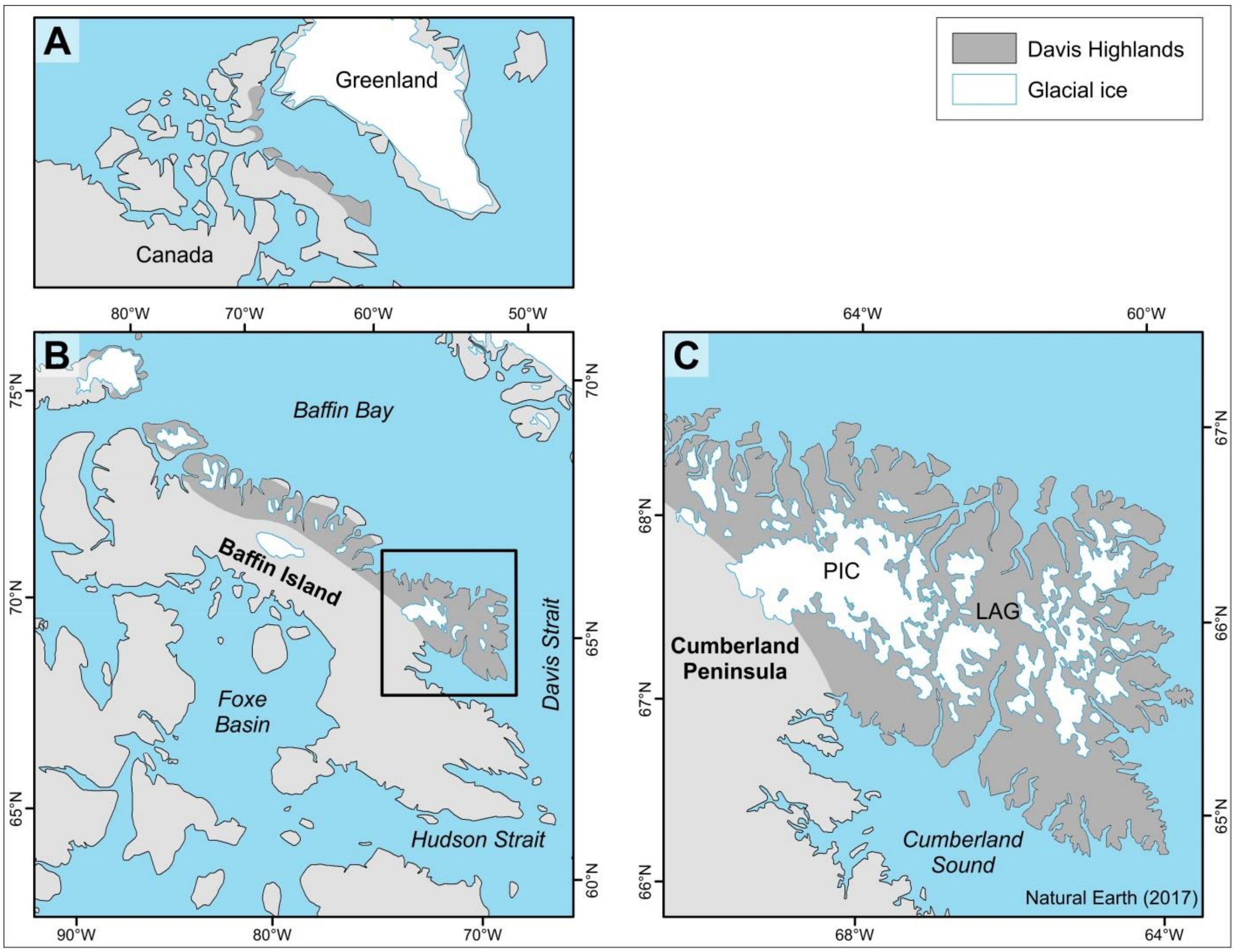

Figure 2.1: Baffin Island and Cumberland Peninsula with surrounding environs. A) The full extent of the Davis Highlands throughout the CAA (Bostock, 2014). B) Baffin Island and the surrounding water bodies; not pictured is the Labrador Sea (Atlantic Ocean) to the southeast. C) Cumberland Peninsula and its two glacial systems: Penny Ice Cap (PIC) and Local Alpine Glaciation (LAG).

2.1.1 Glacial erosion and fjord morphology

Fjords and inland glacial valleys are excavated by glaciers flowing through pre-existing depressions, such as fluvial valleys and fault lines (Augustinus, 1992; Bennett & Glasser, 2009; Benn & Evans, 2010). The process of glacial erosion includes the sub-processes of abrasion and quarrying: Abrasion occurs as basal ice flow drags rock tools across the underlying bedrock, while quarrying refers to the overall transport of rock fragments by the glacier regardless of contact with the bedrock. Subglacial meltwater can also participate in abrasion when flowing at high speeds with a sediment load, and act as the medium for chemical dissolution (especially in limestone terrains) (MacGregor et al., 2000; Anderson et al., 2006; Trenhaile, 2010); however, an in-depth analysis of fluvial erosion is beyond the scope of this thesis.

It is understood that glacial erosion, via abrasion and quarrying, increases with glacier discharge, a function of ice mass/thickness and flow speed (Holtedahl, 1967; Haynes, 1972; Roberts & Rood, 1984; Augustinus, 1992; MacGregor et al., 2000; Anderson et al., 2006; Foster et al., 2008; Kessler et al., 2008; Trenhaile, 2010).

Greater ice thickness increases the pressure of rock tools against the bedrock, thus increasing the rate of erosion (so long as friction does not become excessive) (Trenhaile, 2010). The effects of ice thickness can be observed at overdeepenings in the valley/fjord floor, which often occur within the inner-third of the valley (close to the accumulation zone where the ice is thickest) and the junctions with tributary glaciers (where the influx of ice intensified downward erosion) (Anderson et al., 2006).

Flow speed is partly controlled by ice thickness via compressive stress (Kessler et al., 2008; Trenhaile, 2010), but also by the ice temperature (or thermal regime) at the base of the glacier

(Bennett & Glasser, 2009; Benn & Evans, 2010; Trenhaile, 2010). Because the pressure melting point of water decreases at higher pressure, it is possible for liquid water to exist at temperatures below 0°C under the weight of a glacier. When the basal ice temperature is at or near the pressure melting point, it is referred to as *warm-based ice* and a thin film of liquid water will form, which reduces friction and increases ice velocity. In contrast, when the basal ice temperature remains below the pressure melting point, it is *cold-based ice* and freezes directly to the substrate, reducing ice velocity (Trenhaile, 2010). As a result, warm-based glaciers generally display greater velocity and erosion potential than cold-based glaciers, which are associated with either minor or no glacial erosion (Bennett & Glasser, 2009; Benn & Evans, 2010; Trenhaile, 2010). Multiple studies have interpreted the northeast coast of Baffin Island and Cumberland Peninsula as glaciated by warm-based outlet glaciers flowing through fjords and valleys while cold-based ice occupying the inter-fjord highlands (Miller et al., 2002; Kaplan & Miller, 2003; Briner et al., 2005; Miller et al., 2005; Margreth, 2015; Brouard & Lajeunesse, 2017).

Moreover, it has been observed that the rate of erosion is also influenced by the underlying bedrock mass strength: weaker (sedimentary) bedrock erodes rapidly into broad, shallow valleys while stronger (igneous) bedrock erodes more slowly into steeper, narrower valleys (Augustinus, 1992; Brook et al., 2004). An in-depth review of bedrock composition and rock mass strength across Baffin Island is beyond the scope of this thesis. However, geological mapping of Baffin Island shows exposed plutonic (Rae craton) and granite (Qikiqtarjuaq suite) bedrock to occupy most of the island along the northeast coast and Cumberland Peninsula, with sedimentary cover limited to Home Bay and central Cumberland Peninsula (St-Onge et al., 2015). Therefore, most of the fjords included in this thesis are expected to occupy igneous bedrock terrains, with only a few incising the sedimentary cover.

Depending on the pre-glacial conditions, some fjords may require less glacial erosion than others to reach a specific size. For example, a given fault line (10 km) may be significantly longer than an adjacent fluvial valley (1 km), and thus will develop into a longer fjord over the same interval of glaciation. Nonetheless, when the basal thermal regime and bedrock mass strength are equal, a larger glacier is anticipated to be overall more erosive over the duration of a given glacial period (Augustinus, 1992; Anderson et al., 2006; Bennett & Glasser, 2009). This is further supported by observations of the effects of ice thickness on individual fjord dimensions (i.e., depth, length, width).

Depth: As explained above, a thicker glacier favours a deeper fjord due to the influence of ice thickness on erosion rate (Holtedahl, 1967; Anderson et al., 2006; Kessler et al., 2008; Trenhaile, 2010). However, maximum fjord depth is also limited by the ratio of water depth to ice thickness. As ice does not float until the water depth is ≥90% of the ice thickness, a thicker glacier is thus able to excavate to a greater maximum depth before floatation separates the ice from the seafloor (Flint, 1971).

Length: Logically, as glacial erosion lowers the overall valley floor below sea level, the fjord head (situated at the land-sea interface) is simultaneously moved further inland, thus lengthening the fjord. Even after floatation limits the downward erosion of the maximum basin depth, erosion at the fjord head will likely continue at a rate controlled by glacier discharge (and thus, ice thickness).

Width: A thicker glacier exerts greater compressive stress on the valley sidewalls (Trenhaile, 2010), although lateral erosion on sidewalls may be minimal due to a lack of available rock tools

(Holtedahl, 1967; Nesje & Whillans, 1994). Nonetheless, a greater ice mass will most likely cover, and thus excavate downwards, a wider swath of valley floor (Fig 2.9; Roberts & Rood, 1984; Foster et al., 2008). As explained above, the mass strength of the eroded bedrock influences valley/fjord width, although most fjords along the northeast coast and Cumberland Peninsula incise strong, igneous rock.

Drainage basin: Multiple studies have found positive relationships between drainage-basin area and various dimensions of glacial valley size (length, width, depth, cross-section area, volume, etc.) for regions affected by continental and local alpine glaciation, which supports hypothesis that glacier size is an important control on fjord morphology (Haynes, 1972; Roberts & Rood, 1984; Dowdeswell & Andrews, 1985; Augustinus, 1992; Bennett & Glasser, 2009; Patton et al., 2016). These studies have also used the size of the drainage basin surrounding a fjord as a proxy for ice supply, an assumption that this thesis also makes. This use of the total fjord drainage basin is justified, as only analyzing the portion of the drainage basin inland from the fjord head would exclude the contribution of tributary glaciers. Moreover, while inter-fjord uplands along Baffin Island may have been partly unglaciated, but some were also glaciated with cold-based ice which, while not fast, would have presumably flowed downhill to coalesce with fjord glaciers.

Elevation: The elevation of the mountains surrounding a fjord is a product of the uplift cause by the corresponding orogeny, but can be modified by alpine glacial erosion of the headwall. The rate of elevation change will be influenced by the ongoing uplift rate and underlying bedrock lithology, but also by glacier size (Foster et al., 2008). These changes in alpine elevation and relief may trigger positive feedbacks on glacial mass-balance and erosion via increasing the frequency of avalanches (MacGregor et al., 2009). Although the inter-fjord uplands of Baffin Island are interpreted as previously glaciated by cold-based ice, many fjords (and their inland-valley components) capture multiple hanging valleys, which indicate tributary glaciers that may have altered mountain elevation via erosion throughout the drainage basin. Thus, elevation data can indicate potential differences in glacial erosion along the fjord sidewalls and throughout the surrounding uplands, as well as provide a proxy measurement for fjord incision where bathymetry is unavailable.

Therefore, other variables notwithstanding, one should anticipate a positive relationship between glacier size, drainage-basin area, and fjord dimensions, while a limit on glacier size should likewise limit fjord size.

2.1.2 Regional setting

This study of fjord morphometry is situated along the east coast of Baffin Island, located in the eastern margin of the Canadian Arctic Archipelago (CAA; Fig. 2.1). Along the northeast coast are the Baffin Island mountains, a subset of the Davis Highlands (Bostock, 2014), which were uplifted by the rifting event that opened Baffin Bay and separated Greenland from North America (Clarke & Upton, 1971; MacLean & Falconer, 1979; MacLean et al., 1990; Keen & Beaumont, 1990; Hosseinpour et al., 2013). A fracture zone (horst and graben) has developed along this rift margin, wherein linear troughs cross-cut the NW-SE faults parallel to the rift, creating a trellis drainage pattern (Manchester & Clarke, 1973; MacLean et al., 1990; Funck et al., 2007, 2012). These features are conducive to fjord development, and their initial dimensions reduce the amount of glacial erosion necessary to reach a specific size. At the easternmost edge of Baffin Island sits Cumberland Peninsula, delimited on the south by Cumberland Sound. The sound lies parallel to the cross-cutting valleys that run through the Baffin Island mountains, and is interpreted to have formed as a subsiding graben (Hood & Bower, 1975; MacLean & Falconer, 1979; MacLean et al., 1990).

The onset of Quaternary glaciation drove the excavation of multiple glacial valleys and fjords throughout the Baffin Island mountains (Miller et al., 2005; Kessler et al., 2008). The northeast margin of the Laurentide Ice Sheet (LIS) is understood to have covered the majority of Baffin Island and fed multiple outlet glaciers along its northeast coast. Cumberland Sound became the locus of an LIS ice stream which flowed to the south of Cumberland Peninsula. This allowed the Penny Ice Cap and Local Alpine Glaciation (PIC-LAG) complex to occupy the peninsula as an independent glacial system (Fig. 2.2 and 2.3; Jennings, 1993; Margreth, 2015). The LIS was much larger than the PIC-LAG complex in both area and volume, and thus capable of feeding much larger outlet glaciers. In the present day, the fjords of Baffin Island are relatively unglaciated, facilitating comprehensive study of fjord morphology, while the two separate glacial systems, LIS and PIC-LAG, enable comparisons between how glacier scale and outlet dynamics affected fjord morphology.

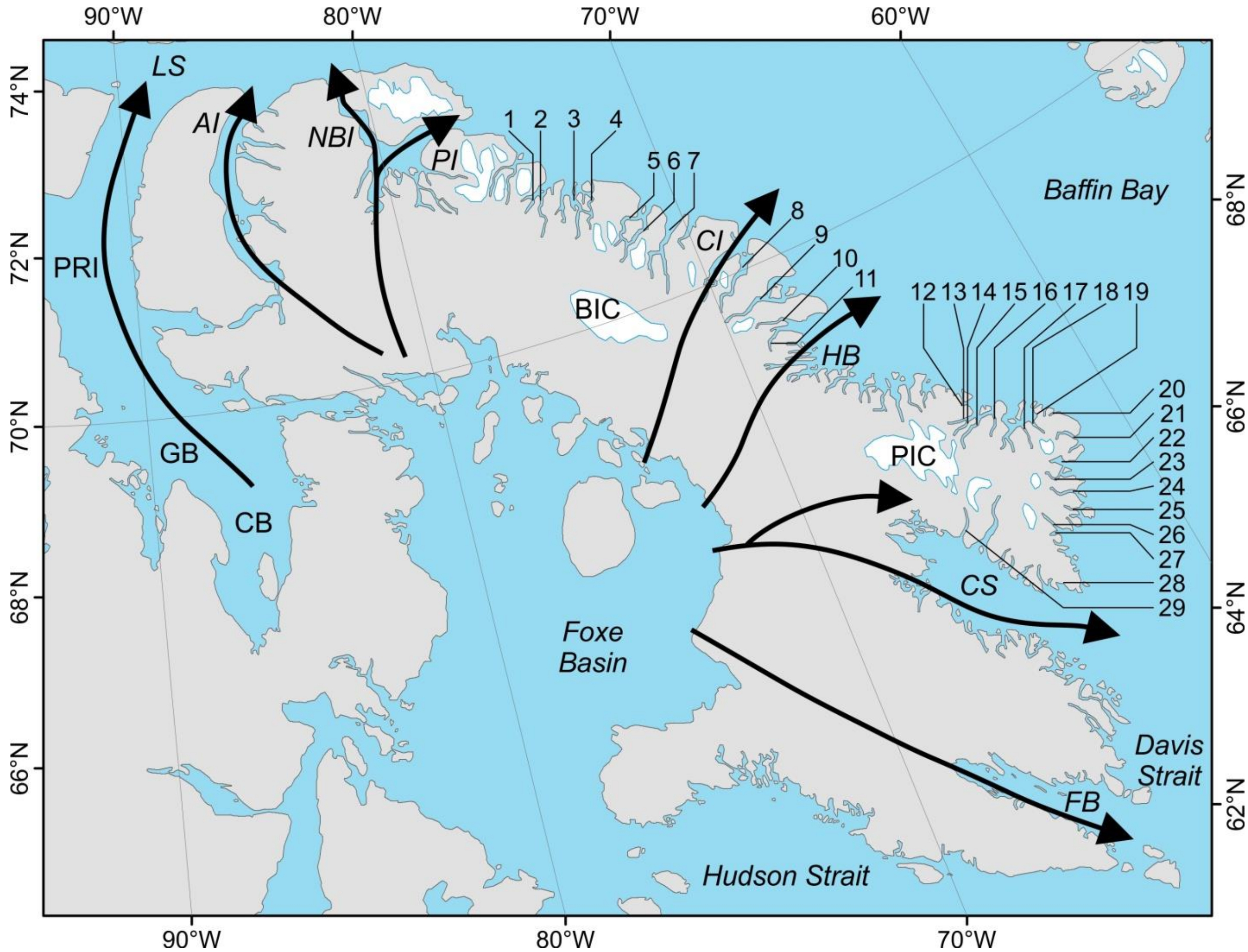

Figure 2.2: Arrows illustrate the major directions of the Laurentide Ice Sheet (Margold et al., 2015; Margreth, 2015). Notice how flow directions essentially bifurcate around Cumberland Peninsula. The positions of Baffin Island fjords included in the study are numbered, with names listed in Table 2.1 (section 2.3 Results). The positions of the Barnes Ice Cap (BIC), Penny Ice Cap (PIC), Committee Bay (CB), Gulf of Boothia (GB), Prince Regent Inlet (PRI), Lancaster Sound (LS),Admiralty Inlet (AI), Navy Board Inlet (NBI), Pond Inlet (PI), Clyde Inlet (CI), Home Bay (HB), Cumberland Sound (CS), and Frobisher Bay (FB) are marked. Glaciers are from Natural Earth (2017), land and ocean from Natural Resources Canada (2017).

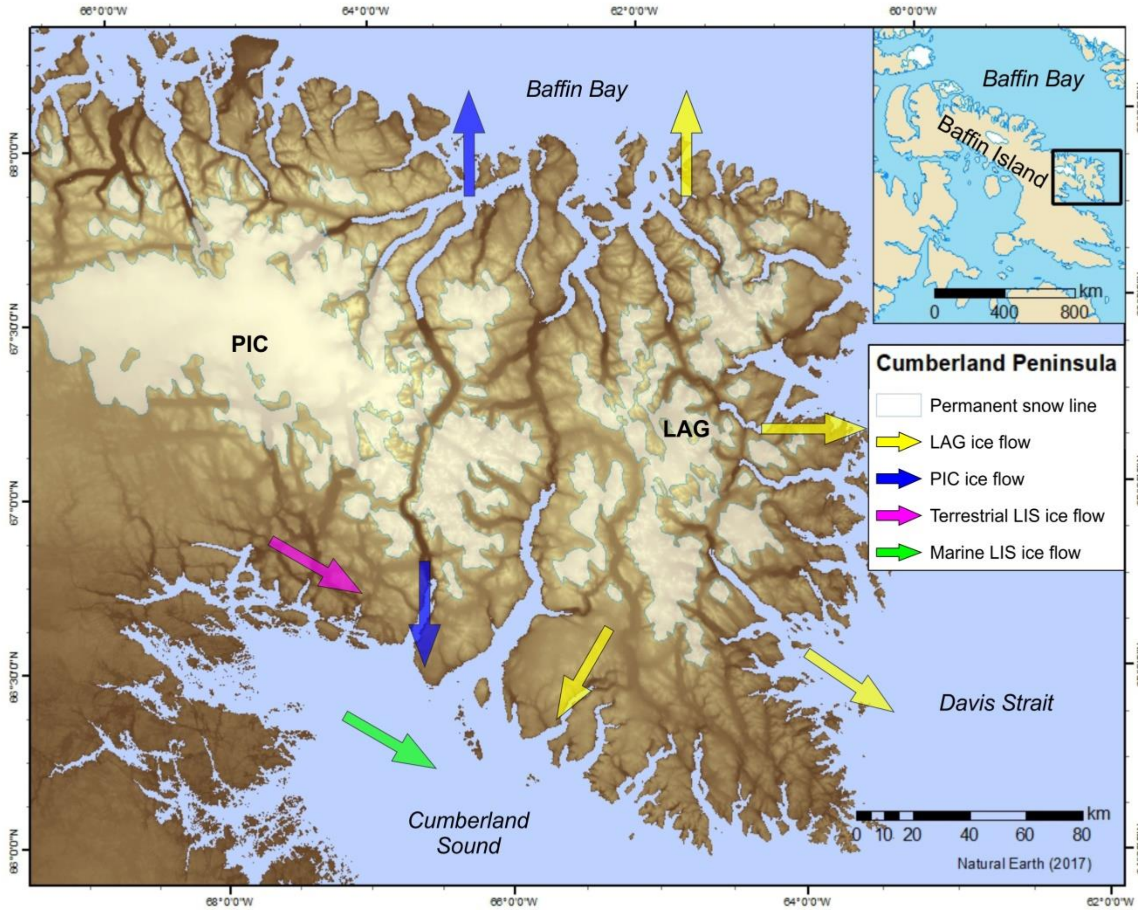

Figure 2.3: Diagram illustrating the general ice-flow of the Penny Ice Cap (PIC) and Local Alpine Glaciation (LAG) compared to the Laurentide Ice Sheet (LIS). Ice-flow directions are further illustrated in Margreth (2015).

2.1.3 Previous research on Baffin Island fjords

Baffin Island fjord morphometry has previously been described for ten fjords by Gilbert and MacLean (1984) as part of the Sedimentology of Arctic Fjords Experiment (SAFE). Gilbert and MacLean suggested that glacial characteristics may have varied between fjords, as glaciers farther north are more likely to be cold-based and slow-moving ice may be less erosive, but made no inferences on regional differences. Their morphometric data for certain parameters have been incorporated into the current study, as described under Methodology.

A contemporary study by Dowdeswell and Andrews (1985) conducted a thorough statistical analysis of Baffin Island fjord morphometry using 29 parameters and a sample of 227 fjords (Fig. 2.4). They used a cluster analysis to aggregate fjords together based on shared values for morphometric parameters, and identified two fjord groups: east coast and north/south coast. These two groups roughly overlap with the northeast coast and Cumberland Peninsula regions described above; however, as seen on Figure 2.4, the Dowdeswell and Andrews groups are not spatially exclusive, showing notable areal overlap with the eastern coast of Cumberland Peninsula as a transition zone. It is possible that these individual cases of overlap indicate local exceptions to regional trends in processes or conditions. Moreover, their discriminant analysis found only one parameter, maximum elevation along the fjord, to be significantly different between the two groups (larger for the east coast). It is interesting that two groups based on similar attributes could not be found to have many significant differences between them. The current study does not use as many parameters and has a much smaller sample size, but tests for differences between two spatially-exclusive regions and uses modern software for measurements.

Following the third SAFE data report in 1987, marine-survey-based research on Canadian Arctic fjords experienced a hiatus, while land-based research continued. Such research included Miller et al. (2002), which described a new paradigm for Last Glacial Maximum glacial extent, and other papers that investigated paleoclimate (e.g., Syvitski et al., 1990; Kaplan et al., 2001; Moore et al., 2001). Marine-based Canadian Arctic fjord research was later renewed by ArcticNet and Government of Nunavut research initiatives, beginning in 2003. The current phase of Arctic fjord research utilizes improved data collection and analysis abilities due to newer technology, such as multibeam bathymetry, which enhances study of maximum basin and sill depths.

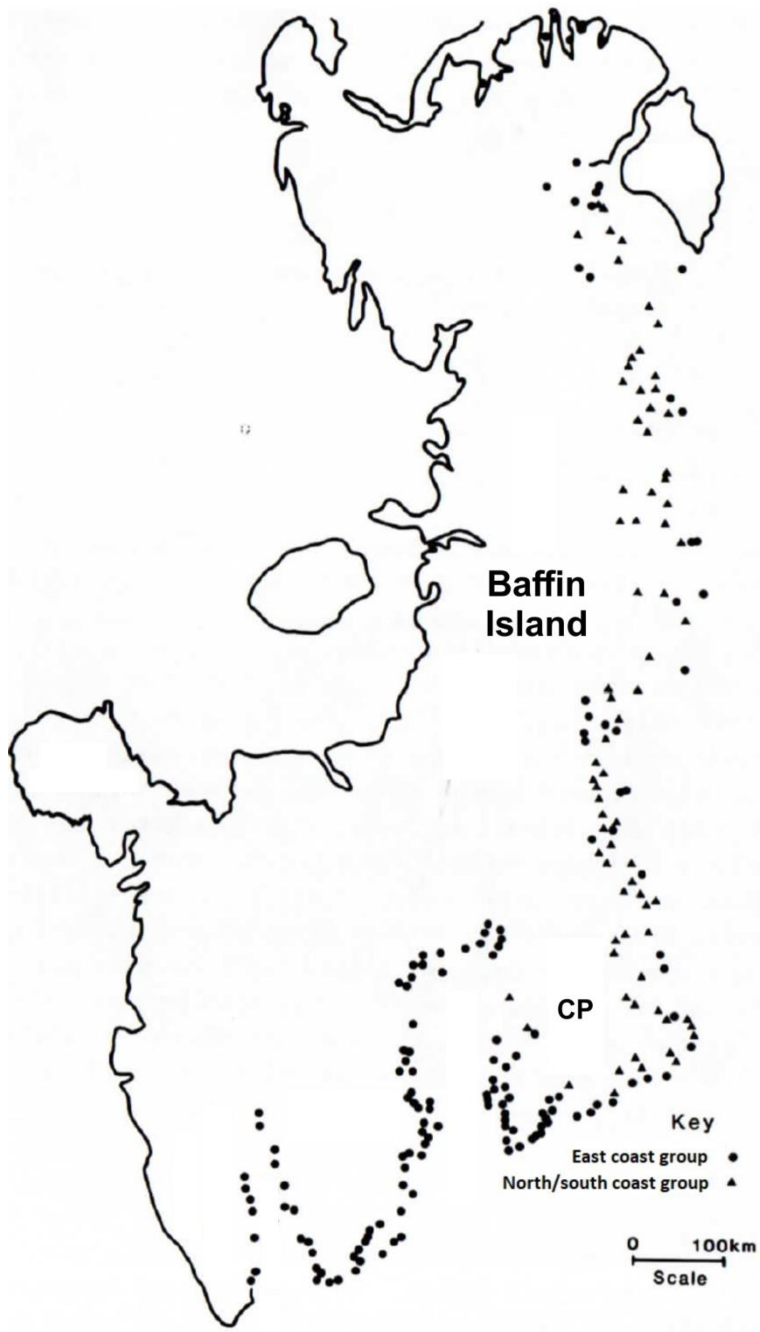

Figure 2.4: Fjords of Baffin Island as classified by cluster analysis, modified from Dowdeswell and Andrews (1985). Note how the two groups overlap spatially, with fjords of either group occurring along the northeast coast and Cumberland Peninsula (CP).

2.1.4 Research questions

Using multibeam bathymetry and GIS software, this study compiles an updated survey of fjord morphology along the Baffin Island coast. This database provides a foundation for determining how glacial style affects fjord morphology, by enabling statistical comparisons between two regions on Baffin Island glaciated by separate glacial systems, the LIS and PIC-LAG complex. The LIS was a massive ice source capable of feeding larger ice stream and outlet glaciers than the PIC-LAG complex. Given that glacial discharge correlates positively with glacial erosion (Holtedahl, 1967; Haynes, 1972; Roberts & Rood, 1984; Augustinus, 1992; Foster et al., 2008; Kessler et al., 2008; Trenhaile, 2010), it is expected that the LIS excavated larger fjords than the PIC-LAG. If so, then a distinct size difference should be found between the majority of fjords on Baffin Island's northeast coast (LIS) and those on Cumberland Peninsula (PIC-LAG). Whether this size difference occurs is tested by selecting several morphometric parameters (i.e., length, width, depth, and drainage-basin area) from the database and testing for a significant difference of means between the two regions.

The database is also used to test other reported observations on fjord morphometry for the Baffin Island sample population. The Kessler et al. (2008) model predicts that the preglacial valley with a greater initial relief experiences greater erosion and thus deepens more rapidly, especially if associated with thicker, warm-based ice. The database makes it possible to expand on this observation by testing the correlation between a fjord's maximum values for basin depth and sidewall elevation. Meanwhile, Patton et al. (2016) found a positive relationship between the length and width of glacial overdeepening beneath continental ice sheets, and multiple studies have found strong correlations between drainage-basin area and glacial valley size (Haynes, 1972; Roberts & Rood, 1984; Dowdeswell & Andrews, 1985; Augustinus, 1992; Patton et al., 2016). The current study uses the database to test these correlations for the fjords of Baffin Island. The extent to which control of each morphometric parameter can be attributed to glacial erosion versus inherited topography is also discussed.

2.2 Methodology

2.2.1 Sampling and analysis strategy

This study was structured to statistically determine whether the fjords situated along the northeast coast (NC) and Cumberland Peninsula (CP) of Baffin Island represent one or two populations on the basis of morphology. Thus, the null hypothesis posits that both groups, NC and CP, represent one population, with the alternative hypothesis that the groups represent two distinct populations.

In order to test this hypothesis, morphometric data were collected for a total of 29 fjords across the NC and CP regions. An initial 21 fjords were analyzed and measured using ArcGIS and multibeam bathymetry, digital elevation model, and topographic map data files. For this morphometric analysis, a total of 13 parameters were measured for each fjord:

- Orientation;
- Sinuosity;
- Surface area;
- Length;
- Mean, minimum, and maximum width;
- Maximum basin, sill, and outer depth;
- Maximum sidewall elevation;
- Surface area of the surrounding drainage basin;

- Maximum elevation of the surrounding drainage basin.

However, this initial analysis was limited to the fjords within the study regions for which multibeam bathymetry data were available. Recognizing the potential for statistical bias because of the small sample size and the selection of fjords for multibeam surveys, morphometric data for an additional seven fjords were imported directly from Gilbert and MacLean (1984). Data for one fjord (Sunneshine Fiord) is a combination of ArcGIS analysis and depth measurements from Syvitski et al. (1986) and Andrews et al. (1994).

The 13 morphometric parameters were in turn used to calculate descriptive and inferential statistics. However, the Gilbert and MacLean dataset only includes 7 of the 13 parameters, and thus could not reduce uncertainty in the statistical analysis of the missing parameters.

2.2.2 Geophysical data sources

The morphometric analysis of Baffin Island fjords was conducted using multibeam bathymetry, a publically available digital elevation model, and topographic map data files.

The multibeam bathymetry data used in this study were originally collected by ArcticNet researchers aboard the *CCGS Amundsen* (2003–2014) and the Government of Nunavut research vessel *MV Nuliajuk* (2012-2014). *CCGS Amundsen* used a Kongsberg EM-302 30 kHz multibeam echosounder (Amundsen Science, 2017), while *MV Nuliajuk* used Kongsberg EM-3002 300 kHz (2012–2013) and EM-2040 200 kHz (2014) multibeam echosounders (Cowan, 2015). Bathymetry raster files were downloaded from the Ocean Mapping Group website at the University of New Brunswick (UNB) (Hughes-Clarke et al., 2015), specifically, the *Google Maps ArcticNet Interface, 2003–2013* and *Google Maps SE Baffin Island, 2012–2014* map products..

Subsets of the Canadian Digital Elevation Model (CDEM) were retrieved as GeoTiff data files from Natural Resources Canada, via the Geospatial Data Extraction service (https://maps.canada.ca/czs/index-en.html) provided on the GeoGratis website. One DEM file was requested with a Predefined Clipping Area corresponding to each of the following drainage basins: Southwestern Baffin Bay (10UD001 and 10UD002), Northwestern Davis Strait (10UE001 and 10UE002), and Northern Cumberland Sound (10UF000). From these regional DEMs, several smaller DEMs localized to specific fjord systems were clipped. The additional data options offered by the Geospatial Data Extraction service remained at the default settings. CanVec topographic data (shapefiles illustrating hydrology and elevation) were also retrieved as geographic databases as part of the submitted requests. The DEMs provided data on the maximum elevations of fjord sidewalls and the areas of drainage basins. CDEM elevations have a grid spacing of 20 m and vertical precision of 5–10 m.

Digital topographic map data (1:50 000) for each fjord were retrieved from the Toporama Interactive Map service (https://atlas.gc.ca/toporama/en/index.html), when the Toporama collection was still supported by GeoGratis, and additional base maps were later retrieved as needed from the online archive (https://ftp.maps.canada.ca/pub/nrcan_rncan/raster/toporama/). Multiple map files were required to illustrate the full areal extent of most fjords in the study. These map files were imported into ArcGIS under the Canada Albers Equal Area Conic projection, and used to trace the shoreline of each fjord.

2.2.3 Parameter definition

The fjord morphometric analysis used ArcGIS mapping software to generate a digital representation of each fjord and measure it as a proxy of the actual landscape. Twenty-one of the

29 fjords selected for this analysis were those within the NC and CP study regions for which bathymetry files were available from UNB Ocean Mapping Group; this selection was made so that depth below sea level could be included in the analysis of each fjord. Sunneshine Fiord was analyzed similarly, but maximum depth data was instead cited from Syvitski et al. (1986) and Andrews et al. (1994).

The 13 morphometric parameters derived in this study were defined as follows.

- **Mean orientation (°)** was defined as the overall direction of ice flow as indicated by the fjord alignment, and is illustrated in Figure 2.6. It was calculated for each fjord by measuring the orientation and length of all individual fjord segments, and then calculating a weighted mean (Appendix A). In Table 2.1 (2.3 Results), the weighted mean orientation for a fjord is presented as a negative angle when >330° (e.g., 338° = -22°), and this negative value is used in calculating all descriptive and inferential statistics. This prevents artificial skewing caused by the gap in the data distribution between 214° and 338° where no values occurred. For example, a fjord oriented 330° is only angled 30° differently from a fjord oriented 0°, but if the former is not adjusted, then the mean of 0° and 330° will be calculated as 165°.

- **Sinuosity** was defined as the quotient of fjord length over the linear distance between the fjord mouth and head. This provides a metric of each fjord's deviation from a straight line.

- **Fjord surface area (km^2)** was defined as the area of the water body contained within the sidewalls. The measurements, as currently reported, exclude all sidewall intrusions and subaerial deltas, but include all islands situated within a fjord. These direct measurements of fjord surface area are more accurate than the product of length and mean width.

- **Length (km)** was defined as the distance along the midline of the fjord, from mouth to head. The fjord mouth was most often interpreted as the space between the opposing headlands where the fjord fed into a larger water body, while the head was interpreted as the interface between the water surface and the subaerial delta or valley floor (Roberts & Rood, 1984; Cowan, 2015).

- **Width (km)** was defined as the distance between opposite sidewalls at the water surface. For each fjord, measurements were taken along its length at either 2.5 or 1.25 km intervals (depending on length), and used to calculate the mean width of the fjord. The minimum and maximum widths recorded were also used in statistical analyses.

- **Maximum depth (m bsl)** was recorded from the bathymetry for three separate components of each fjord: basin, sill, and outer (mouth) depths. Maximum *basin* depth refers to the deepest point of the seafloor within the interpreted fjord surface area. Maximum *sill* depth refers to the deepest point of a sill where uninterrupted water flow occurs, and is presented for the deepest sill within a fjord basin. Maximum *outer* depth refers to the deepest known point of the basin adjacent to the fjord mouth. Multiple basin and sill depths were recorded for the majority of fjords, with only the greatest value for each reported and used in statistical analysis. However, due to the limited bathymetric coverage of some fjord systems, the reported maximum depths may still be underestimated (e.g., Boas Fiord and Totnes Road). For the same reason, all measurements for maximum outer depth report only a minimum measured value (with the exception of Durban Harbour, where the adjacent seafloor basin has been thoroughly mapped). It should be noted that all depths only describe the fjord-floor surface, which typically consists of deposited sediments. The depth of the bedrock below the fjord floor (deepest glacial erosion) is beyond the scope of this analysis.

- **Maximum sidewall elevation (m asl)** was defined as the highest point among the mountains that sloped directly into the fjord. These data may include the elevation of both glaciated and unglaciated summits.

- **Drainage-basin area (km^2)** was defined as the land area of the entire drainage basin surrounding and feeding into each fjord system.

- **Maximum drainage-basin elevation (m asl)** was defined as the highest point within the entire drainage basin surrounding and feeding into each fjord system. The dataset for the maximum drainage-basin elevation may include elevation data for the Penny Ice Cap, in the case of data from Gilbert and MacLean (1984), in addition to unglaciated summits.

The measurements for most parameters were acquired by drawing either a polyline or polygon feature class, using either the topographic map or DEM as a template, and recording either the distance or area measurement provided by the ArcGIS Measure tool. The measurements for depth and elevation were taken directly from the bathymetry and DEM, respectively. Each feature class was originally drawn under the WGS 1984 Mercator map projection, and then re-projected to either Canada Albers Equal Area Conic for the polygons (area measurements) or North America Equidistant Conic for the polylines (distance measurements). These same map projections were applied to the data frame during the collection of the corresponding measurements. Many of the fjord systems included in this study contained tributary fjords, large side-entry bays, and channels that fed into the main fjord (i.e., the submerged valley feeding directly into Baffin Bay, Davis Strait, or Cumberland Sound). During the morphometric analysis, these features were partitioned off from the main fjord to be measured separately. For this study, statistical analysis is applied only to the main fjords.

2.2.4 Sample classification

The total compilation of 29 fjords—21 from the ArcGIS morphometric analysis, 7 from Gilbert and MacLean (1984), and Sunneshine Fiord—are sorted into two regional groups: northeast coast (11 fjords) and Cumberland Peninsula (18 fjords) (Fig. 2.5).

Fjords were assigned to each group based on their position along the Baffin Island coastline. For the purposes of this study, the northeast coast is defined as extending from the eastern mouth of Eclipse Sound southward to Home Bay, and Cumberland Peninsula as extending from Home Bay clockwise to the head of Cumberland Sound. This interpretation is informed by Figure 2.2, which illustrates how the LIS is interpreted as feeding into Home Bay and Cumberland Sound, while Cumberland Peninsula is interpreted as having been glaciated separately by the PIC-LAG complex (Margreth, 2015). Thus, Home Bay and Cumberland Sound represent the limits of LIS ice-flow and influence on fjords. Given the spatial separation between each sample population, the positioning of Home Bay as the division between the regional groups does not affect the sample classification.

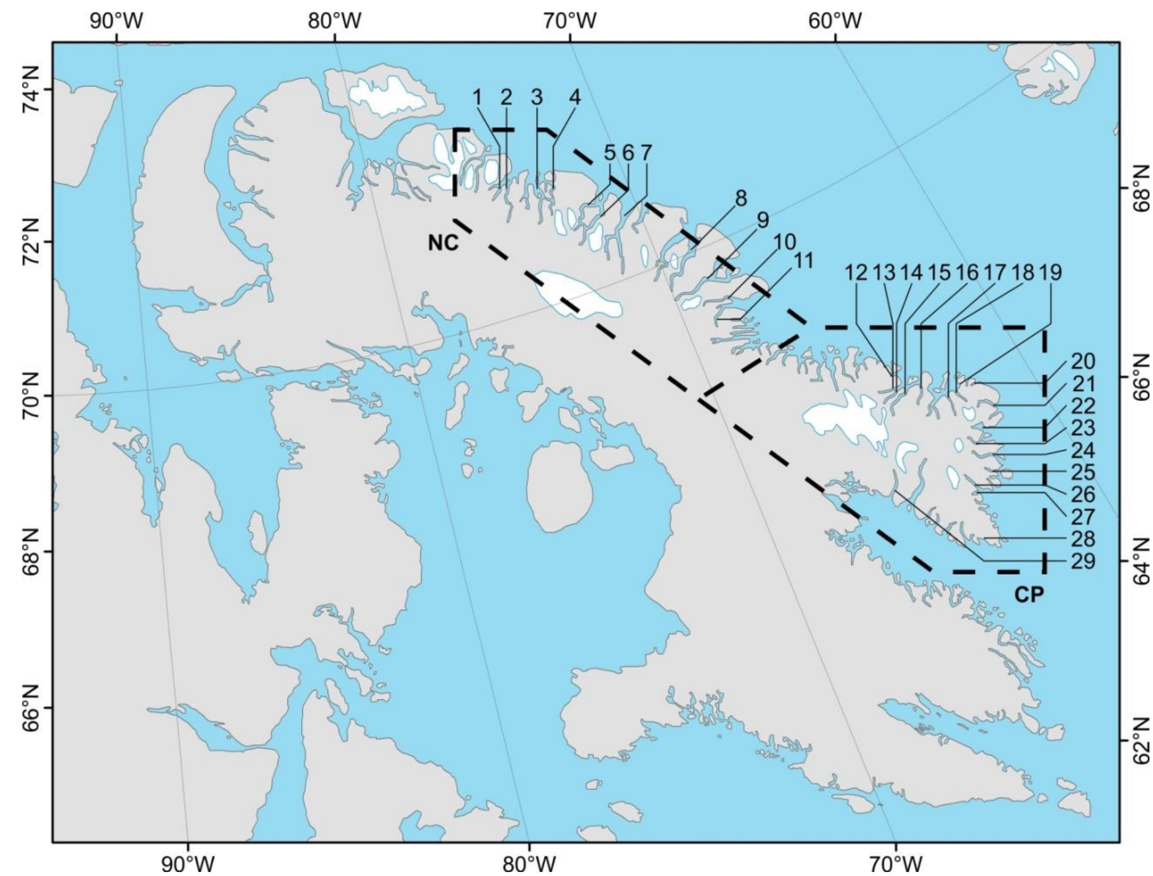

Figure 2.5: Map of Baffin Island with the boundaries of the two study regions, northeast coast (NC) and Cumberland Peninsula (CP), outlined. The positions of Baffin Island fjords included in the study are numbered, with names listed in Table 2.1.

2.2.5 Statistical analyses

Three separate sets of statistical analyses were conducted: descriptive, inferential, and correlation. Each statistic mentioned below is described in depth in Appendix A, and was calculated based on its definition within McGrew and Monroe (2000).

2.2.5.1 Descriptive statistics

Descriptive statistics were calculated in order to describe the average values for each region, and to analyze the distribution for each parameter within each regional group (Table 2.2). The descriptive statistics calculated are: mean, range, standard deviation, standard error, variance, coefficient of variation, skewness, and kurtosis. Skewness and kurtosis were used to determine which statistical tests would be appropriate for the inferential analyses (Table 2.3).

Parametric tests assume that samples are taken from a normally-distributed population, while nonparametric tests assume that the distributions of both samples have similar shapes (McGrew & Monroe, 2000). Therefore, kurtosis was analyzed to determine which if any parameters in each group fit the normal distribution (when kurtosis ≈ 3), and skewness and kurtosis were both analyzed to determine if the distribution shape for each parameter was similar across groups. This study arbitrarily accepted a kurtosis of 3.00 ± 0.25 as indicating a normal distribution, and a difference of ≤ 0.25 in both skewness and kurtosis between the two groups for each parameter as indicating similar distributions across both groups. The regional groups were only considered to have similar data distributions for a parameter if both skewness and kurtosis were similar.

2.2.5.2 Inferential statistics

Inferential statistics were calculated in order to test the regional groups (NC and CP) for a significant difference in each parameter. Thus, this study pairs together two separate inferential tests: a parametric two-sample ANOVA, and a nonparametric Wilcoxon rank sum *W* test. Each test involves its own inherent assumptions. The ANOVA test assumes that the samples are independent and random, the variable is measured at either the interval or ordinal scale, and the population that both samples were taken has a normal distribution and equal variance. The Wilcoxon rank sum test assumes that both samples are independent and random, the variable was either measured at ordinal scale or downgraded from interval/ratio, and that both population distributions are similar in shape, though not necessarily normal.

The dataset for this study only satisfies the first two assumptions for each test. As previously mentioned, the 29 fjords studied were selected based on either the availability of bathymetric imagery (the ArcGIS morphometric analysis), or to represent the spectrum of Baffin Island fjords (Gilbert & MacLean, 1984); these combined selections are treated as approximating a random sample. In addition, each fjord parameter is measured at either the interval or ratio scale. A modified Levene's test (Table 2.4) indicates that the equal variance can be assumed for every parameter except surface area and length. However, the population distributions are unknown, and the results for skewness and kurtosis (Table 2.3) indicate that the majority of sample distributions are non-normal and dissimilar. As the assumptions for neither test are satisfied fully, this study will conduct both tests for each parameter, pairing the parametric and nonparametric tests together. In the event that the results of both tests agree, the confidence in their accuracy is reinforced (McGrew & Monroe, 2000). If the results of each test conflict, the study will favour the results of the nonparametric Wilcoxon rank sum test, as the dissimilar distribution shape of each sample is considered to be less problematic for a non-parametric test than the non-normal distribution is for a parametric test.

For each of the 3 tests used—modified Levene's test, one-way ANOVA, and Wilcoxon rank sum test—both classical hypothesis testing (i.e., comparison of the observed test statistic value to a critical value) and probability (*p*) value testing were used to interpret the results. The formulae for each test can be found in Appendix A.

2.2.5.3 Correlation of parameters

Three pairs of parameters were selected to be tested for correlation—fjord area and drainage-basin areas, fjord length and mean width, and maximum basin depth and sidewall elevation—in order to investigate correlations reported by previous studies (e.g., Haynes, 1972; Roberts & Rood, 1984; Dowdeswell & Andrews, 1985; Augustinus, 1992; Kessler et al., 2008; Patton et al., 2016) using the Table 2.1 dataset. For each pair, a positive correlation and casual relationship is hypothesized. A larger drainage basin should feed more ice into the fjord, resulting in more erosion and thus a larger fjord – assuming a warm-based glacier, as previously explained. The fjords of Baffin Island have been observed to widen from head to mouth, and a longer fjord would logically have a greater probability of capturing tributary glaciers to increase lateral erosion; thus, a longer fjord should demonstrate a greater mean width. Modelling work by Kessler et al. (2008) suggests that higher mountain elevations contribute to deeper fjords due to the steeper slope driving greater ice flow, and Dowdeswell and Andrews (1985) have previously reported a weak correlation ($r^2 = 0.36$) between maximum basin depth and sidewall elevation; this study seeks to corroborate this result with the present dataset.

This study uses correlation as both a descriptor of sample data and as an inferential statistic. This was done to calculate the strength and direction of association between the selected parameters, and to test whether the current samples could be used as estimates of the larger populations. Thus, for the same reasons as the inferential statistical analysis, this study pairs a parametric and a nonparametric correlation coefficient together: the Pearson's correlation coefficient and the Spearman's rank correlation coefficient. For both coefficients, the value of r ranges from 1.0, indicating a perfect positive or direct correlation between variables, to -1.0, a perfect negative correlation. A value of 0.0 indicates no correlation between variables. The value of r^2 indicates the proportion of data variance explained by the association between a dependent and independent variable (Dowdeswell & Andrews, 1985; McGrew & Monroe, 2000). The correlation analysis was conducted using both coefficients for the entire dataset as a whole, in addition to the NC and CP groups. The formulae for each coefficient are listed in Appendix A.

2.3 Results

The summary table of fjord morphometrics (Table 2.1) lists all 29 fjords, sorted by regional group, and their value for every parameter included in the statistical analyses as either calculated by the morphometric analysis or listed by Gilbert and MacLean (1984). As previously stated, some fjords lack measurements for certain parameters, as only 7 of the 13 parameters are shared in common by the morphometric analysis and Gilbert and MacLean, and the latter lacks maximum sill depth data for three fjords (Maktak, Coronation, and North Pangnirtung). The results for the descriptive and inferential statistical analyses are described below.

2.3.1 Descriptive statistics

The descriptive statistics for the northeast coast and Cumberland Peninsula regional groups are summarized in Table 2.2. Variance is used in the calculation of the ANOVA tests, and skewness and kurtosis are discussed separately (Table 2.3). Overall, the CP group shows a wider range of values for weighted mean orientation, while the NC group has a greater mean value than the CP group for every other parameter except maximum drainage-basin elevation. The magnitude of difference between the groups is smallest for sinuosity (0.2) and minimum width (0.4 km), and largest for drainage-basin area (1967 km^2).

Skewness and kurtosis

Skewness and kurtosis were calculated for each parameter within each group in order to determine if the data for each were normally distributed, and if the distributions for a parameter were similar between groups. The calculated skewness and kurtosis statistics are summarized in Table 2.3. Normal distributions (accepted as kurtosis = 3.00 ± 0.25) were found for only three parameters (mean width, drainage-basin area, and maximum drainage-basin elevation) in the CP group. Meanwhile, a similar distribution (difference ≤ 0.25) across both regional groups for both measures was only found for length. Thus, the scarcity of normal or similar distributions informed the decision to use paired parametric and nonparametric tests for the inferential statistical analyses.

Table 2.1: Master table of all fjord-morphometry data. Where the weighted mean orientation was adjusted, the initial positive value is included in parentheses.

Group		Fjord	Fjord: Weighted mean orientation (°)	Sinuosity	Area (km^2)	Length (km)	Width (km): Mean	Min.	Max.	Max depth (m bsl): Basin	Sill	Outer	Max sidewall elevation (m asl)	Drainage basin: Area (km^2)	Max elevation (m asl)
Northeast coast	1	Quernbiter Fiord	49	1.05	114	38	3.5	1.6	7.2	749	238	> 751	1319	1728	1412
	2	Cambridge Fiord *	18	1.15	193	65	3.4	1.4	5.4	674	425	> 751	1074	2013	1080
	3	Paterson Inlet *	-22 (338)	1.14	189	46	4.8	1.1	9.2	456	290	> 482	1048	1552	1169
	4	Dexterity Fiord	11	1.33	182	91	2.4	0.2	5.5	381	300	> 502	1251	2363	1476
	5	Clark Fiord	57	1.19	434	102	5.0	1.1	10.3	705	366	> 845	1424	1895	1481
	6	Gibbs Fiord	49	1.09	419	102	4.9	1.2	10.3	708	410	> 845	1375	5699	1835
	7	Kangiqtualuk Uqquqti	28	1.08	725	123	7.3	0.5	27.3	885	448	> 783	1594	6533	1723
	8	Inugsuin Fiord †	-	-	563	98	5.7	-	-	633	121	-	-	2192	1680
	9	McBeth Fiord †	-	-	402	93	4.3	-	-	563	249	-	-	3584	1751
	10	Itirbilung Fiord †	-	-	162	55	3.0	-	-	435	249	-	-	2184	1751
	11	Tingin Fiord †	-	-	218	47	4.6	-	-	523	180	-	-	1228	1432
Cumberland Peninsula	12	Kennelling Fiord	90	1.05	52	29	1.9	0.1	3.5	388	333	>681	1141	523	1498
	13	Maktak Fiord †	-	-	60	26	2.3	-	-	320	-	-	-	1132	2057
	14	Coronation Fiord †	-	-	131	41	3.2	-	-	606	-	-	-	1128	2057
	15	North Pangnirtung Fiord †	-	-	170	48	3.5	-	-	479	-	-	-	2064	2057
	16	Kangiqtugaapiruluk	27	1.10	81	46	1.9	0.04	3.2	242	167	> 270	1114	560	1511
	17	Boas Fiord *	9	1.08	116	38	3.5	1.4	6.0	419	291	> 458	1366	1138	1649
	18	Southwind Fiord *	-19 (341)	1.04	80	27	3.3	1.6	5.5	433	214	> 459	1389	484	1493
	19	Durban Harbour	-12 (348)	1.06	45	18	2.5	0.4	4.5	233	203	601	862	206	1250
	20	Akpait Fiord	69	1.18	38	19	1.8	0.9	4.5	154	88	> 108	1126	247	1442
	21	Sunneshine Fiord ‡	110	1.21	121	42	3.0	0.3	4.5	256	113	> 89	1511	569	1613
	22	Totnes Road *	134	1.10	117	25	4.8	0.2	8.5	266	-	> 185	1388	536	1656
	23	Mermaid Fiord *	100	1.47	88	37	2.6	0.8	4.1	233	100	> 185	1354	1295	1794
	24	Clephane Bay *	125	1.19	95	40	2.4	0.8	4.0	195	114	> 273	1141	995	1756
	25	Ingnit Fiord *	139	1.09	49	24	2.1	0.1	4.3	235	109	> 312	644	465	1090
	26	Touak Fiord *	166	1.06	114	36	3.3	0.1	5.9	193	170	> 238	1273	1018	1756
	27	Nallussiaq Fiord *	103	1.07	55	19	2.8	0.4	4.9	176	104	> 238	513	514	1413
	28	Aktijartukan Fiord *	188	1.12	33	19	1.6	0.1	3.5	155	71	> 121	481	540	691
	29	Pangnirtung Fiord	214	1.12	93	43	2.3	1.1	4.2	169	98	> 162	1485	1860	2123

* Due to the limited extent of bathymetry for these fjords, the measurements for maximum basin and sill depth are possibly understated.

† Fjords were not included in the original ArcGIS analysis; the data were retrieved from published SAFE Data Report Volume 1 (Gilbert & MacLean, 1984).

‡ Maximum basin depth datum taken from the recorded water depth for Lehigh core SU-0.3 (Syvitski et al., 1986), maximum sill and outer depths taken from the acoustic profile in Andrews et al. (1994).

Table 2.2: Summary of descriptive statistics results. Where the weighted mean orientation was adjusted, the initial positive value is included in parentheses.

	Descriptive statistic	Weighted mean orientation (°)	Sinuosity	Area (km^2)	Length (km)	Width (km)			Max depth (m bsl)			Max sidewall elevation (m asl)	Drainage basin	
						Mean	Min.	Max.	Basin	Sill	Outer *		Area (km^2)	Max elevation (m asl)
Northeast coast	Mean	27	1.15	327	78	4.4	1.0	10.7	610	298	708	1298	2816	1526
	Minimum	-22 (338)	1.05	114	38	2.4	0.2	5.4	381	121	482	1048	1228	1080
	Maximum	57	1.33	725	123	7.3	1.6	27.3	885	448	845	1594	6533	1835
	Range	79	0.27	611	85	4.9	1.4	21.9	504	327	363	546	5305	755
	Sample size (n)	7	7	11	11	11	7	7	11	11	7	7	11	11
	Standard deviation (s)	27.6	0.09	195.4	28.7	1.4	0.5	7.6	153.2	104.7	153.0	193.5	1746.7	247.4
	Standard error (SE)	10	0.03	59	9	0.4	0.2	2.9	46	32	58	73	527	75
	Coefficient of variation (CV)	1.03	0.08	0.60	0.37	0.31	0.51	0.71	0.25	0.35	0.22	0.15	0.62	0.16
Cumberland Peninsula	Mean	96	1.13	85	32	2.7	0.6	4.7	286	155	292	1191	849	1606
	Minimum	-19 (341)	1.04	33	18	1.6	0.04	3.2	154	71	89	481	206	691
	Maximum	214	1.47	170	48	4.8	1.6	8.5	606	333	681	1511	2064	2123
	Range	233	0.42	137	30	3.2	1.5	5.3	452	262	592	1030	1858	1432
	Sample size (n)	15	15	18	18	18	15	15	18	14	15	15	18	18
	Standard deviation (s)	70.7	0.11	37.6	10.3	0.8	0.5	1.3	128.2	79.6	180.0	342.2	521.2	367.0
	Standard error (SE)	18	0.03	9	2	0.2	0.1	0.3	30	21	47	88	123	87
	Coefficient of variation (CV)	0.73	0.09	0.44	0.32	0.30	0.92	0.28	0.45	0.51	0.62	0.31	0.61	0.23

* All values for the outer basin are understood to be minimum estimates, with the exception of Durban which has extensive coverage outside the fjord mouth as delineated for this study.

Table 2.3: Summary of skewness and kurtosis values for the northeast coast (NC) and Cumberland Peninsula (CP). Green cells indicate where either skewness and/or kurtosis are similar across NC and CP (difference ≤0.25).

Parameter	Skewness			Kurtosis			Similar distribution
	NC	CP	Difference	NC	CP	Difference	
Orientation	-0.499	-0.171	0.328	1.713	1.846	0.133	No
Sinuosity	0.784	2.044	1.260	2.203	6.833	4.630	No
Fjord area	0.668	0.394	0.274	2.024	2.188	0.164	No
Length	-0.055	0.019	0.074	1.306	1.402	0.096	Yes
Mean width	0.401	0.735	0.334	2.391	**3.112***	0.722	No
Min width	-0.445	0.679	1.124	1.500	1.982	0.482	No
Max width	1.375	1.371	0.004	3.319	4.556	1.236	No
Max basin depth	0.092	0.971	0.879	1.747	2.848	1.100	No
Max sill depth	-0.035	0.960	0.994	1.625	2.602	0.977	No
Outer depth	-0.589	0.835	1.424	1.351	2.403	1.052	No
Max sidewall elevation	0.030	-0.711	0.741	1.465	2.020	0.554	No
Drainage-basin area	1.137	0.875	0.261	2.659	**2.775***	0.116	No
Max drainage-basin elevation	-0.443	-0.602	0.159	1.760	**3.025***	1.265	No

*Kurtosis of 3±0.25 accepted as a normal distribution.

2.3.2 Inferential statistics

The inferential statistics calculated for the regional comparison are tabulated in Table 2.4. The modified Levene's test found that equal variance could be assumed for the majority of parameters, with the exceptions of fjord area and length. The one-way ANOVA found significant difference between the NC and CP regions for the majority of parameters: orientation, fjord area, length, mean width, maximum width, maximum basin and sill and outer depths, and drainage-basin area. Meanwhile, the results of the Wilcoxon ranked sum test found significant differences between the NC and CO regions for all parameters except sinuosity and maximum sidewall and drainage-basin elevations.

The 12 agreements between the paired tests reinforce the confidence in the results for these parameters, despite the assumptions for neither test being fully satisfied. Thus, the current evidence strongly suggests that the NC region is associated with overall larger fjords and drainage basins than the CP region, while the fjords of each region do not differ significantly in terms of sinuosity or maximum elevation of the surrounding sidewalls and drainage basins. Where the paired tests disagree on minimum fjord width, the Wilcoxon ranked sum test is favoured as it does not require the data set to meet the normal distribution. Therefore, this study also interprets minimum and maximum fjord width as likely to be significantly greater in the NC region.

Overall, the current results of the regional group analysis indicate that the northeast coast and Cumberland Peninsula are associated with significantly different measurements for the majority of parameters. Therefore, the current data strongly suggest that the northeast coast and Cumberland Peninsula regions represent two morphometrically-distinct fjord populations, with the fjords of the former showing significantly greater physical dimensions. Further research should address whether these interpretations remain intact with increased sample sizes, and at smaller regional scales.

Orientation

As can be seen below in Figure 2.6, the NC fjords primarily strike towards the north and northeast (range clockwise from 338–60°), while the CP fjords are considerably more radial, striking towards the north, east, and south (range clockwise from 341–214°).

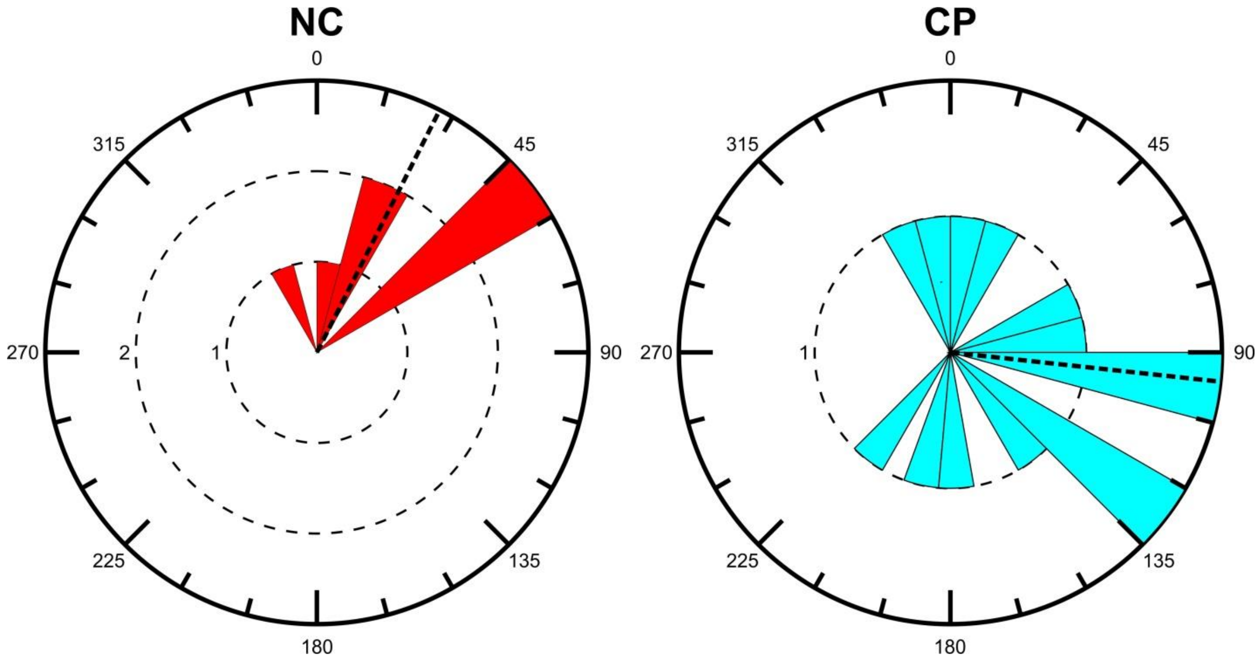

Figure 2.6: Rose diagrams comparing the weighted mean orientations (°) of the northeast coast and Cumberland Peninsula fjord groups. The mean value for each group, NC (27°) and CP (96°), is indicated by the dotted radius.

Table 2.4: Summary of the inferential-statistic results. Green cells indicate where a statistically significant difference between NC and CP was found for a given parameter; yellow cells indicate where equality of variance could not be assumed, thus weakening the inferential power of the ANOVA.

	Statistic	Weighted mean orientation (°)	Sinuosity	Area (km^2)	Length (km)	Width (km)			Max depth (m bsl)			Max sidewall elevation (m asl)	Drainage basin	
						Mean	Min.	Max.	Basin	Sill	Outer *		Area (km^2)	Max elevation (m asl)
NC	Mean (X_1)	27	1.15	327	78	4.4	1.0	10.7	610	298	708	1298	2816	1526
	Sample size (n_1)	7	7	11	11	11	7	7	11	11	7	7	11	11
	Standard deviation (s_1)	27.6	0.1	195.4	28.7	1.4	0.5	7.6	153.2	104.7	153.0	193.5	1746.7	247.4
CP	Mean (X_2)	96	1.13	85	32	2.7	0.6	4.7	286	155	292	1119	849	1606
	Sample size (n_2)	15	15	18	18	18	15	15	18	14	15	15	18	18
	Standard deviation (s_2)	70.7	0.1	37.6	10.3	0.8	0.5	1.3	128.2	79.6	180.0	342.2	521.2	367.0
Hypothesis	H_0	$\mu_1 = \mu_2$	$\mu_1 = \mu_2$	$\mu_1 = \mu_2$	$\mu_1 = \mu_2$	$\mu_1 = \mu_2$	$\mu_1 = \mu_2$	$\mu_1 = \mu_2$	$\mu_1 = \mu_2$	$\mu_1 = \mu_2$	$\mu_1 = \mu_2$	$\mu_1 = \mu_2$	$\mu_1 = \mu_2$	$\mu_1 = \mu_2$
	H_A	$\mu_1 \neq \mu_2$	$\mu_1 > \mu_2$	$\mu_1 > \mu_2$	$\mu_1 > \mu_2$	$\mu_1 > \mu_2$	$\mu_1 > \mu_2$	$\mu_1 > \mu_2$	$\mu_1 > \mu_2$	$\mu_1 > \mu_2$	$\mu_1 > \mu_2$	$\mu_1 > \mu_2$	$\mu_1 > \mu_2$	$\mu_1 < \mu_2$
Levene's Test (Median)	F_{crit} =	4.4	4.4	4.2	4.2	4.2	4.4	4.4	4.2	4.3	4.4	4.4	4.2	4.2
	F_{obs} =	3.8	0.0	11.0	10.6	2.3	0.1	4.3	0.8	0.9	0.2	1.7	3.5	0.9
	p value	0.07	0.96	0.00	0.00	0.14	0.75	0.05	0.39	0.34	0.66	0.21	0.07	0.35
	Result	$\sigma_1^2 = \sigma_2^2$	$\sigma_1^2 = \sigma_2^2$	$\sigma_1^2 \neq \sigma_2^2$	$\sigma_1^2 \neq \sigma_2^2$	$\sigma_1^2 = \sigma_2^2$	$\sigma_1^2 = \sigma_2^2$	$\sigma_1^2 = \sigma_2^2$	$\sigma_1^2 = \sigma_2^2$	$\sigma_1^2 = \sigma_2^2$	$\sigma_1^2 = \sigma_2^2$	$\sigma_1^2 = \sigma_2^2$	$\sigma_1^2 = \sigma_2^2$	$\sigma_1^2 = \sigma_2^2$
ANOVA	F_{crit} =	4.4	4.4	4.2	4.2	4.2	4.4	4.4	4.2	4.3	4.4	4.4	4.2	4.2
	F_{obs} =	6.1	0.2	26.6	39.4	18.6	3.7	9.3	37.6	15.0	27.9	1.6	20.3	0.4
	p value	0.02	0.68	0.00	0.00	0.00	0.07	0.01	0.00	0.00	0.00	0.22	0.00	0.53
	Result	$\mu_1 \neq \mu_2$	$\mu_1 = \mu_2$	$\mu_1 \neq \mu_2$	$\mu_1 \neq \mu_2$	$\mu_1 \neq \mu_2$	$\mu_1 = \mu_2$	$\mu_1 \neq \mu_2$	$\mu_1 \neq \mu_2$	$\mu_1 \neq \mu_2$	$\mu_1 \neq \mu_2$	$\mu_1 = \mu_2$	$\mu_1 \neq \mu_2$	$\mu_1 = \mu_2$
Wilcoxon	Z_{crit} =	± 1.96							1.645					
	Z_W =	2.15	0.81	4.18	4.09	3.24	2.01	3.14	3.96	3.18	3.42	0.81	4.05	0.94
	p value	0.03	0.21	0.00	0.00	0.00	0.02	0.00	0.00	0.00	0.00	0.21	0.00	0.17
	Result	$\mu_1 \neq \mu_2$	$\mu_1 = \mu_2$	$\mu_1 > \mu_2$	$\mu_1 > \mu_2$	$\mu_1 > \mu_2$	$\mu_1 > \mu_2$	$\mu_1 > \mu_2$	$\mu_1 > \mu_2$	$\mu_1 > \mu_2$	$\mu_1 > \mu_2$	$\mu_1 = \mu_2$	$\mu_1 > \mu_2$	$\mu_1 = \mu_2$

2.3.3 Correlations between parameters

The results of the paired Pearson's and Spearman's correlation coefficients are summarized in Table 2.5 and Figure 2.7. Correlations were calculated for three pairs of parameters—fjord and drainage-basin area, length and mean width, and maximum basin depth and sidewall elevation—at three different extents: the NC group, the CP group, and the entire Baffin Island data set.

The results of the Pearson's correlation found statistically significant correlations (p = 0.00 – 0.02) of varying strength between all three pairs of variables for the entire Baffin Island dataset (r^2 = 0.65, 0.48, and 0.18, respectively). However, at the regional scale, statistically significant correlations were only found between fjord and drainage-basin areas (NC: r^2 = 0.41, p = 0.02; CP: r^2 = 0.40, p = 0.00). None of the Pearson's coefficients calculated for length-and-width or depth-and-elevation were found to be statistically significant at the regional scale.

Similarly, the results of the Spearman's rank correlation found statistically significant correlations (p = 0.00 – 0.03) between all three pairs of variables for the entire Baffin Island dataset (r_s^2 = 0.72, 0.39, and 0.18, respectively). However, the results again vary at the regional scale. Within the NC group, the correlations between length-and-width (r_s^2 = 0.37, p = 0.02) and depth-and-elevation (r_s^2 = 0.56, p = 0.02) were found to be statistically significant. Meanwhile in the CP group, only the correlation between fjord and drainage-basin areas (r_s^2 = 0.46, p = 0.00) was found to be significant.

As with the other inferential testing, this study favours the results of the nonparametric test where conflicts occur. Therefore, most of the correlations were found to be statistically significant, with the correlations across the Baffin Island dataset, and between fjord and drainage-basin areas for Cumberland Peninsula, especially reinforced.

Table 2.5: Summary of results for Pearson's and Spearman's correlation analyses. Green cells indicate where a given correlation (r^2) was found to be statistically significant; cyan cells are where $p < 0.05$, which suggests a significant difference despite $t_{obs} < t_{crit}$.

Pearson's correlation coefficient

		Fjord and drainage-basin area (km^2)	Length and width (km)	Max depth (m bsl) and sidewall elevation (m asl)
Baffin Island	r =	0.81	0.69	0.43
	r^2 =	0.65	0.48	0.18
	t_{crit} =	2.05	2.05	2.08
	t_{obs} =	7.10	4.96	2.10
	p =	0.0	0.00	0.02
	Result	$\rho > 0$	$\rho > 0$	$\rho > 0$
Northeast coast	r =	0.64	0.50	0.59
	r^2 =	0.41	0.25	0.35
	t_{crit} =	2.23	2.23	2.45
	t_{obs} =	2.52	1.74	1.63
	p =	0.02	0.06	0.08
	Result	$\rho > 0$	$\rho = 0$	$\rho = 0$
Cumberland Peninsula	r =	0.63	0.21	0.37
	r^2 =	0.40	0.04	0.13
	t_{crit} =	2.11	2.11	2.14
	t_{obs} =	3.23	0.85	1.42
	p =	0.00	0.20	0.09
	Result	$\rho > 0$	$\rho = 0$	$\rho = 0$

Spearman's rank correlation coefficient

		Fjord and drainage-basin area (km^2)	Length and width (km)	Max depth (m bsl) and sidewall elevation (m asl)
Baffin Island	r_s =	0.85	0.62	0.42
	r_s^2 =	0.72	0.39	0.18
	t_{crit} =	2.05	2.05	2.08
	t_{obs} =	8.24	4.12	2.08
	p =	0.00	0.00	0.03
	Result	$\rho_s > 0$	$\rho_s > 0$	$\rho_s = 0$
Northeast coast	r_s =	0.47	0.61	0.75
	r_s^2 =	0.22	0.37	0.56
	t_{crit} =	2.23	2.23	2.45
	t_{obs} =	1.61	2.30	2.54
	p =	0.07	0.02	0.02
	Result	$\rho_s = 0$	$\rho_s > 0$	$\rho_s > 0$
Cumberland Peninsula	r_s =	0.68	0.28	0.45
	r_s^2 =	0.46	0.08	0.20
	t_{crit} =	2.11	2.11	2.14
	t_{obs} =	3.69	1.16	1.82
	p =	0.00	0.13	0.045
	Result	$\rho_s > 0$	$\rho_s = 0$	$\rho_s = 0$

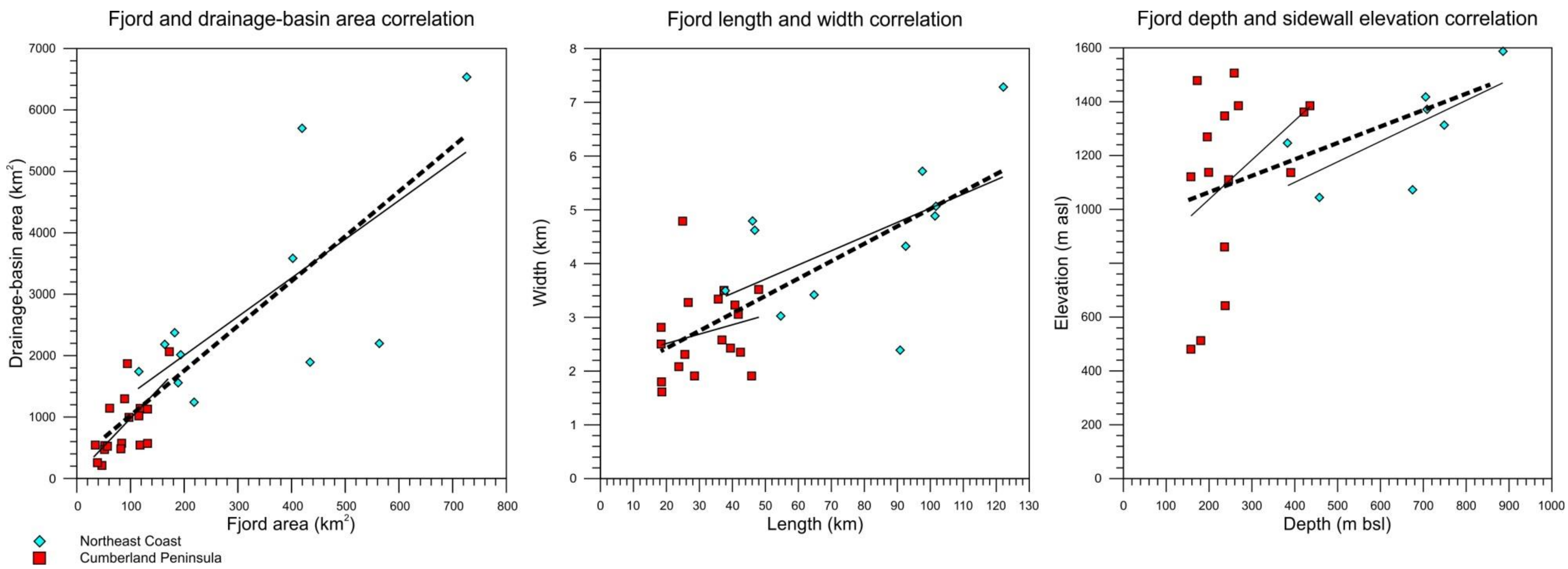

Figure 2.7: Scattergrams illustrating the Pearson's correlation between fjord area and drainage-basin area, fjord length and mean width, and maximum fjord basin depth and sidewall elevation. Solid trendlines illustrate the correlation within the regional groups (NC and CP); dotted trendlines illustrate the correlation across the entire Baffin Island dataset.

2.4 Discussion

2.4.1 Overview of fjord morphometric comparisons

This analysis of fjord morphometry revealed statistically significant differences between the fjords of the northeast coast (NC) and Cumberland Peninsula (CP). The two groups appear to represent morphometrically distinct fjord populations, as NC fjords were found to be significantly different / larger for 10 out of 13 parameters. The three exceptions were sinuosity, maximum sidewall elevation, and maximum drainage-basin elevation. The lack of difference found for sinuosity suggests that the range in fjord shape is similar across regions despite the differences in fjord and ice source size. The similarity between regions for both sidewall and drainage-basin maximum elevation reflects an absence of significant regional variation in mountain elevation along the east coast of Baffin Island, north of Cumberland Sound.

As a result, larger physical fjord dimensions were therefore found to be associated with the larger ice source – the northeast coast is associated with the Laurentide Ice Sheet (LIS), which was much larger than the combined PIC-LAG complex that glaciated Cumberland Peninsula. Overall, the study suggests that greater fjord dimensions are generally associated with the ice sources that could feed larger outlet glaciers.

2.4.1.1 Orientation

Orientation was found to be different between the northeast coast and Cumberland Peninsula regions. Modelling work by Kessler et al. (2008) has demonstrated the excavation of fjords from pre-existing valleys by glacial erosion, with the ice flowing down the slope of least resistance. This indicates that fjord orientation is likely controlled by the pre-existing (or inherited) topography, which itself is influenced by the underlying geologic structure (fault lines and surrounding fracture zone, etc.). Thus, while the differences in overall orientation between NC and CP reflect the different directions of ice flow between the LIS and PIC-LAG, these ice-flow directions can be ultimately attributed to differences in the large-scale physiography of the two regions: NC fjords occur on a single coastline, while CP fjords occur on three coastlines by virtue of their situation on a peninsula.

The LIS was a larger glacial system than the PIC-LAG complex, but this may not be relevant in fjord orientation. Rather than fully glaciating the northeast coast, the LIS outlet glaciers are currently understood to have been funnelled through fjord-onset areas and then into fjords, leaving the adjacent uplands either unglaciated (i.e., *nunataks*) or covered by thin, cold-based ice (Miller et al., 2002; Briner et al., 2008). Therefore, the NC fjords would have been excavated by individual glaciers, each flowing along the path of least resistance, rather than by one unidirectional block of ice. These paths of least resistance would have originated as geologic structures (faults and fractures) related to Baffin Bay rifting and Davis Highlands uplift, before undergoing further topographic development via fluvial erosion prior to glaciation. Outlet glaciers of the smaller PIC-LAG complex would have been similarly constrained by their inherited topography. Therefore, fjord orientation is interpreted to be structurally controlled, with glacial ice flow and fjord excavation occurring along the preglacial paths of least resistance in the direction of the nearest coastline.

However, fjord orientation does not currently appear to be controlled by fault-line orientation, as not all Baffin Island fjords are aligned with currently mapped faults. An extinct seafloor-spreading rift occurs between Baffin Island and Greenland, extending along Baffin Bay and Davis Strait and south into the Labrador Sea (Athavale & Sharma, 1975; Stein et al., 1979; Keen

& Cameron, 1988; Wheeler et al., 1996; Geoffroy et al., 2001; Skaarup et al., 2006; Funck et al., 2007, 2012; St-Onge et al., 2015). Figure 2.8 maps a considerable number of faults on either side of the rift (Funck et al., 2012), but only two of the faults depicted are aligned with Baffin Island fjords (Nedlukseak and Ingnit) while none are aligned with West Greenland fjords; the remainder are all drawn as parallel to the coastlines of Baffin Island and West Greenland. Additional detail is provided by Figure 2.9, a Geological Survey of Canada map of Cumberland Peninsula (Jackson & Sanborn-Barrie, 2014). Inferred and observed thrust faults are drawn across Cumberland Peninsula with the axes tending towards west-east and southwest-northeast. Some of these fault lines do appear aligned with the outer halves of Mermaid Fiord and Clephane Bay (and Iqalujjuaq Fiord), but the remainder are either perpendicular or show no spatial association with other fjords. A map with a similar level of detail for the northeast coast was not found. If these maps are incomplete then there may be other faults that approach the peninsula and northeast coast and align with fjords, but if these maps are fairly representative then perhaps only a few fjords can be associated with fault lines. In the case of the latter, the other fjords could hypothetically have originated as stress fractures in the bedrock caused by rifting and uplift prior to excavation by fluvial and glacial processes. Ultimately, while some glacial valleys and fjords follow pre-existing geologic structures, mapping of structural lineations throughout Cumberland Peninsula shows that some exceptions occur (Dyke et al., 1982). Thus, ice flow is evidently capable of overriding structural geology on occasion.

Dowdeswell and Andrews (1985) reported a mode of north-northeast and a mean of 77.4° for general orientation amongst their Baffin Island fjords dataset. This study corroborates their findings, as the mean of all orientations listed in Table 2.1 is 74° (once corrected for values approaching 360°). The modern ArcGIS study likely improves on Dowdeswell and Andrews by producing a more fine-tuned orientation measurement than was previously possible.

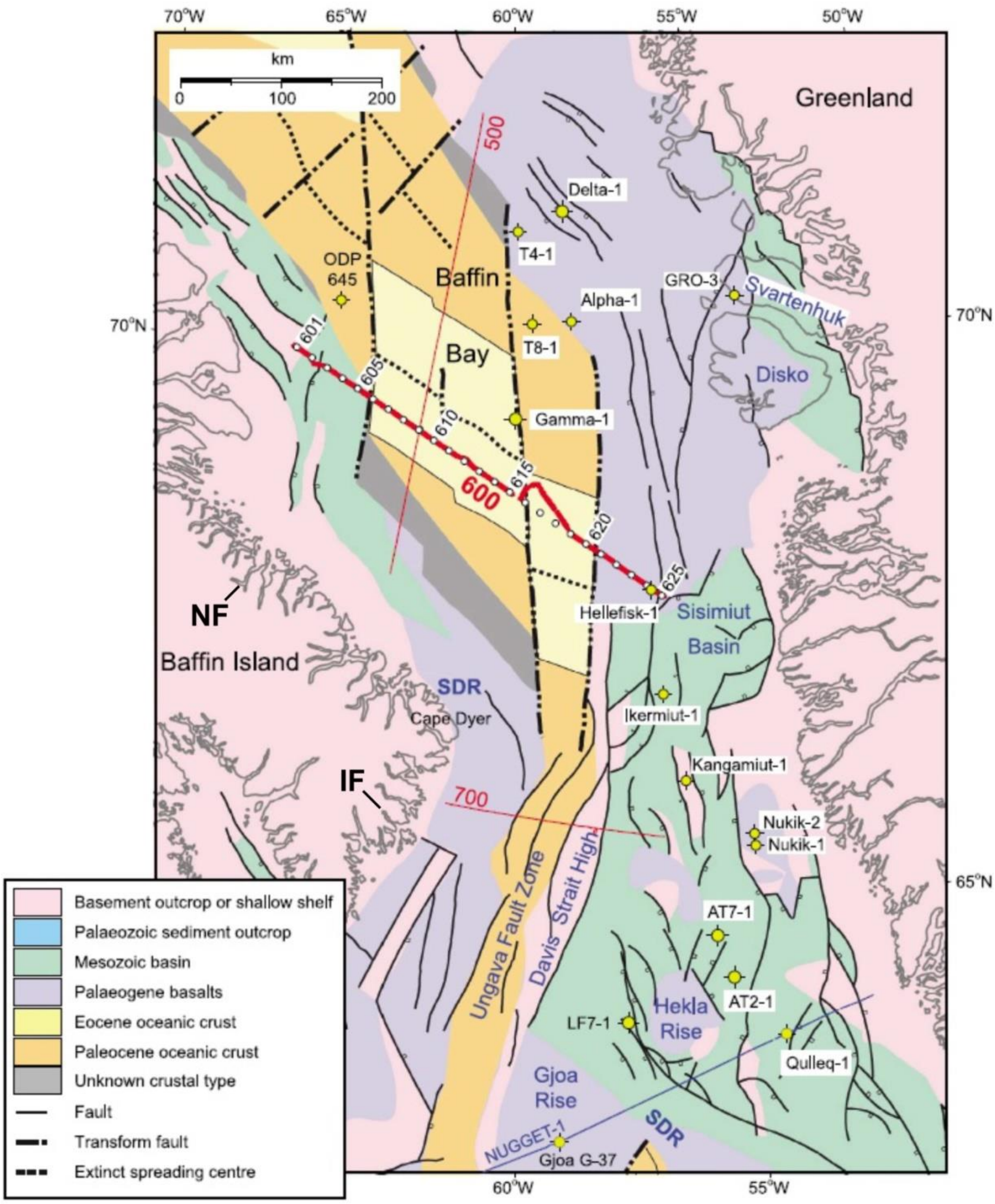

Figure 2.8: Geologic map of Baffin Bay and Davis Strait illustrating multiple seafloor fault lines, modified from Funck et al. (2012). Note that only two faults are aligned with Cumberland Peninsula fjords (NF: Nedlukseak Fiord, IF: Ingnit Fiord), while none are aligned with West Greenland fjords. The nature of Cumberland Sound as a graben is also illustrated.

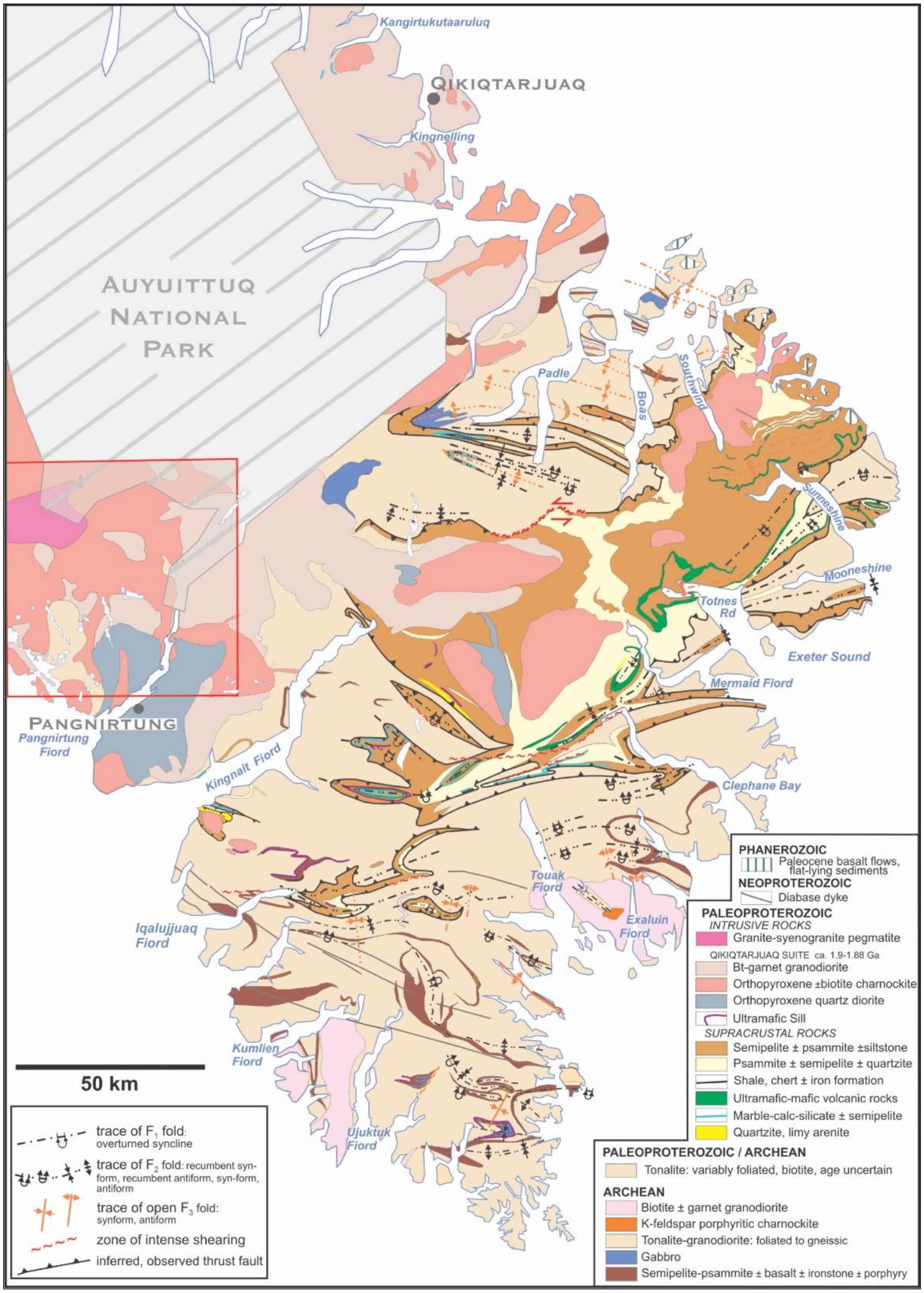

Figure 2.9: A Geological Survey of Canada map of Cumberland Peninsula illustrating inferred and observed thrust faults, modified from Jackson and Sanborn-Barrie (2014). A few fault lines do appear roughly aligned with some fjords (outer Mermaid Fiord and Clephane Bay, Iqalujjuaq Fiord), but most are either perpendicular or show no spatial association with other fjords.

2.4.1.2 Sinuosity

The lack of significant differences in mean sinuosity between NC and CP suggests that the sampled fjords share characteristics of shape, despite the observed differences in fjord length. The inferential results for sinuosity remain true even if either one of the two most sinuous fjords, Mermaid Fiord (1.47) on Cumberland Peninsula and Dexterity Fiord (1.33) on the northeast coast (Fig. 2.10), are removed from the dataset as an outlier (new values of either $Z_W = 1.12$, $p = 0.13$, or $Z_W = 0.39$, $p = 0.35$). This indicates that the controls on fjord sinuosity—be it the straightening of valley sidewall by lateral glacial erosion and or the junction of one or more differently-oriented faults—had no significant regional bias.

The high sinuosity of Mermaid Fiord is due to a sudden right-angle change in orientation. It is possible that the inner segment was originally part of a valley that fed into the Clephane Bay system, before the outer segment intersected and captured it through sidewall erosion. This is supported by a sill at the junction, which might be a submerged col (saddle). The situation could have been set up by intersecting stress fractures or bedrock folds, where fractures/folds normal to the east coast of Cumberland Peninsula were cross-hatched with fractures/folds normal to the north coast. Observations supporting this possibility include: the outer segment of Mermaid Fiord is opposite to a small strait that runs between the eastern headland of Totnes Road and an unnamed island, a trough that runs westward from inner Mermaid Fiord to Touak Fiord, and that the inland glacial valley of Mermaid Fiord appears to connect with the main glacial valley of Boas Fiord.

In the case of Dexterity Fiord, the high sinuosity is attributable to the presence of multiple sidewall spurs that force local detours in the path of the fjord. As explained by Flint (1971) and

Trenhaile (2010), glaciers commonly straighten their valleys by eroding away spurs (the ends of bedrock ridges that the preglacial valleys wove in between) into steep cliff faces labelled truncated spurs. At Dexterity Fiord, it appears that the sidewall spurs are less eroded compared to neighbouring fjords (e.g., Cambridge Fiord, Clark Fiord). In addition to these intact spurs, it is also observed that Dexterity Fiord is the narrowest (2.4 km mean width) and shallowest fjord (381 m bsl max basin depth) in the NC group, despite having one of the largest drainage basins in the entire study sample (2363 km^2). Altogether, this may suggest that glacial erosion is in fact less dominant than structural geology as a control on fjord development. Geological mapping (St-Onge et al., 2015) depicts Dexterity Fiord as incised partly in between the Rae craton and Hudson suite, both units locally consisting of intrusive granite. It is possible that the outer part of Dexterity Fiord followed the contact between these two units. However, it may instead be that the modern drainage-basin area is a poor proxy for glacial ice-catchment area, or is at least misleading in this instance. In contrast to the neighbouring fjords, Dexterity has a relatively short inland glacial-valley ending in a steep headwall instead of an identifiable fjord-onset area. This headwall may have either impeded or prevented LIS ice from funnelling into the fjord, leaving it to be excavated primarily by local alpine glaciers. This interpretation requires that Dexterity be an exception to the assumption that all NC fjords are directly associated with LIS outlet glaciers. Alternatively, other local factors may have limited the amount of lateral erosion despite a large ice-catchment area; the possible effects of additional factors (e.g., basal meltwater conditions, rock tool supply, bedrock material, ice capture by Paterson Inlet, etc.) on the morphology of Dexterity Fiord are beyond the scope of this study.

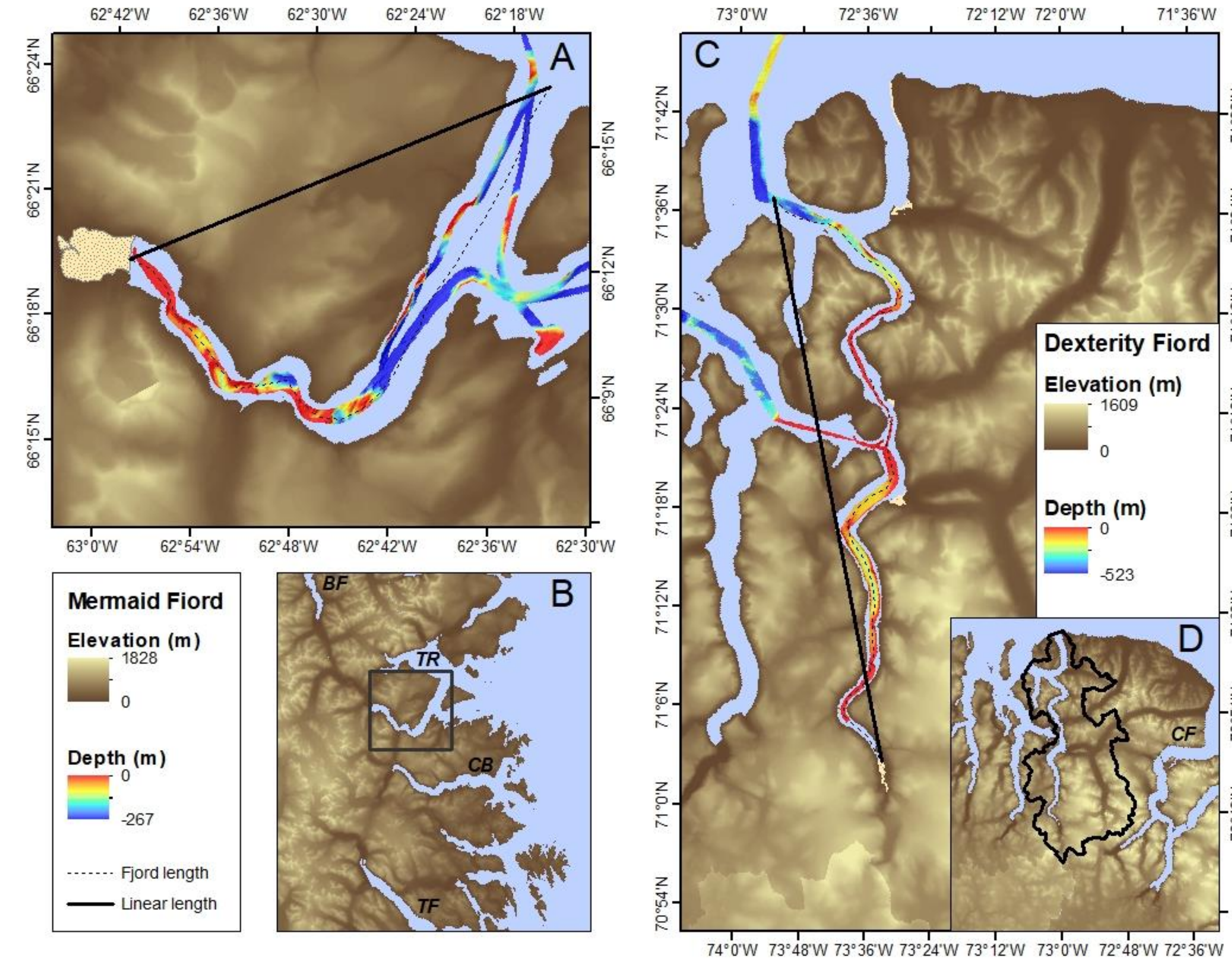

Figure 2.10: Maps of the two fjords with the highest sinuosity values, Mermaid Fiord (1.47) and Dexterity Fiord (1.33). A) Mermaid Fiord's sinuosity is attributable to the near right-angle turn midway along its length. B) Locator map depicting the inland glacial valleys that connect Mermaid to other fjords; BF: Boas Fiord, CB: Clephane Bay, TF: Touak Fiord, TR: Totnes Road. C) Dexterity Fiord's sinuosity may be attributable to a lack of sidewall-spur truncation. D) Despite the size of Dexterity Fiord's drainage basin, its inland glacial-valley component appears shorter than neighbouring fjords; CF: Clark Fiord.

The fjords included in the NC and CP groups are predominantly incised in the Rae craton, which is described as undivided plutonic gneiss and granite suite intrusions (Wheeler et al., 1996; Sanborn-Barrie & Young, 2013; St-Onge et al., 2015). This could lead to a preliminary interpretation that both regions should have a similar resistance to erosion. If true, then significant differences in ice source size do not translate to significant differences in fjord sinuosity. However, specific bedrock material varies within the Rae craton, and some fjords are observed to either cut across or align with thrust faults and various types of geologic folding elements (e.g., Boas Fiord crosses a thrust fault, the head of Iqalujjuaq Fiord aligns with thrust faults and folding) (Fig. 2.9; Sanborn-Barrie & Young, 2013). Thus, bedrock susceptibility to erosion may also vary locally. With the high sinuosity of Mermaid apparently related to the surrounding geological structures, and no evidence that larger outlet glaciers erode straighter fjords, the sinuosity parameter appears to be controlled by the inherited topography.

Dowdeswell and Andrews (1985) did not calculate sinuosity, but instead analyzed the number of fjord bends and the bend angles (i.e., angles closer to 180° indicate an overall straighter fjord). Their dataset found their eastern group (approximating NC) to have a higher mean number of bends than their north/south group (approximating CP), 2.5 to 1.8, with the latter also having a higher percentage of straighter bend angles. This could suggest that the east group (NC) should be more sinuous, but the perceived difference might not be significant enough to conflict with the results of this study.

2.4.1.3 Fjord length (km)

Fjord length was found to be significantly greater for NC than CP. The scope of this study is limited to considering the inherited topography and glacial erosion as controls on fjord length, although fjord length would also be controlled to a small extent by postglacial sedimentation and differential uplift, which would both shorten the fjord by moving the fjord head seawards.

It is understood that fjords develop as ice flow excavates a pre-existing depression (Flint, 1971; Kessler et al., 2008), such as a fault line or fluvial valley. According to Flint (1971), this pre-existing depression may or may not have been submerged prior to glaciation. If the depression was not preglacially submerged and the modern submergence cannot be fully attributed to relative sea level rise, then at least part of the submergence can be attributed to glacial erosion. If the depression was preglacially submerged, then any subsequent glacial erosion would have excavated the fjord beyond its initial condition via downward and headward erosion—the same glacial erosion that deepens the fjord basin also moves the fjord head further inland. MacGregor et al. (2009) cite multiple studies that suggest that glacial valleys are lengthened by erosion of the headwall, but this is a separate phenomenon as the valley headwall rarely coincides with the fjord head. Lacking data on the extent of preglacial submergence, it may not be possible to ascertain the extent to which glacial erosion elongates a fjord from preglacial conditions. Nonetheless, a larger ice source is logically expected to feed larger and more-erosive glaciers. The observation that NC, the group associated with the larger glacial systems, is associated with longer (and deeper) fjords suggests that glacial erosion is the primary control on fjord length. However, topography will ultimately limit the length of a fjord on Cumberland Peninsula or Baffin Island, as the fjord length on any landmass (peninsula or island) will by definition be limited to the length or width of said landmass.

2.4.1.4 Fjord width (km)

All three parameters for fjord width (mean, minimum, and maximum) were found to be significantly greater for NC than CP. This suggests that one or more of the differences between the northeast coast and Cumberland Peninsula regions represent a key control on fjord width. As previously discussed, the two primary controls on fjord morphology considered in this study are glacial erosion and structural geology.

This study analyzed fjord width under the hypothesis that the larger ice source will be associated with larger fjord dimensions due to driving more powerful glacial erosion. Some of the literature appeared to challenge the hypothesis, as Holtedahl (1967) refers to evidence of minimal sidewall erosion by glaciers while Nesje and Whillans (1994) explain that glacial erosion is concentrated on the glacial bed as this is where the rock tools needed for abrasion accumulate. However, Roberts and Rood (1984) illustrate how glacial shear stress is concentrated upon the sidewalls (Fig. 2.11); rock tools may be most prevalent upon the glacial bed, but when they occur along the sidewalls they will be used to maximum effect. Furthermore, while direct glacial erosion of the sidewalls may be limited by rock-tool supply, a larger glacier will nonetheless cover a wider swath of valley and thus excavate a wider valley or fjord (Fig. 2.12).

Moreover, a dismissal of glacial erosion as a driver of fjord width would necessitate major structural control, albeit with possible modification by sidewall mass-wasting (Nesje & Whillans, 1994), which would conflict with observations. While the preglacial valley conditions are most likely a product of the Greenland-Baffin rifting event followed by fluvial erosion, the stress fractures from the rifting alone do not explain the U-shaped valley geomorphology or the regional difference in width (the consulted literature refers to the southern end of the rift opening first, but not to any spatial bias in fracture width; Athavale & Sharma, 1975; Stein et al., 1979; Geoffroy et al., 2001; Skaarup et al., 2006; Funck et al., 2007, 2012). Moreover, while some mass wasting is entirely possible along the fjord sidewalls, it is unlikely to have occurred at a large enough spatial scale to control regional fjord width.

Fjord width is also known to be influenced by the underlying bedrock mass strength, with stronger (igneous) bedrock favouring narrower fjords than weaker (sedimentary) bedrock (Augustinus, 1992; Brook et al., 2004). However, geologic mapping of Baffin Island (St-Onge et al., 2015) indicates that the majority of fjords included in this study are incised in igneous bedrock terrains, with only a few incising the sedimentary cover. Therefore, bedrock material is not expected to have a significant influence on the results of this study.

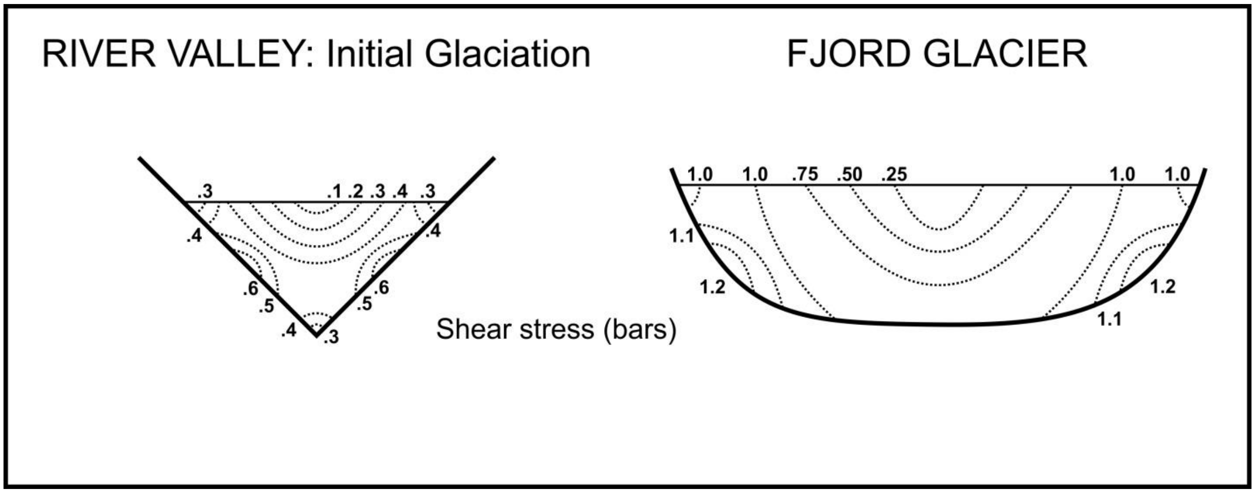

Figure 2.11: Diagram illustrating the distribution of shear stress for a glaciated river valley and the eventual fjord, redrawn from Roberts and Rood (1984). Glacial shear stress is most concentrated along the sidewalls, enabling lateral glacial erosion to be significant despite a relative scarcity of rock tools.

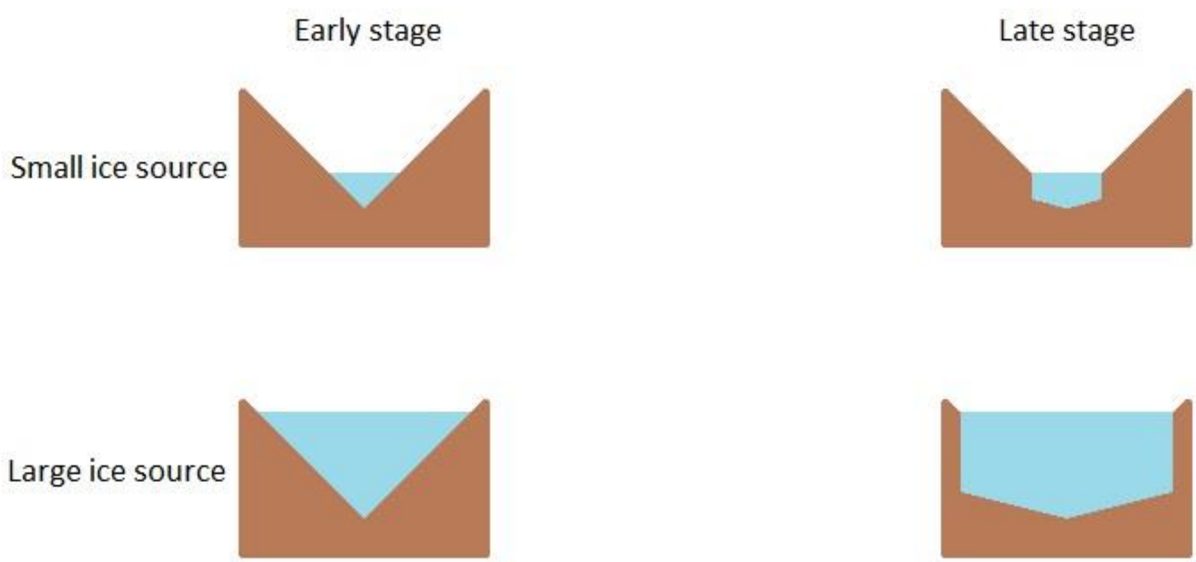

Figure 2.12: Schematic illustrating how a wider initial glacier will result in a wider swath of downwards erosion, and thus a wider glacial valley / fjord.

Overall, it appears reasonable to attribute the significant difference in fjord width between NC and CP to the differences in ice-source and glacial size, which in turn indicates that fjord width is glacially controlled.

2.4.1.5 Fjord depth (m bsl)

Maximum basin depth, maximum sill depth, and outer fjord depth were all found to be significantly greater for the NC group. Holtedahl (1967) stated that fjord depth is based on glacial erosion, which is controlled by glacier thickness. Kessler et al. (2008) demonstrated that fjord depth is a product of a positive-feedback cycle, wherein ice is initially funnelled into a pre-existing depression and the subsequent downward erosion increases the volume of the depression, thereby allowing it to contain more ice, increasing pressure on the floor and therefore erosion. However, this feedback loop is dependent on structural control via the topographic confinement of ice flow (Patton et al., 2016). Nonetheless, as a larger glacier will constantly exert a greater pressure, a fjord excavated by a larger glacier can be expected to extend farther below initial conditions than a fjord excavated by a smaller glacier, so long as the basal ice does not freeze to the substrate. Therefore, the observation that NC, the regional group associated with the larger ice source, demonstrates a greater maximum basin depth suggests a predominant glacial control. It seems unlikely that isostatic subsidence has influenced these results, as the current area of subsidence is known to be eastern Cumberland Peninsula (Cowan, 2015) and therefore any bias caused by subsidence should have favoured the CP group instead. Furthermore, a significant difference in the initial conditions—preglacial depths of the valleys throughout the Baffin Island mountains—could have contributed to the observations, but there has been no reference in the literature to a spatial bias in valley depth due to the rifting event (Athavale & Sharma, 1975; Stein et al., 1979; Geoffroy et al., 2001; Skaarup et al., 2006; Funck et al., 2007, 2012). Other possible controls on fjord depth, such as thermal regime, crustal structure, and bedrock lithology (Patton et al., 2016) are beyond the scope of this study. It should also be noted that some fjords (e.g., Kangiqtualuk Uqquqti, Boas Fiord, Totnes Road) had incomplete or even minimal bathymetric coverage, and further surveying would assist in refining the data on maximum fjord depth.

The above discussion focuses on maximum basin depth, but a similar perspective on maximum sill depth should apply. With the exception of terminal and readvance moraine sills, glacial ice also flows over sills and a thicker glacier should erode them further downwards. However, whether the maximum outer depth parameter is dominated by either structural geology or glacial erosion remains dubious. Both the NC and CP fjords are observed to feed into offshore troughs situated along the margin of Baffin Bay and Davis Strait (MacLean & Falconer, 1979; Gilbert, 1982; Dowdeswell and Andrews, 1985; Google, 2021). Morphometric data on these offshore troughs has not been collected for this thesis, but Google Earth Pro™ suggests that they are more developed along the northeast coast. If the offshore troughs are glacial features, as interpreted by Løken and Hodgson (1971), then this disparity may be another indicator of the greater erosive power of LIS outlet glaciers compared to the PIC-LAG complex.

2.4.1.6 Maximum elevation (m asl)

The maximum elevation of the terrain surrounding each fjord was tested at two spatial scales: along the fjord sidewall, and within the entire surrounding drainage basin. No statistically significant difference in maximum sidewall or drainage-basin elevation was found for NC versus CP. However, this appears to be slightly skewed by the Gilbert and MacLean (1984) data, which lists 2057 m asl as the maximum elevation associated with the Maktak, Coronation, and North Pangnirtung drainage basins without an explanation for the triplicated value. The DEM data indicates that there are glaciated mountains approximating this elevation within the drainage basins of North Pangnirtung Fiord and possibly Coronation, but not Maktak Fiord. The other measurements of maximum elevation (sidewall and drainage basin) retrieved during the ArcGIS analysis corresponded to unglaciated bedrock peaks. Thus, had Maktak, Coronation, and North Pangnirtung been included in the ArcGIS analysis, lower values may have been found for each of them. Despite these suspicions, the Gilbert and MacLean maximum elevation data for these CP fjords are used in the absence of additional data.

The elevation of the Davis Highlands, and thus the fjord sidewalls, would have been initially controlled by tectonic uplift associated with the Baffin-Greenland rifting. Later modifications would have included alpine glacial erosion (Foster et al., 2008) and relative sea level rise due to eustasy and isostasy. The Baffin Bay rift margin is extinct (Athavale & Sharma, 1975; Stein et al., 1979; Geoffroy et al., 2001; Skaarup et al., 2006; Funck et al., 2007, 2012), so any recent uplift is most likely due to isostatic adjustment. The lack of significant difference in maximum sidewall elevation seems reasonable, as preferential behaviour in tectonic uplift is not currently known. Foster et al. (2008) claim that alpine glaciers control alpine elevation via the erosion of susceptible headwall bedrock at a rate controlled by glacier size, uplift rate, and the bedrock lithology. These influences on alpine elevation and relief may trigger feedbacks on glacial mass-balance and erosion via affecting the distribution of alpine precipitation (MacGregor et al., 2009). The current results indicate that glacial erosion (and any feedback effects) has not had a regionally-biased effect on maximum sidewall elevation despite the different-sized ice sources involved, which in turn suggests that geological uplift is the primary control. However, if the lack of significant difference in maximum drainage-basin elevation is due to skewing from the Gilbert and MacLean data, then this may be a possible mechanism for the difference. Egholm et al. (2017) propose that fjord sidewalls were also uplifted by isostasy, following removal of material via erosion, but this interaction is beyond the scope of this study.

Maximum elevation is statistically comparable across the northeast coast and Cumberland Peninsula, which is reasonable for regions of the same contiguous mountain chain. The lack of difference suggests that the LIS and PIC-LAG outlet glaciers had no influence on the rate of alpine erosion via valley glaciers, the process described by Foster et al. (2008). Thus, any modification of alpine elevation within both regions most likely occurred through localized cirque and valley-head glacial erosion.

2.4.2 Correlations

2.4.2.1 Fjord area and drainage-basin area

Statistically significant, positive correlations between fjord area and drainage-basin area were found for both the overall Baffin Island dataset ($r_s^2 = 0.72$, $p = 0.00$) and the CP group ($r_s^2 = 0.46$, $p = 0.00$). The correlation for the NC group approaches statistical significance ($r_s^2 = 0.22$, $p = 0.07$), and hypothetically would become so if Dexterity, Clark, and Tingin fjords were removed from the dataset as outliers (then $r_s^2 = 0.66$, $p = 0.01$): Dexterity Fiord is small for the NC group (182 km^2) but has one of the largest drainage basins (2363 km^2), Clark Fiord is one of the largest NC fjords (434 km^2) but has a small drainage basin relative to the group (1895 km^2), and Tingin Fiord has a medium value for area (218 km^2) but the smallest drainage basin in the NC group (1228 km^2). These correlations generally agree with multiple previous studies, which found positive relationships between drainage-basin area and several parameters of glacial-valley size (length, width, depth, cross-section area, volume, etc.) for regions affected by continental and local alpine glaciation (Haynes, 1972; Roberts & Rood, 1984; Dowdeswell & Andrews, 1985; Augustinus, 1992; Patton et al., 2016).

Altogether, these positive correlations support the hypothesis that a larger drainage basin will be associated with a larger fjord (or glacial valley). Earlier studies typically used drainage-basin area as an indicator of ice supply, and used the positive relationship to argue that a larger ice supply likely excavates a larger fjord (Haynes, 1972; Roberts & Rood, 1984; Augustinus, 1992; Patton et al., 2016). This interpretation is supported by the inferred importance of glacial control on a fjord's physical dimensions (length, width, and depth). An alternative interpretation is that a larger fjord is simply associated with a larger preglacial valley system; however, this is difficult to test. The drainage-basin area is determined not only by the size of the valley surrounding the main fjord, but also by the number and size of all tributary fjords and side-entry valleys that feed into the main fjord. A longer main fjord will have a greater probability of intersecting and capturing adjacent valleys, and thus developing a larger drainage basin. In this respect, the fjord system imitates the preglacial, fluvial drainage basin. Therefore, the correlation between fjord and drainage-basin area may also be influenced by geological structure. However, it is also possible that glacial erosion increases drainage-basin area via head- or sidewall erosion that results in captured valleys.

2.4.2.2 Length and mean width

The overall Baffin Island dataset ($r_s^2 = 0.39$, $p = 0.00$) and the NC group ($r_s^2 = 0.37$, $p = 0.02$) both show a significant positive correlation between fjord length and mean width, while, the CP group ($r_s^2 = 0.08$, $p = 0.13$) does not show a statistically significant relationship, On the surface, this suggests that NC fjords tend to widen with length while CP fjords do not. However, the CP group correlation would improve if Kangiqtugaapiruluk, Totness Road, and Pangnirtung Fiord were hypothetically removed as outliers (then $r_s^2 = 0.20$, $p = 0.04$); the possible justifications for these removals are explained further below. These potential modifications suggest that, barring a few significant outliers, both the NC and CP fjords tend to widen with length, and support the hypothesis that longer fjords will be overall wider. Patton et al. (2016) found a similar trend for the length and width of glacial overdeepenings underneath the Antarctic and Greenland ice sheets. A possible mechanism for this association is that a longer fjord logically has a greater probability of capturing tributary glaciers to increase lateral erosion, and thus width; possible future work could compare fjord width to the number of hanging valleys as a proxy for lateral ice capture.

A noted outlier for the NC group is Dexterity Fiord (Fig. 2.10), which is relatively long (91 km), partly due to its sinuosity, but comparatively narrow (2.4 km)—the fjord narrows abruptly north of the intersection with Patterson Inlet, proximal to where the fjord is observed to shallow, although current bathymetry is insufficient for detailed description. A number of side-entry valleys can be observed and, as previously noted, Dexterity has one of the larger drainage-basin areas in the NC group. The observation that Dexterity is the narrowest fjord in the NC group despite its large drainage basin, implying a large ice catchment, conflicts with the expectation that a larger ice supply should excavate a wider fjord. It is possible that drainage-basin area is an imperfect proxy for ice catchment. Dexterity Fiord was previously noted as an outlier for high sinuosity and weak correlation between fjord and drainage-basin area. Here, it is also observed to be an unexpectedly narrow compared to its length. These observations suggest that Dexterity Fiord is morphologically anomalous within the NC group. As previously mentioned, this may be attributable to its glacial-valley component extending a comparatively short distance before ending at a steep headwall, which may have isolated it from LIS ice-flow and limited it to local alpine glaciation. However, the shape of the fjord is also highly sinuous (1.33; Table 2.1) with 5 sharp bends along its axis, which might have impeded the ice flow and thus inhibited local glacial erosion. The fjord’s relatively low maximum basin depth proximal to the mouth and the relatively shallow depths observed along the fjord’s length also support impeded glacial erosion. The reasons for the apparent anomalous morphology of Dexterity Fiord could bear further investigation.

The outliers identified for the CP group are Kangiqtugaapiruluk (46 km long, 1.9 km wide), Totnes Road (25 km long, 4.8 km wide), and Pangnirtung Fiord (43 km long, 2.3 km wide). Kangiqtugaapiruluk and Pangnirtung are two of the longest CP fjords, but are also among the narrowest in the region. Conversely, Totnes Road is relatively short but is the widest in the region (8.5 km at its widest point).

Kangiqtugaapiruluk and Pangnirtung are both associated with the end-segments of trans-peninsula valleys that cut across Cumberland Peninsula, albeit not with the same valley as each other. The similar structural features could suggest a topographic control. However, North Pangnirtung Fiord is situated on the opposite end of the same valley as Pangnirtung, and unlike Pangnirtung shows a close correlation between its length and width. Similarly, Kingnait Fiord (Fig. ~~2.9~~) is situated on the opposite end of the same valley as Kangiqtugaapiruluk and, while not included in the dataset, can be visually observed from Google Earth Pro™ to be relatively long and wide (Google, 2021). Overall, it seems unlikely that long *and* narrow fjords are strongly associated with these trans-peninsula valleys, lessening the argument for topographic control.

Totnes Road is an anomalously wide feature that may constitute a bedrock-defined bay instead of a genuine, glacially-excavated fjord (pers. comm. Don Forbes), but is included in this analysis until proven otherwise; further bathymetric surveying of the area would be useful for better determining its character. Nonetheless, its width is not shared with any other fjord on

Cumberland Peninsula, making it an isolated case. The slope of the eastern sidewall proximal to the mouth is significantly shallower than is typical of other fjords in the region, suggesting that the width of the feature is structurally controlled; 6 side-entry valleys and 1 tributary fjord feed into the main fjord of Totnes Road, but it is not clear that they would deliver sufficient ice to be responsible for the width.

2.4.2.3 Maximum basin depth and sidewall elevation

Significant correlations between maximum basin depth and sidewall elevation were found for both the overall Baffin Island sample ($r_s^2 = 0.18$, $p = 0.03$) and the NC group ($r_s^2 = 0.56$, $p = 0.02$), with the latter appearing stronger than the former. The CP group was found to show a moderate but statistically insignificant correlation ($r_s^2 = 0.20$, $p = 0.05$). Hypothetically, this correlation would improve in both strength and significance (then $r_s^2 = 0.35$, $p = 0.01$) if Pangnirtung Fiord was removed from the dataset as an outlier (one of the shallowest fiords with the highest sidewalls in the CP group). Thus, there is some support for the hypothesis that higher mountain elevations contribute to deeper fjords due to the steeper slope driving greater ice flow (Kessler et al., 2008).

Pangnirtung Fiord is shallow (max depth of 149 m bsl) compared to other fjords included in the CP group, with its maximum depth occurring in the middle basin. Its maximum elevation (1485 m asl) is adjacent to the fjord head, as part of the mountains in the peninsula’s interior. Pangnirtung is also one of the longest fjords in the CP group, and thus penetrates towards higher mountains near the PIC. In turn, this anomalous length may be attributable to Pangnirtung’s condition as part of a valley that transects the peninsula, which is most likely a structurally controlled feature. On bathymetric and acoustic subbottom imagery, the site where this maximum depth occurs is a pit in the surrounding seafloor and the multiple acoustic units observed beneath it indicates that it does not expose bedrock. Therefore, it may be that the apparent shallowness of Pangnirtung is due to excessive sedimentation. Moreover, Pangnirtung Fiord is located west of the isobase for Cumberland Peninsula's isostatic adjustment, and thus experienced ~50 m of RSL fall between 8.5 and 2 cal ka BP followed by ~5 m of RSL since 2 ka cal BP (Dyke, 1979; Cowan, 2015). Further data collection amongst fjords associated with the PIC and trans-peninsula valleys fjords should help elucidate to what extent Pangnirtung is atypical.

Dowdeswell and Andrews (1985) found a higher correlation (r^2 = 0.36) between maximum fjord depth and sidewall elevation for their much larger sample population (n = 227), suggesting that the limited sample size (n = 29) may influence the current study's results. Both r^2 values indicate a weak to moderate correlation between depth and elevation for the Baffin Island fjords as a group. However, the holistic analysis of Dowdeswell and Andrews does not appear to account for possible regional differences or the influence of outliers. In contrast, the current study found a significant moderate correlation for the NC group and that one outlier (Pangnirtung Fiord) had significant influence on the results for the CP group. Future research may be able to better define any spatial nuances and or anomalies in the depth-elevation relationship.

The controls on basin depth and sidewall elevation vary spatially. Relative sea level change affects basin depth and sidewall elevation simultaneously and in opposite directions, with the magnitude and direction of change largely dependent on the local amount of isostatic adjustment (Kaplan & Miller, 2003; Cowan, 2015). Maximum basin depth is controlled by downward glacial erosion of the initial structural depression, and greater depth has been found to be associated with the larger ice source. Sidewall elevation is controlled by initial geologic uplift, with potential for varying amounts of glacial modification. However, research indicates that the LIS did not erode the plateaus between Baffin Island fjords due to stationary cold-based ice, with the outlet glaciers instead funnelling through the fjord-onset zone (Miller et al., 2002; Briner et al., 2008). Thus, glacial modification of the fjord sidewall lip is not expected for the NC group. Local glaciers are present in both the NC and CP regions, and alpine glaciers have been known to control topography and elevation (Foster et al., 2008). However, neither of the comparisons in this study found a significant difference between groups for maximum sidewall elevation, indicating that there is currently no evidence that the observed alpine glaciers have had any impact on sidewall elevation, or that the geologic uplift showed any spatial preference.

2.4.3 Summary of topographic versus glacial controls

In addition to quantifying the 13 morphometric parameters and using them to identify the northeast coast and Cumberland Peninsula as two distinct fjord populations, this study also uses the comparisons between the fjords associated with the NC and CP regions to attempt to infer how the parameters are controlled by geological structure and glacial erosion. Overall, the topography is understood to control the initial condition of the fjord: an initial depression which glacial erosion later excavates. Glacial erosion controls the dimensions of the end product (length, width, and depth). However, drainage-basin area is defined by topography and was interpreted as a proxy indicator of the ice supply to a fjord, with the understanding that a larger ice-supply leads to greater rates of glacial erosion. Therefore, when ice supply is limited to the drainage basin, it appears that the inherited topography is the ultimate control over a fjord’s morphometry. However, the LIS, unlike alpine glaciers, was not constrained by topography and thus drainage-basin area cannot be interpreted as a hard limit on ice supply for the associated fjords. However, a larger drainage basin still suggests a greater number of tributary glaciers are captured, thus contributing additional ice (and erosive power) to the LIS outlet glacier.

2.4.3.1 Topographic control

Topography is understood to provide the initial conditions under which fjord development occurs, via providing an initial depression for ice flow to accumulate in. Along the Davis Highlands, these initial depressions would have likely originated as geological structures, such as faults and folds related to the Baffin-Greenland rifting, incised by fluvial erosion prior to glaciation. Thus, the inherited topography appears to have predominant control over the parameters that are relicts of the initial depression: orientation, sinuosity, and maximum elevation.

Fjord orientation was attributed to topographic control, as glacial ice flows downhill along the path of least resistance. Along the Baffin Island coast, these paths were most likely established by fluvial excavation of pre-existing stress fractures and or fault lines related to the Baffin-Greenland rifting and uplift events. Tectonic faults are a less likely pathway, as only a few fjords (Nedlukseak, Ingnit, Mermaid, Clephane Bay, Iqalujjuaq; Fig. 2.8 and 2.9) are observed to align with mapped fault lines (Funck et al., 2012; Jackson & Sanborn-Barrie, 2014) and these instances could be coincidental. Furthermore, the significant difference in fjord orientation between NC and CP is evidently due to the intrinsic nature of a peninsula, wherein the additional coastlines provided additional directions for ice flow.

Fjord sinuosity was attributed to topographic control because no statistically significant differences were observed between the groups despite the changes in ice-source size. Moreover, the two most notable outliers in the sinuosity data, Mermaid Fiord and Dexterity Fiord (Fig. 2.10), appear to be associated with unique conditions in the local geology: the former a potential intersection of bedrock folds or stress fractures and the latter a vertical disconformity between separate bedrock materials.

Maximum sidewall and drainage-basin elevation were also attributed to topographic control. The Davis Highlands are understood to have been uplifted by the Baffin-Greenland rifting, and the lack of significant differences for the elevation parameters between NC and CP suggests that glacial erosion has not had a regional impact on alpine elevation despite the different-sized ice sources.

Further investigation into how the topography of NC and CP differ could involve tallying the number of tributary fjords and side-entry valleys that feed into each main fjord and subaerial glacial valley, and the extent to which they intersect.

2.4.3.2 Glacial-erosion control

Glacial erosion is understood to excavate a fjord from its preglacial conditions. Thus, it appears to control the overall spatial dimensions of the excavated fjord: length, width, and depth.

Fjord length was attributed to glacial erosion, given that the NC group, with the statistically greater fjord lengths, is associated with the larger ice source. This also manifests in the situation of maximum sidewall elevation, which was distributed along the length of the LIS fjords, but concentrated near or towards the fjord head for the CP fjords.

Fjord width was attributed to glacial erosion, as a larger outlet glacier, fed by a larger ice source, will cover a wider swath of valley floor and thus excavate a wider fjord. This is supported by the statistically greater mean, minimum, and maximum fjord width for NC compared to CP.

Maximum basin depth was attributed to glacial erosion, as the NC group, associated with the larger ice source, was observed to have greater maximum basin depths. This supported the expectation that a thicker outlet glacier, fed by a larger ice source, will exert greater abrasive pressure and erode downwards at a greater rate (provided that said glacier is not cold-based).

The control of glacial erosion over fjord dimensions (length, width, and depth) is supported by the observed correlations between fjord area (length and width) and drainage-basin area (interpreted as a proxy for ice supply). However, while glacial erosion appears to be the main control on fjord dimensions, topography still imposes a larger-scale control on how and where glacial processes are able to act. For example, drainage-basin area itself is strongly controlled by the inherited topography. Similarly, Cumberland Peninsula has three major coastlines which diffuse the ice flow (and thus erosive potential) of the PIC-LAG complex in three major directions, as opposed to the unidirectional flow of the LIS across the northeast coast. Thus, the erosive power of an innately smaller ice source is further limited by the presence of additional topographic-drainage options. However, were it not for the existence of Cumberland Sound, through which the LIS flowed around Cumberland Peninsula (Margreth, 2015), then the LIS may have fully engulfed the PIC-LAG complex and left no independent glacial system in the area, leaving the regional effects of glaciation relatively more uniform. Moreover, a topographic barrier to LIS ice entering Dexterity Fiord may be why the fjord is anomalously narrow compared to others along the northeast coast. Therefore, it seems that ice supply, the predominant control over glacial erosion and thus fjord dimensions, is itself controlled by the inherited topography and the underlying structural geology.

2.4.4 Comparison to previous research

Previous research by Dowdeswell and Andrews (1985) found only 1 parameter, maximum elevation along the fjord, to show significant difference at the 95% confidence level (89% of variance explained) between their east and north/south groups. In contrast, this study tested for the difference of means between two regionally-defined groups and found significant differences between the NC and CP groups for 10 out of 13 parameters, but interestingly this does not include maximum sidewall elevation. The instances of overlap between the Dowdeswell and Andrews (1985) fjord groups (Fig. 2.4) may indicate local exceptions to regional trends in processes or conditions – the anomalously short glacial-valley component of Dexterity Fiord and its potential impact on fjord sinuosity and width (and thus, area) could be an example of this.

It is possible that these different results could be attributed to the vastly different sample sizes and the different inferential tests used. The total sample size of the Dowdeswell and Andrews study was 227 fjords, as opposed to 29 for this study. As future data collection adds to the dataset compiled for this study, the mean calculated for each parameter will shift to a more comprehensive value. Nonetheless, this study utilizes more recent geophysical data and mapping software, and thus can be confident of testing more precise and accurate data. The technical details of the discriminant analysis are beyond the scope of this study, but the technique is described by Dowdeswell and Andrews (1985) as evaluating "the amount of separation between groups and addresses the research hypothesis that distances between group means in n-dimensional space are significantly different". In contrast, the Wilcoxon ranked-sum sum test was specifically intended to test for a difference of means between samples that were not known to be from normally distributed populations, and in many instances its results were reinforced by a two-sample *t*-test. The Dowdeswell and Andrews analysis compared two groups of fjords based on similar parameter values, and thus their east and north/south groups should be more different from each other than this study's NC and CP groups, which grouped fjords together based on location regardless of parameter value. Therefore, the different group classification is unlikely to be the cause for different findings on significant difference.

2.5 Conclusions

The character of Baffin Island fjords has been found to vary along the coastline. The NC and CP regions appear to represent two morphometrically-distinct fjord populations, as the group formed by outlet flow from the continental-scale Laurentide Ice Sheet was found to be significantly different or larger for the majority of parameters tested (10 of 13). The three exceptions are sinuosity, maximum sidewall elevation, and maximum drainage basin-elevation. Overall, larger fjord dimensions appear to be associated with the larger ice-source. This leads to the interpretation that glacial erosion controls the development of the fjord dimensions (length, width, and depth), while geological structure and inherited topography may control the remnant properties of the fjord's preglacial conditions (orientation, sinuosity, and maximum elevation).

2.6 References

Amundsen Science (2017). *CCGS Amundsen*: Capacity/scientific equipment. Retrieved from http://www.amundsen.ulaval.ca/capacity/scientific-equipment.php

Anderson, R.S., Molnar, P., & Kessler, M.A. (2006). Features of glacial valley profiles simply explained. *Journal of Geophysical Research,* 3: F01004. doi: 10.1029/2005JF000344

Andrews, J.T., Syvitski, J.P., Osterman, L.E., Williams, K.M., Mode, W.N., Kravitz, J.E. & Locke, W.W. III. (1994). *Quaternary geology of Sunneshine Fiord (Baffin Island).* Geological Survey of Canada, Open File 3004. doi:10.4095/195129

Athavale, R.N. & Sharma, P.V. (1975). Paleomagnetic results on early Tertiary lava flows from West Greenland and their bearing on the evolution history of the Baffin Bay-Labrador Sea region. *Canadian Journal of Earth Sciences, 12*(1): 1–18.

Augustinus, P.C. (1992). Outlet glacier trough size-drainage area relationships, Fiordland, New Zealand. *Geomorphology, 4*: 347–361.

Benn, D.I. & Evans, D.J.A. (2010). *Glaciers & Glaciation* (2nd ed.). Routledge: London & New York.

Bennett, M.R. & Glasser, N.F. (2009). *Glacial Geology: Ice Sheets and Landforms* (2nd ed.). Wiley-Blackwell: West Sussex, UK.

Bostock, H.S. (2014). *Geology, Physiographic Regions of Canada*; Geological Survey of Canada, Map 1254A (2nd edition), scale 1:5,000,000. doi:10.4095/293408

Briner, J.P., Miller, G.H., Davis, P.T., & Finkel, R.C. (2005). Cosmogenic exposure dating in arctic glacial landscapes: implications for the glacial history of northeastern Baffin Island, Arctic Canada. *Canadian Journal of Earth Sciences,* 42: 67-84. doi:10.1139/E04-102

Briner, J.P., Miller, G.H., Finkel, R., & Hess, D.P. (2008). Glacial erosion at the fjord onset zone and implications for the organization of ice flow on Baffin Island, Arctic Canada. *Geomorphology, 97*: 126–134. doi: 10.1016/j.geomorph.2007.02.039

Brook, M.S., Kirkbride, M.P., & Brock, B.W. (2004). Rock strength and development of glacial valley morphology in the Scottish Highlands and northwest Iceland. *Geografiska annaler, 86 A* (3): 225-234.

Brouard, E. & Lajeunesse, P. (2017). Maximum extent and decal of the Laurentide Ice Sheet in Western Baffin Bay during the last glacial episode. *Scientific Reports*, 7: 1-8. doi: 10.1038/s41598-017-11010-9

Clarke, D.B. & Upton, B.G.J. (1971). Tertiary basalts of Baffin Island: field relations and tectonic setting. *Canadian Journal of Earth Sciences*, 8: 248–258. https://doi.org/10.1139/e71-025

Cowan, B. (2015). Shorelines beneath the sea: Geomorphology and characterization of the postglacial sea-level lowstand, Cumberland Peninsula, Baffin Island, Nunavut. Master's thesis: Memorial University of Newfoundland, Geography Department.

Dowdeswell, E.K. & Andrews, J.T. (1985). The fjords of Baffin Island: description and classification. In J.T. Andrews (Ed.), *Quaternary Environments: Eastern Canadian Arctic, Baffin Bay and Western Greenland* (pp. 93–123). London: George Allen & Unwin Publishers.

Dyke, A.S., Andrews, J.T., & Miller, G.H. (1982). *Quaternary Geology of Cumberland Peninsula, Baffin Island, District of Franklin.* Geological Survey of Canada, Memoir 403. 32 p. https://doi.org/10.4095/116169

Egholm, D.L., Jansen, J.D., Braedstrup, C.F., Pedersen, V.K., Andersen, J.L., Ugelvig, S.V., ... & Knudsen, M.F. (2017). Formation of plateau landscapes on glaciated continental margins. *Nature Geoscience, 10*: 592–599.

Flint, R. F. (1971). *Glacial and Quaternary Geology.* John Wiley and Sons: New York.

Foster, D., Brocklehurst,S.H., & Gawthorpe, R.L. (2008). Small valley glaciers and the effectiveness of the glacial buzzsaw in the northern Basin and Range, USA. *Geomorphology, 102*: 624–639.

Funck, T., Jackson, H.R., Louden, K.E., & Klingehofer, F. (2007). Seismic study of the transform-rifted margin in Davis Strait between Baffin Island (Canada) and Greenland: What happens when a plume meets a transform. *Journal of Geophysical Research, 112,* B04402: 1-22. https://doi.org/10.1029/2006JB004308

Funck, T., Gohl, K., Damm, V., & Heyde, I. (2012). Tectonic evolution of southern Baffin Bay and Davis Strait: Results from a seismic refraction transect between Canada and Greenland. *Journal of Geophysical Research, 117*. B04107: 1-24. https://doi.org/10.1029/2011JB009110

Gilbert, R. (1982). The Broughton Trough on the continental shelf of eastern Baffin Island, Northwest Territories. *Canadian Journal of Earth Sciences,* 19: 1599-1607.

Gilbert, R. & MacLean, B. (1984). Geophysical studies based on conventional shallow and Huntec high resolution seismic surveys of fiords on Baffin Island. In J.P.M. Syvitski & C.P. Blakeney (Eds.), *Sedimentology of Arctic Fjords Experiment: HU 82-031 Data Report, Volume 1* (GSC Open File No. 960). Dartmouth, NS: Bedford Institute of Oceanography.

Geoffroy, L., Callot, J., Scaillet, S., Skuce, A., Gélard, J.P., Ravilly, M., Angelier, J., Bonin, B., Cayet, C., Perrot, K., & Lepvrier, C. (2001). Southeast Baffin volcanic margin and the North American-Greenland plate separation. *Tectonics, 20*(4): 566–584.

Google. (2021). *Google earth pro* (Version 7.3.3). https://www.google.com/earth/

Haynes, V. M. (1972). The relationship between the drainage areas and size of outlet troughs of the Sukkertoppen Ice Cap, west Greenland. *Geografiska Annaler*, 54A, 66–75.

Holtedahl, H. (1967). Notes on the formation of fjords and fjord valleys. *Geografiska Annaler*, 49AL 188–203.

Hood, P. & Bower, M. (1975). Aeromagnetic reconnaissance of Davis Strait and adjacent areas [Abstract]. *Canada's Continental Margins and Offshore Petroleum Exploration*, 4: 433-451.

Hosseinpour, M., Müller, R.D., Williams, S.E., & Whittaker, J.M. (2013). Full-fit reconstruction of the Labrador Sea and Baffin Bay. *Solid Earth*, 4(2): 461-479. https://doi.org/10.5194/se-4-461-2013

Hughes-Clarke, J.E., Muggah, J., Renoud, W., Bell, T., Forbes, D.L., Cowan, B., & Kennedy, J. (2015). Reconnaissance seabed mapping around Hall and Cumberland peninsulas, Nunavut: opening up southeastern Baffin Island to nearshore geological investigations. *Summary of Activities 2014*. Canada-Nunavut Geoscience Office: 133-144.

Jackson, G. D. & Sanborn-Barrie, M. (2014). *Geology, Pangnirtung Fiord, Baffin Island, Nunavut*; Geological Survey of Canada, Canadian Geoscience Map 4 (preliminary), scale 1:100,000.

Jennings, A. (1993). The Quaternary history of Cumberland Sound, southeastern Baffin Island: The marine evidence. *Géographie physique et Quaternaire*, *47*(1): 21-42.

Kaplan, M.R. & Miller, G.H. (2003). Early Holocene delevelling and deglaciation of the Cumberland Sound region, Baffin Island, Arctic Canada. *Geological Survey of America Bulletin, 115* (4): 445–462.

Kaplan, M., Miller, G., & Steig, E. (2001). Low-gradient outlet glaciers (ice streams?) drained the Laurentide ice sheet. *Geology*, 29: 343–346.

Keen, C.E. & Beaumont, C. (1990). Geodynamics of rifted continental margins. In M.J. Keen & G.K. Williams (Eds.), *Geology of the Continental Margin of Eastern Canada* (pp. 391-474). Geological Survey of Canada, *Geology of Canada*, 2. https://doi.org/10.4095/132690

Keen, M. J. & Cameron, G. D. M. (1988). *Tectonic element map of the Continental Margin of Eastern Canada*; Geological Survey of Canada, Map 1706A, scale 1:5,000,000.

Kessler, M.A., Anderson, R.S., & Briner, J.P. (2008). Fjord insertion into continental margins driven by topographic steering of ice. *Nature Geoscience,* 1: 365–369.

Løken, O. H., & Hodgson, D. A. (1971). On the submarine geomorphology along the east coast of Baffin Island. *Canadian Journal of Earth Sciences, 8*(2): 185–195.

MacGregor, K.R., Anderson, R.S., Anderson, S.P., & Waddington, E.D. (2000). Numerical simulations of glacial-valley longitudinal profile evolution. *Geology*, 28: 1031-1034.

MacGregor, K.R., Anderson, R.S., & Waddington, E.D. (2009). Numerical modelling of glacial erosion and headwall processes in alpine valleys. *Geomorphology, 103*: 189–204.

MacLean, B. & Falconer, R.K.H. (1979). Geological/geophysical studies in Baffin Bay and Scott Inlet-Buchan Gulf and Cape Dyer-Cumberland Peninsula areas of the Baffin Island Shelf. *Geological Survey of Canada*, Paper 79-1B: 231–244. https://doi.org/10.4095/105432

MacLean, B., Williams, G.L., & Srivasta, S.P. (1990). Geology of the Labrador Shelf, Baffin Bay, and Davis Strait. Part 2: Geology of Baffin Bay and Davis Strait. In M.J. Keen &

G.K. Williams (Eds.), *Geology of the Continental Margin of Eastern Canada* (pp. 293-350). Geological Survey of Canada, *Geology of Canada*, 2. https://doi.org/10.4095/132690

Manchester, K.S. & Clarke, D.B. (1973). Geological structure of Baffin Bay and Davis Strait as determined by geophysical techniques. In M.G. Pitcher (Ed.) *Arctic Geology*, American Association of Petroleum Geologists, Memoir 19: 536-541.

Margold, M., Stokes, C.R., & Clark, C.D. (2015). Ice streams in the Laurentide Ice Sheet: Identification, characteristics and comparison to modern ice sheets. *Earth-Science Reviews*, 143: 117-146.

Margreth, A. (2015). Climate sensitivities of polythermal ice sheet, ice cap, and alpine ice dynamics and related episodic erosion on Cumberland Peninsula, Baffin Island, Nunavut. Doctoral dissertation: Dalhousie University, Department of Earth Sciences.

McGrew, J. C. & Monroe, C. B. (2000). *An introduction to statistical problem solving in geography* (2nd ed.). Long Grove, IL: Waveland Press, Inc.

Miller, G.H., Wolfe, A.P., Steig, E.J., Sauer, P.E., Kaplan, M.R., & Briner, J.P. (2002). The Goldilocks dilemma: big ice, little ice, or “just-right” ice in the Eastern Canadian Arctic. *Quaternary Science Reviews, 21*: 33–48.

Miller, G.H., Wolfe, A.P., Briner, J.P., Sauer, P.E., Nesje, A. (2005). Holocene glaciation and climate evolution of Baffin Island, Arctic Canada. *Quaternary Science Reviews, 24*: 1703–1721.

Moore, J.J., Hughen, K.A., Miller, G.H., & Overpeck, J.T. (2001). Little Ice Age recorded in summer temperature reconstruction from varved sediments of Donard Lake, Baffin Island, Canada. *Journal of Paleolimnology*, 25: 503-517.

Natural Earth. (2017). *Downloads*. [Shapefiles]. Retrieved October 30, 2017, from https://www.naturalearthdata.com/downloads/

Natural Resources Canada. (2017). *Geospatial Data Extraction* [CanVec shapefiles]. Retrieved March 4, 2021, from https://maps.canada.ca/czs/index-en.html

Nesje, A. & Whillans, I.M. (1994). Erosion of Sognefjord, Norway. *Geomorphology, 9*: 33–45.

Patton, H., Swift, D.A., Clark, C.D., Livingstone, S.J., & Cook, S.J. (2016). Distribution and characteristics of overdeepenings beneath the Greenland and Antarctic ice sheets: Implications for overdeepening origin and evolution. *Quaternary Science Reviews*, *148*: 128–145.

Roberts, M.C. & Rood, R.M. (1984). The role of ice contributing area in the morphology of transverse fiords, British Columbia. *Geography Annuals*, 66A (4): 381–393.

Sanborn-Barrie, M. & Young, M. (2013). *Geology, Durban Harbour, Baffin Island, Nunavut*; Geological Survey of Canada, Canadian Geoscience Map 38 (preliminary), scale 1:100,000.

Skaarup, N., Jackson, H.R., & Oakey, G. (2006). Margin segmentation of Baffin Bay/Davis Strait, eastern Canada based on seismic reflection and potential field data. *Marine and Petroleum Geology, 23*: 127–144.

St-Onge, M. R., Harrison, J. C., Paul, D., Tella, S., Brent, T. A., Jauer, C. D. & Maclean, B. C. (2015). *Tectonic map of Arctic Canada*; Geological Survey of Canada, Canadian Geoscience Map 187 (preliminary), scale 1:4,000,000

Stein, S., Sleep, N.H., Geller, R.J., Wang, S., & Kroeger, G.C. (1979). Earthquakes along the passive margin of eastern Canada. *Geophysical Research Letters, 6*(7): 537–540.

Syvitski, J.P.M., Schafer, C.T., Asprey, K.W., Hein, F.J., Hodge, G.D., & Gilbert, R. (1986). *Sedimentology of Arctic fjords experiment: PA-85-062 expedition report.* (GSC Open File 1234). https://doi.org/10.4095/130052

Trenhaile, A. (2010). *Geomorphology: A Canadian perspective* (4th ed.). Oxford University Press: Don Mills, ON.

Wheeler, J. O., Hoffman, P. F., Card, K. D., Davidson, A., Sanford, B.V., Okulitch, A.V. & Roest, W.R. (1996). *Geological map of Canada*; Geological Survey of Canada, Map 1860A, scale 1:5,000,000.

CHAPTER 3: PROBING THE LATE- AND POSTGLACIAL SEDIMENTARY RECORD OF EASTERN CUMBERLAND PENINSULA FJORDS, BAFFIN ISLAND

Abstract

Cumberland Peninsula hosts a diversity of fjords carved by outlet glaciers from the Penny Ice Cap and local alpine ice. The fjords on the peninsula's eastern coast were deglaciated c. 14 ka cal BP and have predominantly experienced lower-than-present relative sea level (RSL). This study documents the acoustic stratigraphy and sedimentary facies of fjord sediments in Boas Fiord, Durban Harbour, and Akpait Fiord, the focus of recent marine surveys, and compares results with published data for Sunneshine Fiord. All show a similar glacial-to-postglacial stratigraphy, with ice-contact units overlain by glacial marine or proglacial deposits, in turn overlain by postglacial mud with ice-rafted gravel, in line with the archetypal pattern for Canadian east-coast fjords. Specific sedimentary features (lowstand proglacial deltas and a shallow sill with spillover deposits) were associated with local facies: deltaic bottomset sediments were relatively fine-grained, to the point of resembling some post-submergence mud units, while the spillover deposit was notably coarser, with multiple silty sand lenses likely reflecting gravity flows. Calibrated radiocarbon dates from shell samples enable mean sedimentation rates to be estimated for the study sites: MSRs in the fjord-head areas showed large differences comparable to the differences in drainage-basin area, while MSRs in the outer-fjord areas showed variations with depth that likely reflect pre- versus post-deglaciation periods. A new radiocarbon date from Durban Harbour, combined with Cowan's (2015) earlier interpretation, associates the postglacial lowstand with the Preboreal-Cockburn transition at ~9.5 cal ka BP.

3.1 Introduction

Fjords, carved by glacial erosion, provide natural basins for the accumulation of glacial, proglacial, and postglacial sedimentary deposits. By studying the character and age of the sedimentary record within a fjord, one can interpret the timing and style of glacial recession, sediment discharge, and the subsequent sedimentary environment. Prior sedimentological research has been conducted for some fjords of eastern Arctic Canada (e.g., Gilbert, 1978, 1982, 1985; Cole & Blakeney, 1984; Gilbert & MacLean, 1984; Hein & Longstaffe, 1984; Syvitski et al., 1986; Syvitski & Hein, 1991; Broom et al., 2017; Normandeau & Dietrich, 2019; Normandeau et al., 2019a), but many more have had only reconnaissance surveys or remain unsurveyed. One under-explored region is Cumberland Peninsula (CP), the easternmost extent of Baffin Island. Previous research conducted here includes the Sedimentology of Arctic Fjords Experiment (SAFE) in Sunneshine Fiord during the 1980s (e.g., Gilbert & MacLean, 1984; Syvitski et al., 1986; Andrews et al., 1994; 1996), and other studies referenced above. However, it has only been in the last decade that the first marine geological surveys utilizing multibeam bathymetry have been conducted in the region, enhancing the quality of seabed mapping (Hughes Clarke et al., 2015), coastal and submerged shoreline mapping (Cowan, 2015; Cowan et al. 2021), and investigations on turbidity currents and submarine slope failures (Normandeau et al., 2019b, c).

The fjord sedimentology of Cumberland Peninsula can be expected to reflect the distinctive glacial and relative sea-level (RSL) history of the area relative to other fjords of the Baffin coast. During the Last Glacial Maximum (LGM), the Laurentide Ice Sheet (LIS) covered most of Baffin Island, but flowed around Cumberland Peninsula as it fed outlet ice streams through Cumberland

Sound and Home Bay (#7, Fig. 3.1C). Instead, Cumberland Peninsula was locally glaciated by the Penny Ice Cap (PIC) and local alpine glaciation (LAG; Fig. 3.1; Kaplan & Miller, 2003; Margreth, 2015). Because the PIC and LAG ice masses were limited in spatial extent compared to the LIS, their outlet glaciers may have transported much less sediment. Carter (Chapter 2) found that Cumberland Peninsula fjords have markedly smaller drainage basins (mean area of 848 km^2, range 206–2064 km^2) than fjords elsewhere along the northeast Baffin coast (mean 2816 km^2, range 1228–6553 km^2), and also that Cumberland Peninsula fjords are 3–4 times smaller (33–170 km^2) than northeast Baffin fjords (114–725 km^2). In addition, Cowan (2015) documented multiple submerged shoreline features throughout northeastern Cumberland Peninsula, evidence of a postglacial RSL lowstand first identified by Miller and Dyke (1974). When compared to the pattern of glacio-isostatic uplift and emergence over most of Baffin Island (Andrews, 1989), it is apparent that the sea-level histories of Cumberland Peninsula and other submergent marginal areas on Baffin Island – outer Frobisher Bay (Miller et al., 1980) and the northernmost coast (St-Hilaire-Gravel et al., 2015) – are distinctly different. These regional factors suggest that the marine sedimentary record of fjords on Cumberland Peninsula, hitherto largely unknown, would be an important topic of investigation.

This paper focuses on the sedimentary environments and depositional records of three fjords in the northeastern corner of the peninsula: Boas Fiord, Durban Harbour, and Akpait Fiord[5] (Fig. 3.1B). Within each of these systems, specific areas of interest were surveyed and cored to investigate submerged shoreline features (Cowan, 2015) and the acoustic stratigraphy, lithology, and geochronology of fjord basin sediments. These data are used for the first time to constrain the age of the Holocene sea-level lowstand on eastern Baffin Island. New data collected from these

[5] Canadian official place names use ‘fiord’ spelling

fjords were combined with older published research from Sunneshine Fiord to provide a more comprehensive analysis of the regional postglacial chronology. Material from this chapter (calibrated radiocarbon dates and sedimentological interpretations) has been submitted for publication in Cowan et al. (2021).

This paper has the following aims:

1) to examine the deglacial and postglacial sedimentary record of relatively small fjord systems associated with alpine ice sources on the northeast coast of Cumberland Peninsula, by analyzing acoustic and lithofacies data;
2) to date mollusc-shell samples from sediment cores to constrain the timing of glacial recession, postglacial sedimentation, and RSL changes, including a lowstand that occurred in this region; and
3) to compare sedimentation rates through time and between fjords;

All four fjords discussed in this chapter (Boas, Durban, Akpait, and Sunneshine) still contain alpine ice in their drainage basins, which may raise concerns over the meaning of the term “postglacial sediments”. For the purposes of this study, glaciomarine sediments are defined been released from a tidewater glacier directly into the marine water column and settled within a relatively short timeframe. In contrast, postglacial sediments are defined as those deposited following ice retreat from the fjord basin. This includes deltaic deposits which accumulated at river mouths, and marine muds (composed of very fine biogenic and mineral sediments) which have been suspended in the marine water column for an extended period.

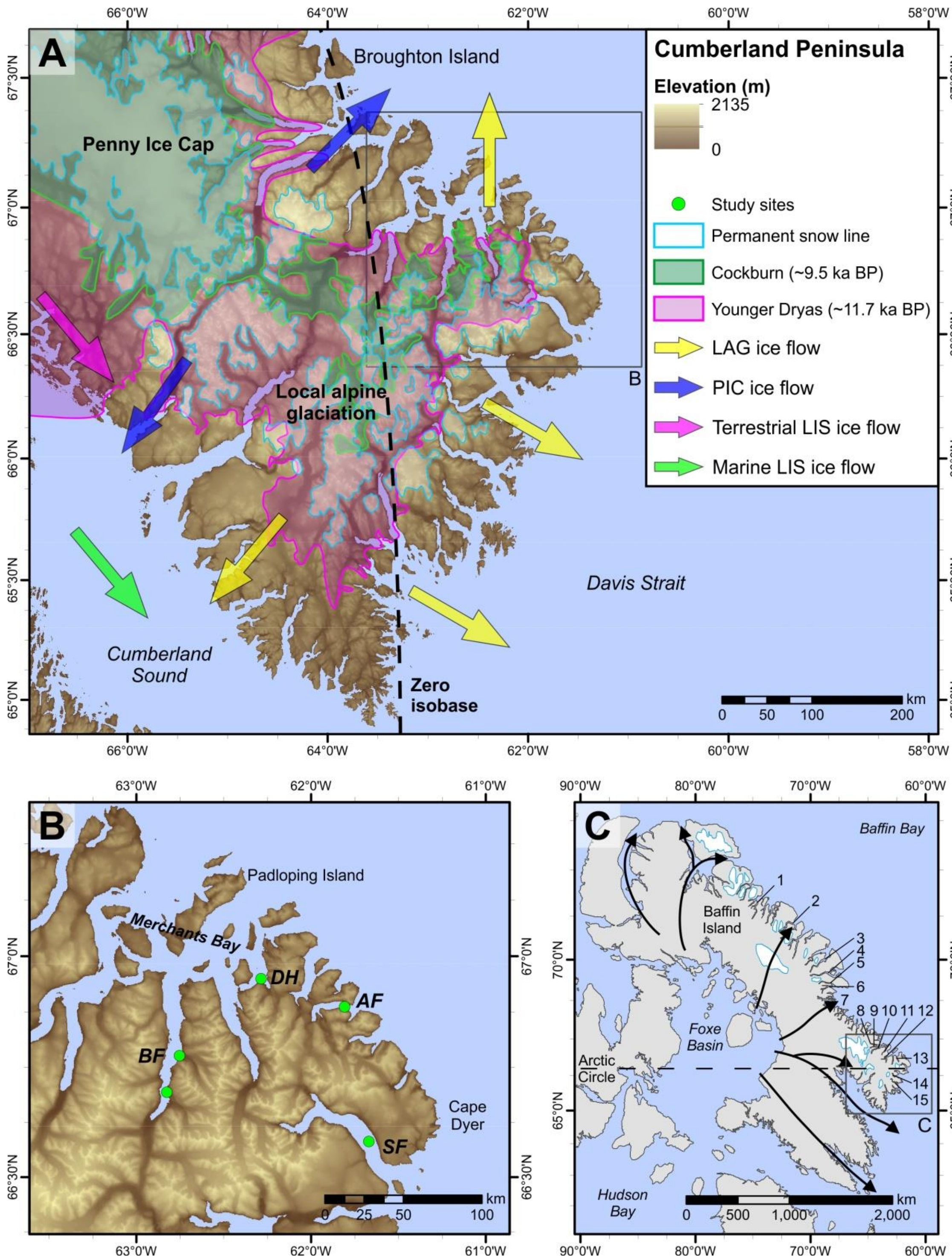

Figure 3.1: Maps of Cumberland Peninsula with glaciers from Natural Earth (2017), illustrating: A) The zero-isobase from Cowan (2015) and the Younger Dryas and Cockburn Substage ice extents as mapped and interpolated by Margreth (2015). B) The four study sites: Boas Fiord (BF), Durban Harbour (DH), Akpait Fiord (AF), Sunneshine Fiord (SF). C) The position of Cumberland Peninsula within the eastern Canadian Arctic, with additional locations labeled: 1) Cambridge Fiord, 2) Clark Fiord, 3) Inugsuin Fiord, 4) McBeth Fiord, 5) Itirbilung Fiord, 6) Tingin Fiord, 7) Home Bay, 8) Maktak Fiord, 9) Coronation Fiord, 10) North Pangnirtung Fiord, 11) Kangert Fiord, 12) Padle Fiord, 13) Southwind Fiord, 14) Mermaid Fiord, and 15) Clephane Bay.

3.2 Regional setting: Cumberland Peninsula, Baffin Island

Cumberland Peninsula is the northernmost of three peninsulas on southeastern Baffin Island, bordered by Baffin Bay to the north, Davis Strait to the east, and Cumberland Sound to the southwest (Fig. 3.1C). From west to east, the peninsula is dominated by the Qikiqtarjuaq plutonic suite, the exposed Rae Craton metamorphics, and sedimentary cover rocks (St-Onge et al., 2015). The peninsula experiences an Arctic climate (average annual temperature of -8 to -11°C; Pheasant & Andrews, 1973; Dyke, 1979) and presents a high-relief landscape of glaciated uplands with intervening deep glacial valleys and fjords. The uplands form part of the eastern rim of Baffin Island, which was uplifted when Greenland rifted away from North America and opened Baffin Bay (Clarke & Upton, 1971; MacLean & Falconer, 1979; MacLean et al., 1990; Keen & Beaumont, 1990; Hosseinpour et al., 2013). During this rifting event, Cumberland Sound developed from a subsiding graben, which simultaneously produced Cumberland Peninsula (Hood & Bower, 1975; MacLean & Falconer, 1979; MacLean et al., 1990), with multiple fault-controlled valleys oriented parallel and perpendicular to Davis Strait.

The glacial history and paleoclimate of Baffin Island and Cumberland Peninsula have been investigated in multiple studies (e.g., Lamb, 1965; Miller & Dyke, 1974; Andrews & Ives, 1978; Bradley et al., 2003; Kaufman et al., 2004; Miller et al., 2005; Anderson et al., 2008; Briner et al., 2009a, b; Margreth, 2015). With the onset of glaciation, both Cumberland Sound (MacLean et al., 1986; Jennings, 1993; Jennings et al., 1996; Kaplan & Miller, 2003) and the preglacial valleys were glacially excavated, with the latter giving rise to a large number of fjords along the coastline (Syvitski et al., 1987; Kaplan & Miller, 2003; Miller et al., 2005; Kessler et al., 2008). Following the LGM, the deglaciation of Cumberland Peninsula was underway after 16 – 15 cal ka BP (Miller et al., 2005; Margreth, 2015), although interrupted by multiple glacial readvances. This study discusses the glacial history of Cumberland Peninsula as early as the Bølling-Allerød interstadial, an early post-LGM glacial recession (Table 3.1). Glacial readvances were associated with at least three subsequent cooling events – the Younger Dryas (YD), Cockburn Substage, and Neoglaciation – while glacial recessions are associated with the Preboreal interstadial (following the YD) and the Holocene Thermal Maximum (following the Cockburn).

Table 3.1: Glacial history outline for Cumberland Peninsula of Baffin Island. All dates given are calendar-year equivalent, where BP (Before Present) refers to 1950 CE.

Epoch	Timeline (~ cal ka BP)	Glacial event		References
Pleistocene	14.6–12.8	Bølling-Allerød	Recession	6, 7
	12.8–11.7	Younger Dryas	Readvance	6
Holocene	11.7–9.5	Preboreal	Recession	2, 6
	9.5–8.5	Cockburn Substage	Readvance	2
	8.0–5.2	Holocene Thermal Maximum	Recession	3
	4.9*–0.1	Neoglacial	Multiple readvances	3, 4
	1.1–0.7	Medieval Warm Period	Recession	1, 4, 5
	0.7–0.1	Little Ice Age	Readvance	1, 4, 5

References: 1) Anderson et al. (2008) 2) Briner et al. (2009b) 3) Gajewski (2015) 4) Margreth (2015) 5) Miller et al. (2012) 6) Rasmussen et al. (2006) 7) Stanford et al. (2011)

*Gajewski (2015) dated the Neoglacial onset in eastern Arctic Canada at ~5.15 cal ka BP, while Margreth (2015) dated it at 4.7 cal ka BP for Cumberland Peninsula.

Although smaller, on average, than the LIS-fed fjords of the northeast Baffin coast, the fjords of Cumberland Peninsula provided a sheltered environment for basin sedimentation and the accumulation of coastal sediments such as deltas, both relict and active (Miller & Dyke, 1974; Hughes Clarke et al., 2015; Cowan, 2015). In general, fjord sedimentation is expected to have increased during glacial recessions and decreased during advances, as a function of meltwater discharge available for sediment transport. However, sediment delivery may have declined with time during recessions as the glacial cover and meltwater discharge diminished (Normandeau et al., 2019a). Early postglacial remobilization of glacial deposits by precipitation runoff may also have fed paraglacial sedimentation, which would also have declined rapidly with time (Church & Ryder, 1972).

Direct evidence of lower RSL on the eastern CP was provided by England and Andrews (1973), who observed river channels incised in bedrock below sea level (bsl) along the coast of Broughton Island, and Miller and Dyke (1974), who identified six submerged terraces interpreted as deltas (32 to 38 m bsl) in Cumberland Peninsula fjords (Padle, Boas, Southwind, Durban; Fig. 3.1C). Although age control was lacking, Miller and Dyke hypothesized that the submerged deltas may be related to a collapsing peripheral bulge, based on: a) the emerged deltas to the northwest associated with the end of the Cockburn readvance (Andrews et al., 1972a, b), now dated to 8.5 cal ka BP (Briner et al., 2009b), and b) their estimate that eustatic sea level change since the Cockburn ended was limited to 16–20 m. Dyke (1979) also posited that an early Holocene shoreline, tilted upwards to the west, must pass below modern sea level eastward.

Cowan (2015) conducted a mapping survey using multibeam bathymetry to target submerged shoreline features around Cumberland Peninsula. She documented eight submerged deltas and several other shore-zone features. The depths of the submerged deltas (19–45 m bsl) were well-described by a least-squares linear gradient (-0.35 m/km toward the east) similar to that of the raised shoreline features on the western Cumberland Peninsula (Dyke, 1979). Together, these observations indicate that the raised and submerged shoreline features were both affected by the same glacial-isostatic crustal motion, and thus likely formed synchronously as part of the same shoreline (Figure 3.2). These observations are consistent with the inward collapse of a peripheral bulge (Chapter 1), with the zero isobase bisecting the peninsula N-S: uplift occurs to the west and subsidence to the east (Figs. 3.1A; Pheasant & Andrews, 1973; Clark et al., 1978; Dyke, 1979; Cowan, 2015). Cowan's study lacked age control on the submerged deltas, but nonetheless was able to interpret them as having likely formed during a postglacial lowstand that followed either the Younger Dryas (post-11.7 cal ka BP) or Cockburn Substage (post-8.5 cal ka BP) ice readvances.

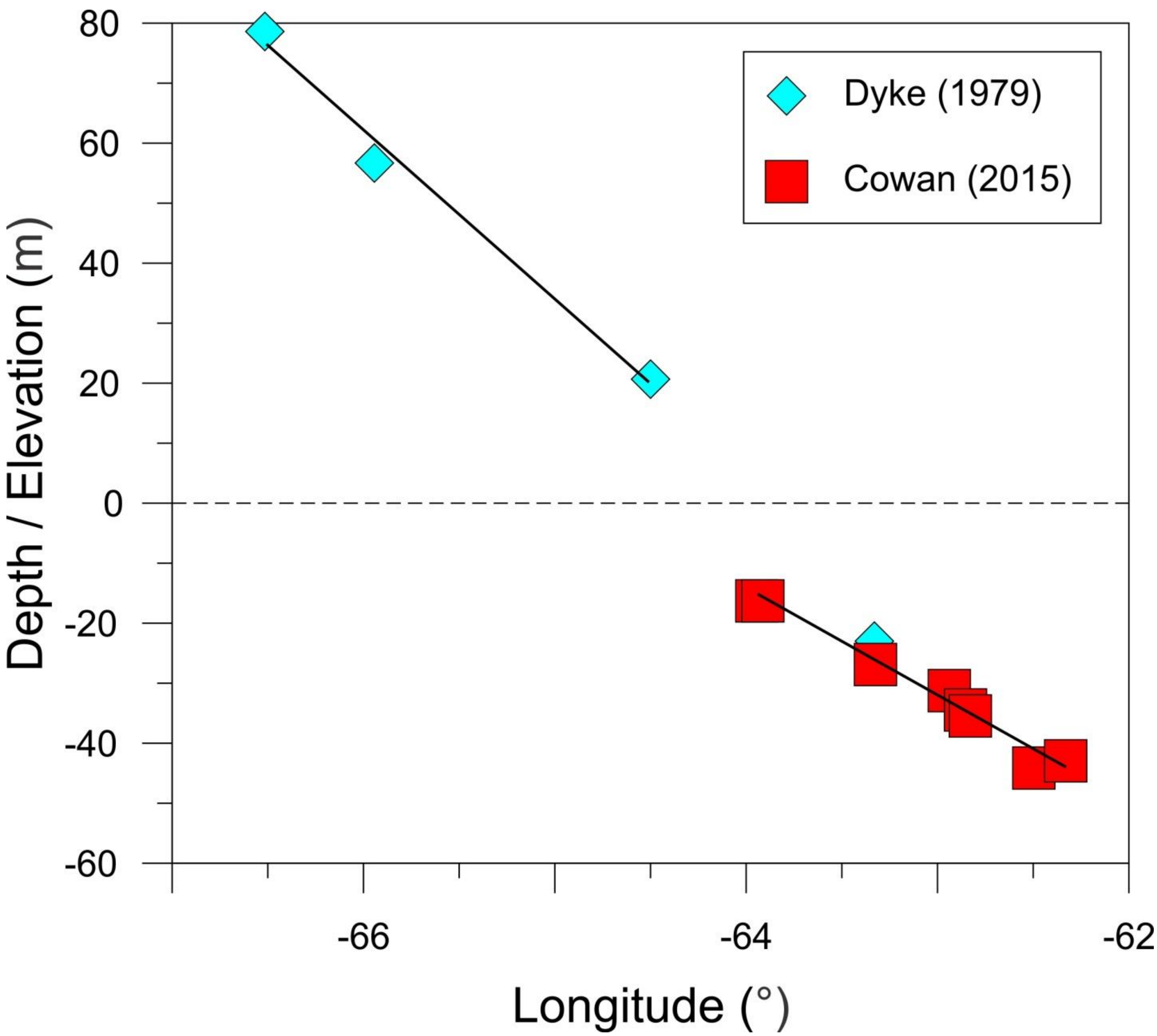

Figure 3.2: Graph illustrating the similar gradients of the subaerial and submerged marine deposits observed throughout Cumberland Peninsula, based on Dyke (1979) and Cowan (2015). Subaerial deposits (>0 m) are observed west of the zero isobase, and submerged deposits (<0 m) to the east.

3.3 Methods and materials

3.3.1 Data collection

The key data used in this study are acoustic subbottom profiles and sediment cores.

The acoustic subbottom profiles image the stratigraphy below the seabed at the coring sites and in the surrounding basins, enabling interpretation of the local sedimentary history. Profiles were collected by *MV Nuliajuk* and *CCGS Amundsen* between 2012 and 2015, using a Knudsen 3.5 kHz subbottom profiler. For Boas Fiord and Durban Harbour, the coverage of the subbottom data corresponds to the bathymetric coverage, roughly extending from mouth to head. However, the acoustic profile coverage for Akpait Fiord is restricted to the proximity of the fjord-mouth sill due to an equipment malfunction during the 2013 *MV Nuliajuk* cruise (Cowan, 2015), which was the only cruise to traverse the length of the fjord.

The sediment cores were acquired to validate interpretation of the upper acoustic stratigraphy, and provide mollusc-shell carbonate for radiocarbon dating. The calibrated radiocarbon ages provide data points that can be used to constrain the timing of the postglacial lowstand, and to estimate mean rates of sedimentation. In 2014, *MV Nuliajuk* collected gravity cores of post-submergence sediments draping the submerged fjord-head delta terrace in Boas Fiord. In 2014 and 2015, *CCGS Amundsen* collected paired piston and trigger-weight cores of prodelta sediments from inner Durban Harbour, and fjord-basin and spillover-deposit sediments from Akpait Fiord.

During the SAFE 1982 cruise (HU82031), CSS *Hudson* collected acoustic profiles in Sunneshine Fiord using a 40 cubic inch air gun and a Huntec deep-tow seismic system (Gilbert & MacLean, 1984). Acoustic units were later interpreted and presented by Andrews et al. (1994, 1996). The current study uses image-analysis software (ImageJ) in conjunction with the Andrews et al. interpretations to estimate the maximum depths of the acoustic units. Gravity and piston cores were also collected from the inner and outer fjord during the 1982 cruise. The current study does not examine these cores directly, but instead uses published results (Cole & Blakeney, 1984; Hein & Longstaffe, 1984; Andrews et al., 1985, 1994, 1996) to inform comparisons with the other three study sites.

The sites for core sampling were selected in advance using multibeam bathymetry, previously collected by *MV Nuliajuk* and *CCGS Amundsen* and processed by the Ocean Mapping Group at the University of New Brunswick (Hughes Clarke et al., 2015). *MV Nuliajuk* used Kongsberg EM-3002 300 kHz (2012–2013) and Kongsberg EM-2040 200 kHz (2014) multibeam echosounders (Cowan, 2015), while *CCGS Amundsen* used a Kongsberg EM-302 30 kHz multibeam echosounder (Amundsen Science, 2017). The coring sites were also targeted with reference to subbottom records to sample specific acoustic units (e.g., Figs. 3.7, 3.8, Appendix B).

3.3.1.1 Sample collection

Interpretation of acoustic stratigraphy was validated by collection of sediment cores, allowing direct observation of lithology and texture, in addition to sampling organic material for radiocarbon dating.

Relict deltas directly indicate a prior RSL, and thus are useful for constraining the timing of RSL change. In order to obtain minimum and maximum age constraints for the postglacial lowstand, the coring sites were chosen specifically to target delta terrace post-submergence muds in Boas

Fiord and prodelta bottomset sediments in Durban Harbour. Sediment coring in Akpait Fiord targeted the fjord basin and the spillover deposit.

Although we were unable to bring a larger vessel into Boas Fiord, *MV Nuliajuk* provided a platform for collection of gravity cores in 2014. These were obtained using a 2.6-m-long gravity corer with a 10-cm-diameter liner. For Durban Harbour and Akpait Fiord, piston cores were obtained from *CCGS Amundsen* in 2014 and 2015, using a 9-m-long piston corer and the same liner. Trigger-weight gravity cores were collected at the same sites for two cores (AF2 and AF7). The cores were split into 1.5 m sections, sealed, and stored upright and refrigerated at 4°C until they could be delivered to the Bedford Institute of Oceanography.

3.3.2 Data analysis

Analysis of the sedimentary history was conducted by interpreting the acoustic stratigraphy of subbottom profiles, and ground-truthing these interpretations using sediment cores. Chronology from the sediment cores provided age control for some of the observed acoustic units, and the postglacial lowstand.

3.3.2.1 Acoustic stratigraphy

The majority of acoustic subbottom profiles used in this study were initially retrieved as KEB files from the ArcticNet database at Memorial University of Newfoundland. The KEB files were first converted to SEGY files using the Knudson Conversion Utility, then converted from SEGY to JP2 using the SegyJp2 program, and saved as JPEG images using SegyJp2 Viewer (Courtney, 2012).

Acoustic profiles were selected for the study by comparing the associated ship-track files to the coring site locations and seafloor bathymetry in ArcGIS. Ship tracks that intersected or lay near the coring sites, approximated straight lines, and or crossed interesting seafloor features were prioritized. The selected acoustic profiles were then visually analyzed to identify acoustic reflectors, which were interpreted as either contacts between different acoustic units or internal reflectors within units. By using acoustic units as proxies for sediment facies, a preliminary framework for interpreting the sedimentary history was developed. Acoustic units were labelled A to G in stratigraphic order, beginning with bedrock.

Where possible, the maximum thickness was determined for each acoustic unit (Table 3.3). Acoustic unit thickness was estimated by recording the depth of each contact, as provided by the SegyJp2 Viewer software, at regular distance intervals along each profile, and then subtracting the difference between units at each interval. All SegyJp2 Viewer depth measurements were computed from the acoustic records using a sound velocity of 1500 m/s (average speed of sound in sea water); variations in water properties (pressure, temperature, salinity, air bubbles or suspended sediment) will affect the measurement of seabed depth, and properties of the subbottom units (bulk density, other factors) affect the speed of sound in sediment. Multisensor track measurements on cores collected in this study showed a range of sound velocity from 1405 to 1673 m/s, indicating that in denser facies the sediment thickness is underestimated using the speed of sound in water.

Each acoustic unit was described in terms of acoustic strength and character, stratification, and unit contacts. These descriptions are summarized below in section 3.5 Results; the full list of descriptions, per core and fjord, is compiled in Appendix B.

3.3.2.2 Lithostratigraphy and subsampling

Laboratory analyses of the collected sediment cores were conducted at the Bedford Institute of Oceanography (Geological Survey of Canada – Atlantic), and included: x-radiography, photography, visual description, the extraction of grain-size and mollusc-shell samples, and additional physical properties (magnetic susceptibility, p-wave velocity, bulk density, shear strength, and L*, a*, and b* colour values; see Appendix C). The x-radiographs were used to identify sedimentary structures for facies interpretation and to locate mollusc shell fragments for extraction as subsamples. Lithofacies were interpreted based on grain-size distribution in addition to sedimentary structure and colour, and labelled based on the Folk (1954) particle size distribution classification.

3.3.2.3 Age determination

Mollusc shells were extracted from various depths in the cores for radiocarbon age determination. Shell samples – bivalves (paired or single valves) and gastropods – were selected from available material to bracket lithostratigraphic unit boundaries and to provide estimates of mean sedimentation rates through time. Samples were cleaned, imaged, and identified to species where possible by PALEOTEC Services (Alice Telka) and submitted to the University of California, Irvine for AMS radiocarbon analysis (Telka, 2015, 2016). The reported ^{14}C ages were calibrated using Calib 8.2 (Stuiver et al., 2021) and the MARINE20 data curve (Heaton et al., 2020). The ΔR correction used was 48 ± 38 yr; this value is the mean of the two regional ΔR values calculated by the Calib8.2 Marine Reservoir Correction Database for northeast Baffin Island (82 ± 18 yr) and southeast Baffin Island (14 ± 58 yr), thus updating the regional ΔR values originally defined by Coulthard et al. (2010) (220 ± 20 yr and 150 ± 60 yr, respectively). The calibrated radiocarbon dates were used to calculate mean sedimentation rates from age-depth curves, and to interpret minimum and maximum constraints on the postglacial lowstand timing. Reported radiocarbon dates for the Sunneshine Fiord cores were retrieved from Andrews et al. (1989) and Manley and Jennings (1996), and given a modern calibration using the above method.

3.3.2.4 Acoustic and lithostratigraphic correlation

The observed lithostratigraphy of each core was compared to the corresponding acoustic unit(s). This provided lithological validation for the interpretation of acoustic stratigraphy. The length of the cores restricted this direct comparison to the near-surface units. In the current study, sampling in Boas Fiord was restricted to the uppermost post-lowstand unit, as a piston-coring vessel could not be brought into the fjord. In the other two fjords, where piston cores were collected, most of the acoustic facies were sampled but deeper units in the fjord basins were beyond the reach of the cores. Unfortunately, without a vibracorer, the sediments composing the Durban Harbour submerged delta terrace and the Akpait sill could not be cored.

Comparison of subbottom depths in cores and acoustic records is subject to uncertainties intrinsic to each data source. During coring, sediments undergo compaction, an effect that is detectable when apparent penetration is recorded for comparison with the retained core length. However, piston cores can also, in some cases, bypass the uppermost sediment (e.g., SU-5 in Sunneshine Fiord), and any loss of sediment at the base of the core can lead to uncertainty about the effective core length. In addition, the depth of a contact in the acoustic records (the depths of the seabed and subsurface contacts) are subject to errors associated with the estimation of sound velocity, as discussed above.

3.4 Study sites

From 2012 to 2015, multiple research cruises by the *CCGS Amundsen* and the *MV Nuliajuk* collected acoustic subbottom profiles and sediment cores from three fjords on Cumberland Peninsula: Boas Fiord, Durban Harbour, and Akpait Fiord. This original research is compared to the previously collected acoustic stratigraphy and sediment cores from Sunneshine Fiord, which was explored by SAFE between 1982 and 1985 (Syvitski & Blakeney, 1984; Syvitski, 1985; Syvitski & Praeg, 1987). The morphometries of all four fjords were previously tabulated in Chapter 2, and are summarized in Table 3.2 below.

Table 3.2: Fjord-morphometry summary for the study sites and Sunneshine Fiord.

Site	Orientation (°)	Sinuosity	Fjord area (km^2)	Length (km)	Mean width (km)	Max basin depth (m bsl)	Max sill depth (m bsl)	Max sidewall elevation (m asl)	Drainage-basin area (km^2)	Max drainage-basin elevation (m asl)
Boas Fiord	9	1.08	116	38	3.5	>419	291	1366	1138	1649
Durban Harbour	348	1.06	45	18	2.5	233	203	862	206	1250
Akpait Fiord	69	1.18	38	19	1.8	154	88	1126	247	1442
Sunneshine Fiord	110	1.21	121	42	3.0	256*	113†	1511	569	1613

* Syvitski et al. (1986)
† Andrews et al. (1994)

3.4.1 Boas Fiord

Boas Fiord opens into the head of Merchants Bay, and formerly fed into an ice-stream along the east side of Padloping Island (Fig. 3.1). Inland from the fjord head, the main valley merges with the glacial valley at the head of Mermaid Fiord (#14, Fig. 3.1C). The present drainage basin of Boas Fiord has an area of 1140 km^2, of which 22% is glaciated, and includes mountains that rise to 1650 m asl. The bedrock is primarily Archean tonalite, granodiorite, and tonalite gneiss. The drainage-basin extends in the west into some areas of the Qikiqtarjuaq granite suite (Sanborn-Barrie & Young, 2013; Sanborn-Barrie et al., 2013; St-Onge et al., 2015).

The first sill is located 7 km from the fjord head and has a depth of 75 m (Figs. 3A, C). The basin behind this sill is the primary depocentre for sediment delivered from the main valley and has a maximum depth of 88 m. Other sills (with depths) are located 9 km (51 m; <10 m across ~80% of the fjord width), 11 km (105 m), 13 km (176 m), 20 km (291 m), 34 km (>232 m), and 35 km (>269 m) downfjord. The enclosed basins have maximum depths of 89 m, 136 m, 195 m, 324 m, >413 m, and >281 m, respectively (the latter two sill-basin pairs are known from incomplete bathymetry).

A broad outwash plain (sandur) occurs at the head of Boas Fiord and appears to extend seaward beyond the delta lip (Fig. 3.3B, C). Satellite imagery shows that this glaciofluvial system continues to deliver sediment (Google, 2021). Multibeam bathymetric surveys have revealed submerged delta terraces at the fjord head and in a cove at the mouth of a side-entry valley (Cowan, 2015). The submerged fjord-head delta consists of an extensive submerged delta plain with relict streams, which extends ~5 km down-fjord from the present waterline, and merges with a terrace along the eastern sidewall (Fig. 3.3 C). The submerged side-entry delta consists of a large primary terrace, with foreslope chutes cut back into the delta front, and a smaller secondary terrace (Fig. 3.3 B). The secondary terrace may either have been deposited by a short-lived fluvial reactivation, or represents a readvance moraine now draped by deltaic sediment.

Multiple moraine ridges have been mapped along the sidewalls of Boas Fiord, and throughout its associated main-stem and side valleys. Neoglacial moraines are present within many of the tributary valleys (Dyke, 2013b).

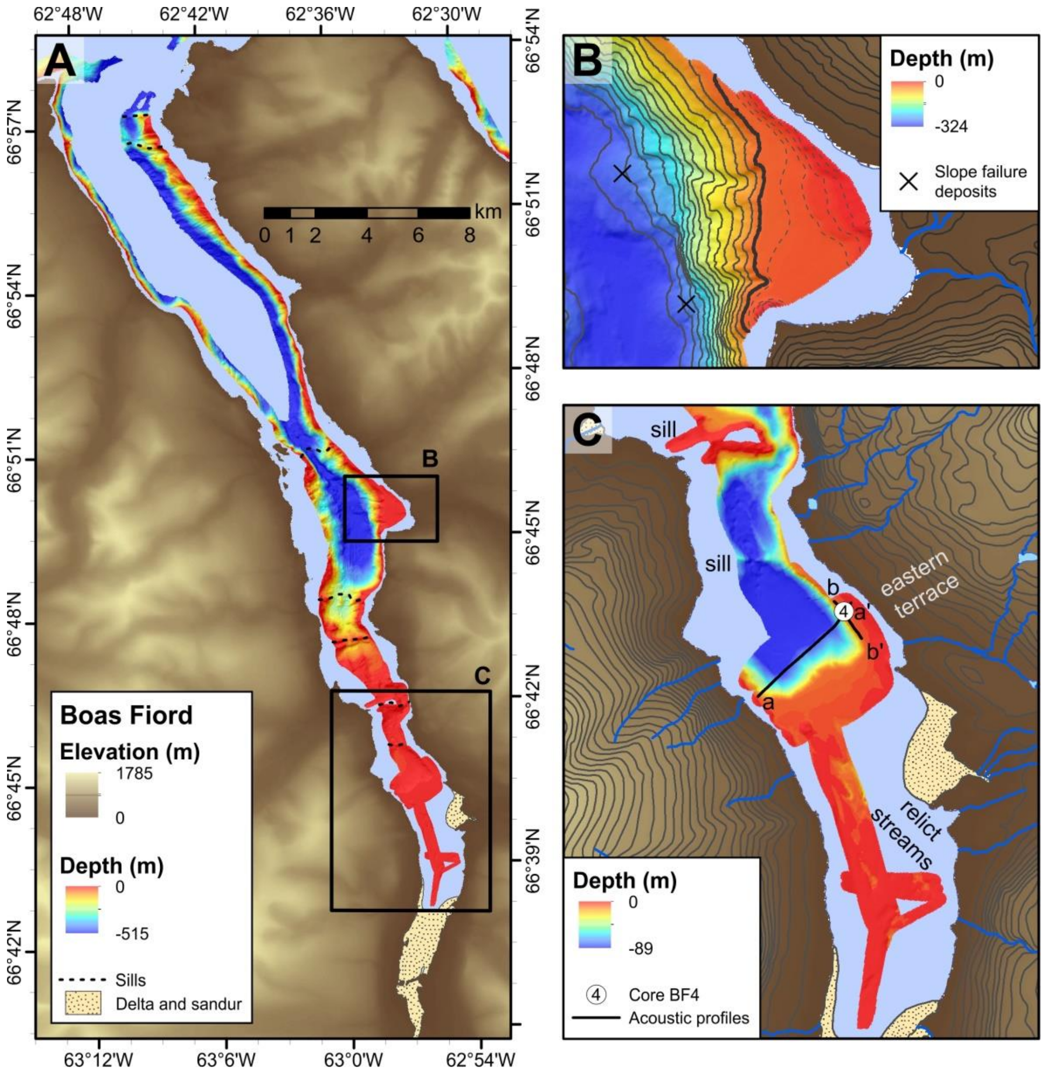

Figure 3.3: A) Map of Boas Fiord, with insets outlining the side-entry embayment and fjord-head regions. B) Side-entry embayment with the secondary terrace outlined and the positions of observed slope-failure deposits indicated. Bathymetric contours are in 20 m intervals below 40 m bsl (bolded) and 5 m intervals above. C) Bathymetry of the fjord head, with the surrounding topography (contour interval 40 m) and the locations of acoustic profiles and a sediment core.

3.4.2 Durban Harbour

Durban Harbour is a complex fjord system, consisting of one main fjord with three channels branching off to the northeast, west, and southwest; the main fjord and the western channel both open into the eastern part of Merchants Bay, while the northeast channel opens into Davis Strait and the southwest (almost closed by a mostly emergent sill) into Southwind Fiord (Fig. 3.4A). Technically, the name "Durban Harbour" refers to the northeastern branch, but is used here for the overall fjord system. The present drainage basin of Durban Harbour is small, with an area of ~206 km^2, of which 7% is glaciated, and includes mountains that rise to 1250 m asl. The bedrock is primarily Archean tonalite-granodiorite (Sanborn-Barrie & Young, 2013; St-Onge et al., 2015).

The first sill is perpendicular to the submerged delta, located 4 km from the fjord head at a depth of 90 m. It encloses a small basin with a maximum depth of 102 m. Other sills (with depths) are located 6 km (109 m), 15 km (173 m), and 18 km (203 m) downfjord (Fig. 3.4A). The enclosed basins have maximum depths of 140 m, 217 m, and 233 m, respectively. Similar to Boas, multibeam bathymetric surveys have revealed a submerged delta terrace at the fjord head (Fig. 3.4B; Cowan, 2015).

Multiple patches of ground moraine have been mapped along the sidewalls of Durban Harbour, though moraine ridges are only observed on Block Island and within the main valley, where some are Neoglacial (Dyke, 2013a, b).

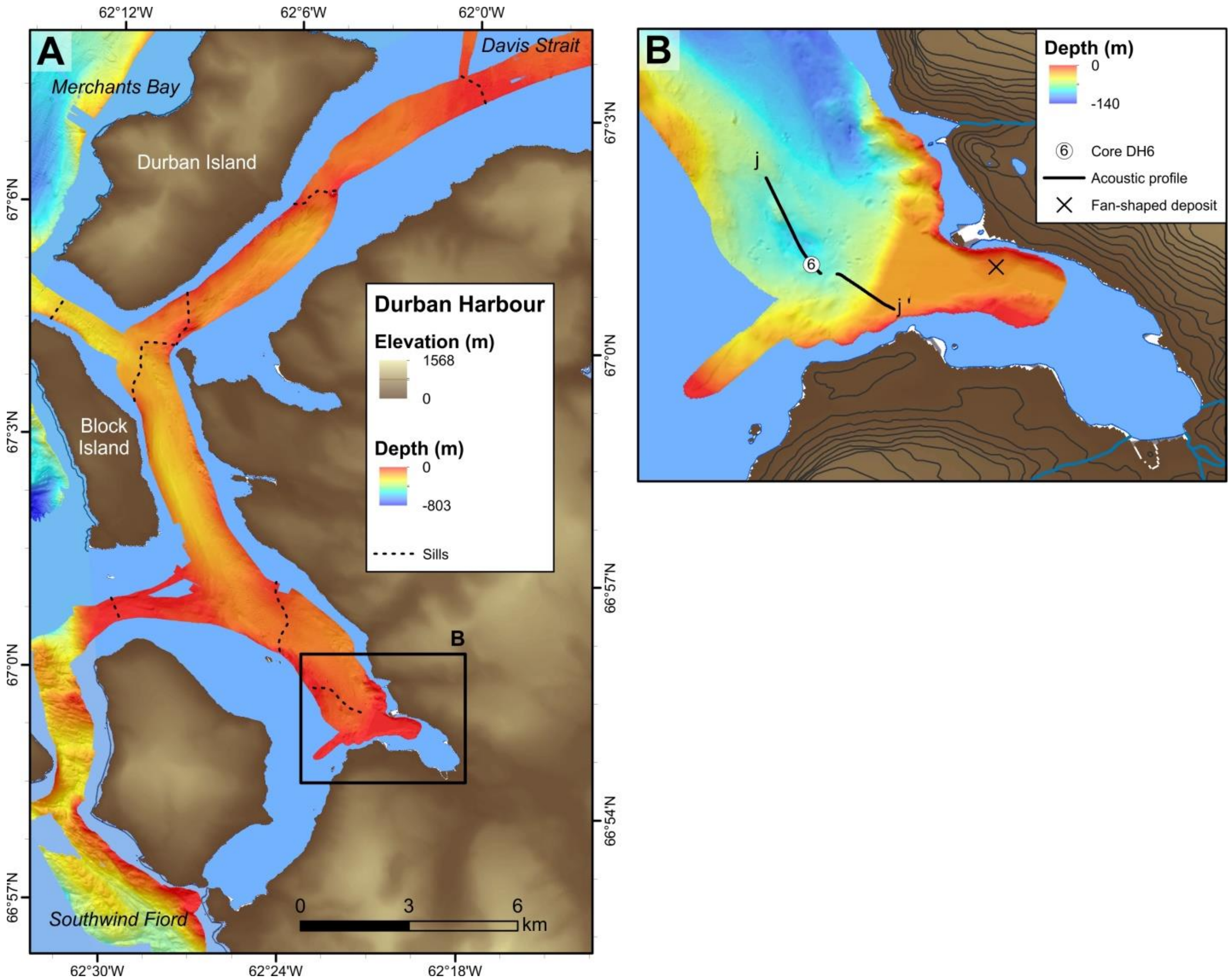

Figure 3.4: A) Map of Durban Harbour, with inset outlining the fjord-head region. B) Bathymetry of the fjord head, with the surrounding topography (contour interval 40 m) and the locations of an acoustic profile and a sediment core.

3.4.3 Akpait Fiord

Akpait Fiord opens into Davis Strait (Fig. 3.5A), while the main valley inland from the fjord head eventually merges with a tributary valley to Sunneshine Fiord. The present drainage basin of Akpait Fiord has an area of 247 km^2 (just 20% larger than Durban Harbour). It is 20% glaciated and includes mountains that rise to 1440 m asl. The bedrock is primarily Paleoproterozoic semipelite, psammite, and pelite (Sanborn-Barrie & Young, 2013).

Only two sills are observed in Akpait Fiord (Figs. 3.5A, B). The inner sill is located 13 km from the fjord head and has a depth of 88 m. The basin behind the inner sill, constituting the majority of the fjord, has a maximum depth of 154 m. The outer sill, located at the fjord mouth (Fig. 3.5B), is a large shallow platform, >7 km^2 in area and 51 m deep, and interpreted by Cowan (2015) as a moraine. It is relatively even and featureless, except for two gravel spits situated upon its western arm, which Cowan attributes to longshore drift during a period of lower sea level (Fig. 3.5B). The western arm of the outer sill is contiguous with the inner sill, and the small basin enclosed between them is at least 129 m deep and is partially filled with sediments interpreted as a spillover deposit from the outer sill.

Small Neoglacial moraine ridges are present on the sidewalls on either side of the fjord mouth and within the main valley (Dyke, 2013b).

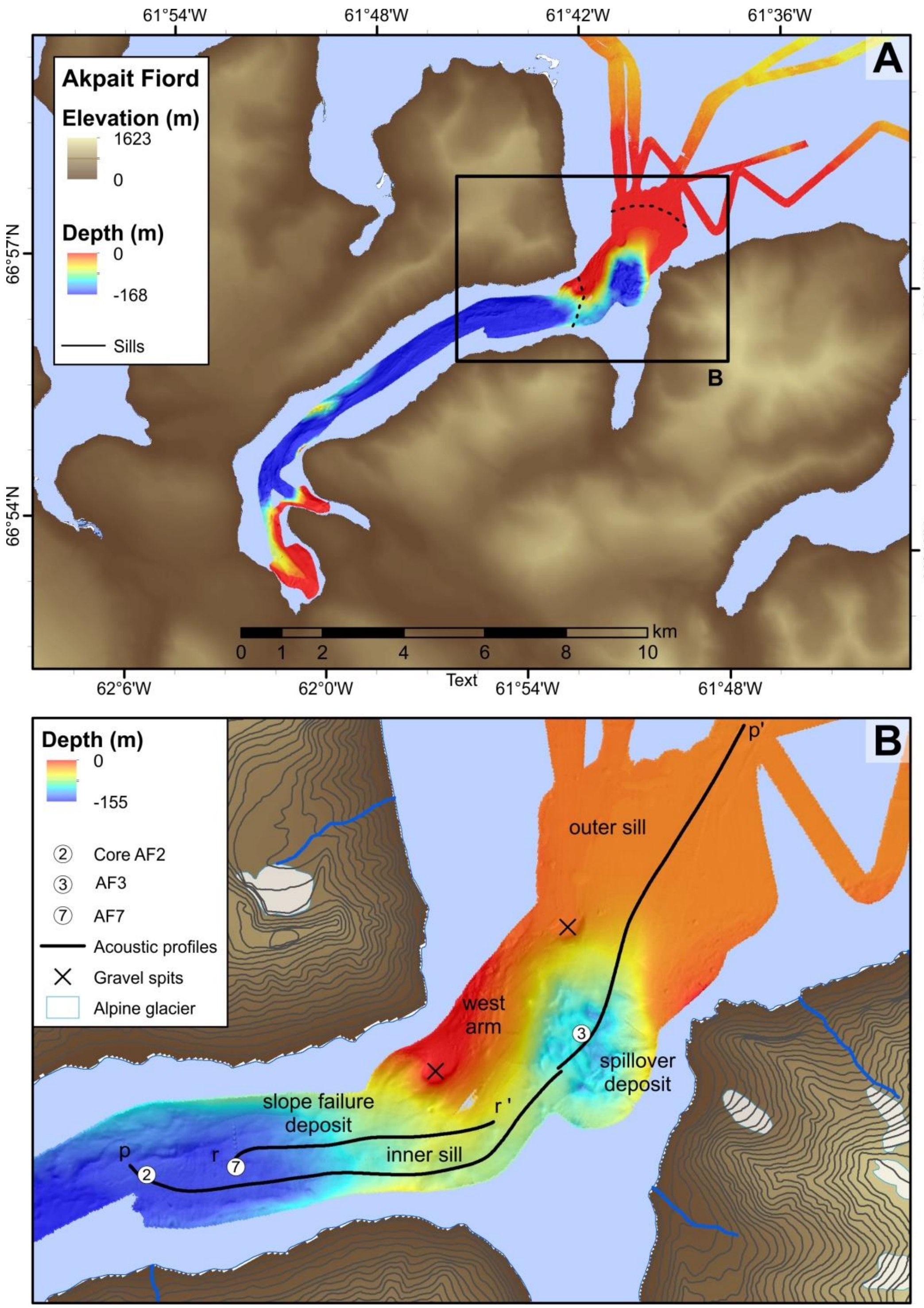

Figure 3.5: A) Map of Akpait Fiord, with inset outlining the site of interest. B) Bathymetry of the inner and outer sills, with the surrounding topography (contour interval 40 m) and the locations of acoustic profiles and sediment cores.

3.4.4 Sunneshine Fiord

Sunneshine Fiord lies adjacent to Cape Dyer and opens into Davis Strait (Fig. 3.1A). Inland from the fjord head, the main valley intersects the glacial valley of Southwind Fiord, while the northern tributary valley merges with the main glacial valley of Akpait Fiord. The present drainage basin of Sunneshine Fiord has an area of 569 km^2, of which 27% is glaciated, and includes mountains that rise to 1613 m asl. The bedrock is primarily Archean and Paleoproterozoic metamorphic rock (Sanborn-Barrie et al., 2013).

The fjord has not been surveyed using multibeam bathymetry, but at least two basins and sills are observed on seismic records of the outer fjord (Fig. 3.6B). The inner sill is ~113 m deep and encloses a basin with a maximum depth of ~164 m, while the outer sill is a long fjord-mouth platform ~52 m deep (similar to Akpait Fiord) enclosing a smaller basin ~125 m deep (Gilbert & MacLean, 1984; Andrews et al., 1994, 1996). A third basin in the inner fjord (~256 m deep) is reported from submersible exploration (Syvitski et al., 1986).

Extensive ground moraine, with a few lateral moraine ridges, drapes the sidewalls along the outer half of Sunneshine Fiord. Along the inner half of the fjord, small Neoglacial moraine ridges are associated with tributary glaciers (Dyke, 2013b).

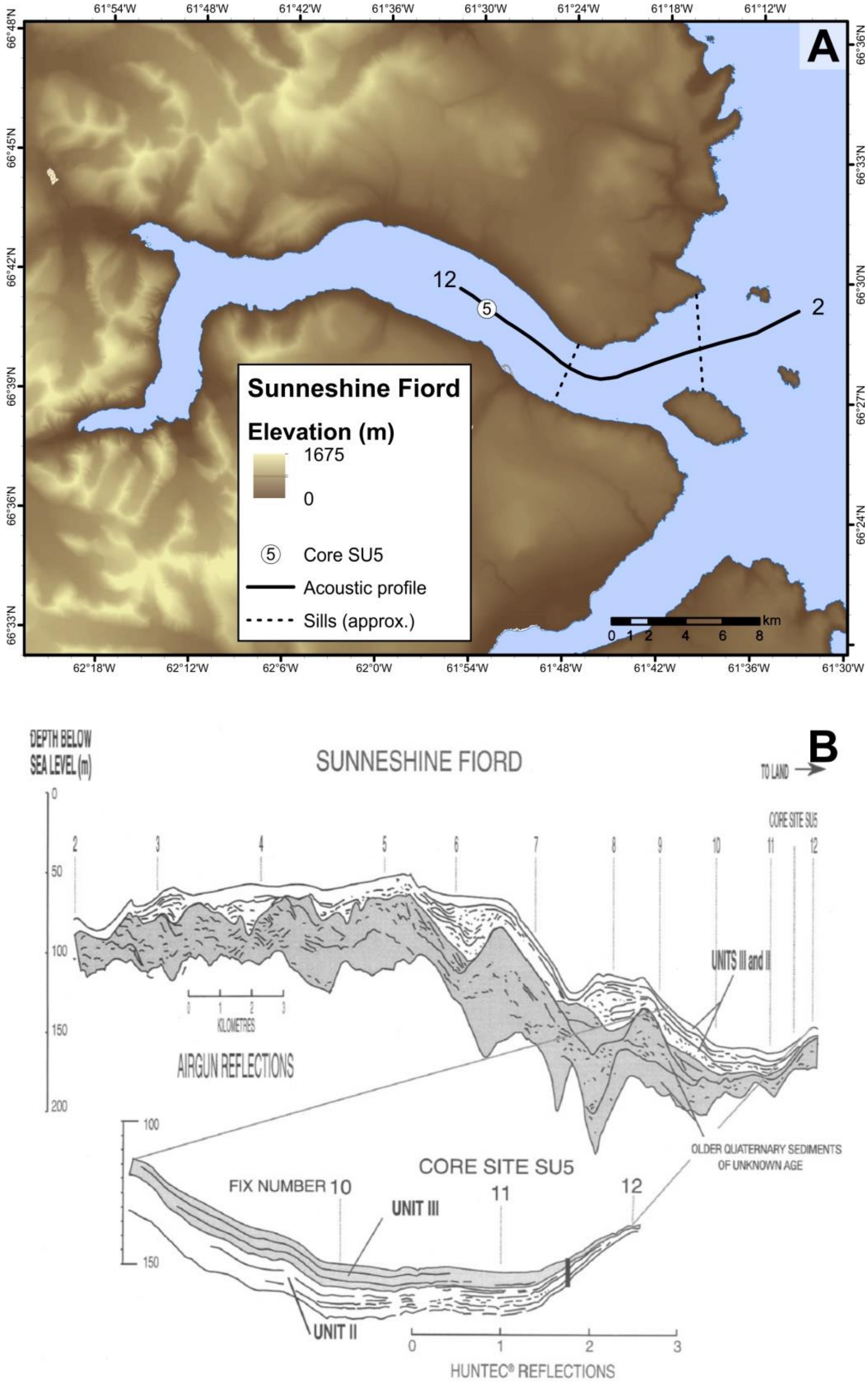

Figure 3.6: A) Map of Sunneshine Fiord, with the locations of the SU5 core (vertical thick black line) and the Gilbert and MacLean (1985) acoustic profile indicated. B) The acoustic profile of Sunneshine Fiord as interpreted by Andrews et al. (1996), containing 3 acoustic units, from bottom to top: Quaternary sediments, Unit II, and Unit III. These acoustic units are discussed further below (3.5.1 Acoustic stratigraphy). The acoustic profile is reversed from its orientation on map A.

3.5 Results

Three of the fjords discussed in this study were targeted based on distinctive seafloor features observed on the multibeam bathymetry. Boas Fiord and Durban Harbour both contain submerged deltas, while Akpait Fiord features a large fjord-mouth sill and adjacent spillover deposit. The remaining fjord, Sunneshine Fiord, has not been bathymetrically surveyed, but the inclusion of its acoustic profile and sediment core data provides a more comprehensive understanding of Cumberland Peninsula fjords.

3.5.1 Acoustic stratigraphy

Across the three fjord systems for which acoustic stratigraphy was analyzed (Boas Fiord, Durban Harbour, and Akpait Fiord), seven acoustic units are interpreted: A to G, in approximate stratigraphic order. Four of these units (A, B, C, and E) are interpreted as representing the anticipated sequence of deglacial sedimentation; the remaining three units (D, F, and G) are explicitly associated with specific geomorphic features. Table 3.3 summarizes where each unit was observed. The profiles most illustrative of key features and core locations included as Figures 3.6 and 3.7; the full collection of analyzed profiles is in Appendix B.

Table 3.3: Estimated thickness of acoustic units and total sediment package from acoustic profiles at each study site.

Unit	Interpretation	Estimated range of acoustic unit thickness (m) Min. (Mean) Max.				
		Boas Fiord		Durban Harbour	Akpait Fiord	Sunneshine Fiord
		Fjord-head	Side-entry			
G	Spillover deposit	—	—	—	0.9 (7) 8	—
F	Sill cover	—	—	—	2 (8) 19	—
E	Marine mud	0.6 (3) 12	0.1 (0.2) 0.2*	0.1*	2 (4) 6	1 (8) 17
D	Deltaic sediment	1 (6) 20	3 (13) 22	0.5 (6) 21	—	—
C	Glaciomarine sediment	5 (16) 25	7 (9) 11	—	2 (5) 16	1 (14) 23
B	Ice-contact sediment	3 (10) 19	?	1 (4) 6	?	12 (32) 49
A	Bedrock	?	—	?	—	—
Known sediment thickness		2 (15) 34	0.1 (7) 22	0.5 (7) 21	0.9 (7) 26	22 (49) 84

*Thickness from cores BF5 to BF7 and DH6, not acoustic profiles.
? = unknown unit thickness
— = absent unit

Unit A: This unit is most often inferred as underlying unit B (ice-contact sediment) at an undetermined depth, but is occasionally observed as an acoustically strong ridge with little to no acoustic penetration or stratigraphy, and prominent acoustic multiples. The unit is spatially associated with bathymetric features such as bedrock sills, shoals, and sidewall intrusions. The unit is interpreted as *bedrock*, based on its acoustic character and feature associations.

Unit B: This unit is observed to be acoustically strong and structureless-to-chaotic, frequently inferred to overlie bedrock and observed to underlie most other acoustic units. Across the entire study, the unit ranges from 1 to 19 m thick where known. It is associated with the central core of the inner and outer sills in Akpait Fiord. The unit is interpreted as *ice-contact sediment*, based on its coarse acoustic texture, stratigraphic position overlying unit A (bedrock), and association with the outer Akpait sill which is interpreted as a moraine (Cowan, 2015).

Unit C: This unit is observed to be acoustically stratified and conformable, overlying ice-contact sediments and underlying units D and E. In this study, it is only observed near the head of Boas

Fiord and in the outer basin of Akpait Fiord, appearing thinner but more distinctly stratified in the latter. Where penetrated, the unit ranges from 2 to 25 m thick. It is interpreted as *glaciomarine*, based on its acoustic character and stratigraphic position overlying unit B (ice-contact).

Unit D: The unit is typically identified by a distinct tripartite structure of bottomset (D1), foreset (D2), and topset beds (D3), and a direct spatial association of the profile with the submerged deltas observed on bathymetry. The upper contact tends to be strong, but acoustic penetration in most cases is minimal due to attenuation by coarse sediments. Large-scale clinoform strata are identified as foresets where associated with other deltaic features. The unit is observed to overlie ice-contact and glaciomarine sediments and underlie unit E (marine muds). The unit ranges from 0.5 to 22 m thick, with similar thickness at the heads of Boas and Durban (mean 6 m) but seemingly greater thickness at the Boas side-entry delta. It is interpreted as *deltaic deposits*, based on its tripartite structure and association with the submerged deltas.

Unit E: The unit is typically surficial and conformable, overlying either deltaic, glaciomarine, or ice-contact sediment, and appears as acoustically weak with few internal reflectors (transparent to faintly stratified). The unit ranges from 0.1 to 12 m thick. It is interpreted as *marine mud*, based on its acoustic character and surficial position. In the context of the submerged deltas of Boas Fiord and Durban Harbour, this unit is also referred to as *post-submergence mud*.

Unit F: This unit is acoustically weak, with a few uneven, weak-to-moderate reflectors. It is surficial, overlying the ice-contact sediment of the Akpait fjord-mouth sill. The unit ranges from 2 to 19 m thick. It is interpreted as *fine-grained, wave-worked sediment on the sill* (aka *sill cover*), based on its acoustic character and video footage described by Cowan (2015).

Unit G: This unit is bounded by a strongly reflective upper contact and contains multiple internal reflectors (hummocky). The two reflectors nearest the upper contact are strongest, while the others quickly weaken with depth. In this study, this unit is only observed landward of the Akpait fjord-mouth sill. It is a surficial unit, onlapping the adjacent ice-contact and sill-cover sediments. The unit ranges from 1 to 8 m thick. It is interpreted as *spillover deposits*, based on its hummocky acoustic character and position adjacent to the outer sill.

For Sunneshine Fiord, Andrews et al. (1996) described three acoustic units (I to III) in the airgun and Huntec DTS records, which penetrated much deeper than the 3.5 kHz subbottom records available for the other three fjords (Fig. 3.6B). The current study uses the Andrews et al. results to analyse the sedimentary record of Sunneshine Fiord within the acoustic stratigraphic framework described above, using the following associations: Unit I is equated with unit B of this study (ice-contact sediment), unit II with unit C (glaciomarine sediment), and unit III with unit E (marine mud). These associations are based on descriptions and illustrations provided by Andrews et al. (1994, 1996).

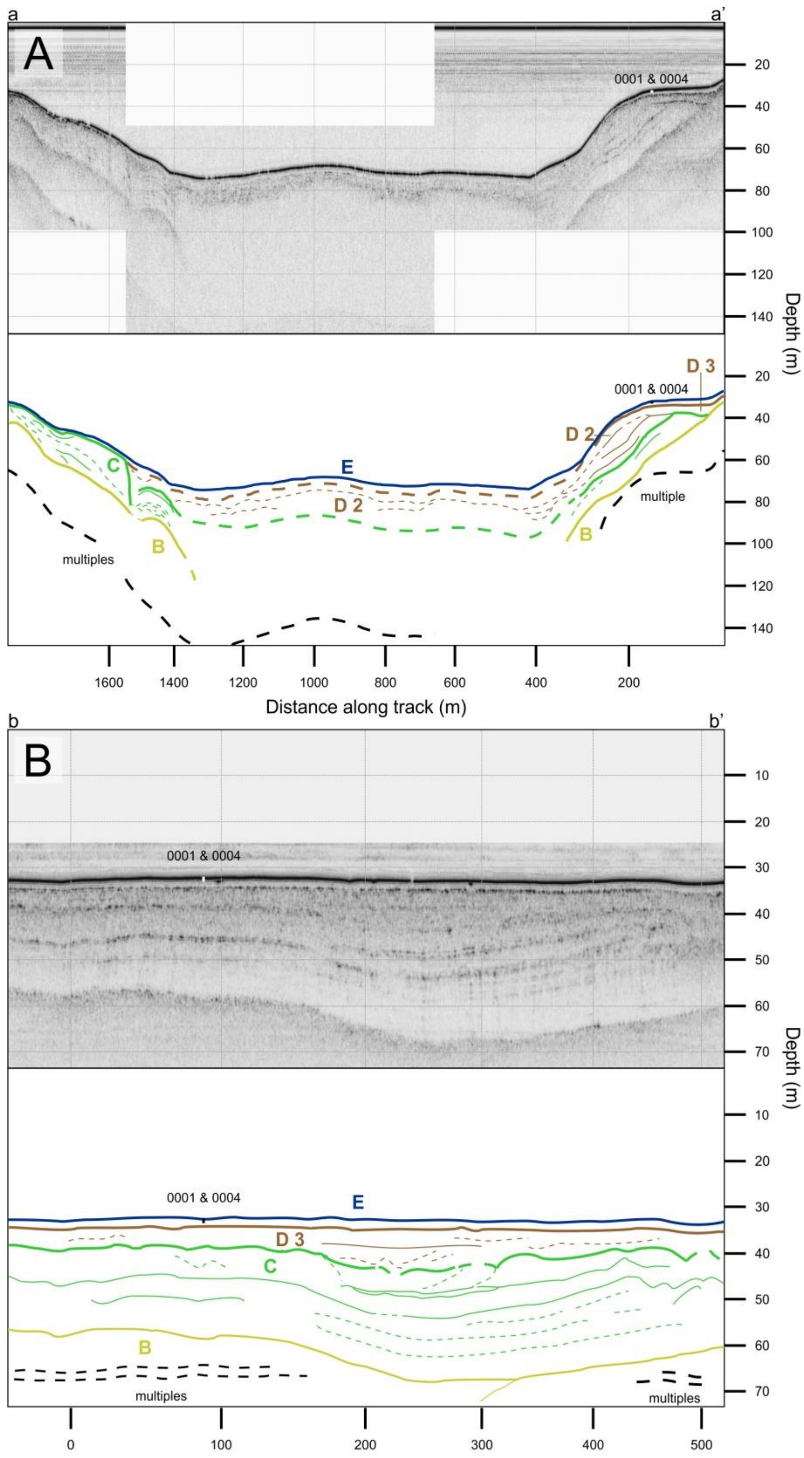

Figure 3.7: Acoustic profiles from the head of Boas Fiord illustrate acoustic units B to E. Dashed black lines represent acoustic multiples, and unit contacts (heavy lines) and internal stratification are colour-coded. Note the change in vertical scale between panels A and B. A) Profile *a-a'* extends across the slope of the submerged fjord-head delta, and shows the western and eastern side-terraces and the foreset beds on the delta slope (depth ~60 m). B) Profile *b-b'* displays a frontal cross-section of the eastern side-terrace, illustrating the typical postglacial sedimentary sequence. See Figure 3.3C for location of profiles.

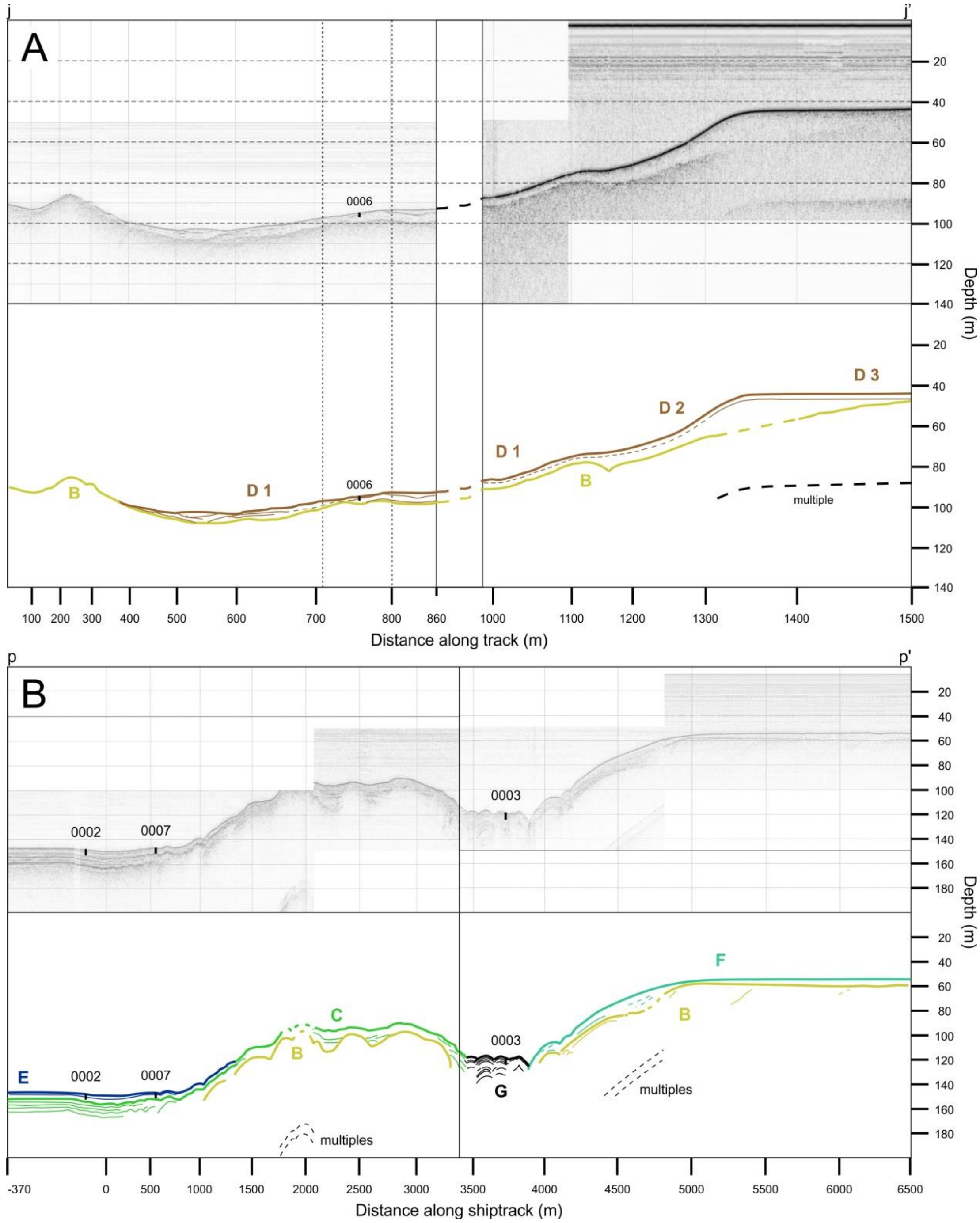

Figure 3.8: Acoustic profiles from Durban Harbour and Akpait Fiord (see Figs. 3.4B and 3.5B for locations). Dashed black lines represent acoustic multiples, and unit contacts (heavy lines) and internal stratification are colour-coded. Note the change in vertical scale between Panels A and B. Sediment core locations and numbered. A) Profile *j-j'* is a composite of two separate acoustic profiles from inner Durban Harbour, covering the prodelta and submerged fjord-head delta. B) Profile *p-p'* is a composite of two separate profiles from outer Akpait Fiord, covering the outer fjord basin, mid-fjord sill, spillover deposit, and fjord-mouth sill.

3.5.2 Lithofacies

The term *lithofacies* is used in this study to refer to units of sediment interpreted primarily on grain-size distribution. Across the three fjord systems where new sediment cores were collected (Table 3.4), six lithofacies are interpreted: L1 to L6, in approximate stratigraphic order. No single core was observed to contain all six facies, though cores DH6, AF3, and AF7 (Figs. 3.9 – 3.11) provide the most inclusive examples. The properties of each facies are summarized below and in Table 3.5. Comprehensive descriptions of each sediment core are compiled in Appendix C.

L1: Muddy gravel. Lithofacies 1 was only observed at the base of cores from the prodelta of Durban Harbour (4 to 16 cm thick). As a unit, it is coarse grained (mean size 1.61 ϕ; medium sand) and poorly sorted (standard deviation 4.55 ϕ), composed of gravel (38%) and almost equal parts of sand (26%) and silt (25%), with some clay (11%). L1 displays one of the highest average magnetic susceptibilities in Durban Harbour (Fig. 3.9). On the x-radiography, it appears as a cluster of gravel. Visually, the unit appears grey (Munsell 5Y 4/1) with a visibly coarse texture.

L2: Silt. Lithofacies 2 was observed in cores taken from the submerged prodelta deposits at the heads of Boas Fiord and Durban Harbour, ranging in thickness from 60 to 235 cm. It is fine grained (mean 6.75 ϕ; fine silt) and partially sorted (SD 1.77 ϕ), composed mostly of silt (72%) and clay (23%) with very little sand (5%). L2 contains the highest values for magnetic susceptibility and shear strength in Durban Harbour (Fig. 3.9). On the x-radiography, its appearance varies from massive to faintly bedded (>1 cm thick), with scattered dropstones ranging in size from granules to cobbles. The unit is a pale grey-brown (5Y 4/1 and 5Y 5/1) with varying amounts of mottling.

L3: Sandy silt. Lithofacies 3 was observed in cores taken from the prodelta of Durban Harbour (8.5 to 37 cm thick) and the spillover deposit in Akpait Fiord (569 cm thick). It is medium grained (mean 4.96 ϕ; coarse silt) and partially sorted (SD 1.95 ϕ), composed mostly of silt (57%) and sand (34%) with a little clay (9%) and rare gravel (0.2%) from dropstone deposits. L3 contains intermediate values for magnetic susceptibility, bulk density, and shear strength for both Durban Harbour (Fig. 3.9) and Akpait Fiord (Fig. 3.10). On the x-radiography, the unit appears as inclined and wavy non-parallel bedding in Durban Harbour cores, and faint horizontal-to-inclined bedding and laminae (<1 cm thick) with massive sections in Akpait Fiord cores. The unit varies in colour from yellow-brown (2.5Y 3/2) to dark grey-brown (10YR 3/1) in Durban Harbour, and from blackish to pale grey-brown (5Y 2.5/1 to 5Y 3/1) in Akpait Fiord.

L4: *Muddy sandy gravel*. Lithofacies 4 was observed only at the top of core DH1 (Fig. C.20), which was collected from the foot of the delta slope. It is 10 cm of coarse-grained (mean 0.87 ϕ; coarse sand) and poorly sorted (SD 4.3 ϕ) sediment, composed of gravel (41%) and sand (32%) with some silt (24%) and very little clay (3%). This unit has the second-lowest magnetic susceptibility for Durban Harbour, but also the highest bulk density. On the x-radiography, pebbles are observed oriented both horizontally and diagonally. The unit is yellow-brown (2.5Y 3/2) near the surface where oxidized, changing downward to pale grey-brown (5Y 4/1).

L5: *Sandy silt*. Lithofacies 5 was observed in cores from the side-entry delta in Boas Fiord (12 to 20 cm thick), prodelta in Durban Harbour (14 cm thick), and basin of Akpait Fiord (450 to 516 cm thick). It is fine grained (mean 5.86 ϕ; medium silt) and partially sorted (SD 1.98 ϕ), composed mostly of silt (67%) with some sand (18%) and clay (15%) and rare gravel (0.1%) from dropstone deposits. The unit has the lowest mean values for magnetic susceptibility, bulk density, and shear strength in either Durban Harbour or Akpait Fiord. On the x-radiography, the unit shows faint horizontal bedding in Durban Harbour, while in Akpait it appears to be mostly massive, with occasional faint horizontal or inclined bedding. Visually, the unit shows a yellow-brown (5Y4/3) component near the seabed in both fjords, but in Akpait darkens downwards to blackish-grey mottling (5Y 3/2 and 5Y 4/1 and black).

L6: *Silty sand*. Lithofacies 6 represents multiple silty sand units observed throughout Boas Fiord, Durban Harbour, and Akpait Fiord, typically either adjacent to or interbedded within L3 and L5 (Figs. 3.10, 3.11, C.11, and C.13). The silty sand units are primarily thin lenses ranging from 1 to 9 cm thick, except for a 34-cm-thick unit in the lower part of AF7 (Fig. 3.11). This facies is coarse grained (mean 3.40 ϕ; very fine sand) and partially sorted (SD 1.71 ϕ), mostly composed of sand (71%) with some silt (25%) and very little clay (4%). This unit has the highest averages and values for magnetic susceptibility and bulk density in Akpait Fiord. On the x-radiography, the silty sand lenses appear as lighter bands of varying thickness with horizontal bedding, while the larger unit appears bright with some fine lamination (Figs. 3.10, 3.11, Appendix C). The thick sand unit in AF7 is a distinct grey (2.5Y 3/1 and 2.5Y 4/1) with a few darker bands and streaks. Short silty sand units (5.5-10 cm) were also sampled from the topset bed of the Boas side-entry delta and foreset bed of the Durban fjord-head delta (cores BF6 and DH5; Appendix C). Core SU5 (Fig. 3.12) was interpreted as also including multiple sand lenses (Cole & Blakeney, 1984).

Table 3.4: Summary table of the sediment cores discussed in the present study.

Fjord	Sediment core #	Station #	Location Lat.	Location Long.	Water depth (m)	Length (cm)	Apparent penetration (cm)	Acoustic facies units(s)	Lithofacies	No. of C^{14} dates
Boas Fiord	BF1	2014NULIAJUK-0001 GC	66.694°N	62.827°W	31	94	-	E	L2	-
	BF2	2014NULIAJUK-0002 GC	66.680°N	62.854°W	29	76	-	E	L2	-
	BF3	2014NULIAJUK-0003 GC	66.666°N	62.861°W	28	60	-	E	L2	-
	BF4	2014NULIAJUK-0004 GC	66.694°N	62.827°W	31	135	-	E	L2	1
	BF5	2014NULIAJUK-0005 GC	66.776°N	62.755°W	36	12	-	E [1]	L5	-
	BF6	2014NULIAJUK-0006 GC	66.776°N	62.754°W	36	17.5	-	D, E [1]	L5, L6	-
	BF7	2014NULIAJUK-0007 GC	66.777°N	62.741°W	25	20	-	E [1]	L5	-
Durban Harbour	DH1	2014805-0001 PC	66.951°N	62.279°W	80	261.5	350	B, D	L1, L2, L3, L4	-
	DH5 [2]	2015805-0005 PC	66.949°N	62.277°W	71	~10	-	D	L6	-
	DH6	2015805-0006 PC	66.950°N	62.29°W	95	244	450	B, D, E [1]	L1, L2, L3, L5	1
Akpait Fiord	AF2 [3]	2014805-0002 PC	66.889°N	61.824°W	142	517	750	E	L5	2
	AF3	2014805-0003 PC	66.883°N	61.743°W	112	603	920	G	L3, L6	3
	AF7	2015805-0007 PC	66.887°N	61.809°W	147	489	830	B, E	L5, L6	4
Sunneshine Fiord	SU5 [4]	HU82-SU5 G	66.575°N	61.672°W	146	232	-	E	-	1
		HU82-SU5 PC	66.575°N	61.672°W	146	770	~870	B, C, E	-	7

[1] Although unobserved on the acoustic stratigraphy, the presence of acoustic unit E is suggested by the lithology.
[2] Bagged sample of unsorted sediment.
[3] Missed the upper 6 cm of sediment.
[4] Water depth and length data from Natural Resources Canada (2017); location data are an estimate; piston core missed the upper ~1 m of sediment (Andrews et al., 1996).

Table 3.5: Summary data for the six lithofacies observed in sediment cores collected from Durban Harbour and Akpait Fiord.

Litho Units:	Photo.	% Gravel	% Sand	% Silt	% Clay	Bulk Density (Mg/m^3)	Shear Strength (kPa)	Average Colour (L* a* b*)
L6		0	44.68 – 97.60	1.90 – 49.19	0.51 – 11.86	1.54 – 2.19	6.28 – 11.52	33.12 -0.61 3.35
L5		0 – 5.09	9.30 – 29.67	56.97 – 77.99	10.83 – 24.76	1.40 – 1.89	2.88 – 16.94	31.07 -1.28 5.22
L4		41.25	32.07	23.85	2.82	1.83 – 2.14	n/a	38.41 -0.83 6.66
L3		0 – 4.22	27.34 – 40.72	51.11 – 65.23	5.99 – 12.66	1.52 – 2.11	4.21 – 17.59	29.19 -0.94 4.75
L2		0	1.28 – 11.21	59.72 – 77.93	16.23 – 32.51	1.52 – 1.98	4.34 – 13.62	42.46 -1.09 6.17
L1	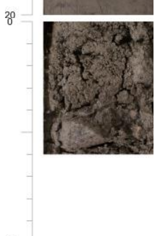	31.99 – 43.15	12.82 – 39.63	12.82 – 36.95	4.40 – 18.23	n/a	n/a	42.29 -1.24 5.55

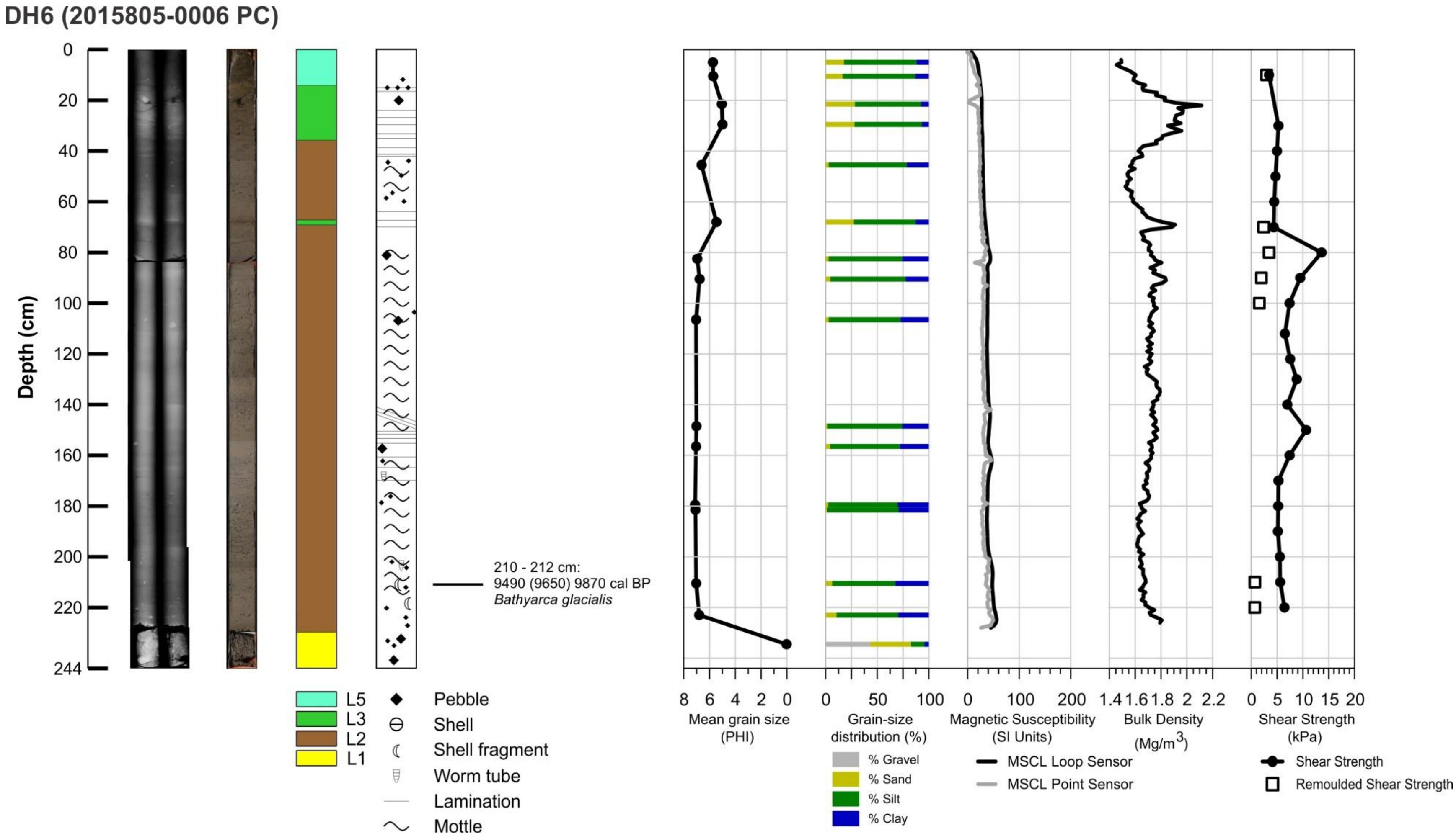

Figure 3.9: Core DH6 (2015805-0006 PC), collected from the prodelta area of Durban Harbour. See Fig. 3.4 for coring site location.

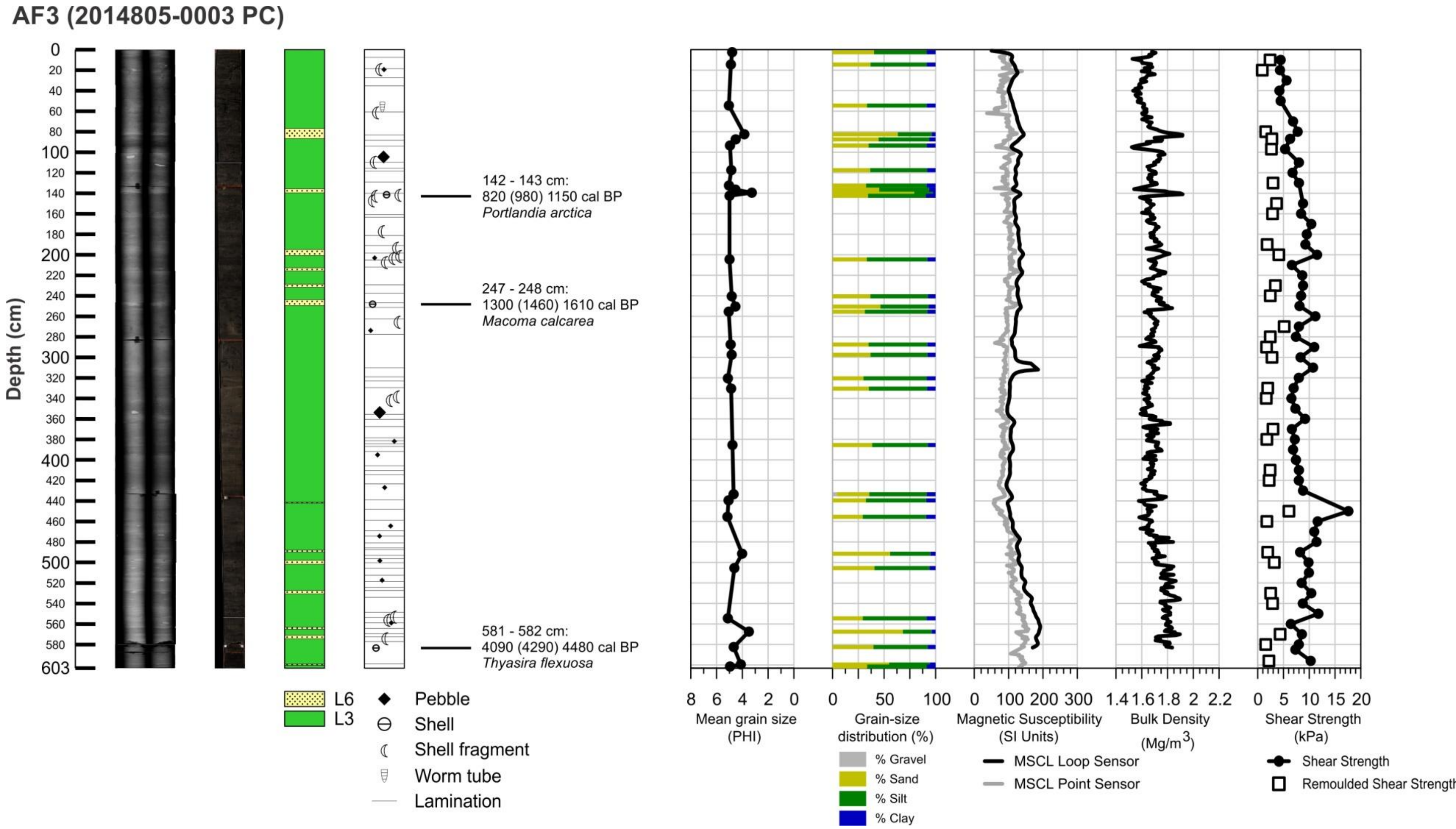

Figure 3.10: Core AF3 (2014805-0003 PC), collected from the spillover deposit, adjacent to the fjord-mouth sill, of Akpait Fiord. See Fig. 3.5 for coring site location.

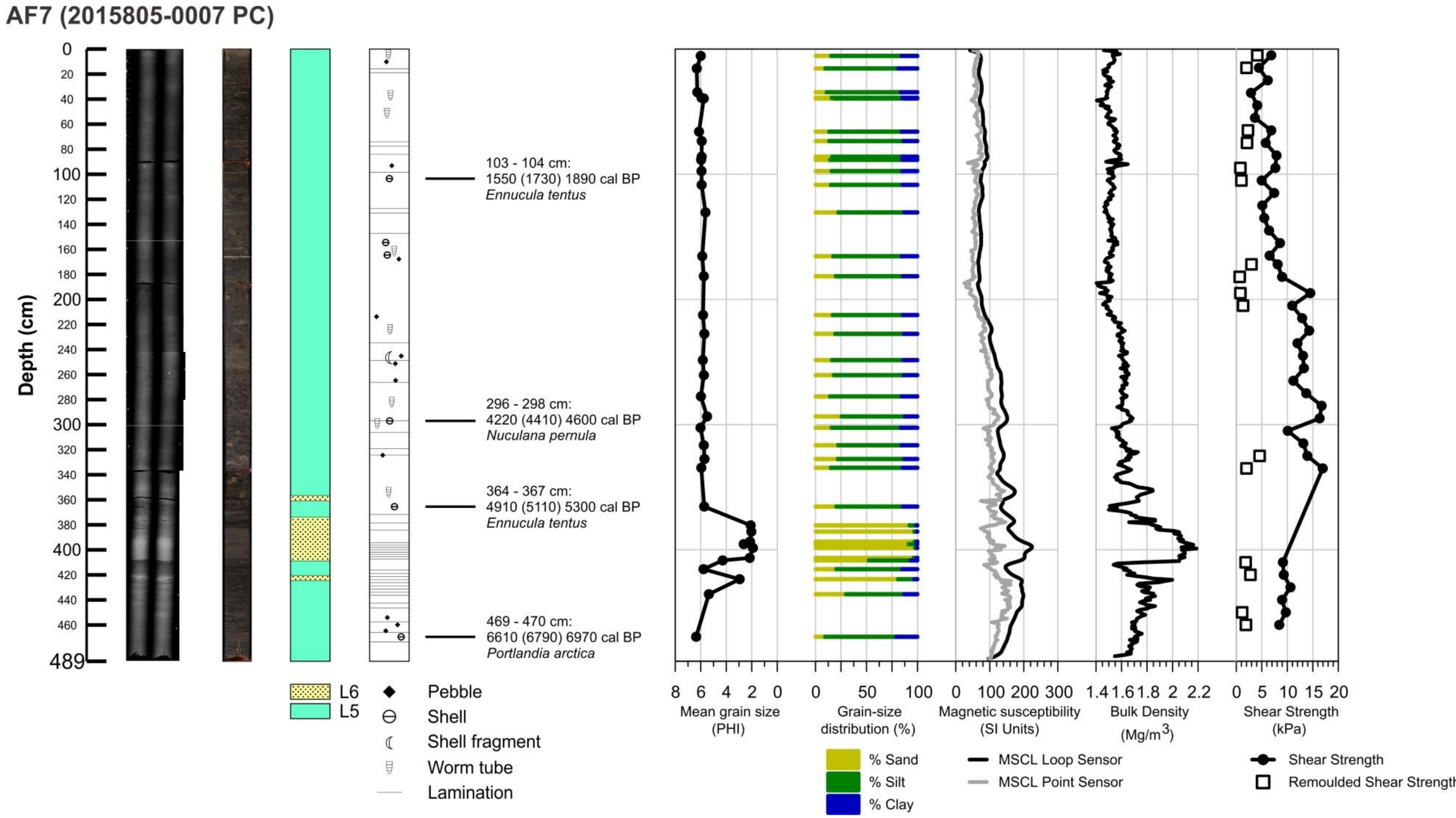

Figure 3.11: Core AF7 (2015805-0007 PC), collected from the fjord basin of Akpait Fiord. See Fig. 3.5 for coring site location.

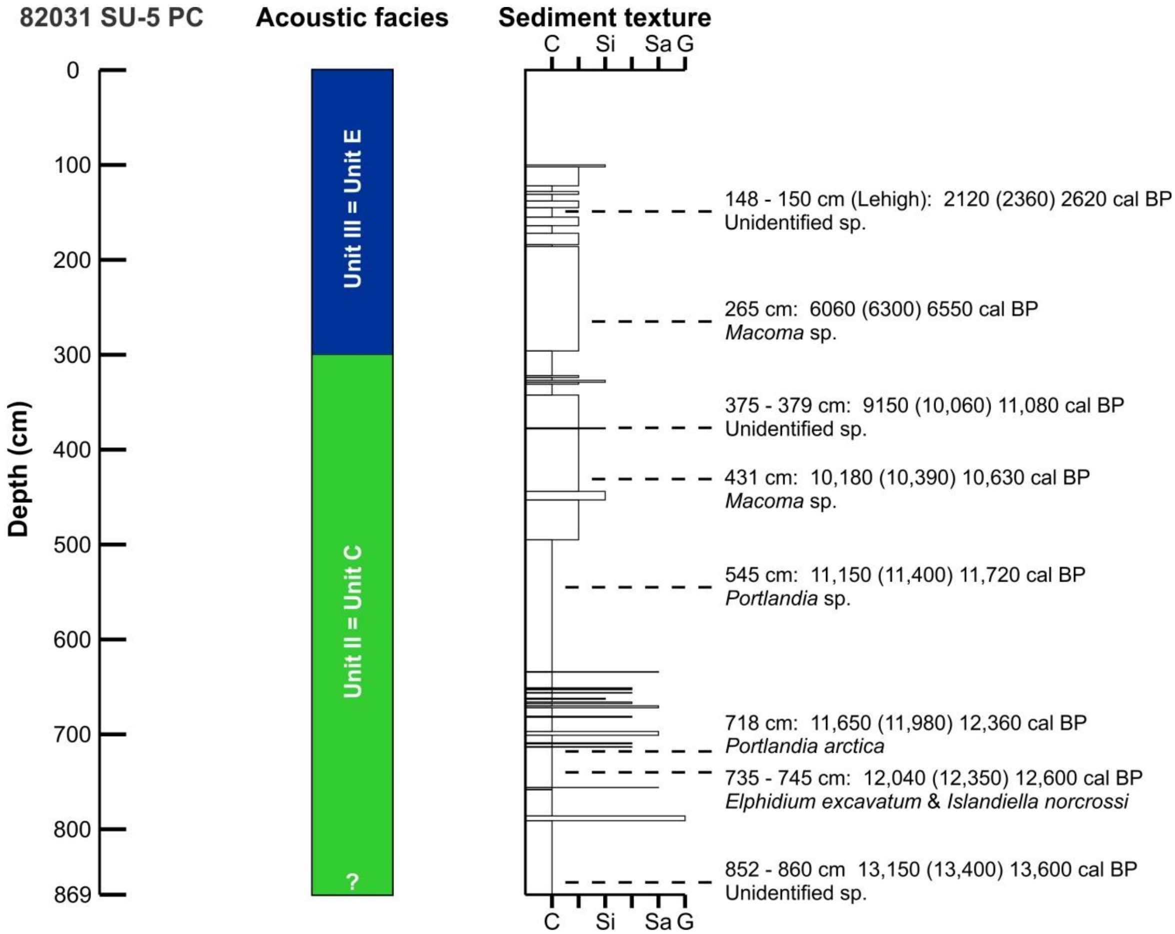

Figure 3.12: Litho log of HU82-SU5 PC, reconstructed from the lithology description in Cole and Blakeney (1984) and corrected for the missing 1.0 m of sediment (Andrews et al., 1996). See Fig. 3.6A for location of core. Log illustrates a composition that transitions from predominantly clay-silt to clay, with various inclusions. Several of the coarse-sediment lenses may represent gravity flows. The positions of the samples are indicated, along with the associated calibrated radiocarbon dates. Acoustic facies were interpreted by Andrews et al. (1996).

3.5.3 Acoustic-lithological correlation

Based on the acoustic stratigraphy and core lithology described above, this section considers the correlation between the acoustic units and lithofacies (Table 3.6). Acoustic unit A is interpreted as bedrock, so it cannot be associated with a sediment lithofacies. Similarly, lithofacies 4 is interpreted as ice-rafted material (3.6.2.2 Sources of sediment and lithofacies) that does not appear on the acoustic profile, but is logically associated with acoustic unit B (ice-contact sediment).

Table 3.6: Correlation of acoustic units to lithofacies summarized.

Acoustic unit	Interpretation	Lithofacies	
A	Bedrock	n/a	
B	Ice-contact sediment	L1	Muddy gravel
		L4	Muddy sandy gravel
C	Glaciomarine sediment	L2 [a]	Silt
		L5 [b]	Sandy silt
		L6 [c]	Silty sand
D	Deltaic sediment	L2	Silt
E	Marine mud	L2	Silt
		L5	Sandy silt
F	Sill cover	L3 [d]	Sandy silt
G	Spillover deposit [e]	L3	Sandy silt
		L6	Silty sand

[a] Cores DH1 and DH6 may sample unit C; if so, then L2 is locally indistinguishable between units D and C.
[b] The bottom of cores AF2 and AF7 may contact uppermost unit C; if so, then L5 is locally indistinguishable between units E and C.
[c] Unit C is likely the origin of the sand units (L6) in core AF7, as the source of gravity flows.
[d] Hypothesis: unit F was not cored, but it may be the primary source of the spillover deposit (unit G) which is dominated by L3.
[e] Unit G may represent either the same sediment as unit F, or a mixture of units B and F.

Unit B: Ice-contact sediment → L1 (muddy gravel) and L4 (muddy sandy gravel).

Acoustic unit B (ice-contact sediment) is associated with two lithofacies, L1 (muddy gravel) and L4 (muddy sandy gravel), observed in cores DH1 and DH6. The coarse, poorly sorted sediments of L1, and its position at the bottom of DH1 and DH6, match with the coarse sediment indicated by the acoustically strong, chaotic-to-structureless character of unit B. Although the interpreted position and length of both cores are offset from the unit B contact on Figures 3.7 and B.20, this can be attributed to small errors in coordinate position and/or acoustic thickness. Alternatively, the interpreted core-position and -length on Figures 3.7 and B.20 may be accurate and L1 instead represents ice-rafted deposits similar to L4; however, this seems less likely due to the similar depths of L1 between cores DH1 (254 cm) and DH6 (228 cm) despite the distance (~440 m) between the two coring sites.

Unit C: Glaciomarine sediment → L6 (silty sand); possibly L2 and L5.

Unit C (glaciomarine sediment) is not easily associated with a lithofacies. The only core clearly identified as penetrating unit C is SU5 from Sunneshine Fiord, which was not analyzed the same way as the other cores. Andrews et al. (1996) interpret unit C as extending from 300 to 860 cm core depth, while sedimentation rate data suggest that glaciomarine deposition continued until somewhere between 377 and 431 cm. These interpretations combined with Figure 3.12 suggest that unit C eventually coarsens upward, from predominantly clay interbedded with multiple coarser lenses to predominantly clay-silt.

In contrast, cores from Durban Harbour and Akpait Fiord may sample unit C, but it is not apparent from the acoustic profile or lithology. Unit C is not observed on any Durban profiles (Figs. 3.8A, B.19 to B.23) but may simply be too thin for image resolution, like the local unit E. Thus, if unit C is present at Durban, it is expected to lie between units B (ice-contact) and D (deltaic), as observed in Boas. However, no distinct unit is observed between L1 (muddy gravel) and L2 (silt) in cores DH1 and DH6. The only possible (but tenuous) indication is in DH6 from 219 to 228 cm, where mottling disappears and horizontally-bedded pebbles become frequent.

Thus, if unit C has been sampled in Durban, then it must be lithologically similar to L2. Similarly in Akpait Fiord, the bottom of cores AF2 and AF7 may penetrate uppermost unit C, but if so then unit C is lithologically indistinguishable from unit E and L5. Given how unit C drapes the inner sill and presumably lower sidewalls in Akpait Fiord, it is a possible source of the L6 (silty sand) interbedding observed in AF7.

Unit D: Deltaic sediment → L2 (silt).

Acoustic unit D (deltaic sediment) is associated with L2 (silt) as it dominates the composition of cores DH1 and DH6, which penetrate unit D1 (Fig. 3.8A, B.20). The prodeltaic sediments are relatively fine-grained (mean 6.78 ϕ) in the bottomset beds (D1), but coarsen towards the foreset beds (D2) (mean 3.98 ϕ in DH5). Further coarsening toward the topset beds is indicated by the acoustic stratigraphy, marked by the strong internal reflectors observed in D3 and the attenuation of the underlying unit B (Figs. B.19, B.21, B.23).

Unit E: Marine mud → L2 (silt) and L5 (sandy silt).

Acoustic unit E (marine mud) is strongly associated with L5 (sandy silt) in Akpait Fiord, as it dominates the composition of cores AF2 and AF7, which penetrate unit E (Fig. 3.8B). Based on this association, L5 may also comprise the top 300 cm of SU5 (Andrews et al., 1996). On the other hand, at the head of Boas Fiord, cores penetrating unit E (BF1 to BF4) lithologically correspond to L2 (silt). Unit E was not observed on any acoustic profiles from the Boas side-entry embayment or Durban fjord-head, but the lithology of cores BF5 to BF7 (Figs. C.6 to C.8) and DH6 (Fig. 3.9) indicate that L5 is present as a thin veneer (12–20 cm).

Unit F: Sill cover → L3 (sandy silt).

Unit F, the surface of the Akpait fjord-mouth sill, was not cored and thus is not easily associated with a sediment lithofacies. Nonetheless, it was described by Cowan (2015) as fine-grained sediment from video footage and is likely similar to L3, which forms the spillover deposit (unit G). Alternatively, the unit F lithology may be similar to L2 or L5, the two finest-grained lithofacies identified in the study.

Unit G: Spillover deposit → L3 (sandy silt) and L6 (silty sand).

Unit G, the spillover deposit, is associated with the two lithofacies observed in core AF3, L3 (sandy silt) and L6 (silty sand). The strong internal reflectors may indicate the silty sand lenses observed in AF3 (Figs. 3.10, B.28). The hummocky character of the unit may reflect the sediment draping the topography of a dead-ice moraine. As the spillover deposit is interpreted as reworked sediment from the outer sill (Cowan, 2015), acoustic unit G and lithofacies 3 may represent either the same sediment as unit F or a mixture of units B and F. The latter possibility is suggested as L3 has a higher sand content than L5 from AF2 and AF7. L3 is also observed in core DH6 without a clear correlation to an acoustic unit.

3.5.4 Chronology

The field research conducted for this study yielded a total of 11 new radiocarbon dates from three fjords on Cumberland Peninsula: Boas Fiord, Durban Harbour, and Akpait Fiord (Table 3.7). In addition, eight previously recorded radiocarbon dates from Sunneshine Fiord have been updated with new calibrations (Table 3.8). The range of mean sedimentation rates has been calculated for each interval between calibrated radiocarbon dates (Table 3.9, Figure 3.13). Cores BF4 and DH6 each returned only one radiocarbon date, and thus Boas Fiord and Durban Harbour are represented by age-depth plots based on only one data point; this lack of resolution is suboptimal, but is the only data available from current samples. The $CaCO_3$ content was found to be 0 for the entire length of every sediment core listed in Table 3.8.

Table 3.7: Summary table of original calibrated radiocarbon dates rounded to the nearest decade, with species identified by Telka (2015; 2016).

Sediment core	Sample depth (cm)	Lithofacies	Laboratory # (UCIAMS-)	Conventional C^{14} data (±σ)	cal BP 2σ age range (median)	Species
BF4 (2014NULIAJUK-0004 GC)	103–104	L5	155824	1570 ± 20 BP	740 (910) 1060	*Hiatella arctica*
DH6 (2015805-0006 PC)	210–212	L2	169710	9165 ± 25 BP	9490 (9650) 9870	*Bathyarca glacialis*
AF2 (2014805-0002 PC)	236–237	L5	155825	2990 ± 20 BP	2360 (2550) 2710	*Curtitoma incisula*
	503–504	L5	155826	6945 ± 25 BP	7040 (7220) 7390	*Portlandia arctica*
AF7 (2015805-0007 PC)	103–104	L5	169711	2340 ± 15 BP	1550 (1730) 1890	*Ennucula tenuis*
	296–298	L5	169712	4485 ± 15 BP	4220 (4410) 4600	*Nuculana pernula*
	364–367	L5	169713	5035 ± 15 BP	4910 (5110) 5300	*E. tenuis*
	469–470	L5	169714	6560 ± 20 BP	6610 (6790) 6970	*P. arctica*
AF3 (2014805-0003 PC)	142–143	L3	155827	1775 ± 20 BP	970 (1120) 1270	*P. arctica*
	247–248	L6	155828	2245 ± 20 BP	1440 (1620) 1790	*Macoma calcarea*
	581–582	L3	155829	4530 ± 20 BP	4270 (4470) 4680	*Thyasira flexuosa*

UCIAMS: Keck Carbon Cycle AMS Lab, University of California, Irvine.

Boas Fiord: Sample BF4 (103–104 cm), a single valve fragment of *Hiatella arctica*, returned an age of 740 (910) 1060 cal BP, giving a mean sedimentation rate of 0.976 (1.14) 1.39 mm/yr for the top 104 cm in the core. The sample is interpreted as within acoustic unit E (marine mud) and lithofacies 2 (silt); by extrapolating downward to the acoustic unit D contact (2.0 m below seafloor), the minimum age constraint for the onset of RSL transgression (and thus the end of the postglacial lowstand) is estimated at ~1440 (1750) 2050 cal BP.

Durban Harbour: Sample DH6 (210–212 cm), a single valve of *Bathyarca glacialis*, returned an age of 9490 (9650) 9870 cal BP. The sample is interpreted as within acoustic unit D1 (deltaic bottomsets) and lithofacies 2 (silt); based on this interpretation, the date provides a maximum age constraint for the postglacial lowstand. The mean sedimentation rate is estimated to be 0.214 (0.219) 0.222 mm/yr for the interval of 0–211 cm.

Akpait Fiord: A total of nine calibrated radiocarbon ages were obtained across two separate environments within Akpait Fiord; six dates from the outer fjord basin (unit E and L5), and three from the spillover deposit (unit G and L3 and L6). The uppermost sample from the fjord basin, AF7 (103–104 cm), returned an age of 1550 (1730) 1890 cal BP, while the lowermost, AF2 (503–504 cm), returned an age range of 7040 (7220) 7390 cal BP. The mean sedimentation rates estimated for the fjord basin range from 0.531 (0.572) 0.617 to 0.636 (0.976) 2.22 mm/yr. Ages returned from the spillover deposit (AF3) range from 970 (1120) 1270 cal BP near the top (142–143 cm) to 4270 (4470) 4680 cal BP near the bottom (581–582 cm). The mean sedimentation rates estimated for the spillover deposit are generally two to three times greater than for the distal fjord basin, ranging from 1.03 (1.17) 1.34 to 1.28 (2.13) 6.00 mm/yr.

Sunneshine Fiord: Eight calibrated radiocarbon ages were returned from cores HU82-SU5 G and PC, ranging from 2120 (2360) 2620 cal BP at the top (149 cm) to 13 150 (13 400) 13 660 cal BP at the bottom (852–860 cm). The upper two samples likely correspond to the unit E (marine mud), while the lower six likely correspond to unit C (glaciomarine sediment). A notable change in the mean sedimentation rates occurs at 377 cm (~10.1 cal ka BP), with post-10.1 cal ka BP sedimentation slowing by nearly an order-of-magnitude (Fig. 3.14).

Table 3.8: Previously published radiocarbon dates from Sunneshine Fiord (SU5), updated using the calibration process described above under Methodology. The topmost sample was retrieved from HU82-SU5 G, while all underlying samples are from HU82-SU5 PC with their depths corrected for a missing 1 m of sediment (Andrews et al., 1996).

Sample #	Depth (cm)	Conventional ^{14}C data (yr BP)	cal BP 2σ age range (median)	Species
CAMS-13511 [2]	149	2840 ± 60	2120 (2360) 2620	Bivalve
CAMS-11814 [2]	265	6120 ± 80	6060 (6300) 6550	*Macoma* sp.
AA-0412 [1]	377	9450 ± 360	9150 (10 060) 10 630*	Bivalve
CAMS-11815 [2]	431	9710 ± 60	10 180 (10 390) 10 630	*Macoma* sp.
AA-13053 [2]	545	10 430 ± 80	11 050 (11 400) 11 630	*Macoma* sp.
AA-13054 [2]	718	10 805 ± 80	11 650 (11 980) 12 360	*Portlandia arctica*
CAMS-17398 [2]	735-745	11 060 ± 70	12 040 (12 350) 12 600	*Elphidium excavatum forma clavata*, *Islandiella norcrossi*
AA-13052 [2]	852-860	12 125 ± 90	13 150 (13 400) 13 660	Foraminifera

* Positive error originally exceeded the positive error of the underlying sample, so it was constrained to be equal.
AA: University of Arizona AMS Laboratory
CAMS: Center for Accelerator Mass Spectrometry, Lawrence Livermore National Laboratory.
[1] Andrews et al. (1989)
[2] Manley & Jennings (1996)

Table 3.9: Summary of mean sedimentation rates per core for all three study sites and Sunneshine Fiord.

Fjord	Sediment core	Sediment interval (cm)	Mean sedimentation rate range (mm/yr)
Boas Fiord	BF4 (2014NULIAJUK-0004 GC)	0-103.5	0.976 (1.14) 1.39
Durban Harbour	DH6 (2015805-0006 PC)	0-211	0.214 (0.219) 0.222
Akpait Fiord	AF2 (2014805-0002 PC)	0-236.5	0.874 (0.929) 1.00
		236.5-503.5	0.531 (0.572) 0.617
	AF7 (2015805-0007 PC)	0-103.5	0.547 (0.599) 0.666
		103.5-297	0.635 (0.721) 0.832
		297-365.5	0.636 (0.976) 2.22
		365.5-469.5	0.505 (0.622) 0.791
	AF3 (2014805-0003 PC)	0-142.5	1.12 (1.27) 1.47
		142.5-247.5	1.28 (2.13) 6.00
		247.5-581.5	1.03 (1.17) 1.34
Sunneshine Fiord	HU82-SU5 G	0-149	0.570 (0.633) 0.704
	HU820SU5 PC	149-265	0.262 (0.294) 0.337
		265-377	0.245 (0.298) 0.430
		377-431	0.365 (1.66) >1.66
		431-545	0.739 (1.13) 2.21
		545-718	1.42 (2.99) >2.99
		718-740	0.230 (0.593) >0.593
		740-856	0.715 (1.10) 2.12

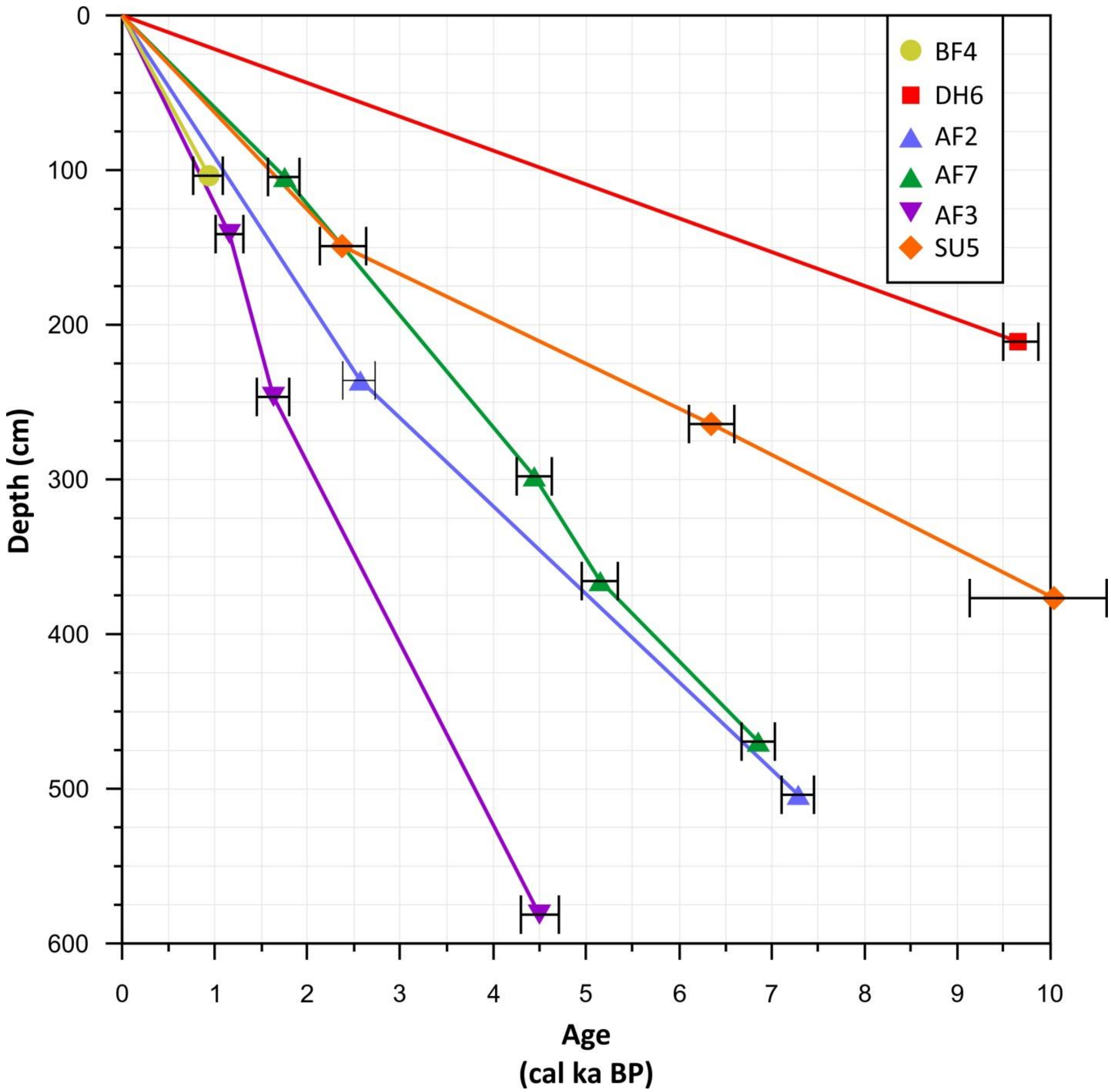

Figure 3.13: Age-depth curves for cores from Boas Fiord, Durban Harbour, and Akpait Fiord. It is assumed that the top of the core corresponds to the present (0 cal ka BP), but may be older; if so, then the first interval of each core represents a minimum mean sedimentation rate.

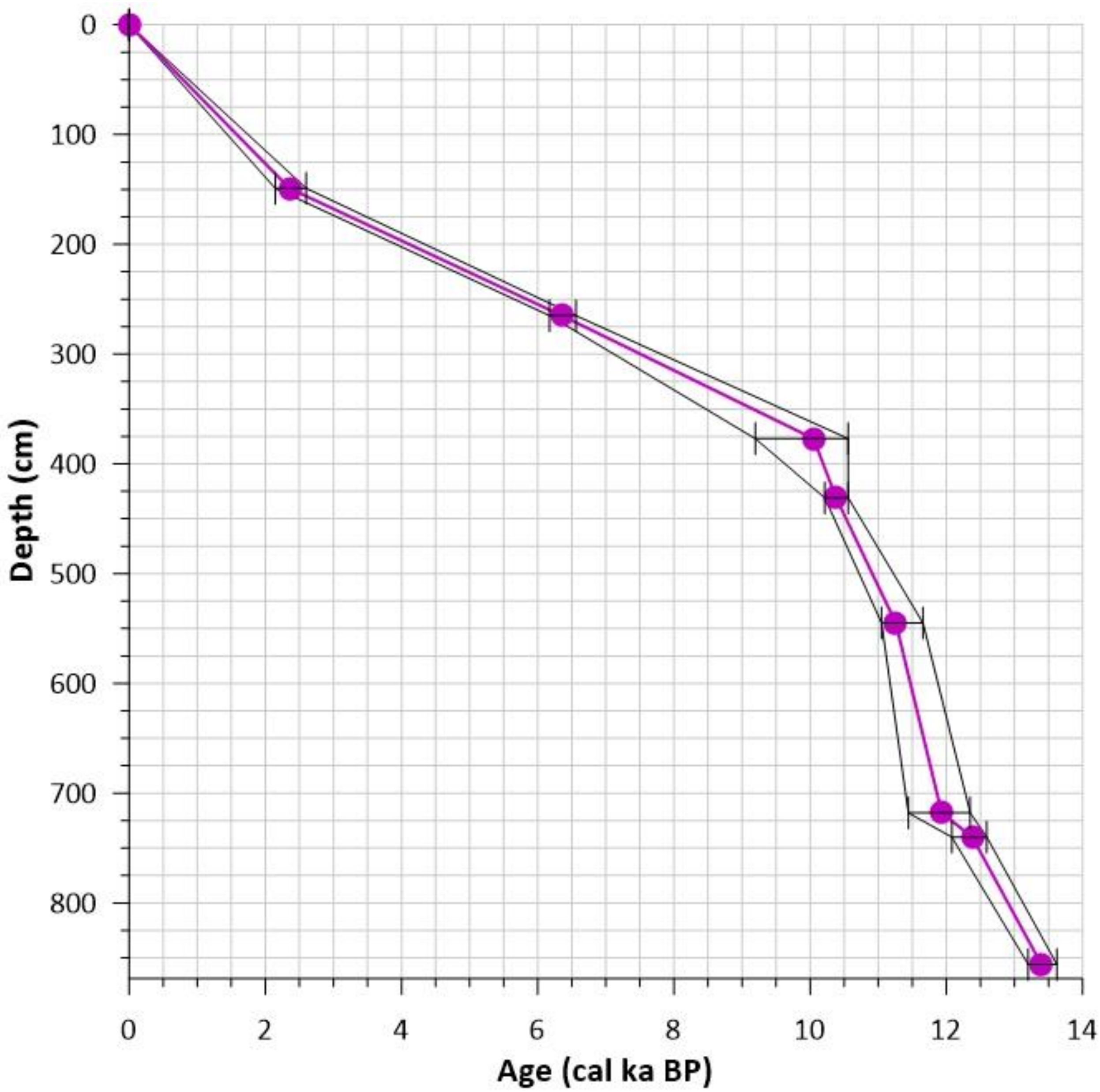

Figure 3.14: Age-depth plot for core HU82-SU5 PC from Sunneshine Fiord, illustrating the change in the possible mean sedimentation rates. Three breaks in sedimentation rate are observed: near surface interval (less reliable), postglacial interval, and ice-proximal interval. The ice-proximal interval (>10 ka) shows higher sedimentation than postglacial interval (<10 ka), which is expected.

3.6 Discussion

This study addresses multiple aspects of the sedimentary environment and depositional record in Cumberland Peninsula fjords: the timing of deglaciation; the sediment sources, delivery processes, and rates of accumulation through time; the timing of the postglacial lowstand; the range of erosional and depositional morphological features contained within each basin; and how the fjords of Cumberland Peninsula compare to those elsewhere along the Baffin Island coast.

3.6.1 Deglaciation

The sediment-core chronologies are consistent with the ice-margin timeline established by Margreth (2015), with most of the studied fjords (Boas, Durban, and Akpait) having fully deglaciated >2 kyr before the oldest returned calibrated dates. No dates were retrieved from ice-contact sediment, but minimum age constraints for local ice retreat are established by the oldest postglacial-sediment date in each core.

According to Margreth, Boas Fiord was the most recent study site to fully deglaciate (~9.5 cal ka BP), while Durban Harbour and Akpait Fiord were both fully deglaciated by ~11.7 cal ka BP. At every study site, the local timing of deglaciation predates the oldest (or only) available radiocarbon date (~0.9 cal ka BP in BF4; ~9.6 cal ka BP in DH6; ~7.2 cal ka BP in AF2). The offset between deglaciation and oldest available date is greatest in Boas, but this is explained by core BF4 targeting post-submergence sediments instead of the fjord-basin sediments that are likely older.

In Sunneshine Fiord, the coring site deglaciated during the ice retreat between 14.6 cal ka BP and ~13.4 cal ka BP, the oldest date returned from SU5. Figure 3.14 indicates a notable decrease in the mean sedimentation rate around ~10.1 cal ka, which falls within the Preboreal warm interval between 11.7 and 9.5 cal ka BP and thus may reflect the cessation of local glaciomarine deposition due to the full withdrawal of ice from the fjord (Chapter 4).

3.6.2 Fjord sedimentation

3.6.2.1 Boas Fiord versus Durban Harbour

This study has compared the sedimentology of two separate fjord-head environments, Boas Fiord and Durban Harbour. Both environments feature submerged deltas overlying ice-contact sediments. However, the Boas system also includes thick glaciomarine and post-submergence sediments, which do not appear on Durban profiles. Submerged fjord-head terraces are also present in Akpait Fiord (where no data beyond bathymetry were obtained) and other fjord-head settings on Cumberland Peninsula (Cowan, 2015; Hughes Clarke et al., 2015)

Glaciomarine sediments are typically fine-grained (silt dominated), released by the glacier directly into the water column before they settle out of suspension. Durban Harbour has a smaller drainage basin (206 km^2) than Boas Fiord (1138 km^2) and thus likely drained a smaller volume of ice, which would result in less glacial sediment production. Thus, it is possible that a glaciomarine unit is present at Durban Harbour but too thin to be resolved in the acoustic imagery. This interpretation suggests that the local glaciomarine and deltaic bottomset sediments may be acoustically and lithologically indistinguishable, as no separate acoustic unit or lithofacies was observed between ice-contact (L1) and deltaic sediment (L2) within the Durban profiles and cores.

In Boas Fiord the sediment deposition upon the submerged delta continued as RSL rose, as indicated by the post-submergence unit (unit E, mean ~3 m thick), while in Durban Harbour the sedimentation effectively ceased. Analysis of grain-size data for cores BF1-4 (Appendix C) indicates that the post-submergence muds overlying the fjord-head delta have equivalent grain size as the deltaic bottomsets (L2) cored in Durban Harbour. In addition, satellite imagery from December 2016 depicts the modern river's sediment plume as extending over most of the submerged delta terrace / sandur (Google, 2021), and acoustic profiles indicate that the post-submergence unit thickens towards the head of Boas. Thus, it appears that post-submergence sedimentation is strongly influenced by fluvial input. In contrast, the post-submergence unit at the head of Durban appears to be represented by a thin (14 cm) unit of sediment resembling what was collected from the Boas side-entry delta (L5). Thus, it appears that post-submergence muds also accumulate in areas of low-fluvial activity. The difference in post-submergence units can be again attributed to differences in drainage-basin area and runoff volume: the larger Boas drainage-basin contains multiple valley glaciers that feed ongoing fluvial activity and sediment transport, while the smaller Durban drainage-basin has less glacial-ice cover (7%) to feed fluvial discharge and more lakes to trap sediments.

3.6.2.2 Sources of sediment and lithofacies

The four fjords examined – Boas, Durban, Akpait, and Sunneshine – were sampled at different locations along their length, where different sediment sources are expected to predominate (Table 3.10). The focus of work in Boas and Durban was at the fjord-head, where sedimentation is typically dominated by fluvial processes after the ice retreats inland, as documented in numerous other fjords (Syvitski et al., 1987; Syvitski & Hein, 1991). Boas was also investigated in a side-entry embayment with minimal postglacial fluvial deposition. The focus in Akpait and

Sunneshine was in the outer fjord, where late- to postglacial sedimentation would be controlled initially by the tidewater glacier, and then by marine deposition following ice retreat. Akpait was also studied in proximity to a fjord-mouth sill, which supplied reworked sediments to the basin.

Table 3.10: Summary of sediment sources per lithofacies.

Lithofacies	Sediment source
L1: Muddy gravel	Glacial deposition.
L2: Silt	Fluvial transport
L3: Sandy silt	Reworked sediment – gravity flows and spillover deposit.
L4: Muddy sandy gravel	Ice-rafting.
L5: Sandy silt	Post-submergence deposition, including fluvial (meltwater) input.
L6: Silty sand	Fluvial transport and gravity flows.

The six lithofacies identified in this study can be associated with the following sediment sources:

L1 (muddy gravel) was interpreted as ice-contact material, and thus was weathered and eroded from the bedrock by glacial action. As each fjord was previously glaciated, L1 was likely deposited along the length of each fjord at some depth below the seafloor, and at some time prior to local deglaciation.

L2 (silt) was interpreted as deltaic bottomset sediment, formed by settling from suspension of the river plume. It was cored in the prodelta region in Durban Harbour, as expected, and likely occurs in the prodelta environments at the head and side-entry embayment in Boas Fiord as well.

L3 (sandy silt) appears to be associated with reworked sediment. In Durban Harbour it is interpreted as indicating gravity flows on the delta front, while in Akpait Fiord it forms the spillover deposit adjacent to the fjord-mouth sill. It remains unknown how the spillover deposit compares to its source, the sill-cover unit, which was never cored. A plausible hypothesis is that waves remobilized sediments on top of the sill, washing them towards and over the inner lip where oversteepening occurred, leading to slumping and gravity flows (including potential turbidity currents) in a setting closely analogous to the fjord-head deltas (e.g., Piper & Normark, 2009). Sand may also be carried into the basin in suspension, as documented in Emerald Basin on the Scotian Shelf and other wave-dominated inlets and shelf edges (Kontopoulos & Piper, 1982; Yang et al., 2020). Because RSL was lower in the past (possibly as low as the sill), the potential for wave-driven transport over the sill would have been much greater and is gradually diminishing (3.6.3.2 Submerged sill).

L4 (muddy sandy gravel) consists of coarse grained, poorly sorted sediments from at the top of DH1. Due to its notable similarity to L1 (muddy gravel interpreted as ice-contact material) but surficial position, L4 is interpreted as ice-rafted material, which ultimately derives from glacial action prior to transportation via iceberg. Upon release from the iceberg into the water column, coarser materials may fall out together in a concentrated deposit while finer materials are dispersed. Ice-rafted material may occur anywhere along a fjord at any depth, but is most likely wherever icebergs become trapped.

L5 (sandy silt) was interpreted as marine / post-submergence mud, the fine-grained sediment which remains suspended for a prolonged period before settling and or is produced in the water column via biotic processes. It is observed as thin veneers overlying the topset beds of the Boas side-entry delta and the Durban bottomset beds (12–20 cm), and as a thicker unit (~2–6 m) on the basin floor in Akpait Fiord. It likely includes a pelagic-biogenic component, but is also clearly influenced by fluvial input (meltwater outwash) based on: the active fluvial input seen in both Boas and Akpait (Google, 2021) where unit E is thickest, and the similar grain sizes between L5 (post-submergence) in Boas and L2 (delta bottomsets) in Durban. Sources of postglacial sediment documented in other fjords include shelf-fjord exchanges, aeolian transport, and fjord-wall mass transport (Syvitski & Hein, 1991).

L6 (silty sand) appears to be associated with deltaic foreset and topset beds, and gravity flows. In Boas Fiord and Durban Harbour, silty sand units (10-12 cm) were sampled from the topset beds of the side-entry delta and foreset beds of the fjord-head delta, respectively. These samples are in line with expectations that topset and foreset beds are coarser than the bottomsets, as coarser sediments fall out of fluvial suspension first. In Akpait Fiord, a large sand unit interrupts the fjord-basin marine muds (AF7, Fig. 3.11), while multiple silty sand lenses are interbedded throughout the spillover deposit (AF3, Fig. 3.10). The large sand unit (>90% sand, 34 cm thick) in AF7 resembles a large grain flow as it appears coarsest in the middle, but also features horizontal laminae at its base before transitioning upwards to bedding and then massive sediment; this study lacks the data required to be conclusive, but identifies the AF7 sand unit as a potential turbidite, similar to those observed in Broom et al. (2017) and discussed by Normandeau et al. (2019a), originating from glaciomarine sediments draping the inner sill and sidewalls of the fjord. Similarly, the silty sand lenses in AF3 may have been formed by wave re-suspension on the sill, oversteepening and slope failure, and possible gravity flows (either grain flows or turbidity currents) activation at the inner lip or upper backslope of the sill.

3.6.2.3 Rates of accumulation

The mean sedimentation rates calculated in this thesis are compared based on their specific fjord environment: fjord head (Boas and Durban), outer fjord (Akpait and Sunneshine), and spillover deposit (Akpait). The comparison of MSR to fjord environment is tabulated below in Table 3.11.

Table 3.11: Comparison of fjord area, drainage-basin area, and mean sedimentation rates, organized by fjord environment.

Environment	Fjord	Fjord area (km^2)	Drainage-basin area (km^2) Total	Delta-specific	MSR* (mm/yr)
Fjord head	Boas	116	1138	658	1.14
	Durban	45	206	85	0.219
Outer fjord	Akpait	38	247	-	0.572 – 0.976
	Sunneshine	121	569	-	0.294 – 0.633† 0.593 – 2.99‡
Spillover	Akpait	38	247	-	1.17 – 2.13

* Column only includes the mean sedimentation rates calculated using the median calibrated radiocarbon ages (Table 3.7 & 3.8).
† Post-10.1 cal ka BP
‡ Pre-10.1 cal ka BP

As seen in Figure 3.13, the MSR curve for Boas is relatively steep (1.14 mm/yr), reflecting the effects of active fluvial deposition, while the curve for Durban is long and shallow (0.219 mm/yr), reflecting a low amount of sediment accumulation over a prolonged period. This difference in MSR at the fjord-head environment is comparable to the difference in drainage-basin area inland of the two fjord heads (658 versus 85 km^2, see Table 3.11). Both rates are calculated using only a single radiocarbon date from each site, which impairs chronologic resolution, and cover very different timeframes (0.9 vs 9.6 ka), which makes comparing them directly problematic. However, the same distinction is also observed in the accumulated post-submergence muds, which are at least 135 cm thick in BF4 (and estimated to be up to ~200 cm thick on profile b, Fig. 3.7B), but only 12 cm in DH6. Overall, the greater sedimentation at the head of Boas can be attributed to its larger drainage basin, which contains multiple meltwater sources (valley glaciers) and no significant lakes to trap sediment. In contrast, the smaller Durban drainage basin contains fewer glaciers to feed meltwater and more lakes to filter out sediments, thus limiting sediment deposition at the fjord-head.

The MSR curves for AF2 and AF7 are similar, reflecting their shared outer-fjord environment; the post-10.1 cal ka BP curve for SU5 is also similar. Outer-fjord sedimentation has occurred at partially overlapping rates in Akpait (0.572–0.976 mm/yr) and Sunneshine (0.294–0.633 mm/yr), with the former being overall higher. Given that Akpait has the smaller drainage basin (247 vs 569 km^2), this seems to reverse the trend seen with Boas and Durban. However, it is possible that the MSR difference between Akpait and Sunneshine is not statistically significant, and/or that the drainage basins are close enough in size (same order of magnitude) that other factors dominate.

Spillover-deposit sedimentation at the mouth of Akpait Fiord shows the highest postglacial mean rates in the study, likely reflecting the effects of mass transfer from the adjacent fjord-mouth sill. The spillover deposit may receive sediment from the sill via wave action and gravity flows, in addition to marine deposition. Core AF3 indicates that the spillover deposit has a notable sand content throughout (minimum 29%), but at least 6 distinct sand lenses (>45 % sand, range 1 – 9 cm thick, mean 3.7 cm) suggest periods of high-magnitude deposition through heightened wave-action during storms, periods of reduced sea ice with greater wave fetch, or both (Fig. 3.10).

Core SU5 provides a deeper and older sedimentary record for Sunneshine Fiord than is available for any other study site (Fig. 3.12). The corresponding age-depth plot (Fig. 3.14) shows an inflection point at ~10.1 cal ka BP (377 cm), when the initially rapid sedimentation rate decreases by an order of magnitude. The ~10.1 cal ka BP inflection point is interpreted as reflecting the local cessation of glaciomarine deposition due to glacial retreat from the fjord, which correlates with Sunneshine Fiord and its drainage basin having fully deglaciated by 9.5 cal ka BP (Margreth, 2015). This is supported by Figure 3.12 depicting the glaciomarine-to-marine interface at 300 cm, which can be interpolated to date to ~ 9.6 cal ka BP when using the MSR of 1.66 mm/yr from the underlying interval (Table. 3.9).

Overall, based on the data available from this study, deltaic bottomset deposition at the fjord head appears to be influenced by drainage-basin area and the number of meltwater sources, and limited by the presence of lakes. When shallow fjord-mouth sills are exposed to wave-action, spillover deposits can accumulate more rapidly than fjord-head deltas. Sunneshine Fiord appears to have deglaciated around ~10.1 cal ka BP (and possibly as late as ~9.6 cal ka BP).

3.6.2.4 Marine mud

Marine muds are observed at the head and side-entry embayment of Boas Fiord, the head of Durban Harbour, and the basin floor of Akpait Fiord. At the head of Boas and floor of Akpait, the marine muds form thick deposits (unit E). In contrast, at the side-entry embayment of Boas and head of Durban, marine muds are only present as thin veneers (L5).

The marine mud strata (unit E) observed on Boas and Akpait profiles vary between 2 and 6 m thick (except for the Boas prodelta, where unit E is up to 12 m thick). Grain-size analysis of cores BF1 to BF4 (Appendix C) indicate that unit E near the head of Boas Fiord resembles L2 (deltaic bottomset beds) from Durban Harbour more than L5 in Akpait. This observation suggests that the muds overlying the submerged fjord-head delta originate from the same source as the bottomset beds of the transgressive delta, which has migrated up-valley with rising sea level to culminate in the modern, active, subaerial delta. Therefore, active fluvial deposition at least partly accounts for the marine mud thickness in the head of Boas Fiord. Marine muds in Akpait also likely include a fluvial component, based on Google Earth Pro™ imagery (Google, 2021), in addition to more marine processes: the settling of very fine and biogenic sediments. Other sources of postglacial sediment documented in other fjords include shelf-fjord exchanges, aeolian transport, and fjord-wall mass transport (Syvitski & Hein, 1991).

The thin veneers of marine mud (L5) observed in cores from the Boas embayment and Durban head, versus the thick unit cored from the Akpait basin, can be partly attributed to shorter timespans for local marine deposition. Marine deposition in Akpait presumably became the dominant sediment source some time following fjord deglaciation, pre-11.7 cal ka BP (Margreth, 2015). In contrast, marine deposition in the Boas Fiord side-embayment and head of Durban Harbour most likely were initiated much later, as lowstand deltas were flooded by rising RSL (prior to ~1.8 cal ka BP, based on BF4).

Even accounting for the different timespans, the marine-mud veneers at Boas and Durban seem disproportionately thin compared to Akpait and Sunneshine. Based solely on data from core AF2 (L5), marine muds at Akpait have accumulated a thickness of ~5 m since ~7.2 cal ka BP, at mean sedimentation rates ranging between ~0.531 and 1.00 mm/yr. In contrast, the BF5 and BF6 coring sites accumulated only 0.12 or 0.20 m of marine mud since delta submergence prior to 1.4 (1.8) 2.0 cal ka BP (3.5.4 Chronology). These data result in MSRs of either 0.059 (0.069) 0.084 mm/yr (where thickness is 12 cm) or 0.098 (0.11) 0.14 mm/yr (where thickness is 20 cm); if earlier dates for submergence are used, the MSR estimates become even smaller. Thus, even accounting for a delayed onset, the marine muds across the four study sites demonstrate a tendency for sediment thickness to increase with depth.

3.6.3 Marine submergence

The postglacial lowstand that occurred along Cumberland Peninsula (Cowan, 2015) is reflected in certain geomorphic features of the studied fjords. Well-preserved, submerged deltas are located within Boas Fiord and Durban Harbour, marking the position of the palaeo-sea-level. The

Akpait fjord-mouth sill is shallow enough to have been levelled by wave-action, and thus supply sediment to the basin (spillover deposit), during the lowstand.

3.6.3.1 Submerged deltas

Cowan (2015) previously interpreted eight submerged, Gilbert-style deltas located in inlets along the coast of Cumberland Peninsula as forming synchronously during a postglacial lowstand. In order to constrain the timing of the lowstand, the current study collected sediment cores from two submerged deltas. The maximum age constraint was established by targeting the bottomset beds at the head of Durban Harbour, and the minimum by targeting the topset beds at the head of Boas Fiord.

The Durban Harbour bottomset beds were most likely deposited when the delta was still an active fluvial system, and thus should constrain the maximum age of submergence when dated. Sample DH6 210-212 cm was extracted near the bottom of the deltaic sediment (unit D, L2), and returned an age range of 9490–9870 cal BP. Therefore, this date indicates that local delta progradation, and thus the lowstand, was occurring at some point during the interval 9.5–9.9 cal ka BP, which corresponds closely to the 9.5 cal ka BP transition between the Preboreal recession and the Cockburn Substage readvance (Table 3.1). However, kettle holes observed on the submerged delta terrace in Kangert Fiord (Cowan, 2015) indicate that delta progradation occurred (at least locally) in an ice-proximal environment, making a late-Preboreal pulse less likely.

The Boas Fiord topset beds are draped by post-submergence marine muds, and thus constrain the minimum age of submergence. Core BF4 103–104 cm was extracted from the marine mud (unit E, L2) and returned an age range of 740–1060 cal BP. Based on this date range, mean sedimentation rates of 0.976–1.393 mm/yr are calculated for the interval between 0 and 103.5 cm in BF4. When these rates are extrapolated downwards to the unit D contact at ~2 m below seafloor (Fig. B.5), the minimum age constraint for the postglacial lowstand is estimated at ~1440–2050 cal BP, corresponding to the Neoglacial (5.7–0.05 cal ka BP). However, this is most likely an underestimate, as the true sedimentation rate for BF4 most likely varied over time: initially increasing with water depth during RSL transgression, before decreasing as the river mouth retreated up-valley and became distal.

Overall, the postglacial lowstand can be constrained to sometime in between 9.9–9.5 and 2.0–1.4 cal ka BP. These constraints can in turn be associated with the Preboreal-Cockburn transition (9.5 cal ka BP) and the latter half of the Neoglacial (5.7–0.05 cal ka BP).

3.6.3.2 Submerged sill

It has been hypothesized that the fjord-mouth sill of Akpait Fiord may have been subaerial during the lowstand (Cowan, 2015). The two gravel spits associated with the outer sill (Fig. 3.5B), at ~31 and ~50 m bsl, were interpreted by Cowan (2015) as formed by longshore drift during the postglacial lowstand. This is corroborated by the submerged-delta shoreline, which reaches palaeo-sea-levels of 45–46 m bsl (below present sea level) at Durban Harbour and Clephane Bay (Cowan, 2015). If assumed for Akpait mouth, these palaeo-sea-levels would leave the current sill platform (~51 m bsl) at 5–6 m below contemporary sea level, within range of the wave base assuming some open water in Baffin Bay. Given its morainal origin, the outer sill was likely higher prior to levelling by wave-action, and thus possibly subaerial. Furthermore, based on the submerged shoreline's overall trend of -0.35 m/km east (Cowan, 2015), the palaeo-sea-level at the mouth of Akpait Fiord may have been even lower at 54–58 m bsl. Therefore, in either palaeo-sea-level scenario (45–46 or 54–58 m bsl), it is possible that the outer sill may have been subaerial during the lowstand.

If the sill was subaerial during the lowstand, then Akpait Fiord would most likely have been either a freshwater or brackish lake instead of a fjord. However, no mollusc shells or microfossils retrieved from Akpait cores thus far have indicated a freshwater or brackish environment. The current lack of empirical evidence for the subaerial-sill hypothesis suggests that the outer sill was either never subaerial, or was only subaerial at some time before 7.0–7.4 cal ka BP based on the oldest Akpait radiocarbon date. Deeper penetration of the Akpait basin and the coring of older sediments may eventually resolve the present ambiguity.

The spillover deposit (unit G) features some of the highest sedimentation rates (1.03–6.00 mm/yr) included in the study. The spillover deposit contains reworked sediment, so some AF3 dates cannot be interpreted as dating the feature. However, sample AF3 581–582 cm, dating to 4.3–4.7 cal ka BP, appears to represent *in situ* deposition (horizontal bedding in x-radiography); therefore, it provides an age constraint on all underlying and overlying sediments. The other AF3 samples (142–143 cm and 247–248 cm) may occupy reworked sediment (massive, bioturbated on x-radiography). However, even if these molluscs originally died on the sill and were later transported to the spillover deposit, they still provide maximum age constraints (albeit with an unknown amount of lag) on all overlying sediments. However, without evidence that the sill was once subaerial, an age constraint on reworking cannot be treated as a constraint on RSL rise.

3.6.3.3 RSL lowstand restriction of icebergs

During the sea-level lowstand, the major sill in inner Boas Fiord would have greatly restricted water flow from the innermost basin. As indicated by the submerged fjord-head delta, the palaeo-sea-level at the fjord head was 38 m bsl (Cowan, 2015). The major sill near Boas head has a maximum depth of 51 m, but the majority of it (11 to 38 m bsl) would have been subaerial during the lowstand. The resulting lack of disturbance from waves and or water circulation may explain the sediment thicknesses near the fjord-head delta. It would also restrict the entry of icebergs (thus, ice-rafted material) to the innermost basin.

In contrast, in Durban Harbour, the palaeo-sea-level was 45 m bsl at the fjord head. Thus, the lowstand would have likely restricted water flow through the west branch (maximum sill depth of 53 m) and southwest branch (minimum known depth of 13 m). However, there is no indication that water flow, and thus icebergs, would be restricted at any point along the main fjord, and thus prevented from reaching the head of Durban Harbour. Therefore, it remains likely that lithofacies 4 in core DH1 originated from an ice-rafted deposit. Moreover, the resulting susceptibility of the delta to waves and water circulation may have also contributed to the lack of observable glaciomarine and marine sediments.

3.7 Conclusions

The deglacial and postglacial sedimentary record of Boas Fiord, Durban Harbour, and Akpait Fiord is represented by a sedimentary sequence of: bedrock, ice-contact sediment, glaciomarine sediment, deltaic deposits (where applicable), and marine mud. In addition, Akpait Fiord appears to show two acoustic units unique to its locality, a sedimentary sill-cover and a spillover deposit. With the exception of the acoustic units associated with specific features (deltas and sills), inner Boas Fiord and outer Akpait Fiord show a late- and postglacial sedimentary succession similar to what was previously interpreted for outer Sunneshine Fiord. Inner Durban Harbour appears distinctly different, in that glaciomarine sediments are largely absent and marine muds are extremely thin at the fjord head. This appears to be related to its smaller drainage basin and earlier deglaciation.

Radiocarbon dates from mollusc-shell samples corroborate the timings of deglaciation established by Margreth (2015). Moreover, the synchronous formation of Cowan's (2015) submerged deltas, and thus the postglacial lowstand, was ongoing at some point between 9.5–9.9 cal ka BP, which closely corresponds to the 9.5 cal ka BP transition between the Preboreal interstadial and the Cockburn Substage. Therefore, delta progradation may have either begun pre-9.5 cal ka BP and continued during the Cockburn and following HTM, or may have occurred in a single pre-9.5 cal ka BP pulse toward the end of the Preboreal. Kettle holes observed by Cowan in Kangert Fiord suggest an ice-proximal environment for delta progradation, making the latter hypothesis less likely. Additional dates from higher in the deltaic sediment column may better resolve the timeline of delta formation, and how its deposition varied from the late Preboreal and into or after the Cockburn Substage.

The sedimentation rates compared to other fjords indicate that an order-of-magnitude change in MSR can be associated with fjord deglaciation, as the supply of glaciomarine sediment is cut off. This transition appears to have occurred in Sunneshine Fiord at ~10.1 cal ka, but was not captured in the other Cumberland Peninsula fjords examined here.

3.8 References

Amundsen Science (2017). *CCGS Amundsen*: Capacity/scientific equipment. Retrieved from http://www.amundsen.ulaval.ca/capacity/scientific-equipment.php

Anderson, R.K., Miller, G.H., Briner, J.P., Lifton, N.A., & DeVogel, S.B. (2008). A millennial perspective on Arctic warming from ^{14}C in quartz and plants emerging from beneath ice caps. *Geophysical Research Letters*, 35: L01502. doi:10.1029/2007GL032057

Andrews, J.T. (1989). Postglacial emergence and submergence. In R.J. Fulton (Ed.), *Quaternary Geology of Canada and Greenland* (pp. 546-562). Geological Survey of Canada, *Geology of Canada*, 1. https://doi.org/10.4095/127905

Andrews, J.T., Barry, R.G., Bradley, R.S., Miller, G.H., & Williams, L.D. (1972a). Past and present glaciological responses to climate in eastern Baffin Island. *Quaternary Research*, 2(3): 303-314.

Andrews, J.T, & Ives, J. (1978). “Cockburn” nomenclature and the Late Quaternary history of the eastern Canadian Arctic. *Arctic and Alpine Research*, 10: 617–633.

Andrews, J.T., Jull, A.J.T., Donahue, D.J., Short, S.K., & Osterman, L.E. (1985). Sedimentation rates in Baffin Island fiord cores from comparative radiocarbon dates. *Canadian Journal of Earth Sciences,* 22: 1827-1834.

Andrews, J.T., Laymon, C.A., & Briggs, W.M. (1989). Radiocarbon date list III: Labrador and northern Quebec, Canada and radiocarbon date list VI: Baffin Island, N.W.T., Canada. *INSTAAR Occasional Paper No. 46,* University of Colorado, Boulder.

Andrews, J.T., Mears, A., Miller, G.H., & Pheasant, D.R. (1972b). Holocene late glacial maximum and marine transgression in the eastern Canadian Arctic. *Nature Physical Science,* 239 (96): 147–149.

Andrews, J.T., Osterman, L.E., Jennings, A.E., Syvitski, J.P.M., Miller, G.H., & Weiner, N. (1996). Abrupt changes in marine conditions, Sunneshine Fiord, eastern Baffin Island, NWT during the last deglacial transition: Younger Dryas and H-0 events. *Late Quaternary Palaeoceanography of the North Atlantic Margins,* Geological Society Special Publication No. 111: 11-27.

Andrews, J.T., Syvitski, J.P., Osterman, L.E., Williams, K.M., Mode, W.N., Kravitz, J.E. & Locke, W.W. III. (1994). *Quaternary geology of Sunneshine Fiord (Baffin Island).* Geological Survey of Canada, Open File 3004. doi:10.4095/195129

Bradley, R.S., Hughes, M.K., & Diaz, H.F. (2003). Climate in Medieval time. *Science,* 302: 404–405.

Briner, J.P., Bini, A.C., & Anderson, R.S. (2009a). Rapid early Holocene retreat of a Laurentide outlet glacier through an Arctic fjord. *Nature Geoscience,* 2: 496–499.

Briner, J.P., Davis, P.T., & Miller, G.H. (2009b). Latest Pleistocene and Holocene glaciation of Baffin Island, Arctic Canada: key patterns and chronologies. *Quaternary Science Reviews*, 28: 2075–2087.

Broom, L.M., Campbell, D.C., & Gosse, J.C. (2017). Investigation of a Holocene marine sedimentary record from Pond Inlet, northern Baffin Island, Nunavut. *Summary of Activities 2017,* Canada-Nunavut Geoscience Office, Iqaluit, 93-104.

Church, M. & Ryder, J.M. (1972). Paraglacial sedimentation: a consideration of fluvial processes conditioned by glaciation. *Geological Society of America Bulletin,* 83: 3059-3072.

Clark, J.A., Farrell, W.E., & Peltier, W.R. (1978). Global changes in postglacial sea level: A numerical calculation. *Journal of Quaternary Research,* 9: 265–287.

Clarke, D.B. & Upton, B.G.J. (1971). Tertiary basalts of Baffin Island: field relations and tectonic setting. *Canadian Journal of Earth Sciences,* 8: 248–258. https://doi.org/10.1139/e71-025

Cole, F. & Blakeney, C.P. (1984). Description and X-radiographs of the Baffin fjord cores. In J.P.M. Syvitski & C.P. Blakeney (Eds.), *Sedimentology of Arctic Fjords Experiment: HU 82-031 Data Report, Volume 1.* Geological Survey of Canada, Dartmouth, Open File 960. doi: 10.4095/129793

Courtney, B. (2012). *SEGYJP2Viewer* [computer software]. Natural Resources Canada; Geological Survey of Canada.

Coulthard, R. D., Furze, M.F.A., Pieńkowski, A.J., Nixon, F.C., & England, J.H. (2010). New marine ΔR values for Arctic Canada. *Quaternary Geochronology*, 5: 419–434.

Cowan, B. (2015). *Shorelines beneath the sea: Geomorphology and characterization of the postglacial sea-level lowstand, Cumberland Peninsula, Baffin Island, Nunavut*. Master's thesis: Memorial University of Newfoundland, Geography Department.

Cowan, B., Carter, J., Forbes, D.L., & Bell, T. (2021). Postglacial sea-level lowstand on Cumberland Peninsula, Baffin Island, eastern Arctic Canada. *Canadian Journal of Earth Sciences* (manuscript in review).

Dyke, A.S. (1979). Glacial and sea-level history of southwestern Cumberland Peninsula, Baffin Island, N.W.T., Canada. *Arctic and Alpine Research,* 11 (2): 179–202.

Dyke, A.S. (2013a). Surficial geology, Broughton Island–Padloping Island, Baffin Island, Nunavut, NTS 16-M, NTS 16-N, and parts of NTS 26-P. *Geological Survey of Canada, Canadian Geoscience Map 23* (ed. prelim.). doi:10.4095/288968

Dyke, A.S. (2013b). Surficial geology, Cape Dyer North, Baffin Island, Nunavut, NTS 16-L northeast and NTS 16-K northwest. *Geological Survey of Canada, Canadian Geoscience Map 22* (ed. prelim.). doi:10.4095/288967

England, J.H. & Andrews, J.T. (1973). Broughton Island—a reference area for Wisconsin and Holocene Chronology and sea-level changes on Eastern Baffin Island. *Boreas*, 2 (1): 17–32.

Folk, R.L. (1954). The distinction between grain size and mineral composition in sedimentary-rock nomenclature. *The Journal of Geology*, 62(4): 344-359.

Gajewski, K. (2015). Quantitative reconstruction of Holocene temperatures across the Canadian Arctic and Greenland. *Global and Planetary Change*, 128: 14–23.

Gilbert, R. (1978). Observations on oceanography and sedimentation at Pangnirtung Fiord, Baffin Island. *Maritime Sediments*, 14(1): 1-9.

Gilbert, R. (1982). Contemporary sedimentary environments on Baffin Island, N.W.T., Canada: Glaciomarine processes in fiords of eastern Cumberland Peninsula. *Arctic and Alpine Research*, 14(1): 1-12.

Gilbert, R. (1985). Quaternary glaciomarine sedimentation interpreted from seismic surveys of fiords on Baffin Island, N.W.T. *Arctic*, 38 (4): 271-280.

Gilbert, R. & MacLean, B. (1984) Geophysical studies based on conventional shallow and Huntec high resolution seismic surveys of fiords on Baffin Island. In J.P.M. Syvitski & C.P. Blakeney (Eds.), *Sedimentology of Arctic Fjords Experiment: HU 82-031 Data Report, Volume 1*. Geological Survey of Canada, Dartmouth, Open File 960. doi: 10.4095/129793

Google. (2021). *Google earth pro* (Version 7.3.3). https://www.google.com/earth/

Heaton, T.J., Kohler, P., Butzin, M., Bard, E., Reimer, R.W., Austin, W., Ramsey, C.B., Grootes, P.M., Hughen, K.A., Kromer, B., Adkins, J., Burke, A., Cook, M.S., Olsen, J., & Skinner, L.C. (2020). Marine20–the marine radiocarbon age calibration curve (0-55,000 cal BP). *Radiocarbon,* 62: 779-820. doi:10.1017/RDC.2020.68

Hein, F.J. & Longstaffe, F.J. (1984). Geotechnical sedimentology and mineralogical investigations in Arctic fjords. In J.P.M. Syvitski & C.P. Blakeney (Eds.), *Sedimentology of Arctic Fjords Experiment: HU 82-031 Data Report, Volume 1*. Geological Survey of Canada, Dartmouth, Open File 960. doi: 10.4095/129793

Hood, P. & Bower, M. (1975). Aeromagnetic reconnaissance of Davis Strait and adjacent areas [Abstract]. *Canada's Continental Margins and Offshore Petroleum Exploration,* 4: 433-451.

Hosseinpour, M., Müller, R.D., Williams, S.E., & Whittaker, J.M. (2013). Full-fit reconstruction of the Labrador Sea and Baffin Bay. *Solid Earth*, 4(2): 461-479. https://doi.org/10.5194/se-4-461-2013

Hughes Clarke, J.E., Muggah, J., Renoud, W., Bell, T., Forbes, D.L., Cowan, B., & Kennedy, J. (2015). Reconnaissance seabed mapping around Hall and Cumberland peninsulas, Nunavut: opening up southeastern Baffin Island to nearshore geological investigations. *Summary of Activities 2014*. Canada-Nunavut Geoscience Office: 133-144.

Jennings, A. (1993). The Quaternary history of Cumberland Sound, southeastern Baffin Island: The marine evidence. *Géographie physique et Quaternaire*, 47 (1): 21-42.

Jennings, A.E., Tedesco, K.A., Andrews, J.T., Kirby, M.E., 1996. Shelf erosion and glacial ice proximity in the Labrador Sea during and after Heinrich events (H-3 or -4 to H-0) as shown by foraminifera. *Geological Society, London, Special Publications*, 111: 29–49.

Kaplan, M.R. & Miller, G.H. (2003). Early Holocene delevelling and deglaciation of the Cumberland Sound region, Baffin Island, Arctic Canada. *Geological Survey of America Bulletin*, 115 (4): 445–462.

Kaufman, D.S., Ager, T.A., Anderson, N.J., Anderson, P.M., Andrews, J.T., Bartlein, P.J., Brubaker, L.B., Coats, L.L., Cwynar, L.C., Duvall, M.L., Dyke, A.S., Edwards, M.E., Eisner, W.R., Gajewski, K., Geirsdóttir, A., Hu, F.S., Jennings, A.E., Kaplan, M.R., Kerwin, M.W., ... Wolfe, B.B. (2004). Holocene thermal maximum in the western Arctic (0–180°W). *Quaternary Science Reviews*, 23: 529–560.

Keen, C.E. & Beaumont, C. (1990). Geodynamics of rifted continental margins. In M.J. Keen & G.K. Williams (Eds.), *Geology of the Continental Margin of Eastern Canada* (pp. 391-474). Geological Survey of Canada, *Geology of Canada*, 2. https://doi.org/10.4095/132690

Kessler, M.A., Anderson, R.S., & Briner, J.P. (2008). Fjord insertion into continental margins driven by topographic steering of ice. *Nature Geoscience*, 1: 365-369.

Kontopoulos, N. & Piper, D.J.W. (1982). Storm graded sand at 200 m water depth, Scotian Shelf, eastern Canada. *Geo-Marine Letters*, 2(1-2): 77-81. https://doi-org /10.1007/BF02462804

Lamb, H.H. (1965). The early medieval warm epoch and its sequel. *Palaeogeography, Palaeoclimatology, Palaeoecology*, 1: 13–37.

MacLean, B. & Falconer, R.K.H. (1979). Geological/geophysical studies in Baffin Bay and Scott Inlet-Buchan Gulf and Cape Dyer-Cumberland Peninsula areas of the Baffin Island Shelf. *Geological Survey of Canada*, Paper 79-1B: 231–244. https://doi.org/10.4095/105432

MacLean, B. Williams, G.L., Jennings, A.E. & Blakeney, C. (1986). Bedrock and surficial geology of Cumberland Sound, N.W.T. *Current Research Part B*. Geological Survey of Canada, Paper 86-1B: 605-615. doi:10.4095/120622

MacLean, B., Williams, G.L., & Srivasta, S.P. (1990). Geology of the Labrador Shelf, Baffin Bay, and Davis Strait. Part 2: Geology of Baffin Bay and Davis Strait. In M.J. Keen & G.K. Williams (Eds.), *Geology of the Continental Margin of Eastern Canada* (pp. 293-350). Geological Survey of Canada, *Geology of Canada*, 2. https://doi.org/10.4095/132690

Manley, W.F. & Jennings, A.E. (1996). Radiocarbon date list VIII: Eastern Canadian Arctic, Labrador, northern Quebec, East Greenland Shelf, Iceland Shelf, and Antarctica. *INSTAAR Occasional Paper No. 50*, University of Colorado, Boulder.

Margreth, A. (2015). Climate sensitivities of polythermal ice sheet, ice cap, and alpine ice dynamics and related episodic erosion on Cumberland Peninsula, Baffin Island, Nunavut. Doctoral dissertation: Dalhousie University, Department of Earth Sciences.

Miller, G.H. & Dyke, A.S. (1974). Proposed extent of late Wisconsin Laurentide Ice on Eastern Baffin Island. *Geology,* 2 (3): 125–130.

Miller, G.H., Lock, W.W., III, & Locke, C.W. (1980). Physical characteristics of the southeastern Baffin Island coastal zone. In S.B. McCann (Ed.), *The Coastline of Canada*: *Littoral Processes and Shore Morphology*. Geological Survey of Canada. Paper 80-10, 251-265. https://doi.org/10.4095/102212

Miller, G.H., Wolfe, A.P., Briner, J.P., Sauer, P.E., & Nesje, A. (2005). Holocene glaciation and climate evolution of Baffin Island, Arctic Canada. *Quaternary Science Reviews,* 24: 1703–1721.

Miller, G.H., Geirsdóttir, Á., Zhong, Y., Larsen, D.J., Otto-Bliesner, B.L., Holland, M.M., Bailey, D.A., Refsnider, K.A., Lehman, S.J., Southon, J.R., Anderson, C., Björnsson, H., & Thordarson, T. (2012). Abrupt onset of the Little Ice Age triggered by volcanism and sustained by sea-ice/ocean feedbacks. *Geophysical Research Letters,* 39: L02708.

Natural Earth. (2017). *Downloads*. [Shapefiles]. Retrieved October 30, 2017, from https://www.naturalearthdata.com/downloads/

Natural Resources Canada. (2017). *Expedition 82031*. [Data file]. Available from http://ed.gdr.nrcan.gc.ca/index_e.php

Normandeau, A. & Dietrich, P. (2019). *Distribution of potentially active turbidity currents in eastern Baffin Island fiords*. Geological Survey of Canada, Open File 8512, 1 sheet. doi:10.4095/314733

Normandeau, A. Dietrich, P., Hughes Clarke, J., van Wychen, W., Lajeunesse, P., Burgess, D. & Ghienne, J.F. (2019a). Retreat pattern of glaciers controls the occurrence of turbidity currents on high-latitude fjord deltas (eastern Baffin Island). In *The Arctic*, an AGU joint special collection. *Journal of Geophysical Research, Earth Surface*, 124 (6): 1559-1571. doi:10.1029/2018JF004970

Normandeau, A., Robertson, A.G., Philibert, G., Regular, K. & Sedore, P. (2019b). *R/V Nuliajuk expedition 2019Nuliajuk: marine geohazards near Qikiqtarjuaq, Padle Fiord, Southwind Fiord and Pangnirtung, southeast Baffin Island, Nunavut.* Geological Survey of Canada, Open File 8641. doi:10.4095/315676

Normandeau, A., Broom, L.M., Carson, T. & Trottier, A.-P. (2019c). *CCGS Amundsen 2019804 expedition: marine geohazards and sediment transport processes in Baffin Bay, Nunavut.* Geological Survey of Canada, Open File 8649.doi:10.4095/321054

Pheasant, D.R. & Andrews, J.T. (1973). Wisconsin glacial chronology and relative sea-level movements, Narpaing Fiord Broughton Island area, eastern Baffin Island, N.W.T. *Canadian Journal of Earth Sciences,* 10 (11): 1621–1641.

Piper, D.J. & Normark, W.R. (2009). Processes that initiate turbidity currents and their influence on turbidites: a marine geology perspective. *Journal of Sedimentary Research*, 79 (6): 347-362. https://doi.org/10.2110/jsr.2009.046

Rasmussen, S.O., Andersen, K.K., Svensson, A., Steffensen, J.P., Vinther, B.M., Clausen, H.B., Sigaard-Andersen, M.-L., Johnsen, S.J., Larsen, L.B., Dahl-Jensen, D., Bigler, M., Röthlisberger, Fischer, H., Goto-Azuma, K., Hansson, M.E., & Ruth, U. (2006). A new Greenland ice core chronology for the last glacial termination. *Journal of Geophysical Research*, 111: 1–16

Sanborn-Barrie, M. & Young, M. (2013). Geology, Durban Harbour, Baffin Island, Nunavut. *Geological Survey of Canada, Canadian Geoscience Map 38* (ed. prelim.). doi:10.4095/292015

Sanborn-Barrie, M., Young, M., Keim, R., & Hamilton, B. (2013). Geology, Sunneshine Fiord, Baffin Island, Nunavut. *Geological Survey of Canada, Canadian Geoscience Map 6* (ed. prelim.). doi:10.4095/288931

Stanford, J.D., Rohling, E.J., Bacon, S., Roberts, A.P., Grousset, F.E.,& Bolshaw, M. (2011). A new concept for the paleoceanographic evolution of Heinrich event 1 in the North Atlantic. *Quaternary Science Reviews*, 30: 1047-1066.

St-Hilaire-Gravel, D., Forbes, D.L., and Bell, T.(2015). Evolution and morphodynamics of a prograded beach-ridge foreland, northern Baffin Island, Canadian Arctic Archipelago. *Geografiska Annaler A*, 97(3): 615-631, doi:10.1111/geoa.12103.

St-Onge, M.R., Harrison, J.C., Paul, D., Tella, S., Brent, T.A., Jauer, C.D., and Maclean, B.C. (2015). Tectonic map of Arctic Canada. *Geological Survey of Canada, Canadian Geoscience Map 187* (ed. prelim.). doi: 10.4095/295945

Stuiver, M., Reimer, P.J., & Reimer, R.W. (2021). *CALIB 8.2* [www program]. http://calib.org/calib/

Syvitski, J.P.M. (Compiler). (1985). *Sedimentology of Arctic Fjords Experiment: HU 83-028 Data Report, Volume 2.* Geological Survey of Canada, Dartmouth, Open File 1122. doi: 10.4095/129977

Syvitski, J.P.M., & Blakeney, C.P. (Compiler). (1984). *Sedimentology of Arctic Fjords Experiment: HU 82-031 Data Report, Volume 1.* Geological Survey of Canada, Dartmouth, Open File 960. doi: 10.4095/129793

Syvitski, J.P.M., Burnell, D.C., & Skei, J.M. (1987). *Fjords: Processes and products*. Springer-Verlag: New York.

Syvitski, J.P.M. & Hein, F.J. (1991). *Sedimentology of an Arctic basin: Itirbilung Fiord, Baffin Island, Northwest Territories.* Geological Survey of Canada Paper 91-11. doi: 10.4095/132684

Syvitski, J.P.M., & Praeg, D.B. (Compilers). (1987). *Sedimentology of Arctic Fjords Experiment: Data Report, Volume 3.* Geological Survey of Canada, Dartmouth, Open File 1589. doi: 10.4095/130318

Syvitski, J.P.M., Schafer, C.T., Asprey, K.W., Hein, F.J., Hodge, G.D., & Gilbert, R. (1986). *Sedimentology of Arctic Fjords Experiment: PA-85-062 Expedition report*. Geological Survey of Canada, Open File 1234. doi:10.4095/130052

Telka, A. (2015). *Expedition 2014805 Baffin Island shell dating report* [contract research report, unpublished]. Paleotec Services.

Telka, A. (2016). *Expedition 2014805 Baffin Island shell dating report* [contract research report, unpublished]. Paleotec Services.

Yang, Y., Maselli, V., Normandeau, A., Piper, D.J., Li, M.Z., Campbell, D.C., Campbell, C., Gregory, T. & Gao, S. (2020). Latitudinal response of storm activity to abrupt climate change during the last 6,500 years. *Geophysical Research Letters*, 47(19). https://doi.org/10.1029/2020GL089859

CHAPTER 4: SUMMARY AND CONTRIBUTIONS

The presented thesis has advanced our knowledge of the fjord environments of Baffin Island. Fjords are distinctly larger along the northeast coast than on Cumberland Peninsula, attributable to excavation by outlet glaciers fed by the Laurentide Ice Sheet. The sedimentary record of Cumberland Peninsula fjords displays the archetypal pattern for Canadian east-coast fjords (ice-contact, glaciomarine, and marine units), in addition to local facies associated with specific sedimentary features (deltas, sills, and spillover deposit). New radiocarbon dates, combined with Cowan's (2015) earlier interpretation, associates the postglacial lowstand with the Preboreal-Cockburn transition (9.5 cal ka BP). Overall, this thesis provides perhaps the first dataset of modern fjord morphometrics for the Canadian Arctic and the first detailed acoustic description of Cumberland Peninsula fjords, and adds new calibrated radiocarbon dates to the chronology of Cumberland Peninsula. The current results can contribute to testing models of fjord origin and development and guide future sediment coring.

4.1 Summary

Combining multibeam bathymetry, acoustic subbottom profiles, and sediment cores from Baffin Island fjords with previously published data, this study aimed to further our understanding of fjord morphology and the postglacial sedimentary record, with a particular focus on the less-documented, smaller fjords of the eastern Cumberland Peninsula. The study had two main objectives:

(1) to assess the influence of ice source on the morphometric parameters (such as orientation, sinuosity, length, width, and depth) of Baffin Island fjords, in particular whether the

fjords of Cumberland Peninsula can be distinguished statistically from those formed by outlets from the Laurentide Ice Sheet (LIS); and

(2) to interpret the deglacial and postglacial sedimentary record of selected Cumberland Peninsula fjords, including maximum and minimum age constraints for the postglacial lowstand (Cowan, 2015) via radiocarbon dating.

The character of Baffin Island fjords has been found through statistical analyses to vary along the coastline. The northeast coast (NC) and Cumberland Peninsula (CP) regions appear to contain two morphometrically-distinct fjord populations, as the NC group shows significantly greater length, width, depth, and drainage-basin area. Fjord orientation is also significantly different, with the NC fjords mainly orientated toward the north-northeast (27°) within a relatively narrow range (-22° to 57°), while CP fjords were mainly oriented towards the east (96°) within a far wider range (-19° to 214°). However, no significant differences were found for sinuosity, maximum sidewall elevation, and maximum drainage-basin elevation. The larger fjord dimensions appear to be attributable to the larger ice-source, with the Laurentide Ice Sheet (LIS) feeding larger (more erosive) outlet glaciers than the combined Penny Ice Cap (PIC) and Local Alpine Glaciation (LAG). This is supported by the strong correlation between fjord and drainage-basin area found across Baffin Island (Spearman's $r_s^2 = 0.72$), which suggests that (potential) ice supply controls overall fjord size. Meanwhile, the difference in dominant orientation is attributable to the different glacial-flow patterns of the two ice sources: the unidirectional NNE flow of the LIS northeast margin, versus the outward-radial flow of the PIC-LAG complex. Overall, the above findings lead to the interpretation that glacial erosion controls the development of fjord dimensions (length, width, and depth), while geology and tectonics control other properties of the fjord's preglacial environment (sinuosity and maximum elevation). Fjord orientation appears to be influenced by both glacial and geologic controls; most glacial valleys and fjords follow pre-existing structural lineations, yet structural-lineation maps for Cumberland Peninsula show some exceptions (Dyke et al., 1982). Thus, ice flow is evidently capable of overriding structural control in the carving of fjords.

Select fjords from Cumberland Peninsula (Boas Fiord, Durban Harbour, Akpait Fiord, and Sunneshine Fiord) were found to contain a stratigraphic sequence of: ice-contact, glaciomarine, and marine/post-submergence units, with additional acoustic facies associated with local sedimentary features. These local features include submerged deltas in Boas and Durban, and weakly-stratified sill cover and spillover (highly stratified unit with strong, disturbed reflectors) facies in Akpait Fiord. With the exception of the acoustic units associated with specific geomorphic features (deltas, sills, and spillover deposits), inner Boas Fiord and outer Akpait Fiord both show a similar sedimentary succession to that previously interpreted for outer Sunneshine Fiord (Andrews et al., 1994, 1996). Durban Harbour appears to be slightly different, in that glaciomarine sediments and marine muds are extremely thin at the fjord head; this lack of fine-grained sediments and a low mean sedimentation rate may be related to Durban Harbour's smaller drainage basin and earlier deglaciation.

Radiocarbon dating of deltaic and post-submergence sediments via mollusc-shell samples constrained the timing of the postglacial lowstand described by Cowan (2015) to sometime between 9.9 – 9.5 and 2.0 – 1.4 cal ka BP. The maximum age constraint was retrieved from bottomset deltaic sediments deposited during active delta progradation, at the head of Durban Harbour. The minimum age constraint was extrapolated downwards from a shell sample retrieved from post-submergence muds, using the mean sedimentation rate; it is most likely an underestimate, as the true sedimentation rate most likely declines with depth below the seabed, as the corresponding palaeo-sea-level reduces to zero. Earlier, Cowan had constrained the postglacial lowstand to sometime between 11.7 and 8.5 cal ka BP, as some deltas along the tilted shoreline are indicative of ice-proximal and ice-contact environments (Dyke, 1979; Cowan, 2015). Therefore, the maximum age constraint established by this study (9.9 – 9.5 cal ka BP) indicates that delta formation during the postglacial lowstand was initiated prior to the Preboreal-Cockburn transition at 9.5 cal ka BP. It seems unlikely that delta progradation occurred in a single pulse towards the end of the Preboreal, but how the rate of delta progradation may have varied during the Cockburn and following the Holocene Thermal Maximum (HTM, Table 3.1) currently remains unknown.

The radiocarbon dating of mollusc-shell samples allowed mean sedimentation rates (MSRs) to be calculated for some sediment cores. For the current study, these rates ranged from 0.22 to 2.99 mm/yr, with a median value of 0.93 mm/yr. Sunneshine Fiord was unique among the fjords studied in that it displayed an order-of-magnitude decrease in MSR (from $1.66^{+\infty}_{-1.29}$ to $0.30^{+0.13}_{-0.05}$ mm/yr) at ~10.1 cal ka BP (377 cm in core SU5). Based on comparisons to the MSR curves of Clark, McBeth, Tingin, and Coronation fjords (Andrews, 1987, 1990; Syvitski, 1989), the sedimentation rate in Sunneshine Fiord likely declined when the glacier fully retreated from the fjord waterbody and thus reduced the glaciogenic sediment supply. This interpretation is in line with Margreth's (2015) mapping of glacial retreat. None of the cores from the present study penetrated deep enough to intersect the corresponding change in sedimentation rate in Boas or Akpait fjords; although the Durban core may have penetrated ice-contact sediment, its MSR curve is constructed from only one sample (~9.6 cal ka BP) and thus lacks the resolution to inform on MSR changes. Nonetheless, the low MSR for Durban Harbour, combined with the lack of observable glaciomarine or marine acoustic facies at the fjord head, strongly suggests that mean sedimentation was lower in Durban Harbour than the other study sites.

4.2 Contributions

Overall, this thesis contributes new data on Baffin Island fjord morphology, and the sedimentary records of previously unexplored fjords in Cumberland Peninsula. Specifically, this thesis:

- Presents a morphometric dataset of up to 13 parameters for 29 fjords along the northeast coast of Baffin Island and Cumberland Peninsula, which provides a basis for comparing fjords across Baffin Island and elsewhere. Previous morphometric datasets on Baffin Island fjords were provided by Gilbert and MacLean (1984) and Dowdeswell and Andrews (1985); however, the current dataset covers more fjords than the former and is likely better defined than either, due to the use of digital mapping and multibeam bathymetric data.
- Describes the sedimentary record of three fjords on eastern Cumberland Peninsula. As a result, it adds to our understanding of deglacial and postglacial deposition in Baffin Island fjords, specifically those occupied by local alpine glaciers during and since the last glacial maximum.
- Provides new calibrated radiocarbon dates for submerged sediments around Cumberland Peninsula, adding to the regional radiocarbon record and establishing age control for the postglacial lowstand in the eastern Canadian Arctic described by Cowan (2015).
- Calibrates radiocarbon dates previously reported for Sunneshine Fiord (Andrews et al., 1989; Manley & Jennings, 1996) using modern correction factors (Coulthard et al., 2010; Heaton et al., 2020; Stuiver et al., 2021).

4.3 Future Work

The collected morphometry data may be useful in studying other aspects of fjord science. For example, the degree of association between fjord orientation and adjacent fault strikes could be statistically tested. The interaction between postglacial sedimentation and fjord length could be investigated by delimiting the portion of each drainage basin that empties through the fjord head, and comparing the area of said portion, and the number of streams and lakes within it, to fjord length. Investigating the relationship between fjord and drainage-basin areas could involve grouping drainage basins into classes by areal size, and documenting evidence of valley capture through glacial erosion (e.g., cols/saddles, the number of tributary fjords and valleys compared to the size of the local ice source). Other data that have been collected, but not published in this thesis, could be used to investigate how the complexity of fjord systems (fjord + tributaries) varies across Baffin Island, by analyzing the distribution and frequency of tributary fjords versus hanging valleys.

Both the morphometric and acoustic-facies data compiled in this thesis can be used in assessing models of fjord development. The physical dimensions documented in Chapter 2 provide an empirical standard in assessing the outputs of models simulating fjord origin and growth via glacial erosion, especially in respect to how fjord size is influenced by drainage basin and ice source size. Meanwhile, the acoustic records can be used to assess fjord-sediment-accumulation models, especially when modelling fjords associated with alpine glaciation.

Additional research can further develop the fjord-morphometry database presented in this thesis. Priorities include updating the data imported from Gilbert and MacLean (1984) with modern measurements and expanding the database to include all fjords from the northeast coast and

Cumberland Peninsula. Doing so would improve the quality of the database and allow statistical analyses of both fjord populations, rather than samples. Increased sample sizes could confirm that the current results are free from sampling error (i.e., bathymetric surveys may have favoured larger fjords), and allow statistical comparison of fjords associated with the Penny Ice Cap versus local alpine glaciers. Eventually, the dataset could be expanded to include all Baffin Island fjords, and additional parameters listed by Gilbert and MacLean (1984) and Dowdeswell and Andrews (1985) but excluded from this thesis. This could also include a topographic assessment of how directly each fjord along the northeast coast connects to the LIS hinterland; this could identify other potential exceptions to the overall trend like Dexterity Fiord, and add another dimension to the overall assessment of glacial versus structural/topographic control on fjord morphology.

Ideally, expanding the morphometry database as described above would coincide with expanded multibeam bathymetry coverage of Baffin Island fjords. Currently, multiple fjords lack available bathymetry (e.g. Sunneshine Fiord) while others have limited coverage (e.g. Kangiqtualuk Uqquqti, outer Boas Fiord, and Totnes Road). Expanded bathymetric coverage would resolve some uncertainties in maximum fjord depth, and facilitate reliable seafloor-width measurements and calculations of depth-to-width and surface-to-seafloor width ratios.

The sedimentary succession described for Cumberland Peninsula fjords can also be expanded. The acoustic subbottom profiles analyzed in this thesis were selected primarily based on proximity to the coring sites, leaving the down-fjord environments of Boas Fiord and Durban Harbour under-analyzed. Similarly, a large repository of modern acoustic profiles for several Baffin Island fjords also remains to be interpreted. Studying these remaining profiles could reveal how sedimentary environments compare away from the fjord head, how sedimentary facies vary throughout Cumberland Peninsula, and how sediment thickness and the distribution of acoustic facies indicative of local processes (e.g., mass flows and ice-deformed sediment) differs between Cumberland Peninsula and the northeast coast. In addition, acoustic subbottom profiles are yet to be collected for inner Akpait Fiord and multiple other fjords.

The collection of additional sediment cores and radiocarbon dates could refine mean sedimentation rate (MSR) curves, better illustrating past environmental changes and broadening our understanding of the postglacial lowstand timing. At Durban Harbour specifically, additional dates from higher in the deltaic sediment (for which fossils were absent in the cores studied) may better resolve the timeline of delta formation and how sedimentation rates may have varied before, during, and after the Cockburn Substage. Additional radiocarbon-dated shell samples from the other study sites, regardless of their position in the sediment column, would better resolve the current MSR curves. In addition, vibra-coring of the seafloor in Akpait Fiord may be necessary to achieve the sediment penetration required to test the subaerial-sill hypothesis.

The coring and dating of other submerged deltas throughout Cumberland Peninsula could test the synchronicity of delta formation during the postglacial lowstand, in addition to improving the chronological record of the peninsula. This thesis attempted to establish a maximum and a minimum age constraint by targeting the deltaic bottomset beds and the post-submergence muds on the delta terrace, respectively. However, the minimum age constraint from the post-submergence muds appears to be a clear underestimate.

Therefore, in order to test the synchronicity of the postglacial lowstand throughout Cumberland Peninsula, future coring should target the bottomset beds of other submerged deltas and assess how the oldest recoverable dates (ideally near the ice-contact unit) compare to sample DH6 210-212 cm (~9.6 cal ka BP). Older samples (e.g., ~11.7 cal ka BP) may indicate deltas that formed immediately following the Younger Dryas, while younger samples (<9.5 cal ka BP) may indicate that delta formation continued during the Cockburn Substage or resumed afterwards. In Boas Fiord, the prodelta marine muds appear to be thicker (~12 m) than the piston corer previously carried by the *CCGS Amundsen*, so vibra-coring of the potentially coarse-grained delta slope may be advisable. Vibra-coring is also advisable for deeper penetration in Durban Harbour, to test whether the bottoms of cores DH1 and DH6 contacted glacial till or ice-rafted deposits.

Alternatively, future coring might still target the delta terrace. If multiple dates are returned from one post-submergence facies, they may inform on how the MSR changed over time and thus enable a more accurate age extrapolation for the delta contact. Vibra-coring could be used to sample the likely coarse-grained delta topsets, but mollusc fossils may prove scarcer in this environment.

4.4 Comparison to other Baffin Island fjords:

This thesis has, in part, assessed the extent to which Cumberland Peninsula fjords differ from the wider population of Baffin Island fjords.

Studies by Syvitski (1985) and Gilbert (1985) surveyed fjords throughout Baffin Island, and interpreted an overall sedimentary sequence of: ice-contact till → glaciomarine sediment → hemipelagic sediment. This largely parallels the sequence observed in the study sites, minus deltaic sediments. However, Gilbert describes subunits of glaciomarine sediment (lower and upper stratified subunits separated by an unstratified subunit), which are not observed in the study sites. Other distinctions between the thesis study sites and the other Baffin Island fjords are observed in sediment thickness, mean sedimentation rates, and submerged features.

4.4.1 Sediment thickness

This thesis hypothesized that the fjords of Cumberland Peninsula will differ from the rest of Baffin Island sedimentologically, just as they do morphologically. This appears to have already been confirmed by Gilbert (1985), who reported northern fjords as having larger sediment accumulations than southern fjords, which includes North Pangnirtung, Coronation, and Maktak of Cumberland Peninsula. Direct comparisons of sediment thickness between earlier studies (Gilbert & MacLean, 1984; Gilbert, 1985) and this thesis are complicated by changes in acoustic profiling equipment, with modern imagery not penetrating as deep. In addition, this thesis has focused its analysis on specific study sites within Boas, Durban, and Akpait, rather than the full fjord lengths surveyed by Gilbert and MacLean. Nonetheless, a few tentative comparisons can be made using current data from the study sites.

The maximum-known sediment thicknesses from Cumberland Peninsula study sites range from 21 to 35 m (Table 4.1). This range of max sediment thickness is comparable to the maximum thickness in North Pangnirtung Fiord (36 m), but is well below the values for the remaining Cumberland Peninsula fjords surveyed, Maktak (58 m) and Coronation (94 m). In comparison, the maximum sediment thicknesses for fjords along the northeast coast of Baffin Island are known to range between 83 and 174 m (Gilbert, 1985). Thus, it appears that Cumberland Peninsula fjords show overall thinner sediment deposits than elsewhere along Baffin Island, in keeping with expectations that the larger LIS-fed glaciers would have transported more sediments than the smaller PIC-LAG glaciers.

Table 4.1: Maximum (known) sediment thicknesses from fjords in Cumberland Peninsula and the northeast coast.

Region	Fjord	Maximum (known) sediment thickness (m)	Feature / Environment	Source
Cumberland Peninsula	Boas	≥ 34	Inner fjord; delta slope and prodelta	This study
	Durban	≥ 21	Inner fjord; delta slope and prodelta	
	Akpait	≥ 26	Outer fjord; spillover deposit	
	Sunneshine	≥ 35	Outer fjord basin	
	North Pangnirtung	36	Outer fjord basin	SAFE (Gilbert, 1985)
	Coronation	94	Innermost fjord (head)	
	Maktak	58	Inner and outer fjord basins	
Northeast Coast	Tingin	94	Outer fjord (mouth); adjacent to sill	
	Itirbilung	131	Inner fjord basin	
	McBeth	174	Mid-fjord basin	
	Inugsuin	83	Mid-fjord basin	
	Clark	131	Outer fjord basin	
	Cambridge	171	Outer fjord basin	

4.4.2 Sedimentation rates

Table 4.2 combines data from this thesis and other studies to summarize mean sedimentation rates for multiple Baffin Island fjords. Based on the mean sedimentation rates calculated from previously reported ^{14}C dating, it appears that mean sedimentation rates in Cumberland Peninsula fjords are comparable to those along the northeast coast of Baffin Island. While some northeast fjords (Clark and Tingin) show higher maximums and wider ranges, overall there is a considerable amount of overlap between the two regions.

However, much of the chronology data outside of the study sites comes from less accurate acid-insoluble organic-matter samples, and not all of them were corrected to shell-equivalent (Andrews et al., 1986; Andrews, 1987, 1990; Gilbert et al., 1990). Moreover, none of these additional dates are currently calibrated to modern standards. Comparison is also complicated by how some MSR intervals cover non-comparable periods of time. For example, the CO-2 and BF4 rates average time intervals of ~0.74 and ~0.91 kyr, respectively, while the IT1.1 and DH6 rates average ~3.5 and ~9.6 kyr (Appendix D). If additional dates from these cores were available, it would be possible to better assess how the MSR varied throughout the length of each core.

Barring complicating factors, mean sedimentation rate is expected to be highest near the fjord head, the main point-source of sediment, and to decrease with distance until reaching a local minimum at the fjord mouth. Data on the inner-fjord positions is lacking compared to central- and outer-fjord positions, both in terms of fjords cored and number of dates per core. Nonetheless, MSR decreases between the inner/central and outer regions are observed in McBeth and Itirbilung. Core AF3 defies this expectation but is omitted from this discussion as anomalous since no other fjords were cored at spillover deposits.

Across the inner-fjord regions, Itirbilung shows a higher MSR than Boas, which is much higher than Durban. This is reasonable, as the fjord heads of Boas and Itirbilung both show active fluvial input of sediment while Durban appears to be fluvially inactive (Google, 2021). That MSR is higher in Itirbilung than Boas may be attributable to its larger drainage basin (Table 3.14). Thus, it appears that in terms of inner-fjord MSR, CP fjords are comparable to NC fjords where fluvial conditions are similar, but remain limited by their smaller drainage basins.

Across the central-fjord regions the two highest max MSRs are shown by Clark and Coronation fjords. This could suggest that central-fjord sedimentation is similar between Cumberland Peninsula and the northeast coast. However, it must be noted that the central-Coronation rate only averages the period since ~0.74 cal ka BP, and thus was likely influenced by the tidewater glacier (fed by the Penny Ice Cap) occupying the fjord. In contrast, the central-Clark rates all average intervals >1 kyr, with the maximum rate (5.21 mm/yr) dated to the 5.8 – 7.4 cal ka BP interval, which corresponds with the HTM and is thus attributable to deglaciation. As a result, it is difficult to compare central-fjord MSR across Cumberland Peninsula and the northeast coast without comparable time scales. The remaining fjords with central-region MSR data are McBeth and Cambridge, deglaciated fjords with larger drainage basins than Coronation, yet lower max MSR. Yet again, the MSRs being compared average significantly different intervals of time.

Across the outer-fjord regions, Sunneshine has a higher max MSR rate than most of the northeast coast fjords. This max rate of 2.99 mm/yr (12.0 – 11.4 cal ka BP) may reflect a pulse of post-YD ice retreat. Similarly, the maximum MSRs in outer Tingin (4.49 mm/yr during 8.7 – 7.1 cal ka BP) and outer Itirbilung (1.31 mm/yr during 5.8 – 3.7 cal ka BP) can be loosely associated with the HTM, indicating sediment influxes from post-Cockburn ice retreat and the effects of terminal HTM warming, respectively. Ultimately, given how the maximum MSR for Sunneshine falls within the range defined by the max MSRs for the northeast coast fjords, the collected data indicates that there is no difference in sedimentation rates at the fjord mouth between Cumberland Peninsula and northeast coast fjords of Baffin Island.

Table 4.2: Summary table of sedimentation rates across Baffin Island.

Region	Fjord	Fjord area (km^2)	Drainage-basin area (km^2)	Mean sedimentation rate (mm/yr) by position per fjord* Inner	Central	Outer	Source
Cumberland Peninsula	Boas	116	1138	1.14	-	-	This thesis.
	Durban	45	206	0.22	-	-	”
	Akpait†	38	247	-	-	0.57 – 0.98	”
	Sunneshine	121	569	-	-	0.29 – 2.99	”
	Coronation	131	1128	-	3.6	-	E) ^{14}C dated organics.
	Min (Mean) Max =			0.22 (0.68) 1.11	3.6	0.29 (0.94) 2.99	
Northeast Coast	Cambridge	193	2013	-	1.24 [D], 1.32 [C]	-	C & D) ^{14}C dated organics.
	Clark	434	1895	-	0.28 – 5.21	-	A) ^{14}C dated organics corrected to shell-equivalent.
	McBeth	402	3548	-	0.34 – 1.24	0.10 – 0.50	B) ^{14}C dated organics corrected to shell-equivalent.
	Itirbilung	162	2184	1.69	-	0.28 – 1.31	B) ^{14}C dated organics and shells.
	Tingin	218	1228	-	-	0.5 [C]; 0.38 – 4.49 [B]	B) ^{14}C dated organics corrected to shell-equivalent C) ^{14}C dated organics.
	Min (Mean) Max =			1.69	0.28 (1.33) 5.21	0.10 (1.09) 4.49	

Sources: A) Andrews (1987) B) Andrews (1990) C) Andrews et al. (1986) D) Gilbert et al. (1990) E) Syvitski (1989)

*Mean sedimentation rates calculated using only the median radiocarbon age.

†MSRs for the spillover deposit (core AF3) are excluded as anomalous.

The order-of-magnitude MSR change observed in Sunneshine Fiord has also been observed in sediment cores from other fjords. Previous studies have also reported radiocarbon dates from Baffin Island fjords via sediment cores (e.g., Andrews, 1987, 1990; Syvitski, 1989; Deering et al., 2018). When the reported radiocarbon dates are graphed (Fig. 4.1), they indicate that a significant MSR change occurred between 8.7 and 5.8 cal ka BP for McBeth, Tingin, and Clark Fiord. In contrast, Coronation Fiord shows a high MSR, comparable to the earlier rates for Clark and Tingin fjords, approaching the modern day. In addition, it is observed that Clark, McBeth, and Tingin Fiords are deglaciated, while Coronation Fiord contains a modern tidewater glacier. Therefore, these observations suggest that the order-of-magnitude MSR change observed in Sunneshine and other fjords in fact reflects the timing of ice-retreat from the fjord, rather than the effects of a single palaeoclimate event. This is further supported by the observation that the MSR change occurs at different dates for different fjords. Based on the dates available, Sunneshine Fiord appears to have deglaciated before McBeth, Clark, and Tingin fjords. It must be noted that the radiocarbon dates reported by Andrews (1987, 1990) and Syvitski (1989) are derived from bulk organic content instead of shells and are uncalibrated. Thus, the dates and MSRs are likely less accurate than those reported from Sunneshine. Nonetheless, these examples illustrate how MSR changes over time with the retreat of the glacier.

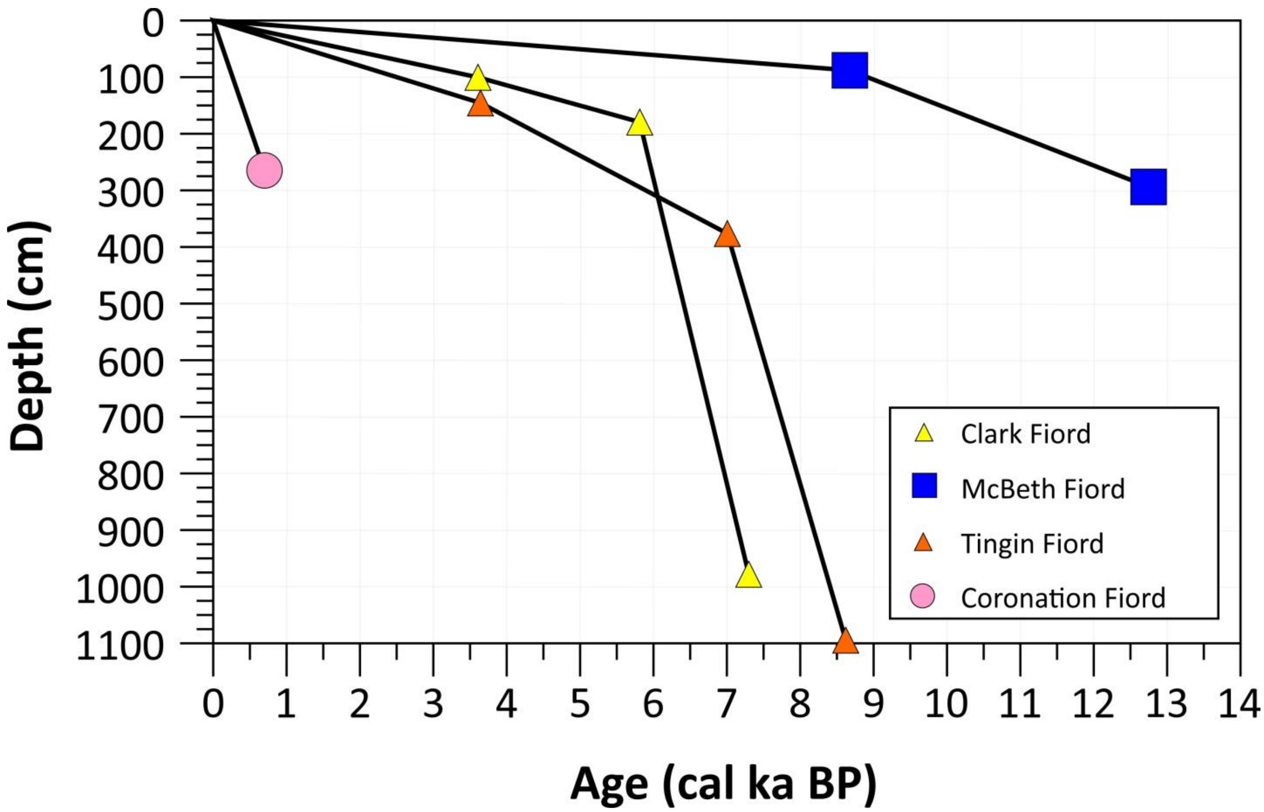

Figure 4.1: Graph comparing the MSR curves for sediment cores collected from Clark Fiord (CL5; Andrews, 1987), McBeth Fiord (MC83.6; Andrews, 1990), Tingin Fiord (TI3; Andrews, 1990), and Coronation Fiord (CO2; Syvitski, 1989). Clark, McBeth, and Tingin fjords were previously glaciated by the LIS. Coronation Fiord, which shows a proglacial sedimentation rate, currently contains a tidewater glacier fed by the PIC.

4.4.3 Submerged features

A core focus of this thesis has been on the sedimentology of submerged deltas in Boas Fiord and Durban Harbour of Cumberland Peninsula.

The NE Baffin coast is expected to have no submerged deltas, as the region is west of the zero-isobase (Cowan, 2015) and none were reported in the literature reviewed thus far (Gilbert, 1982; Syvitski & Blakeney, 1984; Syvitski, 1985; Syvitski et al., 1986; Syvitski & Praeg, 1987; Syvitski & Hein, 1991). However, similar to western Cumberland Peninsula (England & Andrews, 1973; Pheasant & Andrews, 1973; Dyke, 1979), multiple raised marine deposits have been reported along the NE Baffin fjords and dated to ages (<10 cal ka BP) similar to submerged shoreline of eastern Cumberland Peninsula (King, 1969; Andrews et al., 1970; Andrews & Ives, 1978; Stravers, 1987; Briner et al., 2009b). Both regions contain other raised deltas that are located at higher elevations (50 – 85 m asl) and dated to be even older (35 to >57 ka) (Ives & Buckley, 1969; England & Andrews, 1973; Andrews, 1990; Miller et al., 2002).

In addition to relict submerged and raised deltas, active subaerial deltas and sandar are widely observed throughout both regions (Google, 2021). A survey of selected Baffin fjord prodeltas reports no major differences in geomorphic features between NE Baffin Island and Cumberland Peninsula fjords (Syvitski et al., 1984), although the sample population was skewed towards the former. However, other research has summarized NE Baffin fjords as containing larger sediment accumulations than Cumberland Peninsula (Gilbert, 1985). Thus, it is reasonable to hypothesize that deltas throughout the northeast coast should be larger overall, as the larger drainage basins represent larger potential sediment supplies to the prograding deltas, allowing them to reach greater maximum sizes. However, a larger drainage basin may also contain more lakes and other features that sequester sediment, thus inhibiting delta growth. A detailed morphometric survey of subaerial deltas is beyond the scope of this thesis, so it remains an open question how frequently northeast-coast deltas reach their potential maximum size.

To the extent that both regions have been surveyed, Cumberland Peninsula fjords differ from the wider population of Baffin Island fjords in the following respects:

- Cumberland Peninsula fjords show overall thinner sediment deposits than elsewhere along Baffin Island, in keeping with expectations that the larger LIS-fed glaciers would have transported more sediments than the smaller PIC-LAG glaciers.

- Mean sedimentation rates in Cumberland Peninsula fjords appear comparable to those along the northeast coast, with considerable overlap occurring between the two regions.
- Unlike in eastern Cumberland Peninsula, the northeast coast fjords are currently not known to contain any submerged deltas, but do contain multiple raised marine deposits similar to western Cumberland Peninsula. Active subaerial deltas and sandar are observed within fjords of both regions, though are expected to be larger along the northeast coast.

4.5 References

Andrews, J.T. (1987). Late Quaternary marine sediment accumulation in fiord-shelf-deep-sea transects, Baffin Island to Baffin Bay. *Quaternary Science Reviews, 6*: 231-243.

Andrews, J. T. (1990). Fiord to deep sea sediment transfers along the northeastern Canadian continental margin: Models and data. *Geographie Physique et Quaternaire, 44*: 55-70.

Andrews, J., & Ives, J. (1978). “Cockburn” nomenclature and the Late Quaternary history of the eastern Canadian Arctic. *Arctic and Alpine Research*, 10: 617–633.

Andrews, J.T., Buckley, J.T., & England, J.H. (1970). Late-glacial chronology and glacio-isostatic recovery, Home Bay, east Baffin Island, Canada. *Geological Society of America Bulletin,* 81: 1123-1148.

Andrews, J.T., Laymon, C.A., & Briggs, W.M. (1989). Radiocarbon date list III: Labrador and northern Quebec, Canada and radiocarbon date list VI: Baffin Island, N.W.T., Canada. *INSTAAR Occasional Paper No. 46*, University of Colorado, Boulder.

Andrews, J.T., Syvitski, J.P., Osterman, L.E., Williams, K.M., Mode, W.N., Kravitz, J.E. & Locke, W.W. III. (1994). Quaternary geology of Sunneshine Fiord (Baffin Island). *Geological Survey of Canada Open File 3004.*

Andrews, J.T., Osterman, L.E., Jennings, A.E., Syvitski, J.P.M., Miller, G.H., & Weiner, N. (1996). Abrupt changes in marine conditions, Sunneshine Fiord, eastern Baffin Island, NWT during the last deglacial transition: Younger Dryas and H-0 events. *Late Quaternary Palaeoceanography of the North Atlantic Margins,* Geological Society Special Publication No. 111: 11-27.

Briner, J.P., Davis, P.T., & Miller, G.H. (2009). Latest Pleistocene and Holocene glaciation of Baffin Island, Arctic Canada: key patterns and chronologies. *Quaternary Science Reviews*, 28: 2075–2087.

Coulthard, R. D., Furze, M.F.A., Pieńkowski, A.J., Nixon, F.C., & England, J.H. (2010). New marine ΔR values for Arctic Canada. Quaternary Geochronology, 5: 419–434.

Cowan, B. (2015). Shorelines beneath the sea: Geomorphology and characterization of the postglacial sea-level lowstand, Cumberland Peninsula, Baffin Island, Nunavut. Master's thesis: Memorial University of Newfoundland, Geography Department.

Deering, R., Misiuk, B., Bell, T., Forbes, D.L., Edinger, E., Tremblay, T., Telka, A., Aitken, A., & Campbell, C. (2018). Characterization of the seabed and postglacial sediments of inner Frobisher Bay, Baffin Island, Nunavut. *Summary of Activities 2018*, Canada-Nunavut Geoscience Office: 139-152.

Dowdeswell, E.K. & Andrews, J.T. (1985). The fjords of Baffin Island: description and classification. In J.T. Andrews (Ed.), *Quaternary Environments: Eastern Canadian Arctic, Baffin Bay and Western Greenland* (pp. 93–123). London: George Allen & Unwin Publishers.

Dyke, A.S. (1979). Glacial and sea-level history of southwestern Cumberland Peninsula, Baffin Island, N.W.T., Canada. *Arctic and Alpine Research, 11* (2): 179–202.

Dyke, A.S., Andrews, J.T., & Miller, G.H. (1982). *Quaternary Geology of Cumberland Peninsula, Baffin Island, District of Franklin.* Geological Survey of Canada, Memoir 403. 32 p. https://doi.org/10.4095/116169

England, J.H. & Andrews, J.T. (1973). Broughton Island—a reference area for Wisconsin and Holocene Chronology and sea-level changes on Eastern Baffin Island. *Boreas,* 2 (1): 17–32.

Heaton, T.J., Kohler, P., Butzin, M., Bard, E., Reimer, R.W., Austin, W., Ramsey, C.B., Grootes, P.M., Hughen, K.A., Kromer, B., Adkins, J., Burke, A., Cook, M.S., Olsen, J., & Skinner, L.C. (2020). Marine20–the marine radiocarbon age calibration curve (0-55,000 cal BP). *Radiocarbon*, 62: 779-820. doi:10.1017/RDC.2020.68

Gilbert, R. (1982). Contemporary sedimentary environments on Baffin Island, N.W.T., Canada: Glaciomarine processes in fiords of eastern Cumberland Peninsula. *Arctic and Alpine Research*, 14(1): 1-12.

Gilbert, R. (1985). Quaternary glaciomarine sedimentation interpreted from seismic surveys of fiords on Baffin Island, N.W.T. *Arctic,* 38 (4): 271-280.

Gilbert, R. & MacLean, B. (1984). Geophysical studies based on conventional shallow and Huntec high resolution seismic surveys of fiords on Baffin Island. In J.P.M. Syvitski & C.P. Blakeney (Eds.), *Sedimentology of Arctic Fjords Experiment: HU 82-031 Data Report, Volume 1* (GSC Open File No. 960). Dartmouth, NS: Bedford Institute of Oceanography.

Google. (2021). *Google earth pro* (Version 7.3.3). https://www.google.com/earth/

Ives, J.D. & Buckley, J.T. (1969). Glacial geomorphology of Remote Peninsula, Baffin Island, N.W.T., Canada. *Arctic and Alpine Research,* 1 (2): 83-96.

King, C.A.M. (1969). Glacial geomorphology and chronology of Henry Kater Peninsula, east Baffin Island, N.W.T. *Arctic and Alpine Research,* 1 (3): 195-212.

Manley, W.F. & Jennings, A.E. (1996). Radiocarbon date list VIII: Eastern Canadian Arctic, Labrador, northern Quebec, East Greenland Shelf, Iceland Shelf, and Antarctica. *INSTAAR Occasional Paper No. 50*, University of Colorado, Boulder.

Margreth, A. (2015). *Climate sensitivities of polythermal ice sheet, ice cap, and alpine ice dynamics and related episodic erosion on Cumberland Peninsula, Baffin Island, Nunavut*. Doctoral dissertation: Dalhousie University, Department of Earth Sciences.

Miller, G.H., Wolfe, A.P., Steig, E.J., Sauer, P.E., Kaplan, M.R., & Briner, J.P. (2002). The Goldilocks dilemma: big ice, little ice, or "just-right" ice in the Eastern Canadian Arctic. *Quaternary Science Reviews, 21*: 33–48.

Pheasant, D.R. & Andrews, J.T. (1973). Wisconsin glacial chronology and relative sea-level movements, Narpaing Fiord Broughton Island area, eastern Baffin Island, N.W.T. *Canadian Journal of Earth Sciences,* 10 (11): 1621–1641.

Stravers, J.A. (1987). Late Quaternary glacial and raised marine stratigraphy of northern Baffin Island fiords. In J.P.M. Syvitski & D.B. Praeg (Eds.), *Sedimentology of Arctic Fjords Experiment: Data Report, Volume 3*. Geological Survey of Canada, Dartmouth, Open File 1589. doi:10.4095/130318

Stuiver, M., Reimer, P.J, & Reimer, R.W. (2021). *CALIB 8.2*. http://calib.org/calib/

Syvitski, J.P.M. (Compiler). (1985). *Sedimentology of Arctic Fjords Experiment: HU 83-028 Data Report, Volume 2.* Geological Survey of Canada, Dartmouth, Open File 1122. doi: 10.4095/129977

Syvitski, J.P.M. (1989). On the deposition of sediment within glacier-influenced fjords: Oceanographic controls. *Marine Geology*, 85: 301-329.

Syvitski, J.P.M., & Blakeney, C.P. (Compiler). (1984). *Sedimentology of Arctic Fjords Experiment: HU 82-031 Data Report, Volume 1.* Geological Survey of Canada, Dartmouth, Open File 960. doi: 10.4095/129793

Syvitski, J.P.M. & Hein, F.J. (1991). *Sedimentology of an Arctic basin: Itirbilung Fiord, Baffin Island, Northwest Territories.* Geological Survey of Canada Paper 91-11. doi: 10.4095/132684

Syvitski, J.P.M., & Praeg, D.B. (Compilers). (1987). *Sedimentology of Arctic Fjords Experiment: Data Report, Volume 3.* Geological Survey of Canada, Dartmouth, Open File 1589. doi: 10.4095/130318

Syvitski, J., Blakeney, C.P., & Hay, A.E. (1984). SAFE: HU83-031 sidescan sonar and sounder profiles. In J.P.M. Syvitski & C.P. Blakeney (Eds.), *Sedimentology of Arctic Fjords Experiment: HU 82-031 Data Report, Volume 1.* Geological Survey of Canada, Dartmouth, Open File 960. doi: 10.4095/129793

Syvitski, J.P.M., Schafer, C.T., Asprey, K.W., Hein, F.J., Hodge, G.D., & Gilbert, R. (1986). *Sedimentology of Arctic Fjords Experiment: PA-85-062 Expedition report*. Geological Survey of Canada, Open File 1234. doi:10.4095/130052

A DESCRIPTIVE AND INFERENTIAL STATISTICS

Appendix A lists and explains the descriptive, inferential, and correlative statistics used in Chapter 2 for analyzing fjord morphometric parameters. The thirteen parameters analyzed are: fjord surface area, length, orientation, sinuosity, width (mean, minimum, and maximum), maximum depth (basin, sill, outer), maximum sidewall elevation, drainage-basin area, and maximum drainage-basin elevation. The total dataset of 29 fjords are sorted into two sample populations (regional groups): northeast coast (NC; 11 fjords) and Cumberland Peninsula (CP; 18 fjords).

A.1 Descriptive statistics

Descriptive statistics were calculated in order to analyze the distribution of values for each parameter within each regional group. The descriptive statistics calculated are: mean, weighted mean, range, standard deviation, variance, coefficient of variation, skewness, and kurtosis.

The **mean** of each category was calculated as the sum of the series divided by the number of values within it. It was included to illustrate the central tendency of each category, and was later used in the two-sample difference of means tests used for the inferential analysis.

$$\bar{X} = \frac{\sum_{i=1}^{n} X_i}{n}$$

The **weighted mean** was calculated only for fjord orientation, as the sum of the orientation of each individual fjord segment weighted by the length of said segment and divided by the length of the fjord.

$$\bar{Y}_w = \frac{\sum Y_i D_i}{\sum D}$$

The **range** between the maximum and minimum value of each category was included as a simple measure of variability.

The **standard deviation** of each category was included to illustrate the degree to which the parameter values of each category deviate from the mean. As an absolute measure, the magnitude of the standard deviation is directly related to the magnitude of the data set.

$$s = \sqrt{\frac{\sum (X_i - \bar{X})^2}{n-1}}$$

The **standard error** of the mean illustrates how likely the mean calculated for each parameter is likely to deviate from the true mean value for the entire population.

$$SE = \frac{s}{\sqrt{n}}$$

Variance is the square of the standard deviation. It is rarely included in descriptive statistic summaries as its value is often large and difficult to interpret (McGrew & Monroe, 2000), but is included here as it is relevant to the analysis of variance (ANOVA) test described below under the inferential statistics (2.2.4.3).

$$s^2 = \frac{\sum (X_i - \bar{X})^2}{n-1}$$

Coefficient of variation (CV) is a standardized measure that can be used to directly compare the variability of data sets for different regions. It is defined as the standard deviation divided by the mean, therefore removing the influence of the data's magnitude.

$$CV = \frac{s}{\bar{X}}$$

Skewness is defined by McGrew and Monroe (2000) as a measure of the degree of symmetry in a frequency distribution. A skewness value close to zero indicates a symmetric distribution, i.e., an equal number of values above and below the mean. In contrast, a negative skewness indicates that the distribution is skewed below the mean (tail to the left), while a positive skewness indicates that the distribution are skewed above it (tail to the right). Skewness is a standardized measurement, allowing separate categories to be compared directly.

$$\text{Skewness} = \frac{\sum(X_i - \bar{X})^3}{ns^3}$$

Kurtosis describes the peakedness or flatness of a data set—whether the values are clustered or dispersed across a distribution (McGrew & Monroe, 2000). A kurtosis equal or close to 3.0 (mesokurtic) indicates a normal distribution. A kurtosis greater than 3.0 (leptokurtic) indicates a peaked distribution, a cluster of values in one area of the distribution. A kurtosis less than 3.0 (platykurtic) indicates a flattened distribution, a more even dispersion of values across the distribution.

$$\text{Kurtosis} = \frac{\sum(X_i - \bar{X})^4}{ns^4}$$

Skewness and kurtosis, together known as the measures of the distribution of shape, were used to determine which statistical tests would be used for the inferential analyses. Parametric tests assume that samples are taken from a normally-distributed population, while nonparametric tests assume that the distributions of both samples have similar shapes (McGrew & Monroe, 2000). Therefore, kurtosis was analyzed to determine which parameters in a group fit the normal distribution (when kurtosis ≈ 3), and skewness and kurtosis were analyzed together to determine if the distributions for each parameter were similar between groups. This study arbitrarily accepted a kurtosis of 3.00 ± 0.25 as indicating a normal distribution. McGrew and Monroe (2000) do not specify what constitutes similar distribution shapes, so for the purposes of this study it is arbitrarily defined as a difference of ≤ 0.25 for both skewness and kurtosis. Therefore, the regional groups were only considered to have similar data distributions for a given parameter only if both the skewness and kurtosis showed a difference of ≤ 0.25. From the calculated values of skewness and kurtosis (Tables 2.3), it was determined that the vast majority of data distributions for each parameter and group were non-normal and dissimilar between groups. As a result, inferential statistical analysis proceeded by pairing parametric and nonparametric tests together.

A.2 Inferential statistics

Inferential statistics were calculated in order to test the two regional groups (NC and CP) for a significant difference in means for each parameter. Therefore, this study utilizes two-sample difference-of-means testing, which was done using the parametric one-way ANOVA, and the nonparametric Wilcoxon rank sum *W* test.

Each inferential test requires its own inherent assumptions. The one-way ANOVA assumes that the samples are independent and random, the variable is measured at either the interval or ordinal scale, and the populations that the samples are taken from are normally distributed and have equal variance. Meanwhile, the Wilcoxon rank sum test assumes that both samples are independent and random, the variable was either measured at ordinal scale or downgraded from interval/ratio, and that both population distributions are similar in shape. However, not all of these assumptions are met by the dataset.

The 29 fjords included in the fjord morphometry dataset were selected based on either the availability of bathymetric imagery (the ArcGIS morphometric analysis), or to represent the spectrum of Baffin Island fjords (Gilbert & MacLean, 1984); these combined selections are treated as approximating a random sample. In addition, each fjord parameter was measured at either the interval or ratio scale. Thus, the dataset satisfies the first two assumptions for each test. However, the population distributions are unknown, and the results of the skewness and kurtosis analyses suggest non-normal distributions and dissimilar distribution shapes for the vast majority of parameters in each group. In addition, because the one-way ANOVA test assumes equal variance of the populations tested, a modified Levene's test was conducted to whether this assumption was valid. The results of the modified Levene's test indicate that equality of variance could be assumed for most but not all parameters. Therefore, the assumptions for neither statistical test are fully satisfied. In response, this study pairs the parametric and nonparametric tests together by conducting both tests for each parameter. In the event that the results of both tests agree, the confidence in the accuracy of said results will be reinforced (McGrew & Monroe, 2000). If the results of each test conflict, the study will favour the results of the nonparametric

Wilcoxon rank sum test, as the dissimilar distribution of each sample is considered to be less problematic for it than the non-normal distribution is for ANOVA.

For each of the 3 tests used—modified Levene's test, one-way ANOVA, and Wilcoxon rank sum test—both classical hypothesis testing (i.e., comparison of the observed test statistic value to a critical value) and probability (p) value testing were used to interpret the results.

A.2.1 One-way analysis of variance

A one-way analysis of variance (ANOVA) test calculates the quotient of between-group variability and within-group variability. When the variability across all groups in the analysis is larger than the variability of each individual group, the observed F value will be greater than 1. Therefore, when the observed F value was found to be above the critical F value defined by the degrees of freedom for each parameter, unequal variance was assumed for both groups. This study uses a one-way ANOVA to test each parameter separately. This ANOVA was conducted in order to determine whether sample variances could be assumed to be equal or unequal for the two-sample difference of means t test, and thus was calculated using only two samples instead of three or more. The observed F value of each parameter was calculated using the formula below.

$$F = \frac{MS_B}{MS_W}$$

Where MS_B is the between-group mean squares and MS_W is the within-group mean squares. Each mean squares variable was first calculated using its own series of formulae.

$$MS_B = \frac{SS_B}{df_B} = \frac{SS_B}{k-1}$$

Where k is the total number of groups or samples and SS_B is the between-group sum of squares.

$$SS_B = \sum_{i=1}^{k} n_i(\bar{X}_i - \bar{X}_T)^2$$

Where $\bar{X}_i$ is the mean of sample i and $\bar{X}_T$ is the weighted mean of the individual sample means.

$$\bar{X}_T = \frac{\sum_{i=1}^{k} n_i \bar{X}_i}{N}$$

Where N is the total number of observations in all samples.

$$MS_W = \frac{SS_W}{df_W} = \frac{SS_W}{N - k}$$

$$SS_W = \sum_{i=1}^{k}(n_i - 1)\, {s_i}^2$$

A.2.2 Modified Levene's test

The standard Levene's test is conducted by performing an ANOVA on the absolute deviations of each measurement from its sample mean (McGrew & Monroe, 2000). This study utilized a modified Levene's test by instead using the absolute deviations of each measurement from its sample median, in order to account for the non-normal distributions of the data. Absolute deviation from sample median was calculated as:

$$Z_i = \left| x_i - \tilde{X} \right|$$

Where x_i is the value of sample *i* and $\tilde{X}$ is the median of the sample. Due to time constraints, the issue of structural zeroes, wherein the absolute deviation of the median from itself equals zero, was not corrected.

A.2.3 Wilcoxon rank sum *W* test

As previously mentioned, this study pairs the parametric two-sample difference of means *t* test with the non-parametric Wilcoxon rank sum test. The Wilcoxon test does not assume that the samples fit a normal distribution, but does assume that both samples have a similar distribution shape. The test operates by assigning an ordinal rank to every observation included in the analysis (in the case of a tie, the mean of the ranks that otherwise would have been assigned is given to each tying observation), and then taking the sum of the ranks in each sample separately. The test statistic (Z_W) is then calculated as:

$$Z_W = \frac{W_i - \overline{W}_i}{s_W}$$

Where W_i is the sum of ranks for sample *i*, and $\overline{W}_i$ is the mean rank of W_i and s_w is the standard deviation, both calculated as below:

$$\overline{W_i} = n_i \left(\frac{n_1 + n_2 + 1}{2}\right)$$

$$s_W = \sqrt{n_1 n_2 \left(\frac{n_1 + n_2 + 1}{12}\right)}$$

A.3 Correlation of parameters

Three pairs of parameters were selected to be tested for correlation: fjord and drainage-basin areas, fjord length and mean width, and maximum basin depth and sidewall elevation. For each of these pairs, a positive correlation is hypothesized. A larger drainage basin should feed more ice into the fjord, resulting in more erosion and thus a larger fjord. The fjords of Baffin Island have been observed to widen from head to mouth, and a longer fjord would logically have a greater probability of capturing tributary glaciers to increase lateral erosion; thus, a longer fjord should demonstrate a greater mean width. Dowdeswell and Andrews (1985) have previously reported a correlation ($r^2 = 0.36$) between maximum basin depth and sidewall elevation, and this study seeks to corroborate with its dataset. These pairs of parameters were selected in order to inform on the character of Baffin Island fjords.

This study uses correlation as both a descriptor of sample data, and as an inferential statistic. This was done to calculate the strength and direction of association between the selected parameters, and to test whether the current samples could be used as estimates of the larger populations. Thus, for the same reasons as the inferential statistical analysis, this study pairs a parametric and a nonparametric correlation coefficient together: the Pearson's correlation coefficient and the Spearman's rank correlation coefficient. For both coefficients, the value of r ranges from 1.0, indicating a perfect positive or direct correlation between variables, and -1.0, a perfect negative correlation. A value of 0.0 indicates no correlation between variables. The value of r^2 indicates the proportion of data values explained by the association (Dowdeswell & Andrews, 1985). The correlation analysis was conducted, using both coefficients, for the entire Baffin Mountains dataset in addition to the northeast coast and Cumberland Peninsula groups.

A.3.1 Pearson's correlation coefficient

The Pearson's product-moment correlation coefficient is regarded as the most powerful measure of correlation between two variables (McGrew & Monroe, 2000). It assumes: a random sample of paired variables, that variables have a linear association, and that variables are measured at interval or ratio scale. If used inferentially instead of descriptively, both variables should be derived from normally distributed populations. The Pearson's coefficient (r) is calculated as:

$$r = \frac{[\sum(X-\bar{X})\,(Y-\bar{Y})]/N}{S_X S_Y}$$

Where r is the Pearson's correlation coefficient, N is the number of paired data values, and S_X and S_Y are the standard deviations of X and Y, respectively.

The version of the *t* test used to check the significance of the correlation is given by McGrew and Monroe (2000) as:

$$t = \frac{r}{s_r}$$

Where s_r is the standard error estimate, calculated as:

$$s_r = \sqrt{\frac{1-r^2}{n-2}}$$

A.3.2 Spearman's rank correlation coefficient

The Spearman's rank correlation coefficient (r_s) is described as almost as strong as the Pearson's coefficient, but is nonparametric and uses ordinal data. Thus, it is better suited to highly skewed or non-normal data distributions (McGrew & Monroe, 2000). The Spearman's coefficient is calculated as:

$$r_s = 1 - \frac{6(\sum d^2)}{N^3 - N}$$

Where d is the difference in ranks of variables X and Y for each pair of data values, $\sum d^2$ is the sum of the squared differences in ranks, and N is the number of paired data values.

The following version of the t test was used to check the significance of the correlation:

$$t = r\sqrt{\frac{n-2}{1-r^2}}$$

B ACOUSTIC STRATIGRAPHIC ANALYSIS

Across the three fjord systems for which acoustic stratigraphy was analyzed (Boas Fiord, Durban Harbour, and Akpait Fiord), a total of 7 acoustic units are interpreted. Each unit is labelled from A to G and illustrated using a separate colour on Figures B.4 to B.29, excluding maps. Thick lines indicate unit contacts, thin lines indicate internal reflectors, and dashed lines are used when the reflector is either indistinct or inferred. Acoustic multiples are indicated by a black dashed line. No one profile was observed to display all 7 acoustic units, as units F and G are local to the Akpait fjord-mouth sill (Table B.1). Nonetheless, profiles *c* (Fig. B.6) and *p* (Fig. B.31) provide the most inclusive examples.

Table B.1: Summary table of every acoustic unit observed per profile.

Fjord	Acoustic profiles	Acoustic units observed						
		A	B	C	D	E	F	G
Boas Fiord	*a*		X	X	X	X		
	b		X	X	X	X		
	c	X	X	X	X	X		
	d	X	X	X		X		
	e		X		X	X		
	f		X		X			
	g		X		X			
	h				X			
	i		X	X	X			
Durban Harbour	*j*		X		X	X		
	k		X		X			
	l		X		X			
	m	X	X		X			
	n		X		X			
	o	X	X		X			
Akpait Fiord	*p*		X			X	X	X
	q		X				X	X
	r		X			X		
	s		X				X	X

Unit A: Bedrock is illustrated in gray. The unit is most often inferred as underlying the ice-contact sediment at an undetermined depth, but is occasionally identified by a strong unit contact and prominent acoustic multiples.

Unit B: Ice-contact sediments are in yellow. The unit is identified as a coarse, structureless to chaotic unit, frequently inferred to overlie bedrock and observed underlying most other acoustic units.

Unit C: Glaciomarine sediments are in green. This unit is identified as stratified and conformable, overlying ice-contact sediments and underlying deltaic sediments and marine mud. Among the selected profiles, it is only observed at Boas Fiord, mostly around the submerged fjord-head delta.

Unit D: Deltaic sediments are in brown. The unit is typically identified by a distinct tripartite structure of topset, foreset, and bottomset beds, a spatial association of the profile with the submerged deltas observed on bathymetry, and stronger and more chaotic reflectors. It is observed to overlie ice-contact and glaciomarine sediments and underlie marine muds.

Unit E: Marine muds are in blue. The unit is typically surficial, overlying either deltaic or ice-contact sediment, and appears as acoustically weak (light-coloured) with few internal reflectors. In the context of the submerged deltas of Boas Fiord and Durban Harbour, this unit may also be referred to as post-submergence muds.

Unit F: The fine-grained sediments covering the Akpait fjord-mouth sill are in blue-green. It is an acoustically weak unit with a few weak to moderate reflectors. It is surficial, overlying the ice-contact sediment of the sill.

Unit G: The spillover deposit adjacent to the Akpait fjord-mouth sill is in black. The unit is bounded by a strong contact line and contains multiple internal reflectors (wavy-parallel to disturbed). The two reflectors nearest the contact line are strongest, while the others quickly weakening with depth. It is most likely reworked unit, but shows a level of stratification not seen in disturbed sediments in Boas or Durban. It is a surficial unit, onlapping the adjacent ice-contact and sill-cover sediments.

B.1 Boas Fiord

Acoustic subbottom profiles have been collected along the entire length of Boas Fiord by the *MV Nuliajuk* during 2012 and 2014; however, a significant blank region remains along the center line of the fjord's outer basin. Surveying was most concentrated at the two submerged deltas identified by Cowan (2015), located at the fjord-head and the side-entry valley mouth at in the side-entry embayment (Fig. B.1).

B.1.1 Fjord-head delta

The submerged fjord-head delta is observed to occupy an area of at least 3.2 km^2 (but may cover 7.5 km^2), and extent ~5.4 km outwards from the fjord head (defined here as the modern land-water interface). Its terrace runs across the seafloor (~2.0 km wide), with a developed side terrace extending at least ~0.8 km along the eastern sidewall (may extend from 1.4 to 2.8 km long). The delta plain contains physical features which have been interpreted as: partially-infilled relict stream channels, a shallow ridge near the fjord head, and a shoal near the delta terrace (Fig. B.2). The acoustic profiles analyzed in this study transect the submerged fjord-head delta and its eastern side terrace, and the nearby major and minor sills (Fig. B.3).

Overall, five acoustics (A to E) are observed throughout the fjord-head delta.

Unit A (bedrock) is only directly observed on profiles *c* and *d* (Figs. B.6, B.7), as three acoustically strong and massive ridges. The largest ridge is partly surficial and partly overlain by onlapping units B and C and D, the middle ridge is onlapped by B and overlain by C, and the smallest ridge is onlapped by B and C and overlain by E. These ridges, from largest to smallest, are visibly associated with the major sill, the minor sill, and the shoal observed on the bathymetry. The unit is interpreted as bedrock, based on the strength of the contact line (with 4 reflectors observed for the largest ridge) combined with the association with said bathymetric features. Two internal reflectors observed on profile *d* might indicate faults in the rock.

Unit B (ice-contact sediment) is observed throughout the submerged fjord-head delta area, as an acoustically massive unit with a moderate-to-strong and chaotic contact line. The unit is observed to onlap the unit A ridges and is inferred to overlie it elsewhere, and underlies units C, D, and or E depending on location. Where it underlies unit D of the main delta, the contact line instead appears weak and hummocky to contorted, possibly due to attenuation. Where the unit thickness could be estimated, a maximum of 13 m was found along the slope of the major sill (Fig. B.6). The unit was interpreted as ice-contact sediment, based on the strong, chaotic acoustic character indicative of coarse sediments, its position adjacent to unit A (bedrock), and its association with likely lateral moraine deposits at the side terraces. The unit is not observed below the main delta slope (Fig. B.4, B.7), suggesting either attenuation of the shot or gas masking from organic decomposition.

Unit C (glaciomarine sediment) is observed as a significant component of the west and east side-terraces and the minor sill, but not as part of the main delta. It is a draped and stratified unit, with a strong-to-weak contact line and moderate-to-weak internal reflectors (weakening with depth) that conform to the underlying substrate. The unit overlies and occasionally onlaps units A and B, and underlies units D and E. The unit appears to undergo acoustic blanking underneath the main delta (suggesting either attenuation or gas-masking). Where the unit thickness could be estimated, it showed a maximum of 25 m (Fig. B.5) within the eastern terrace. The unit is interpreted as glaciomarine sediment, as it matches the description of highly conformable and stratified character. Within the eastern side-terrace (Fig. B.4), the unit is observed to be truncated by the overlying unit D—this combined with the Gilbert-style delta suggests that the eastern terrace was a higher fluvial activity environment than the western terrace.

Unit D (deltaic sediment) is observed as directly associated with the submerged delta and its eastern side-terrace. As a result, the unit is divided into subunits D1, D2, and D3, corresponding to the bottomset, foreset, and topset beds, respectively. The unit is bounded by a contact line that varies in strength, from strong throughout D3 to moderate-to-weak along D1 and D2. The contact line and internal reflectors seem hummocky-to-chaotic at D1 and D2, and uneven parallel to sub-parallel in D3. At D2, the contact line slopes with a sigmoid-oblique clinoform pattern in the eastern terrace and main delta. The overall unit is observed to overlie and or onlap units A, B and C at different locations, and consistently underlies unit E. It has an estimated maximum thickness of 20 m at the eastern side-terrace. The unit is interpreted as deltaic sediment, based on the observed tripartite Gilbert-style delta structure and direct spatial association with the submerged delta, and supported by the chaotic acoustic character indicating coarse sediments. Little acoustic detail can be observed within the main delta. This is most likely due to either, sufficiently coarse and thick sediment attenuating the shot, or a sufficient decomposing organic content causing gas-masking.

Unit E (post-submergence mud) is observed throughout the fjord-head delta area, except for the summit of the major sill (largest unit A ridge). The unit is acoustically weak to transparent, with two strong point reflectors on the eastern side terrace and a few internal reflectors (sub-parallel to wavy parallel). It is the surficial unit, onlapping unit A and draping units C, along the major and minor sills and the western terrace, and D, along the main delta and eastern terrace. A maximum unit thickness of 12 m was estimated for the prodelta area. The unit was interpreted as post-submergence marine mud, based on its acoustic weakness indicative of fine sediment and its surficial position which indicates deposition following submersion of the delta. This unit has accumulated more thickly on the eastern side-terrace than the western one, possibly suggesting greater stream activity. The unit also thickens on the delta plain towards the fjord head, suggesting that sediment deposition remains ongoing.

B.1.1.1 Profile *a* (0046_2012_285_1905.jp2)

Profile *a* (Fig. B.4) extends across the two opposing side terraces and the lower delta slope in between them, intersecting stations 2014NULIAJUK-0001 and -0004 on the eastern terrace (*a*'). From the acoustic profile and bathymetry, the eastern side terrace is observed to be the more developed of the two, showing a distinct Gilbert-delta shape overlying a sloping substrate and extending ~0.25 km outwards from the eastern sidewall and at least ~0.8 km northwards. In contrast, the western terrace (*a*) conforms to its substrate and only protrudes ~0.10 km outwards from the western sidewall. These differences may be due to the greater number and development of stream systems feeding into the eastern terrace (2 second-order and 2 first-order streams) as opposed to the western terrace (3 first-order streams total); this is supported by the differences in shape (Gilbert-style delta versus conforming), which suggest a depositional rather than structural control.

Unit A: Is not observed on the profile, but is expected to underlie unit B at some distance.

Unit B: Is observed on either end of the profile as a massive unit with a strong, sloping contact line. As the observed basal unit, its thickness could not be estimated; however, unit A is expected to underlie it at an unknown distance. Within the western terrace the unit is onlapped by unit D and overlain by unit E, while inside the eastern terrace it is fully overlain by unit D. Its locations represent the sides of the valley, so these deposits are likely lateral moraines. No reflections are observed below the unit D2 for the main delta slope—this may be due to attenuation of the shot, or gas masking from decomposing organics.

Unit C: Is observed along the western and eastern terraces as a draped, stratified unit with a contact line varying from strong to weak, and weak internal reflectors. It overlies unit B and underlies D and E. It cannot be observed in the middle of the profile, likely due to gas-masking, but is inferred to underlie unit D at an unknown depth. Where the unit could be measured, it has an estimated mean thickness of 14 m, ranging from 7–21 m. The unit is thickest along the western terrace, and is less significant underneath the eastern terrace. This disparity may be due to fluvial input of the nearby stream (Fig. B.3), as the unit appears to be truncated where it contacts the overlying unit D3 (delta topset beds). The fault and slope failure deposit are observed in the unit at the foot of the western terrace, where the weak internal reflectors abruptly transition from sigmoidal to disrupted. The unit is interpreted as glaciomarine sediment.

Unit D: Overall, the unit is described as chaotic reflectors varying from strong to weak, sloping with a sigmoid-oblique clinoform pattern, with an estimated mean thickness of 10 m and range of 1–20 m. It is observed to either overlie or onlap unit C, and underlie unit E. Near the western terrace (*a*), the unit is acoustically weak where it overlies the unit C slope failure deposit and onlaps the unit C fault; here the estimated mean unit thickness is 6 m with a range of 3–9 m. Along the main delta slope, the upper contact is weak and underlain by structureless stratification that is only observed near the surface (indicating either attenuation or gas masking); unit C is not observed in this segment, precluding any estimation of thickness. Along the eastern terrace (*a*'), the contact line strengthens towards the top of the slope, while the subparallel, sigmoid-oblique internal reflectors vary in strength; here the estimated mean unit thickness is 10 m with a range of 1–20 m. The unit, specifically at the eastern terrace, resembles the tripartite structure of a Gilbert-style delta, and thus is interpreted as deltaic sediment.

Unit E: Acoustically transparent surficial unit along the length of the profile. The unit is visibly thickest above the main delta slope and the eastern side-terrace, and thinnest above the western side-terrace. The unit has an estimated mean unit thickness of 3 m and range of 1–5 m. It was interpreted as post-submergence marine mud, with more sediment deposition indicated on the eastern terrace than the western, possibly due to greater stream activity.

B.1.1.2 Profile *b* (0009_2014_247_1648.jp2)

Profile *b* (Fig. B.5) surveys the eastern side-terrace delta along its edge, parallel to the delta slope, intersecting stations 2014NULIAJUK-0001 and -0004. Overall, the profile displays a marine pattern (Holocene/postglacial sediment) observed along the Atlantic coast: ice-contact sediments, overlain by glaciomarine sediments, fluvial-deltaic sediment (silt, sand, gravel), and surficial acoustically transparent mud with dropstones (dark dots).

Unit A: Is not observed on the profile, but is expected to underlie unit B at some distance.

Unit B: Observed as a moderately-strong, massive unit with a chaotic contact line. Possible side-echoes are observed at the 50 and 350 m markers. As the basal unit, its thickness could not be estimated. It is inferred to overlie unit A, and is observed to underlie unit C. The unit is interpreted as ice-contact glacial till, due to the chaotic contact line indicating coarse sediments.

Unit C: Is a stratified unit with a strong contact line, interrupted by an erosional channel with ponded infilling (250–350 m markers). The internal reflectors conform to the underlying unit B, and visibly weaken with depth. The unit has an estimated mean thickness of 21 m, ranging from 18–25 m. The unit is interpreted as conformably draped glacial-marine deposits, due to the conformable stratified character.

Unit D: Is observed to overlie unit C and underlie unit E. The contact line is strong, with weaker, internal reflectors. Most reflectors are uneven parallel, but they become wavy-to-contorted above the erosional channel. The unit has an estimated mean thickness of 5 m, ranging of 4–8 m. The unit was interpreted as representing a frontal plane of the deltaic topset bed.

Unit E: Acoustically transparent unit with two strong point reflectors (indicating dropstones) just below the contact line. The unit conforms to the underlying unit D and overlays the entire profile, with an estimated mean thickness of 2 m and range of 2–3 m. The unit was interpreted as post-submergence marine muds, with the narrow thickness range indicating a roughly even sediment distribution on the delta terrace.

B.1.1.3 Profile *c* (0040_2012_285_1739.jp2)

Profile *c* (Fig. B.6) begins near a shallow mid-fjord sill and travels up-fjord, crossing a feature interpreted as a smaller, deeper sill (1000–2000 m markers) and the prodelta area, and ends above the submerged fjord-head delta / sandur. During the sea level lowstand, when the delta formed, the major sill would have been subaerial and part of it exposed to wave action. This could have resulted in ice-contact sediment being reworked downslope.

The 1000–2000 m feature is currently interpreted as a minor sill, consisting of a bedrock core draped by ice-contact and glaciomarine sediment. In profile *c*, the feature resembles the Nordfjord moraine as surveyed by Aarseth (1997), with a steep-sloping face on the ice-ward side and an uneven, gradual slope on the other (recalling the piled-up sediments of a push moraine). However, profile *d* is more centered in the fjord trough and thus crosses the feature at a deeper point, and depicts the feature as a roughly symmetrical ridge with no resemblance to the Nordfjord moraine. This suggests that what appears as push-piled sediments are instead glaciomarine sediments draping the underlying topography. Furthermore, sloping reflectors can be observed on either side of the ridge in the acoustic basement, suggesting that a bedrock core is present. Therefore, the feature seems more likely to be a bedrock sill draped by conforming ice-contact and glaciomarine sediments, rather than a pure moraine deposit.

Unit A: Is observed to be very acoustically strong and massive, with four associated multiples. As the basal unit, its thickness could not be estimated. The unit appears as a large ridge on the left margin of the profile, and again as smaller ridges near the 2000 and 4000 m markers. At the larger ridge (*c*), unit A appears to be surficial before onlapping by units B, C, and E. At the 2000 m ridge, unit A is overlain by units B and C, while the 4000 m ridge appears to surpass units B and D and instead underlies unit E. The unit is interpreted as bedrock, due to the multitude of associated multiples and the bathymetry suggesting that the major sill is continuous with the sidewall. Thus, the major sill is likely an intrusion of the sidewall, and is potentially draped by lateral moraine material. The 4000 m ridge feature is also interpreted as bedrock, as the bathymetry indicates that this point is located close to the shoal.

Unit B: Is observed primarily in between the major and minor sills, where it overlies unit A and underlies unit C, and to a lesser extent within the delta below unit D. The unit has a moderate, chaotic contact line where it underlies unit C, but appears weaker underneath unit D. Very few distinct internal reflectors are observed. Where it can be measured, the unit has an estimated mean thickness of 5 m and range of 4–7 m. The unit is interpreted as ice-contact sediment, given its chaotic character.

Unit C: Is observed associated with the major and minor sills. The unit is acoustically stratified, with a strong contact line and a relatively continuous, moderate internal reflector. It overlies and conforms to units A and B, and underlies units D and E. The unit undergoes acoustic blanking underneath unit D in the prodelta region. Where it can be measured, the unit has an estimated mean thickness of 11 m and range of 5–15 m, visibly thickest over the minor sill. It was interpreted as glaciomarine sediment for its stratified and conforming character.

Unit D: Is defined by the strong, chaotic contact line throughout the delta plain, which weakens to moderate through the main delta slope (sigmoid-oblique clinoform pattern), becomes strong for a short segment at the foot of the delta slope before weakening significantly through the prodelta region. Where it could be measured, the unit has an estimated mean thickness of 4 m and range of 2–9 m, thickest in the prodelta region and thinnest in the delta plain. Where the prodelta approaches the minor sill, the unit overlies and onlaps unit C, and in the delta plain overlies unit B and onlaps the unit A ridge. The unit overlies unit E along its length. Due to the unit's association with the delta, which covers over half of the profile, unit D was interpreted as deltaic sediment.

Unit E: Is an acoustically weak-to-transparent, surficial unit that drapes most of the profile, overlying units C and D. Where they occur, the weak internal reflectors are either sub-parallel (prodelta) or wavy parallel (delta plain). The unit has an estimated mean thickness of 4 m and range of 2–12 m, reaching its maximum thickness in the prodelta area but also thickening towards the fjord head. The unit was interpreted as post-submergence marine mud.

Multiples: Four multiples represent the major sill, two being very strong and two weaker. This is interpreted as representing exposed bedrock. Only one multiple is present for the submerged fjord-head delta, but is fairly strong, likely indicating coarse sediment.

B.1.1.4 Profile *d* (0077_2012_286_1214.jp2)

Profile *d* (Fig. B.7) is parallel to the upper portion of profile *c*, transecting the major and minor sills closer to the fjord mid-line. This provides a modified view of the minor sill, showing a relatively symmetrical shape conforming to the underlying substrate, which decisively indicates that it should not be interpreted as a push moraine. During the sea level lowstand, when the delta formed, the major sill would have been subaerial and part of it exposed to wave action. This could have resulted in ice-contact sediment being reworked downslope.

Unit A: Is acoustically strong and massive, except for two internal reflectors at the 286 m marker, with four associated multiples. The unit appears as a large ridge on the north end of the profile (*d*), where it is surficial to partly draped by units B, C, and E, and a smaller ridge in between 1686–1886 m, overlain by unit C. As the basal unit, its thickness could not be estimated. Due to the spatial association of the larger ridge with the mid-fjord sill and its acoustic strength, the unit is interpreted as bedrock. The smaller ridge is interpreted as the same, as its contact line is observed to be sharper than and extend below the adjacent and onlapping unit B, suggesting a structural feature. The internal reflectors at 286 m may indicate faults in the bedrock.

Unit B: Is a massive unit with a moderate, chaotic contact line. It partially overlies and onlaps unit A, and underlies unit C. The thickness could only be estimated where it onlaps unit A, which returns a mean of 7 m and range of 3–13 m. Given its chaotic character and position adjacent to the interpreted bedrock, the unit is interpreted as ice-contact sediment.

Unit C: Is a stratified unit with a strong contact line and moderate-to-weak internal reflectors conforming to the underlying units A and B. It has an estimated mean thickness of 16 m, ranging from 11–23 m. The unit appears to contribute considerably to the minor sill, in between 1686–1886 m. Due to its stratified, conformable nature, it was interpreted as glaciomarine sediment.

Unit E: Is an acoustically transparent, surficial unit, observed to drape unit C and onlap and infill unit A. Along the length of profile *d*, the unit has an estimated mean thickness of 3 m and range of 1–11 m, and appears to thicken further south of *d*’. The unit is interpreted as marine mud.

B.1.1.5 Profile *e* (0013_2014_247_1808.jp2)

Profile *e* (Fig. B.8) provides a larger-scale view of the submerged delta plain / sandur from profile *c*, and intersects station 2014NULIAJUK-0002. The contact between units B and D3 (ice-contact sediment and topset bed) is difficult to observe—some part of it can be traced from faint reflectors, but elsewhere the record is unclear. This may be due to a greater presence of gravel in the sandur environment which causes attenuation of the shot, and or gas-masking arising from organic deposits buried in the valley floor. Infilled stream channels may be present.

Unit B: Acoustically weak and difficult to observe contact line, except for a strong segment on the left margin. Equally weak internal reflectors are also observed. The shape of the reflectors appears to be between hummocky and contorted. As the basal unit, thickness could not be estimated. The unit was interpreted as ice-contact sediment.

Unit D: Moderate contact line closely underlain by a strong internal reflector in an uneven, sub-parallel pattern. It overlies unit B and underlies unit E. The estimated mean thickness is 4 m, and ranges between 2–7 m. The unit is interpreted as the delta topset bed.

Unit E: An acoustically transparent surface layer. The unit has an estimated mean thickness of 2 m and range of 2–3 m, and is interpreted as post-submergence marine mud.

Multiples: Correspond to unit D and E. The latter multiple is weaker than the former, suggesting that unit E (post-submergence marine mud) is composed of more weakly reflecting (fine-grained) materials than unit D (coarser deltaic sediments).

B.1.2 Side-entry delta

The submerged side-entry delta occupies a shallow embayment on the eastern shore of Boas Fiord, located 16–17 km from the fjord head. Here, a side-entry valley with three stream systems feeds into the fjord. The southernmost stream is a first-order system, while the other two are third-order. Both third-order streams are observed via Google Earth Pro™ (Google, 2021) to contain both lakes and segments of braided-stream morphology along their length. While the higher stream order initially makes these streams favourable for sediment transport, the lakes and braided morphology indicate areas of decreased water velocity where coarser sediments should settle prior to reaching the delta. Thus, modern sedimentation is not expected to be significant.

The local bathymetry reveals that the side-entry delta includes a primary terrace (>0.8 km^2) which extends across Giff's Cove, and a secondary terrace (>0.2 km^2) which progrades outwards from the northernmost stream mouth. The slope and relief of the two terraces are significantly different, with the former sloping at 18° (~816 m) with a relief of ~280 m bsl, while the latter slopes at 5 to 6° with a relief of ~5 m bsl. A narrow side terrace is also observed, extending northwards along the sidewall. The primary terrace is relatively even and featureless, yet the delta slope contains four well-developed channels, at least two of which are identified as slope-failure scars by the deposits at the foot of the slope (Fig. B.9). The others observed channels may be relict stream channels. The secondary terrace shows faint signs of shallow channels, but its slope shows no distinct features (possibly due to its shallow slope and or low relief relative to the primary terrace). The acoustic profiles analyzed for this study transect the three *MV Nuliajuk* coring sites, the primary and secondary terraces, and the northern sidewall terrace slope (Fig. B.10).

The secondary terrace indicates that a period of fluvial reactivation and delta building occurred sometime after the primary terrace was submerged. However, the size contrast between the two indicates that delta building during the fluvial reactivation was limited, possibly by the sediment supply and or duration of the event. Moreover, the acoustic profiles only depict the secondary terrace as a change in elevation rather than a distinct acoustic appearance. As noted above, the presence of lakes and braided streams in the local stream system should impede coarse sediment deposition, which could explain the limited development of the secondary terrace. However, the duration of the fluvial reactivation remains an open question. Both the primary and secondary terraces of the side-entry delta where targeted for gravity coring by the *MV Nuliajuk* in 2014. A shell subsample was extracted from 2014NULIAJUK-0005 GC, and 2014NULIAJUK-0007 GC was observed to contain shell material. However, this material has not been submitted for radiocarbon dating, so dating control of the two terraces is currently unavailable.

Overall, three acoustic units (B to D) are observed throughout the side-entry delta.

Unit B (ice-contact sediment) is observed underlying the delta slope, before undergoing acoustic blanking, as a moderate-to-weak, massive, chaotic unit. It is the basal unit, observed to underlie units C and D. The unit is interpreted as ice-contact sediment, based on the glacial history of the setting (lateral, median, and or end moraines expected) and the chaotic character of the unit which suggests coarse sediment. The acoustic blanking observed for the unit could indicate either a gas-mask (from decomposed organics) or the attenuation of the shot due to coarse sediments from the overlying unit D.

Unit C (glaciomarine sediment) is only observed underneath the sidewall terrace (Fig. B.14), before either onlapping unit B or undergoing acoustic blanking underneath the delta slope. The unit has a strong-to-moderate contact line with a disturbed to chaotic appearance, but shows no stratification. It overlies and conforms to unit B, and underlies unit D. The unit has an estimated maximum thickness of 11 m. It is currently interpreted as glaciomarine sediment, despite showing no internal stratification, based on its acoustic weakness, suggesting finer sediment, and its position in between units interpreted as ice-contact and deltaic.

Unit D (deltaic sediment) is observed in direct spatial association with the side-entry delta. The unit's acoustic strength and character varies in strength between subunits D2 and D3. Along D2, the contact line varies from strong to moderate, with a few internal reflectors varying from strong to weak. Some disturbed reflectors along the delta slope and sidewall terrace may suggest slump failures, although the bathymetry suggests these feature may represent relict stream channels instead. Along D3, the unit is bounded by a strong contact line, and appears to be acoustically massive except for a single strong, subparallel internal reflector very close to the contact line. A transition between weak to strong internal reflectors occurs at the cusp of the delta slope. The unit is surficial, overlying units B and C, and where its thickness could be estimated it shows a maximum of 22 m at the cusp of the delta slope, along the sidewall terrace. The unit was interpreted as deltaic sediment, based on its direct spatial association with the submerged side-entry delta, and its acoustic strength which suggests coarse sediments. The strong internal reflector along the topset beds (D3) may indicate a pavement of coarse sediments or even gravel, while the lack of other internal reflectors suggests that the shot was attenuated. Two hyperbolic reflectors observed on the sidewall terrace (profile *i*; Fig. B.14) may indicate seabed erratics.

Deltas may contain buried organics, the decomposition of which could lead to the gas build-up necessary for the acoustic masking of unit B. Moreover, build-up of gas deposits can trigger slope failures, similar to the one observed, which should otherwise occur less frequently in a submerged delta than an active one. However, given the lack of an observable overlying acoustic unit, and any age constraints for the slump deposits, there is no evidence to suggest whether the rotational failure occurred pre- or post-submergence.

It is noted that samples 2014NULIAJUK 0005 to 0007 GC contain 12 to 20 cm of clay-silt. This indicates that a stratum of marine mud is also present at the side-entry delta, if much thinner than at the fjord-head delta. However, the thickness of 12–20 cm is evidently below the resolution of the acoustic subbottom imagery, as no acoustic unit corresponding to this sediment stratum appears on any of the local acoustic subbottom profiles. The thinness of this stratum further supports the interpretation of weaker sedimentation at the side-entry delta.

B.1.2.1 Profile *f* (0036_2012_285_1635.jp2)

Profile *f* (Fig. B.11) transects the side-entry delta roughly along its centerline, from the lower delta slope to the secondary terrace, providing a representative view of its overall structure. However, it does not include the foot of the delta slope.

Unit B: Is observed as a single reflector underlying unit D in the delta slope (foreset beds). Its acoustic character is weak and massive with little detail to describe, but the slope of the reflector does not conform to expectations for an additional foreset bed. As the basal unit, its thickness could not be estimated. Based on the glacial history of the setting and the reflector's lack of conformity with the foreset beds, the unit is interpreted as ice-contact sediment.

Unit D: Surficial unit, overlying unit B. The contact line is strong along the delta plain, but shows uneven strength along the delta slope. The delta plain area appears acoustically massive, with no indicators of topset beds. However, it is associated with two multiples—possibly indicating coarser sediments. The delta slope contains a few internal reflectors, and what resemble overlying deposits. Some of the internal reflectors appear to onlap the weaker segment of the unit B contact line. What resembles an overlying deposit, when compared to the bathymetry, seems more likely to be a deltaic structure related to what are likely relict stream channels. The unit thickness could only be estimated where unit B is visible, which returns a mean of 15 m and range of 13–18 m. The unit is interpreted as deltaic sediment.

B.1.2.2 Profile *g* (0093_2012_286_1444.jp2)

Profile *g* (Fig. B.12) extends from the upper delta slope (foreset beds) to the shallow secondary terrace on the main delta plain, intersecting station 2014NULIAJUK-0005. The delta slope shows evidence of a partial rotation failure and slump-failure deposits near the left margin (*g*). The secondary terrace (*g*') indicates a possible reactivation of the delta, possibly as a submarine fan.

Unit B: Is observed as a moderate contact line, extending from the left margin to underneath the delta slope (~150 m marker) where it undergoes acoustic blanking. The unit appears to be massive, with a chaotic pattern. As a basal unit, its thickness could not be estimated. The unit is interpreted as ice-contact sediment, as its chaotic character indicates coarse sediment and its position corresponds to what is expected for a ground moraine. The acoustic blanking of the contact line could indicate either a gas-mask or the attenuation of the shot due to coarse sediments.

Unit D: Surficial unit with a strong contact line and internal reflectors of varying strength. Moderate, disturbed internal reflectors along the slope indicate a slump failure. Strong reflectors lie parallel and close to the contact line along the primary and secondary terrace. The thickness could only be estimated where unit B is visible, which returns an estimated mean thickness of 13 m and range of 12–14 m. The unit is interpreted as deltaic sediment. The topset (D3) contact shows scattering, suggesting gravel, while the lack of internal reflectors suggests that the shot is likely attenuated. The foreset beds (D2) contain few internal reflectors (vaguely sigmoid), along with evidence of a partial rotational failure and slump deposit. Deltas may contain buried organics, the decomposition of which could lead to the gas build-up necessary for masking. Moreover, build-up of gas deposits can trigger slope failures, similar to the one observed, which should otherwise occur less frequently in a submerged delta than an active one. However, given the lack of an observable overlying acoustic unit, and any age constraints for the slump deposit, there is no evidence to suggest whether the rotational failure occurred pre- or post-submergence.

Multiple: A strong seabed multiple represents the delta plain (unit D3), probably indicating sand or gravel in the topset bed. However, the multiple weakens when representing the foreset bed (D2), suggesting the presence of mud.

B.1.2.3 Profile *h* (0016_2014_247_2256.jp2)

Profile *h* (Fig. B.13) begins on the cusp of the delta slope and travels south across the delta, intersecting station 2014NULIAJUK-0006. Only the deltaic sediments are observed on the acoustic profile, although surficial marine muds (0.12 m thick) are indicated by 2014NULIAJUK-0006 GC.

Unit D: Is the only acoustic unit observed in the profile. It is bounded by a strong contact line, with internal reflectors of varying nature. Near the cusp of the delta slope, the reflectors are weak and mostly chaotic, although a weak sloping reflector is also observed. Along the delta plain is a single, uneven subparallel reflector close to the contact line, which peaks in strength in between the 350–450 m markers. The unit was interpreted as deltaic sediment. Moreover, it is noted that the 350–450 m peak in internal reflector strength is similar to what as observed on profile *g*; this may represent a feature, such a pavement of coarse sediments on a topset bed. The weak, sloping reflector near the left margin of the profile likely indicates the foreset bed.

Multiple: A strong multiple is observed in the corner (similar to profile *g*), this time overlain by a potential multiple of the watergun precursor.

B.1.2.4 Profile *i* (0013_2012_285_1352.jp2)

Profile *i* (Fig. B.14) runs parallel to the fjord sidewall and sidewall terrace before curving above the secondary terrace, where it intersects station 2014NULIAJUK-0007. Where the profile runs above the sidewall terrace, it displays possible frontal cross-sections of slump deposits and or stream channels. Unit E is not observed on the acoustic profile, but surficial marine muds (0.20 m thick) are indicated by 2014NULIAJUK-0007 GC.

Unit B: Is bounded by a moderate-strength chaotic contact line. As the basal unit, the thickness could not be estimated. It underlies units C and D, and undergoes acoustic blanking around the 3600 m marker. The unit is interpreted as ice-contact sediment, as it appears to correspond to the lateral moraine. The acoustic blanking observed may be caused by a gas-mask from decomposed organics in the overlying delta sediment, or attenuation of the shot from coarse deltaic sediments.

Unit C: Contact line varies from strong to moderate, with a disturbed to chaotic appearance. It conforms to the underlying unit B, but shows no stratification. The unit is acoustically weaker than the underlying unit B and overlying unit D, suggesting finer sediment. The unit has an estimated mean thickness of 9 m, ranging from 7–11 m. For this reason, it is currently interpreted as glaciomarine sediment.

Unit D: Is bounded by a strong contact line. Along the sidewall terrace (*i*), dips in the contact line may represent either slope failure scares or stream channels, and two hyperbolic internal reflectors may indicate seabed erratics. The internal reflectors underlying the primary and secondary terraces are acoustically strong, show an uneven subparallel pattern, and closely underlie the contact line. It is the surficial unit, overlying units B and C. Where it is possible to measure, the unit has an estimated mean thickness of 11 m and range of 3–22 m. The unit was interpreted as deltaic sediment.

Multiples: Two seabed multiples for the delta are present. The upper multiple appears strongly, indicating coarse material, and disappears below the sidewall terrace. The lower multiple is much fainter.

B.2 Durban Harbour

Acoustic subbottom profiles were collected throughout the Durban Harbour fjord system by the *MV Nuliajuk* in 2012 and 2014, and the *CCGS Amundsen* in 2014 and 2015. However, significant blank regions of the fjord system remain, including the entire southwest branch, the entire tributary fjord off of the northeast branch, and the margins of the northwest and northeast branches and the main trunk (Fig. B.15). Surveying was most concentrated at the submerged fjord-head delta, previously described by Cowan (2015).

As observed on Figure B.16 and Google Earth Pro™ (Google, 2021), three stream mouths feed into the fjord head. The western and eastern streams are both short, first-order systems that drain small ponds on the fjord sidewalls. However, the middle stream system has far more complex morphology. It consists of two major branches, western and eastern, which each drain its own valley before converging at a pseudo-braided segment shortly upstream from the mouth. The western branch drains a short valley, where the stream is fed at the valley head by glacial meltwater, and receives multiple tributaries which drain lakes or ponds. Near the head of the western branch, a braided segment feeds directly into a lake, with two smaller ponds occurring further downstream. Prior to convergence, it is a second-order stream. The eastern branch is longer with more tributaries. The headwaters and some of the tributaries are fed by glacial meltwater, while some other tributaries drain ponds. Along the stream's length, a notable segment of braided morphology occurs where most of the tributaries flow in, and a significant valley lake occurs downstream of all tributaries. Prior to convergence, it is a third-order stream. Although the middle stream drains multiple glaciers, and thus can be expected to transport glacial sediment, the occurrence of multiple braided segments and lakes/ponds along its course suggest multiple opportunities for sediment filtering to occur, thus impeding modern sedimentation.

The submerged fjord-head delta is not surveyed all the way to the fjord head, but is observed to have an area of at least 0.44 km^2. From the bathymetry, the terrace is measured to be ~0.86 km wide at the delta slope and ~0.16 km at the edge of the coverage, and at least ~1.5 km long. The delta plain appears relatively even with only three features of note: a raised feature interpreted as a bedrock shoal originating as a spur of the northern sidewall, a shallow ridge located near the southern sidewall, and a slope-failure deposit (Fig. B.16). This study prioritizes stratigraphic analysis related to the core-sampling sites, but these features may be of note to future research. The acoustic profiles analyzed in this study transect the three *CCGS Amundsen* coring sites, as well as the prodelta and submerged delta terrace (Fig. B.17).

The slope-failure deposit is interesting, as on profile *n* (Fig. B.26) it is clearly onlapped by a weaker acoustic unit to the east, but to the west only displays a subtle transition indicated by weakening internal reflectors. However, the delta plain is observed to be level at nearly the same depth on either side of the deposit, suggesting that the visible eastern unit is continuous with the rest of the delta plain. Thus, the slope failure is interpreted to have occurred either prior to or during delta progradation. The fact that the overlying sediment does not drape the slope-failure deposit indicates a hyperpycnal flow.

Overall, three acoustic units (A, B, and D) are observed throughout the Durban Harbour fjord-head delta. However, it must be noted that additional sedimentary units may be present but too thin to be resolved on the acoustic stratigraphy, as evidenced by cores from Boas Fiord and Durban which contained sediment facies not observed on acoustic profiles.

Unit A (bedrock) is only directly observed on profiles *m* and *o* (Figs. B.25, B.27) where they approach the sidewalls and the shoal. The unit appears as multiple acoustically-strong ridges, with weaker, ridge-shaped internal reflectors. The unit is surficial at select locations, but is predominantly overlain and or onlapped by unit B. The southern flank of the shoal appears to be onlapped by deltaic sediment. As the basal unit, its thickness could not be estimated. The unit is interpreted as bedrock, based on its acoustic strength, ridge shape, and the spatial association with the sidewalls and the shoal. The observed internal reflectors possibly represent either side echoes or faults in the bedrock.

Unit B (ice-contact sediment) is observed throughout the fjord-head area, underlying the submerged delta but also composing the fan-shaped feature. It is predominantly an acoustically massive unit bounded by a strong, chaotic-to-hummocky contact line. The unit is observed to overlie and onlap unit A, and appears to be surficial at the sidewall slopes and distal end of the prodelta area. However, the unit is onlapped by unit D proximal to the delta, and also be unit E in the prodelta depression (profile *j*; Figs. B.18 – B.22). It appears as the basal unit in most profiles analyzed, but is estimated to be at least 6 m thick in profile *l* (Fig. B.24). The unit is interpreted as ice-contact sediment, based on the glacial history of the setting, its bedrock-adjacent position, and its strong, chaotic contact line which suggests gravel and or coarse sediments.

However, within the fan-shaped feature (Fig. B.26), the unit instead appears to contain chaotic-to-disturbed internal reflectors near the contact line, and weak, contorted reflectors deeper below. The feature is partially surficial, onlapped on either side by unit D. The contact line with unit D is distinctly stronger on the right (upfjord) side of the profile, suggesting finer sediment deposition nearer to the fjord head. The fan-shaped feature is hypothesized to be either a slope-failure deposit from the lateral moraine, or a terminal moraine that developed behind the sidewall intrusion.

Unit D (deltaic sediment) is observed in direct spatial association with the submerged fjord-head delta. The unit is bounded by a strong contact line, which is closely underlain by stratified, strong-to-weak internal reflectors. These reflectors are mainly parallel throughout the topset beds, but become subparallel throughout the foreset and bottomset beds. The unit is surficial, overlying unit B and onlapping it at the prodelta and sidewall slope areas (and at the fan-shaped feature). It has an estimated maximum thickness of at least 21 m along the delta slope (profile *k*; Fig. B.23). The unit is interpreted as deltaic sediment, due to its observed spatial association with the submerged fjord-head delta and the prograding clinoform pattern representative of the Gilbert delta. The presence of sand is confirmed by core 2015805-0005 GC. At the fan-shaped feature (profile *n*; Fig. B.26), the contact between units B and D is more distinct along the south face (*n*'), suggesting that unit D consists of finer sediment at this location nearer to the fjord-head.

B.2.1 Profile *j* (0063_2015_295_0924.jp2 & 0008_2012_286_2127.jp2)

Profile *j* (Fig. B.18) transects the prodelta depression, breaks for ~135 m, and continues across the delta, terminating above the delta plain. The ridge observed near the far-left margin visibly resembles a submerged drumlin on bathymetry, but may be more likely to be a sediment-draped bedrock shoal. The profile is composed of segments from two separate acoustic profiles collected by the *CCGS Amundsen* and *MV Nuliajuk*.

Unit B: Underlies the length of the composite profile. The unit is bounded by a strong, chaotic contact line, and appears to be acoustically massive. As the basal unit, its thickness could not be estimated. The unit is partly surficial, and partly overlain and onlapped by units D and E. The unit is interpreted as ice-contact glacial till, given its basal position and the strong and chaotic contact line which likely indicates gravel.

Unit D: Is observed along most of the profile. The unit is bounded by a strong contact line, and contains multiple internal reflectors, discontinuous and sub-parallel, that range from strong to weak. Some may indicate slump features. Overall, the reflectors display a sigmoidal sloping pattern. The unit is surficial, overlying and onlapping unit B, and has an estimated mean thickness of 6 m and range of 1–15 m. The unit is interpreted as deltaic sediment, due to its observed spatial association with the submerged fjord-head delta and prograding clinoform pattern. The strength of some of the reflectors may be attributable to ponded infilling, driving by a hyperpycnal flow. Additionally, on the original profile used for the left segment (not depicted here), the internal reflectors are observed to be continuous with the delta slope.

Multiple: A strong multiple below the delta plain suggests its surface includes sand or gravel.

B.2.2 Profile *k* (0053_2014_247_0100.jp2)

Profile *k* (Fig. B.23) is a segment taken from a much longer shiptrack. It begins near where the seabed begins shallowing, skirts the prodelta depression (see profile *j*), crosses the delta slope, and terminates above the submerged delta plain. The area where the seabed begins to shallow may be associated with the small intra-fjord islands, or the submerged western sidewall; the morphology remains uncertain due to the limits of bathymetric coverage.

Unit B: The basal unit is acoustically strong, massive, and chaotic. It underlies the weaker unit D. As the acoustic basement, the thickness could not be estimated. The unit is interpreted as ice-contact glacial till, based on the glacial history of the area and the strong and chaotic character indicating coarse sediment.

Unit D: The unit is acoustically strong near the contact line, but quickly weakens with depth. Uneven internal reflectors occur near the contact line in a complex sigmoid-oblique pattern, and a few very weak, disturbed reflectors occur below the delta plain. Based on where the unit thickness could be measured, a mean thickness of 5 m and range of 3–9 m was estimated. The unit was interpreted as deltaic sediment, based on the observable tripartite delta structure of topset, foreset, and bottomset beds.

B.2.3 Profile *l* (0013_2012_286_1915.jp2)

Profile *l* (Fig. B.24) is a segment of a longer profile (the remainder of acoustic subbottom profile 0013_2012_286_1915 is fragmented and difficult to use), and details the prodelta area and foot of the delta slope. It intersects stations 2014805-0001 and 2015805-0005.

Unit B: Is an acoustically strong unit. The contact line has a hummocky shape, while the unit interior is massive and chaotic. As the basal unit, its thickness could not be estimated. The unit is interpreted as ice-contact glacial till.

Unit D: Is acoustically lighter than the underlying unit B, with a darker, near-surface internal reflector noticeable between the 1000–1200 m markers, making an oblique-tangential slope. The unit has an estimated mean thickness of 6 m and range of 2–21 m. The unit was interpreted as deltaic sediment, based on the observed structure of a bottomset beds (D1) continuous with the foreset beds (D2), and the presence of sand indicated by 2015805-0005 GC.

Multiples: Strong multiple reflecting the sand known to be present.

B.2.4 Profile *m* (0016_2012_286_1942.jp2)

Profile *m* (Fig. B.25) transects the submerged delta from the lower delta slope to the foot of the southern sidewall slope. Therefore, it provides a representative view of the overall delta.

Unit A: Is observed as three ridges within the southwest sidewall slope (*m*'). The unit is bounded by a strong contact line, with at least two ridge-shaped internal reflectors. It is observed to be partially overlain and onlapped by unit B, and partially surficial. As a basal unit, its thickness could not be estimated. The unit is interpreted as bedrock, based on its ridge-like shape and spatial association with the fjord sidewalls. The ridge-shaped internal reflectors may represent side-echoes.

Unit B: Is observed underlying the delta slope, and draping the sidewall slope. The unit is acoustically massive, bound by a strong, chaotic contact line. It is observed to overlie and onlap unit A, and underlies unit D. Its thickness could not be estimated beneath the delta slope, but within the sidewall slope it shows a thickness of at least 6 m where it onlaps unit A. The unit is interpreted as ice-contact sediment, based on the glacial history of the setting and its chaotic character, indicative of coarse sediment.

Unit D: Extends from the left margin to the sidewall slope, in direct spatial association with the submerged delta. Internal reflectors appear weak-to-moderate within the delta slope, and strengthen to moderate-to-strong along the delta plain. The unit is observed to overlie unit B at the delta slope, and to onlap it at the sidewall slope. Where it could be estimated, the unit has an estimated mean thickness of 7 m, ranging from 4–13 m. The unit is interpreted as deltaic sediment, based on its direct spatial association with the submerged delta.

B.2.5 Profile *n* (0006_2012_286_2117.jp2)

Profile *n* (Fig. B.26) covers the northern edge of the submerged delta plain, towards the edge of the collected bathymetry. It transects the fan-shaped feature.

The fan-shaped feature (0.033 km^2) is located along the northern sidewall, below a small alpine pond (9.5×10^{-3} km^2). The observation of onlapping deltaic sediments on either side indicates that the feature predates at least the most recent topset beds. Its origin was difficult to interpret, with hypothesizes including: alluvial fan, talus fan, draped bedrock, or a minor side-entry moraine. An alluvial fan origin is suggested by its position below the alpine pond, and Google Earth Pro™ (Google, 2021) imagery which faintly suggests an outflowing stream; however, the sediment source is left unexplained. A talus fan origin is suggested the coarse material of the feature, but it lacks the characteristic steepness. The feature could have originated as bedrock draped by ice-contact sediment (and possibly smoothed by wave action), but how often does this result in a fan shape? The feature may also be a moraine deposit from a minor side-entry glacier; localized glacial erosion could explain the topography wherein the sidewall is significantly lower proximal to the alpine pond than it is immediately to the east. Or a minor slope failure scar, although no corresponding slope failure scar is apparent on either the bathymetric or satellite imagery.

Unit B: Is interpreted as making up the fan-shaped feature. The unit is bounded by a strong, chaotic contact line, and appears to contain chaotic-to-disturbed internal reflectors near the contact line and contorted reflectors further below. It is partially surficial, and interpreted to be onlapped by unit D on either side; on the right side (*n*') this contact is clearly visible if uneven in strength, but the contact is much weaker on the left (*n*). As the basal unit, its thickness could not be estimated. The unit was interpreted as ice-contact sediment, based on its strong, chaotic character indicative of coarse sediments, and the glacial history of the setting. See above for discussion of the fan-shaped feature.

Unit D: Is observed as a level delta plain onlapping the fan-shaped feature on either side. The unit is bounded by a strong contact line with a few internal reflectors—these are more apparent on the right side where the unit interior is weaker. The unit has an estimated mean thickness of 8 m, ranging from <1 to 12 m. It was interpreted as deltaic sediment, based on its spatial association with the delta plain.

B.2.6 Profile *o* (0024_2012_286_2034.jp2)

Profile *o* (Fig. B.27) is a frontal profile of the delta, extending from the foot of the southern sidewall and across the width of the delta, the shoal, and a sidewall intrusion.

Unit A: Is observed on either side of the profile, associated with the sidewall and shoal. The unit appears as multiple ridge features, bounded by strong contact lines and containing additional ridge-like internal reflectors. It appears to be occasionally draped by unit B, and occasionally surficial. As the basal unit, its thickness could not be observed. The unit was interpreted as bedrock, based on its ridge shape and the spatial association with the sidewalls and the shoal. The observed internal reflectors possibly represent either side echoes or faults in the bedrock.

Unit B: Appears as an acoustically strong, chaotic unit. It overlies and onlaps unit A, and underlies unit D. The unit has an estimated mean thickness of 2 m, ranging from 1 to 4 m. It was interpreted as ice-contact sediment based on its strong, chaotic character, indicative of coarse sediment, the glacial history of the setting, and its position adjacent to bedrock. An acoustic body next to the 1300 m marker is acoustically weaker than the rest of the unit—this is current attributed to it having been previously disturbed, thus reducing its density and or sorting and weakening its reflection.

Unit D: Is observed along the frontal profile of the delta. The unit is bounded by a strong contact line with strong-to-weak, even to uneven parallel internal reflectors that weaken with depth. The unit is surficial, observed to overlie and onlap unit B at its margins, and likely overlies it along the width of the delta at an unknown depth. Where the unit thickness could be estimated, it shows a mean of 5 m, ranging from 1 m to 9 m. It is interpreted as deltaic sediment, given its spatial association with the submerged delta and its acoustic stratification reminiscent of topset beds.

B.3 Akpait Fiord

Akpait Fiord has been explored by the *MV Nuliajuk* in 2012, 2013, and 2014, and the *CCGS Amundsen* in 2014 and 2015. The majority of these cruises were centered on the fjord-mouth sill and the adjacent portion of the fjord basin. In 2013, the *MV Nuliajuk* collected bathymetry along the length of the fjord; however, due to an equipment malfunction, no acoustic subbottom imagery was collected. As a result, all of the acoustic subbottom profiles are concentrated within the vicinity of the fjord mouth. The current study focuses on inferring the sedimentary history of the fjord-mouth sill and adjacent fjord basin.

As observed on the Toporama base map, multiple short, first-order streams feed into the fjord near the mouth. Some of these streams are observed to be fed by small cirque glaciers.

The most distinctive feature of Akpait Fiord is the fjord-mouth sill. Bathymetric coverage is incomplete, but the sill appears to occupy an area exceeding 7 km^2. As previously noted by Cowan (2015), the sill platform lies at 50–52 m bsl with a relief of 72 m compared to the adjacent basin floor. The limited bathymetry makes an average slope for the outer sill difficult to estimate, but the inner slope is visibly steeper, with more signs of mass transport. The inner slope is also observed to be steeper at the margins (7.6–9.2°), with a shallower ramp along the median (2.7°). This ramp may be related to the adjacent spillover deposit. The sill platform is relatively even and featureless, except for two gravel spits identified by Cowan (one is transected by profile *s*, Fig. B.36). Overall, Cowan interpreted the sill as morainal in origin. A smaller, mid-fjord sill is contiguous with the western arm of the fjord-mouth sill; for brevity, they are referred to as the inner and outer sills, respectively.

The outer part of the western tributary appears to contain a submerged delta (52 m bsl) that was not discussed by Cowan (2015). In addition the head of the main fjord contains a narrow sidewall terrace with an incised stream channel on the west side. At the southwestern corner of the fjord head and edge of current bathymetry, a slope face is observed (~20–30 m bsl) which could belong to either a shallow submerged delta, or a developing subaerial delta. The latter possibility is supported by satellite imagery (Google, 2021) indicating modern sedimentation at the fjord head.

Overall, five acoustic units (B, C, E, F, and G) were observed throughout Akpait Fiord.

Unit B (ice-contact sediment) is observed throughout the fjord-mouth region, underlying the fjord basin and composing the core of the mid-fjord and fjord-mouth sills. The acoustic character of the unit is observed to vary along the fjord: in the fjord basin, the unit appears to be massive with a weak contact line (underlying ~17 m of units C and E); in the mid-fjord sill, the unit shows a moderate, hummocky-to-chaotic contact line with similar internal reflectors; and within the fjord-mouth sill, the unit is bounded by an uneven, weak-to-strong chaotic contact line and contains a few weak, chaotic internal reflectors. It underlies unit C in the basin and inner sill, and unit F along most of the outer sill, but appears to be surficial at the gravel spit. In between the two sills, the unit is predicted to underlie unit G at an unknown depth. As the basal unit, its thickness could not be estimated. The unit is interpreted as ice-contact sediment, based on its spatial association with the mid-fjord and fjord-mouth sills, which are currently interpreted as morainal in origin, and the observed chaotic reflectors indicative of coarse sediment.

Unit C (glaciomarine sediment) is observed to overlie the inner sill and underlie the fjord basin (Figs. B.31, B.32, B.35). It is heavily stratified, with at least 4 even parallel internal reflectors in the fjord basin, but has only one, weak-to-moderate internal reflectors along the mid-fjord sill. The unit overlies and conforms to unit B, and is onlapped by units E and G. The estimated maximum thickness is at least 16 m in the fjord basin. The unit is interpreted as glaciomarine sediment, based on its highly stratified and conformable character, and proximity to ice-contact material.

Unit E (marine mud) is observed to drape the fjord basin and onlap the inner slope of the inner sill (Figs. B.31, B.32, B.35). It is acoustically weak with one strong, even-parallel internal reflector. The unit is surficial, draping and onlapping unit C. The estimated maximum thickness is at least 6 m in the fjord basin. The unit is interpreted as marine mud, based on the expectation for fine-grained sediments to accumulate in the fjord basin, high density of parallel reflectors which may represent structural laminations of fine-grained sediment, and the clay-silt content of core samples 2014805-0002 PC & TWC, 2015805-0007 PC & TWC.

Unit F (sill cover) is observed overlying the fjord-mouth sill (Figs. B.33, B.34, B.36). The unit is acoustically weak, with some uneven weak-to-moderate internal reflectors along the inner slope and a moderate, even parallel reflector along the sill platform. The unit is surficial, overlying unit B, except for the foot of the sill where it is onlapped by the spillover deposit. The unit appears to onlap unit B in proximity to the gravel spit. The estimated maximum thickness is 19 m, where it infills the unit B terrace on the inner slope. The sill cover has been previously interpreted as sand-gravel draped in fine-grained sediments following sea-level rise by Cowan (2015), based on video footage. However, this interpretation poses the question of how fine-grained sediment developed so thickly on top of the fjord-mouth sill; it may originate as glaciomarine sediment. The unit thinness along the sill platform can be attributed to wave-action winnowing.

Unit G (spillover deposit) occupies the small basin in between the bases of the western sill arm and the fjord-mouth sill, appearing on the selected profiles as hump-shaped structures. It contains stratified, disrupted reflectors, strong near the surface and weakening with depth likely due to attenuation. The unit is surficial, and onlaps units B and F at the bases of the western sill arm and fjord-mouth sill, respectively. Its thickness could only be estimated where the onlapping is visible, which returns a maximum thickness of at least 8 m. The structure is spatially associated with the spillover deposit observed on bathymetry (Cowan, 2015), and thus likely consists of fine- and coarse-grained sediment reworked via wave action. This is supported by core sample 2014805-0003 PC. Due to this origin of reworking, spillover deposit is treated as an acoustic unit unto itself.

B.3.1 Profile *p* (0028_2014_277_1352.jp2 & 0066_2015_295_1712.jp2)

Profile *p* (Fig. B.31) is made from two segments of longer profiles (Figs. B.32, B.33). The first segment begins in the outer part of the Akpait Fiord basin and travels eastwards, crossing the mid-fjord sill (possibly a readvance moraine) before turning to the northeast and travelling along the foot of the western arm of the fjord-mouth sill. The profile then transitions to the second segment, which crosses the spillover deposit and the fjord-mouth sill proper as it continues north-by-northeast.

Unit B: Is observed across the entire composite profile, its contact line varying in acoustic strength. In the 1st profile segment, the contact line appears to occur in two separate, vertically offset segments, with the lower segment appearing to underlie and attenuate below the upper segment, while the upper segment appears to laterally transition from one of the unit E internal reflectors. Before attenuating, the lower contact line appears acoustically weak and uneven, and the massive chaotic interior quickly weakens even further with depth. The upper contact line is acoustically stronger, with a reflector pattern that transitions from hummocky to chaotic; signs of ponded infilling occur on either side of the 2500 m marker. A few hummocky internal reflectors are observed underlying the superior contact line. In the 2nd profile segment, the contact line is uneven, ranging between acoustically strong to transparent, while the unit interior appears to be massive. Near the foot of the sill, the contact line appears disturbed. Overall, unit B directly underlies both units E and F, and as a basal unit its thickness could not be estimated. It is interpreted as ice-contact sediment, as it is observed to make up the core of the mid-fjord and fjord-mouth sills, and the chaotic to structureless reflectors indicate coarse sediment.

Unit C: Is observed on the 1st profile segment, within the fjord basin and draping the inner sill. The unit is highly stratified with multiple strong, even parallel reflectors. The unit overlies unit B, and is onlapped by unit E. The unit has an estimated mean thickness of 8 m, with a range of 6–16 m, thinning slightly as it drapes the inner sill. It is interpreted as glaciomarine sediment based on its highly-stratified and conforming nature, and proximity to the ice-contact material. Core sample 2015805-0007 PC contains a large sand unit interbedded within fine-grained sediments, which is a potential turbidite current originating from unit C.

Unit E: Is observed on the 1st profile segment, within the fjord basin. The unit is acoustically weak, with one strong, even parallel reflector. The unit is surficial, overlying unit E along the fjord basin and onlapping it along the inner slope of the mid-fjord sill. The unit has an estimated mean thickness of 5 m, with a range of 2–6 m, thinning rapidly as it onlaps the inner sill. It is interpreted as marine muds based on the expectation for fine-grained sediments to accumulate in the fjord basin, and removal from the fjord head and any immediate major sediment source. This interpretation is supported by the predominately clay-silt composition of cores 0002 and 0007, which clearly appear to penetrate unit E.

Unit F: Is observed on the 2nd profile segment, overlying the fjord-mouth sill. The unit is acoustically weak, with a few uneven weak-to-moderate internal reflectors sloping towards the spillover deposit. It overlies unit B and infills the terrace observed above the 4500 m marker, and is onlapped at the foot of the sill by the spillover deposit. The estimated mean thickness for the unit is 7 m, ranging from 2–14 m. The unit was previously interpreted as fine-grained sediment by Cowan (2015), who observed the sill surface to consist of sand-gravel draped in fine-grained sediments. However, this interpretation does pose the question of how the fine-grained sediment developed so thickly on top of the fjord-mouth sill; it could stem from a combination of fine-grained sediments and upwelling freshwater released by the glaciers retreat, or originate as glaciomarine sediment.

Unit G: Appears as a stratified series of disrupted reflectors, initially strong near the surface but weakening with depth. The spillover deposit onlaps unit F of the fjord-mouth sill and unit B of the western sill arm. As a basal unit, its thickness could not be estimated. The structure is identified as the spillover deposit as its position along the profile corresponds to the feature on the bathymetry. As a spillover deposit, it likely consists of reworked sediment—both coarse- and fine-grained sediment mixed together. The spillover deposit is treated as an acoustic unit unto itself due to its origin of reworking via wave-action.

Multiples: Two separate sets of multiples are observed on the composite profile. On the 1st segment, the multiple illustrates the acoustic structure of the 2000 m ridge, the primary data for which was cut off. On the 2nd segment, the multiple reflects part of the sill slope.

B.3.2 Profile *q* (0047_2014_246_1828.jp2)

Profile *q* (Fig. B.34) is a segment of a longer profile, beginning above the spillover deposit and travelling northeast across the fjord-mouth sill. An adjacent profile was previously interpreted by Cowan (Fig. 3.16 in 2015), which is consulted in this analysis.

Unit B: Is observed as a short segment at the left-margin, corresponding to the flank of the western sill arm, and as the core of the fjord mouth sill. On the left margin, the unit is bounded by a strong even contact line, but appears to be disturbed and contains a few contorted internal reflectors. Within the fjord-mouth sill, the contact line is uneven and has an overall sigmoidal slope with a terrace at 1200 m, and the unit itself appears to be acoustically massive except for a single weak reflector near the right margin. The slope terrace could be interpreted as a scar left by a slope-failure that produced the bulge near the foot of the sill (500–700 m); however, evidence from Cowan (2015) supports a different interpretation described below. The unit is onlapped by the spillover deposit on the left margin, and draped and partially infilled by unit F throughout the fjord-mouth sill. As the basal unit, its thickness could not be estimated. The unit is interpreted as ice-contact sediment, as both the western sill arm and the fjord-mouth sill are currently interpreted as morainal in origin.

Unit F: Is bounded by a strong contact line and contains a few acoustically-weak, sigmoidal reflectors that converge towards the right. The unit is primarily surficial, draping the fjord-mouth sill segment of unit B and infilling the terrace at 1200 m, with only its lower flank onlapped by the spillover deposit. It has an estimated mean thickness of 8 m and range of 2–19 m, visibly thinnest at the right margin and thickest along the inner slope. The unit has been interpreted by Cowan (2015) as fine-grained sediments deposited following sea level rise, based in part on video-footage of the sill surface. Marine mud is expected to drape underlying structures as it settles out of suspension, but the range in unit thickness is unexpected. Cowan attributes the range of thickness to winnowing of fine-grained surface sediments.

Unit G: Appears as two hump-shaped structures containing multiple disrupted reflectors, which are acoustically strong near the contact line but weaken with depth. Core 2014805-0003 PC suggests that attenuation from coarse-grained sediments (sandy silt and silty sand) occurs. Cowan (2015) has previously interpreted this feature as a mass-transport deposit originating from reworking of the sill via wave-action. The unit thickness could only be estimated where it onlaps units B and F, which return an estimated mean thickness of 5 m, ranging from 1 to 8 m.

Cowan (2015) illustrated this area using a different profile (0028_2014_277_1500; Cowan Fig. 3.16), which shows a major difference in the contact line for unit B (unit A in Cowan). In Cowan’s Fig. 3.16, the unit B contact line is observed to have a shallow convex shape, while the 1200 m terrace is where an entirely separate acoustic unit onlaps with unit B. Due to the convex shape, the contact line separating the two units is unlikely to represent an artifact. Cowan interpreted this intervening unit as a wedge-shaped overwash deposit of redistributed sill material. The lower boundary for this unit cannot be observed on profile *q*, where the terrace appears to be continuous with unit B. The only comparable features observed on acoustic subbottom profile 0047_2014_246_1828 are changes in acoustic strength within unit B that resemble a series of ridges and troughs, with the peaks planed off and weaker infill in the troughs. These peak and infill features could represent ridges in the original moraine that were eroded by wave action and the reworked sediment deposited in between them. The difference between Fig. B.34 and Cowan Fig. 3.16 may be attributable to different subbottom echosounders, as the former acoustic profile was recorded by the *MV Nuliajuk* (Knudsen 3200 3.5 kHz) while the latter was recorded by the *CCGS Amundsen* (Knudsen K302R 3.5 kHz).

B.3.3 Profile *r* (0066_2015_295_1712.jp2)

Profile *r* (Fig. B.35) is a segment of a longer acoustic subbottom profile. The profile begins at the outer basin of Akpait Fiord and travels eastwards, crossing the slope of the sill's western arm. The profile intersects coring site 0007. Two acoustic units are interpreted—the acoustic basement and a surficial unit with onlaps it at the foot of the sill's western arm slope.

Unit B: Is the acoustic basement, visibly underlying unit C in between the 1500 m mark and right-hand margin. The unit is bounded by a moderate, chaotic contact line which plunges below the unit C internal reflector. As the basal unit, the thickness could not be estimated. The unit is interpreted as ice-contact sediment due to its association with the inner sill, and the observed chaotic character indicating coarse sediments.

Unit C: Overlies unit B at the summit of the sill, and is onlapped by unit E partway down the slope. The unit is bounded by a strong contact line, which is uneven beneath unit E but even where surficial. Strong, uneven-wavy internal reflectors occur along its length. Where the underlying unit B is visible, unit C has an estimated mean thickness of 2 m and a range of 1.7–2.0 m. The unit is interpreted as glaciomarine sediment, based on how it corresponds to unit C on profile *p*. Core 2015805-0007 PC contains a large sand unit at 378–408.5 cm, which potentially originated as a turbidity current from unit C.

Unit E: Is a moderately strong acoustic unit draping unit B, with an uneven weak-to-moderate internal reflector observed from the left margin to slightly beyond the 250 m marker. The unit has an estimated mean thickness of 4 m and a range of 4–5 m. The unit is surficial, overlying and onlapping unit C. The unit is interpreted as marine mud, which is confirmed by core samples 2015805-0007 PC & TWC. The weak internal reflector towards the left margin possibly represents structural lamination of the fine-grained sediments.

B.3.4 Profile *s* (0049_2014_246_1901.jp2)

Profile *s* (Fig. B.36) is a segment of a longer acoustic subbottom profile. The profile begins at the spillover deposit and travels northeast, crossing the fjord-mouth nearer to the western sidewall. The profile passes adjacent to coring site 0003, and transects one of the gravel spits identified by Cowan (2015). Here, the sill cross-section is distinct from what is observed on profiles *p* and *q*: the slope is steeper, and the unit B appears to emerge as surficial at the edge of the terrace.

Unit B: Is observed making up the core of the fjord-mouth sill. The unit is bounded by an uneven, chaotic contact line, varying from strong to weak. It appears mostly massive, with only a few weak, chaotic internal reflectors observed. The unit underlies unit F along most of the sill platform and inner slope, but it appears to be surficial near the edge of the slope, corresponding to the gravel spit identified by Cowan (2015). As the basal unit, its thickness could not be estimated. The unit is interpreted as ice-contact sediment, based on its association with the morainal fjord-mouth sill. In addition, the observed chaotic character is suggestive of coarse sediments.

Unit F: Is observed along the inner slope of the sill and along the sill platform. The unit is acoustically weak, with an even-parallel reflector along the sill platform, and multiple sloping reflectors along the slope. The unit overlies and onlaps unit B, and is mostly surficial except near the foot of the slope where it is onlapped by the spillover deposit. Has an estimated mean thickness of 8 m, ranging from 3 m above the sill to 14 m along the sill slope. The sill cover unit has been previously interpreted by Cowan (2015) as fine-grained sediments deposited following sea level rise.

Unit G: Is observed near the left margin, at the foot of the sill. The unit is stratified, with strong disturbed internal reflectors overlying some weaker sloping reflectors. It is surficial, and observed to onlap unit F at the foot of the sill. Could only be measured where it onlaps units F, which shows a thickness of 8 m. Cowan (2015) has previously interpreted this feature as a mass-transport deposit originating from reworking of the sill via wave-action.

B.4 Sunneshine Fiord

An acoustic profile of Sunneshine Fiord was collected by Gilbert and MacLean (1984) and analyzed by Andrews et al. (1994, 1996); see Figure B.37. Andrews et al. identified three acoustic units, which have been equated to the acoustic facies described throughout this thesis:

older sediments of Quaternary sediments of unknown age (Unit B), Unit II (Unit C), and Unit III (Unit E).

Table B.2: Summary of maximum sediment thicknesses and drainage-basin areas for fjords from the Northeast Coast and Cumberland Peninsula groups. All values are from Gilbert and Maclean (1984) except where marked.

Group	Fjord	Max. sediment thickness (m)	Drainage-basin area (km^2)
Northeast Coast	Cambridge	290	2013[*]
	Clark	200	1895[*]
	Inugsuin	110	2192
	McBeth	297	3584
	Itirbilung	200	2184
	Tingin	130	1228
	Mean:	*204.5*	*2183*
Cumberland Peninsula	Maktak	70	1132
	Coronation	130	1128
	North Pangnirtung	40	2064
	Sunneshine	84 [**]	564
	Mean:	*81*	*1222*

[*] Values borrowed from Carter (Chapter 2) analysis.
[**] Value estimated based on Andrews et al. (1994) diagram.

B.5 References

Andrews, J.T., Syvitski, J.P., Osterman, L.E., Williams, K.M., Mode, W.N., Kravitz, J.E. & Locke, W.W. III. (1994). *Quaternary geology of Sunneshine Fiord (Baffin Island).* Geological Survey of Canada, Open File 3004. doi:10.4095/195129

Andrews, J.T., Osterman, L.E., Jennings, A.E., Syvitski, J.P.M., Miller, G.H., & Weiner, N. (1996). Abrupt changes in marine conditions, Sunneshine Fiord, eastern Baffin Island, NWT during the last deglacial transition: Younger Dryas and H-0 events. *Late Quaternary Palaeoceanography of the North Atlantic Margins*, Geological Society Special Publication No. 111: 11-27.

Gilbert, R. & MacLean, B. (1984). Geophysical studies based on conventional shallow and Huntec high resolution seismic surveys of fiords on Baffin Island. In J.P.M. Syvitski & C.P. Blakeney (Eds.), *Sedimentology of Arctic Fjords Experiment: HU 82-031 Data Report, Volume 1* (GSC Open File No. 960). Dartmouth, NS: Bedford Institute of Oceanography.

Google. (2021). *Google earth pro* (Version 7.3.3). https://www.google.com/earth/

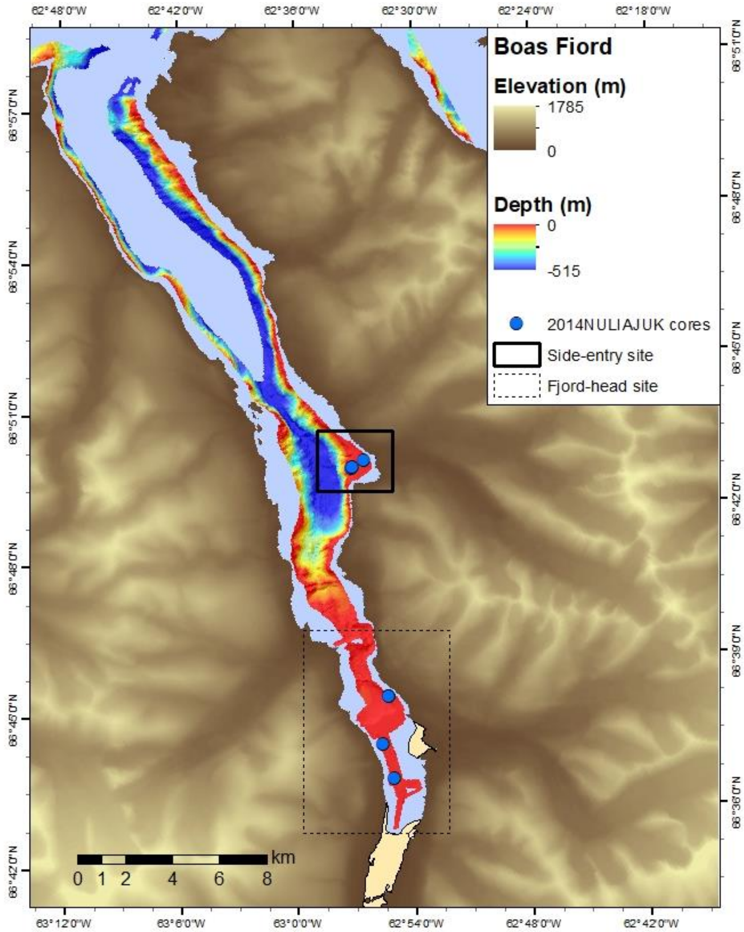

Figure B.1: Map of Boas Fiord, with the submerged delta study sites and their associated coring sites indicated.

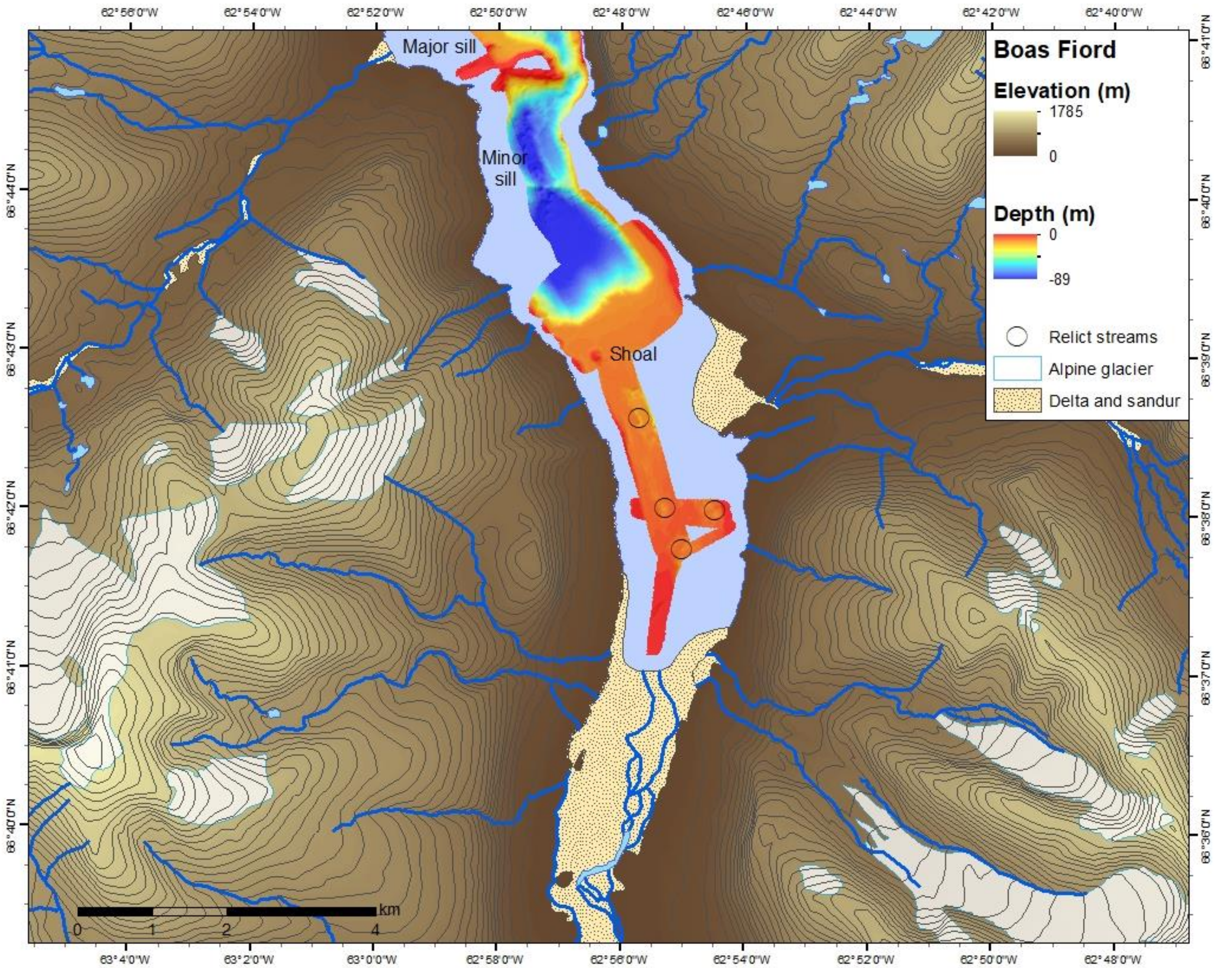

Figure B.2: Map of the submerged fjord-head delta study site at Boas Fiord, with some seafloor geomorphic features indicated.

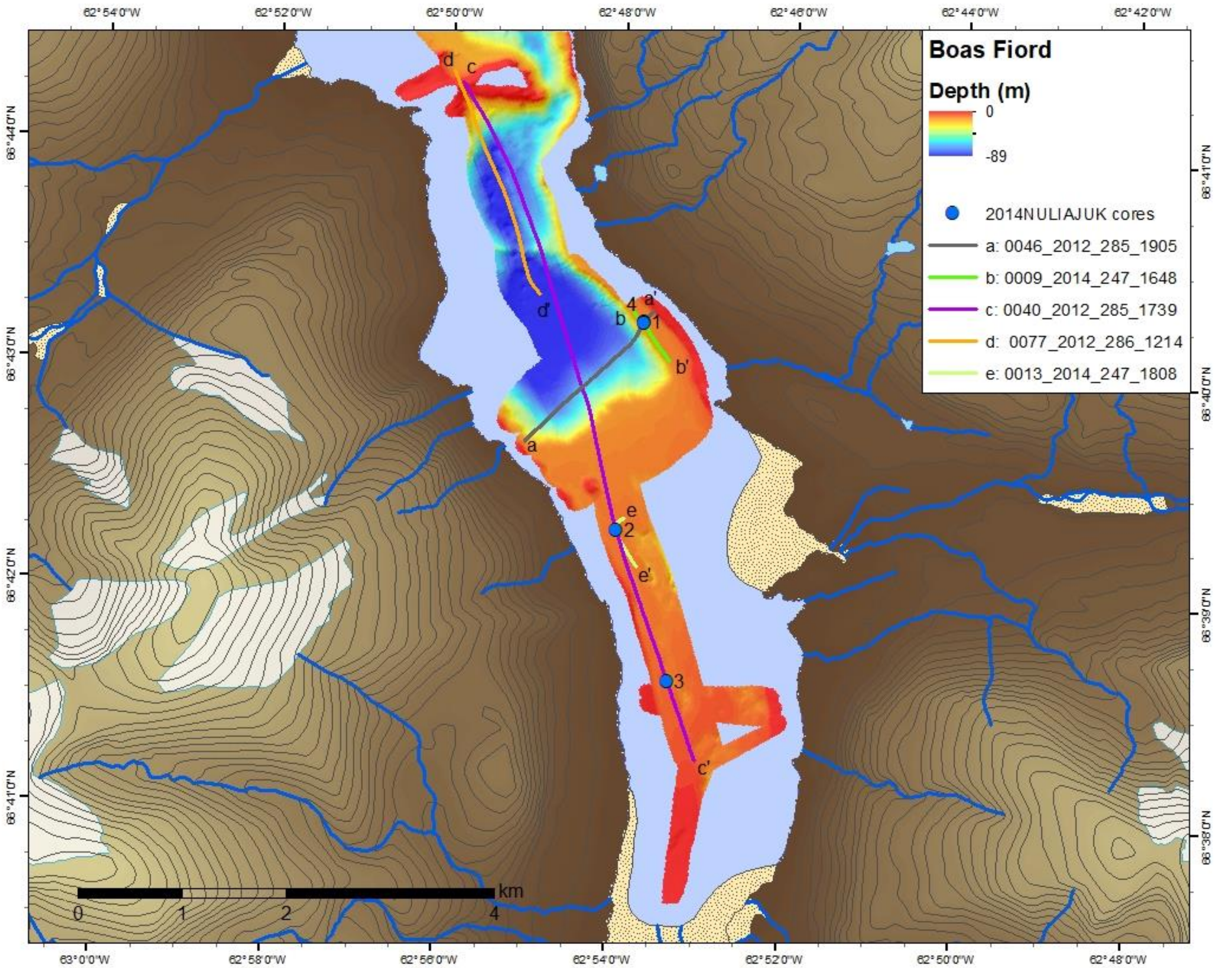

Figure B.3: Map of the submerged fjord-head delta study site at Boas Fiord, with the positions of the coring sites and the analyzed acoustic profiles indicated.

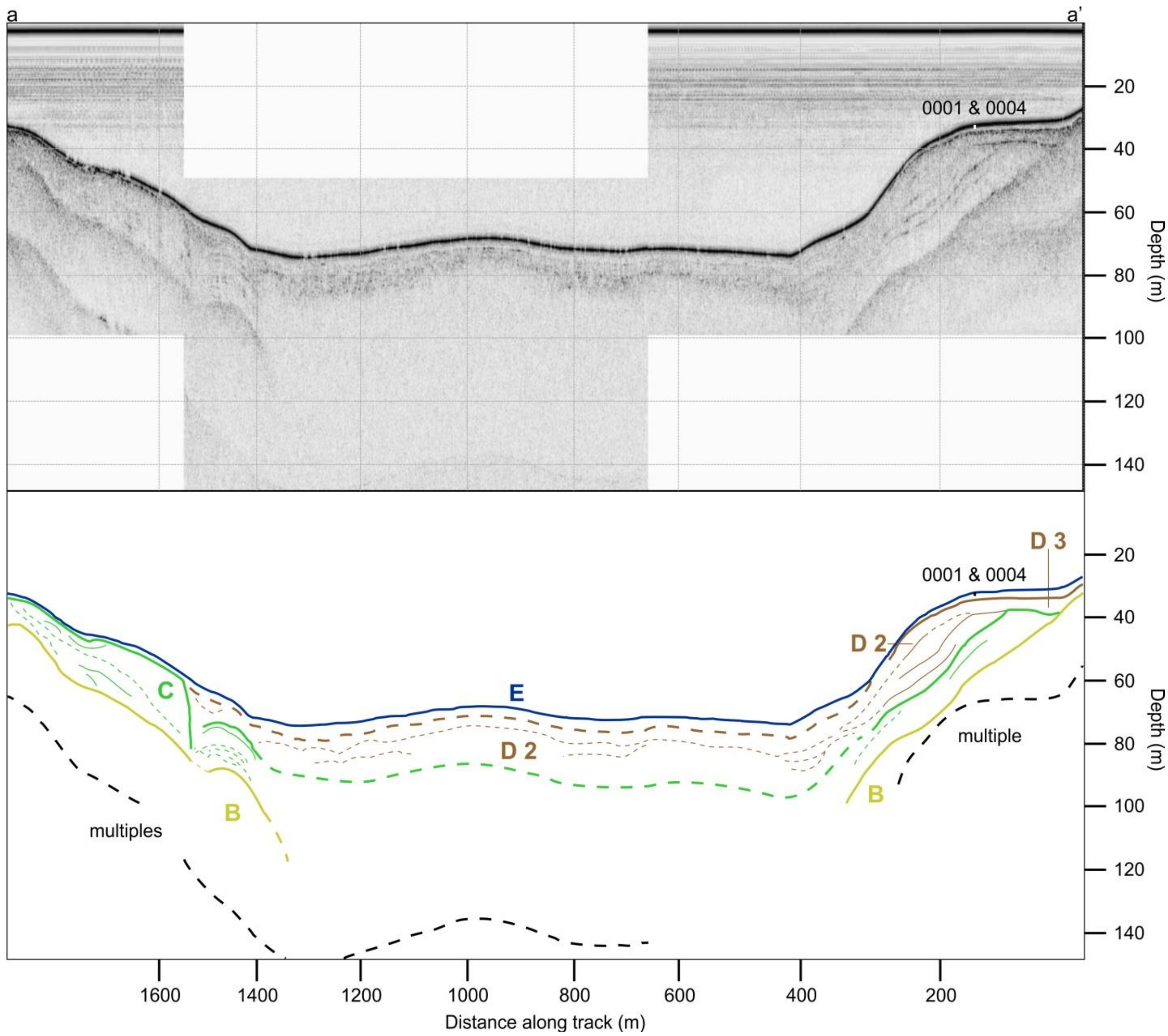

Figure B.4: Boas Fiord fjord-head delta profile *a* crosses the frontal plane of the delta slope. (E) Post-submergence mud, (D3) delta topset beds, (D2) delta foreset beds, (C) glaciomarine sediment, and (B) ice-contact sediment.

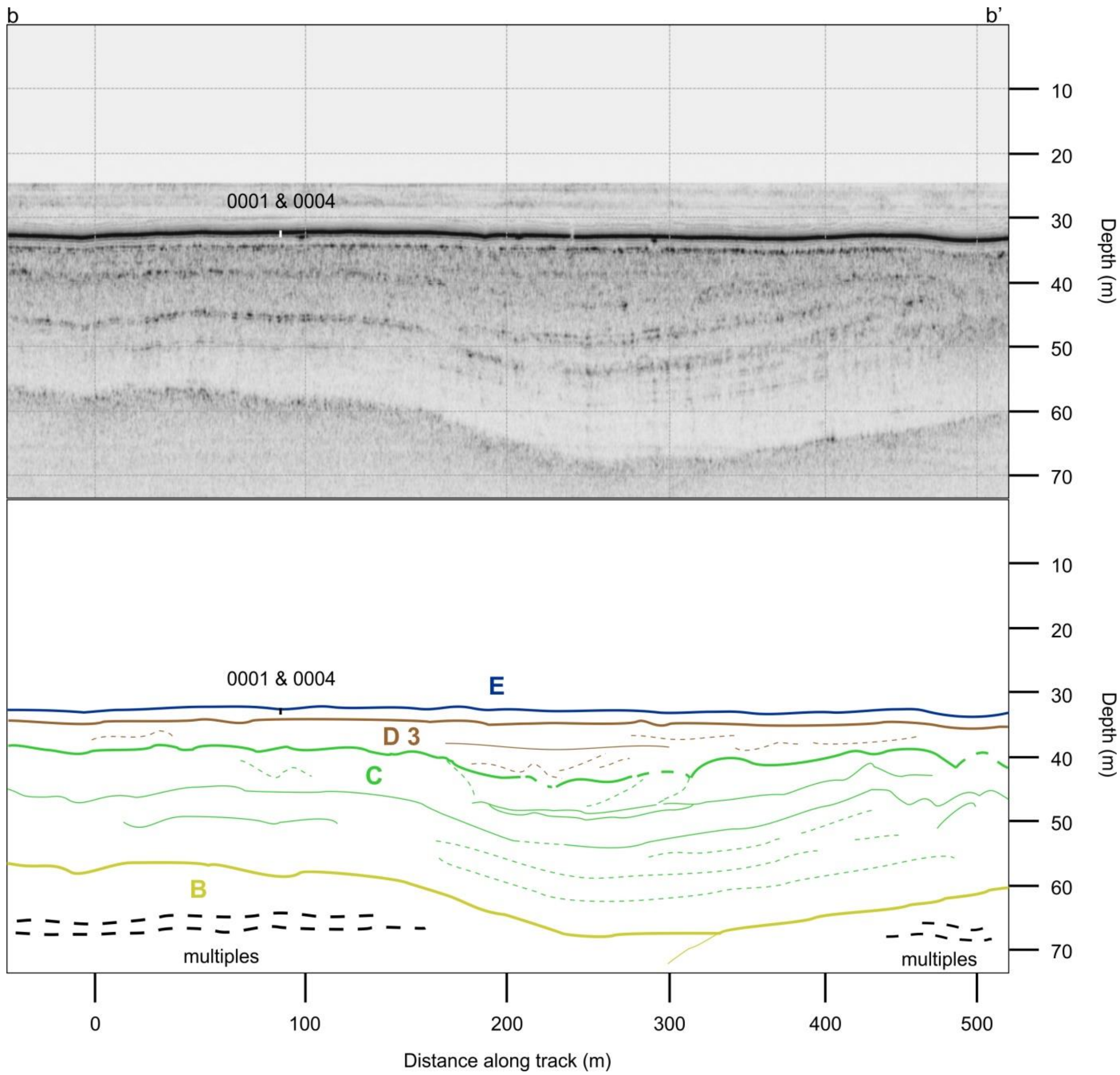

Figure B.5: Boas Fiord fjord-head delta profile *b* crosses the frontal plane of the side-terrace. (E) Post-submergence mud, (D3) delta topset beds, (C) glaciomarine sediment, (B) ice-contact sediment.

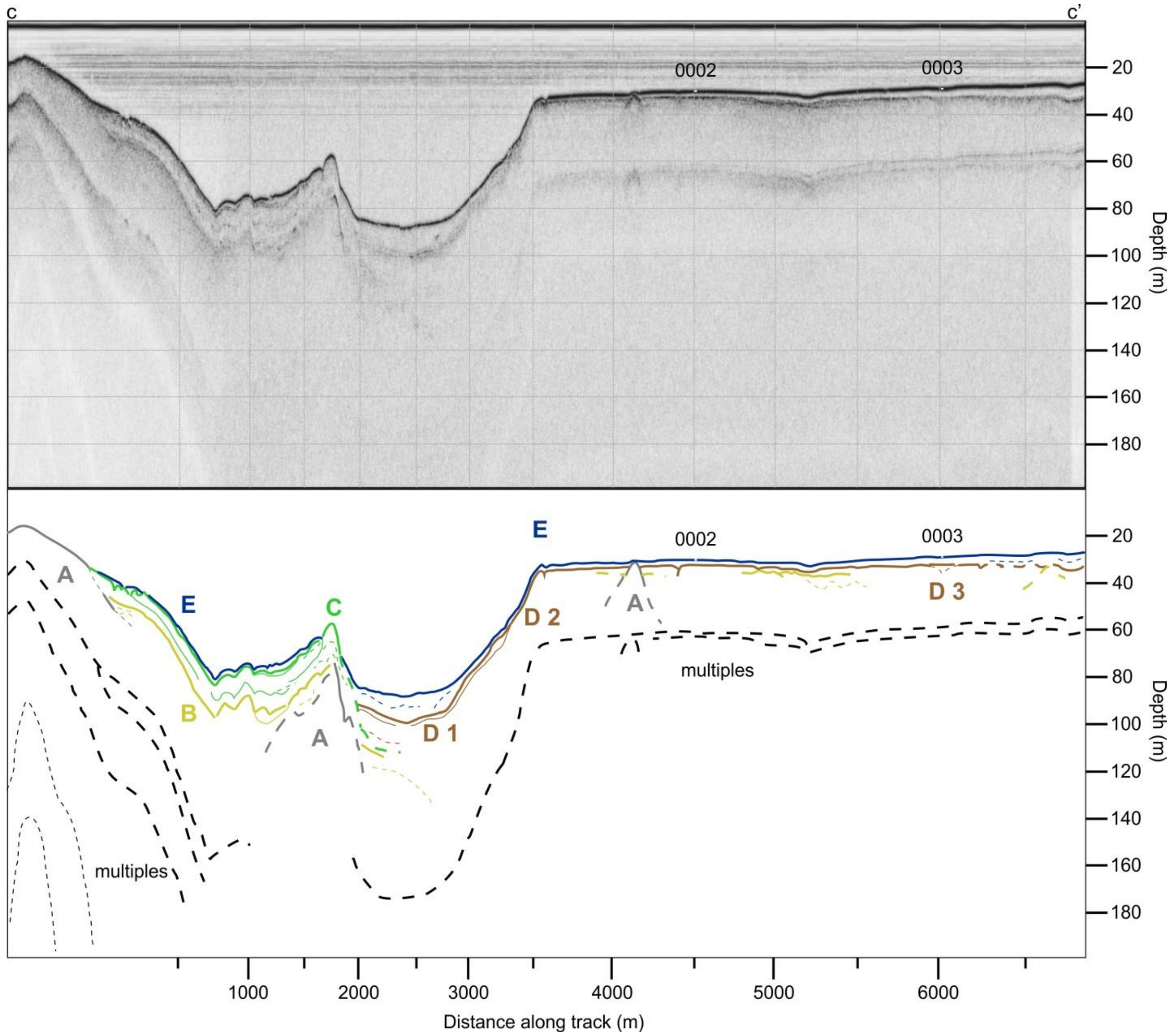

Figure B.6: Boas Fiord fjord-head delta profile *c* crosses the major and minor sills, and the submerged delta terrace. (E) Post-submergence mud, (D3) delta topset beds, (D2) delta foreset beds, (D1) delta bottomset beds, (C) glaciomarine sediment, (B) ice-contact sediment, (A) bedrock.

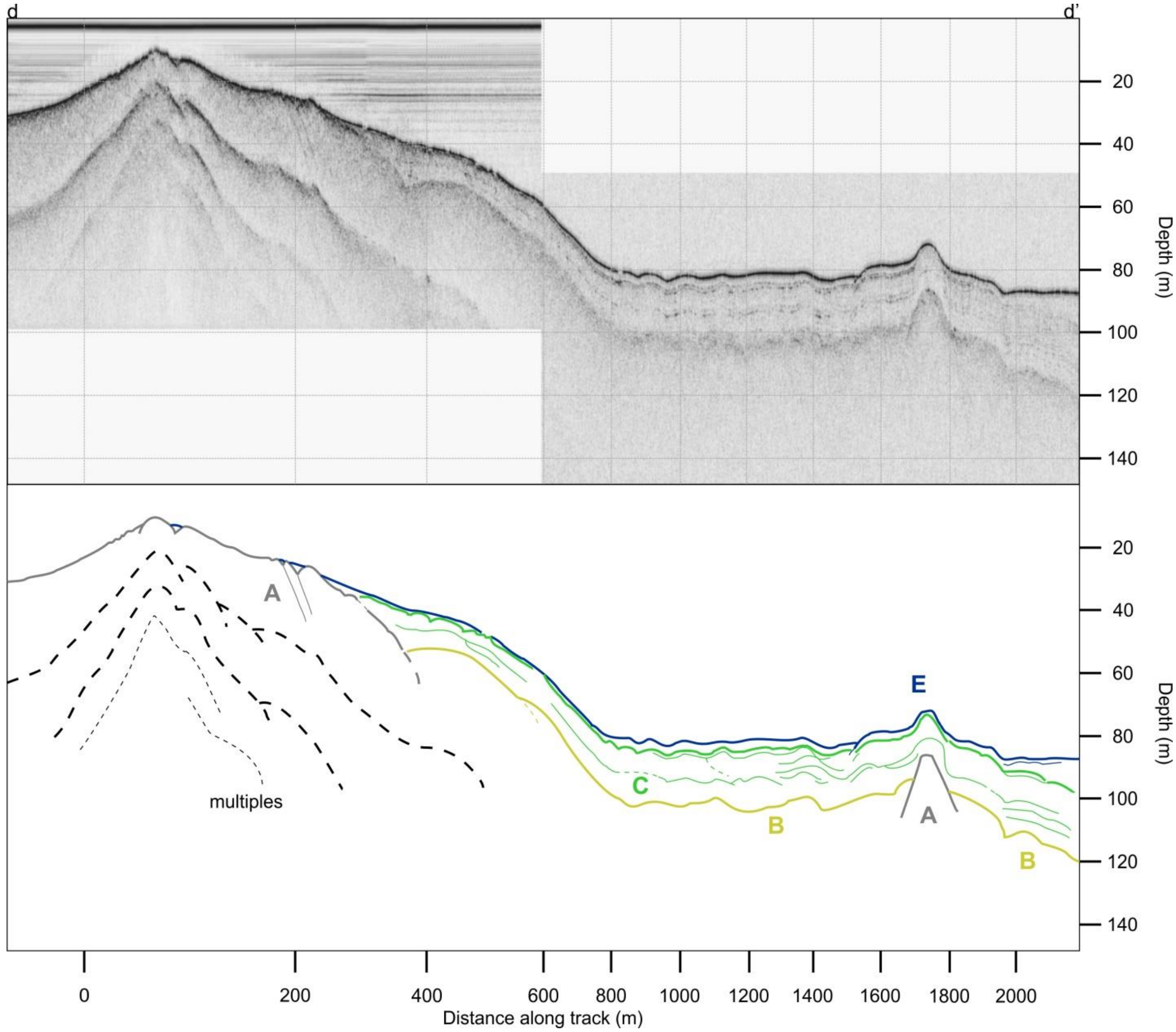

Figure B.7: Boas Fiord fjord-head region profile *d* crosses the major and minor sills. (E) Post-submergence mud, (C) glaciomarine sediment, (B) ice-contact sediment, (A) bedrock.

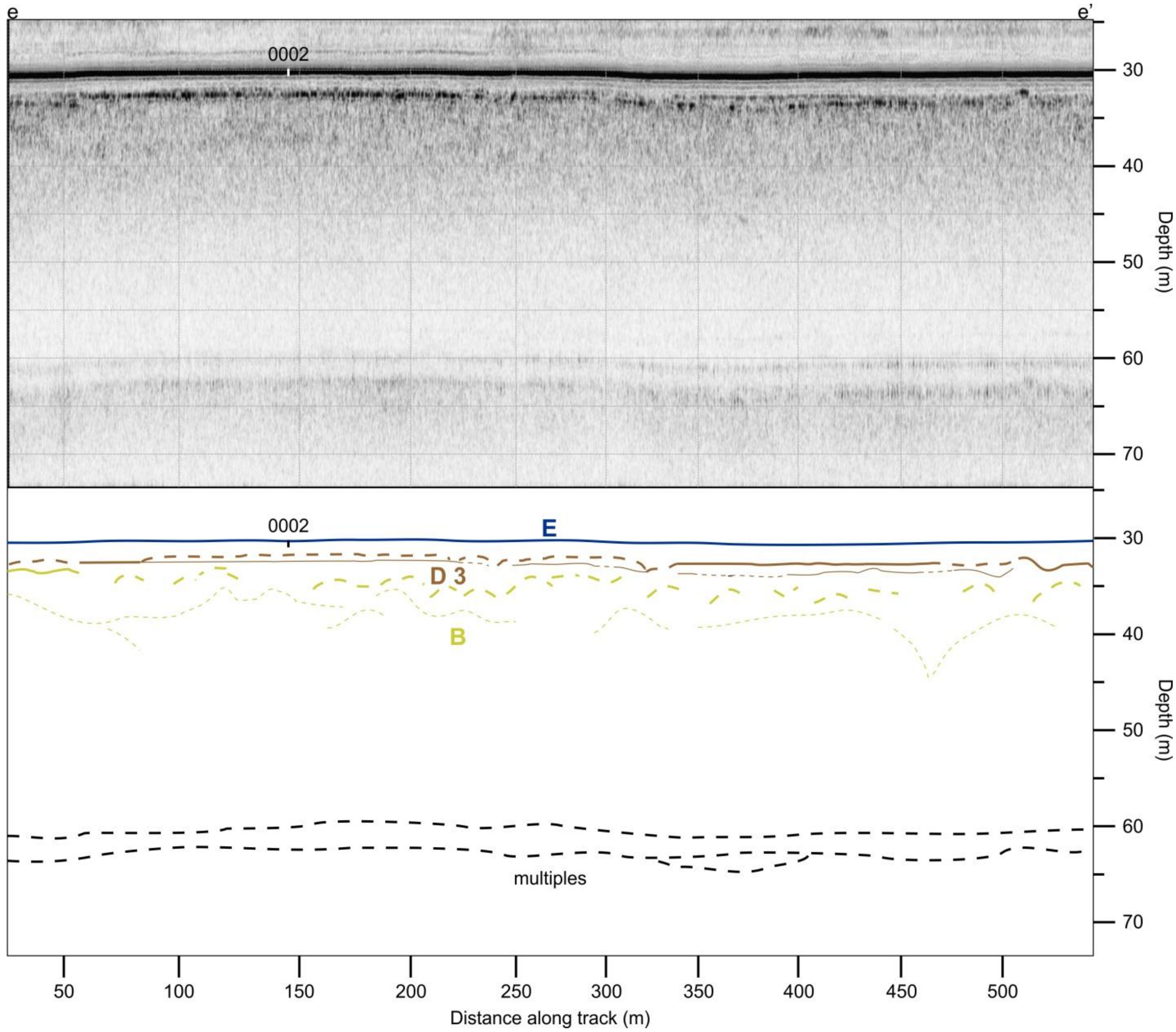

Figure B.8: Boas Fiord fjord-head delta profile *e* covers a small segment of the submerged delta plain. (E) Post-submergence mud, (D3) delta topset beds, (B) ice-contact sediment.

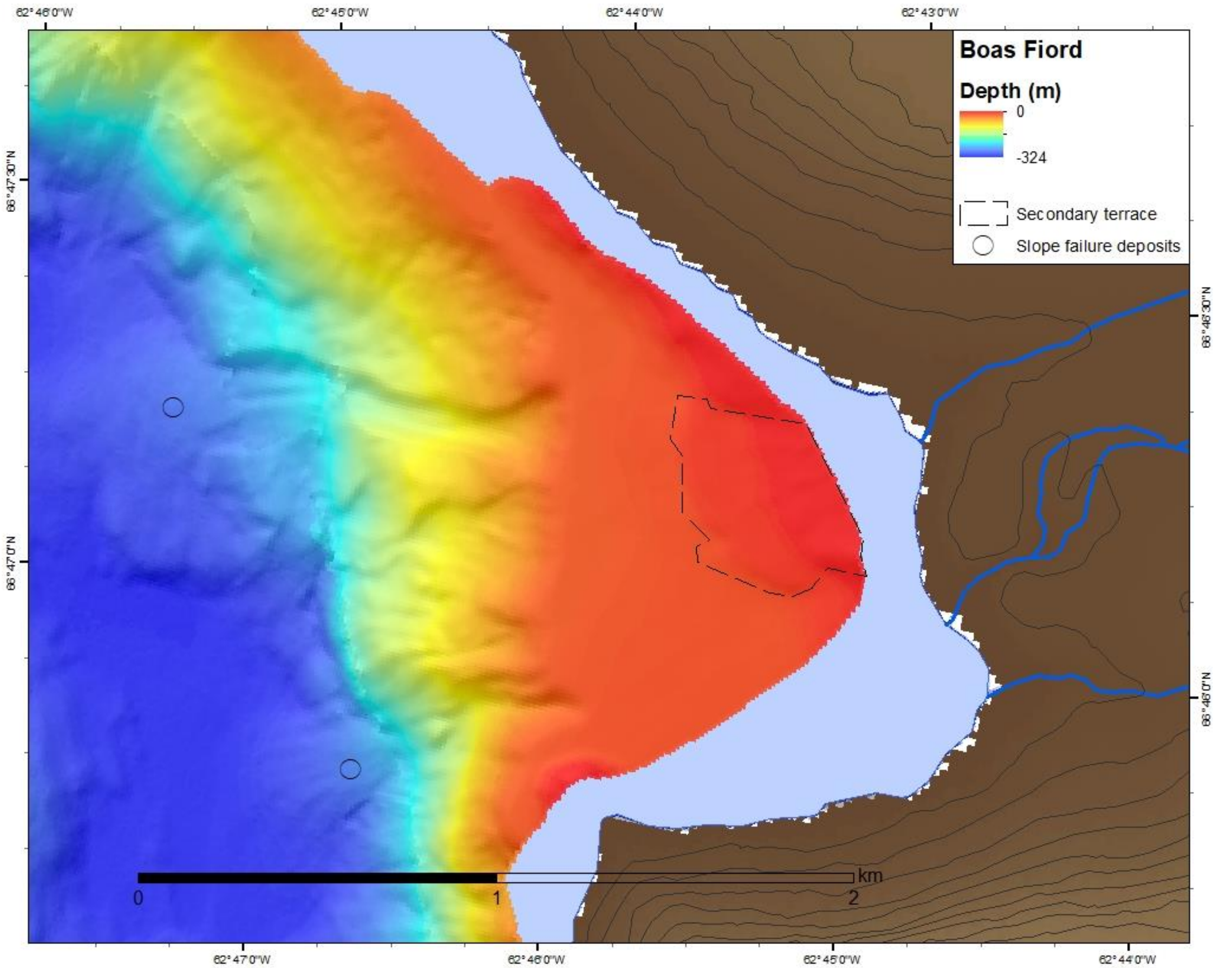

Figure B.9: Map of the submerged side-entry delta study site at Boas Fiord, with some seafloor geomorphologic features indicated.

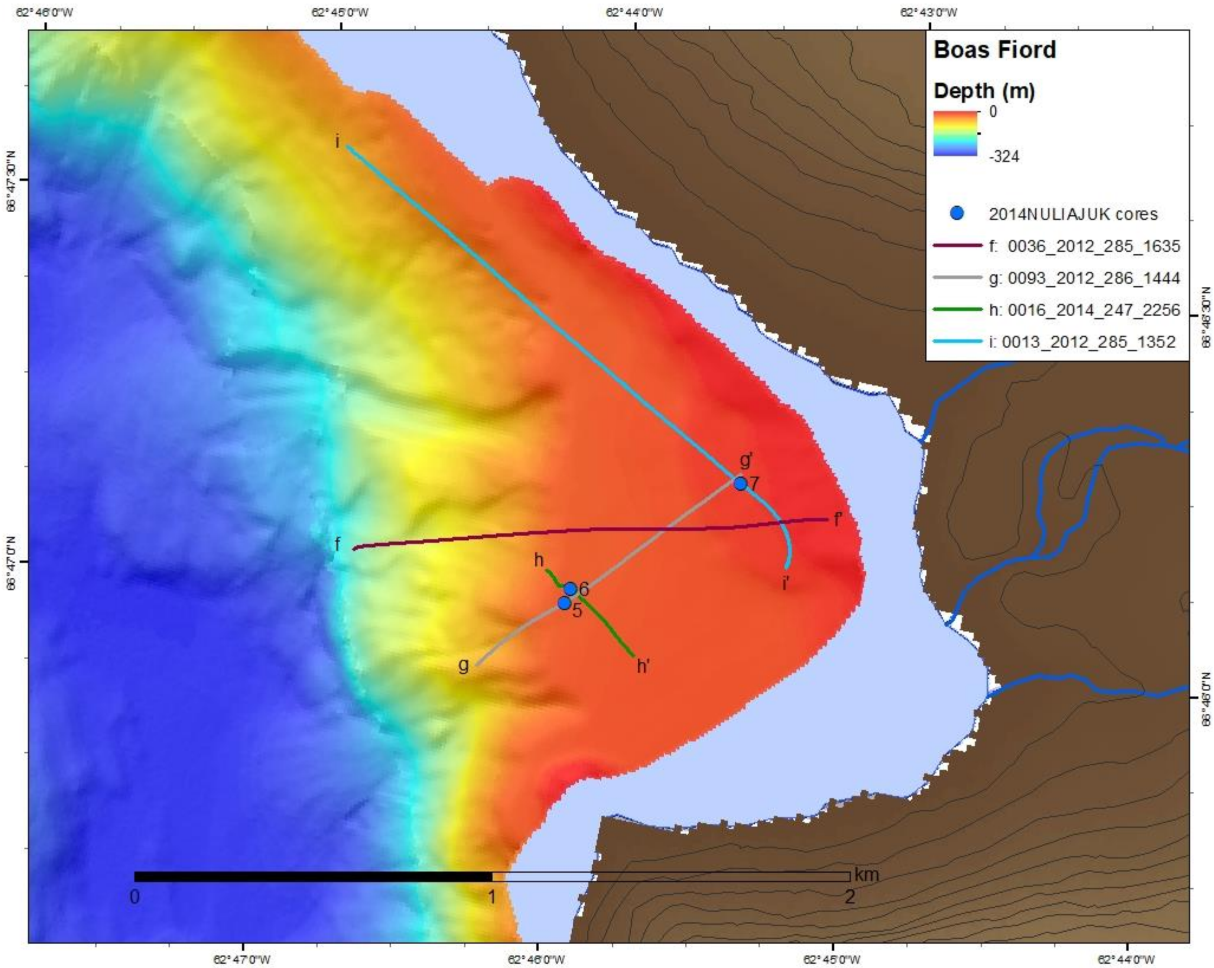

Figure B.10: Map of the submerged side-entry delta study site at Boas Fiord, with the positions of the coring sites and the analyzed acoustic profiles indicated.

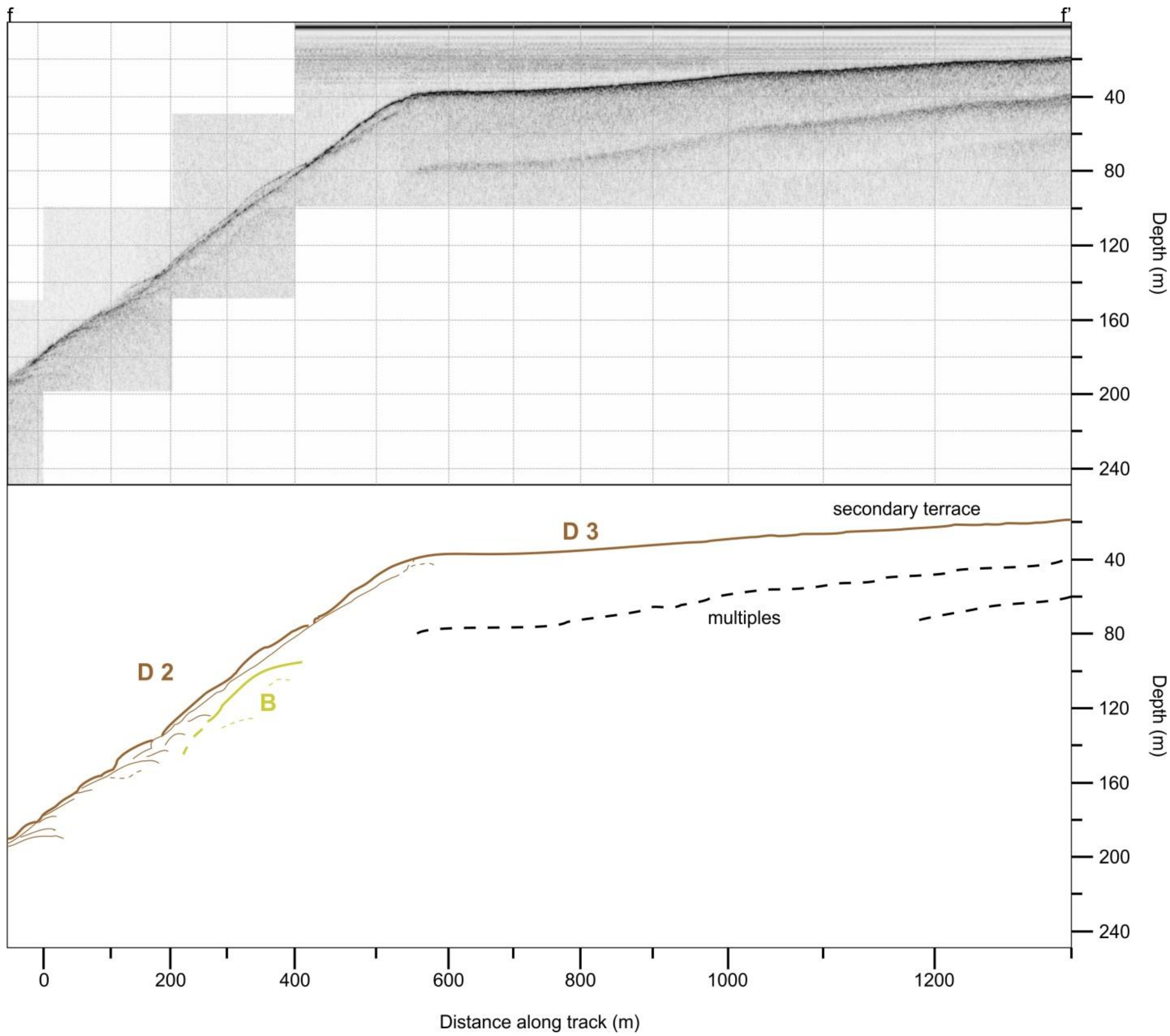

Figure B.11: Boas Fiord side-entry delta profile *f* covers most of the delta slope, and the primary and secondary delta terraces. (D3) delta topset beds, (D2) delta foreset beds, and (B) ice-contact sediment.

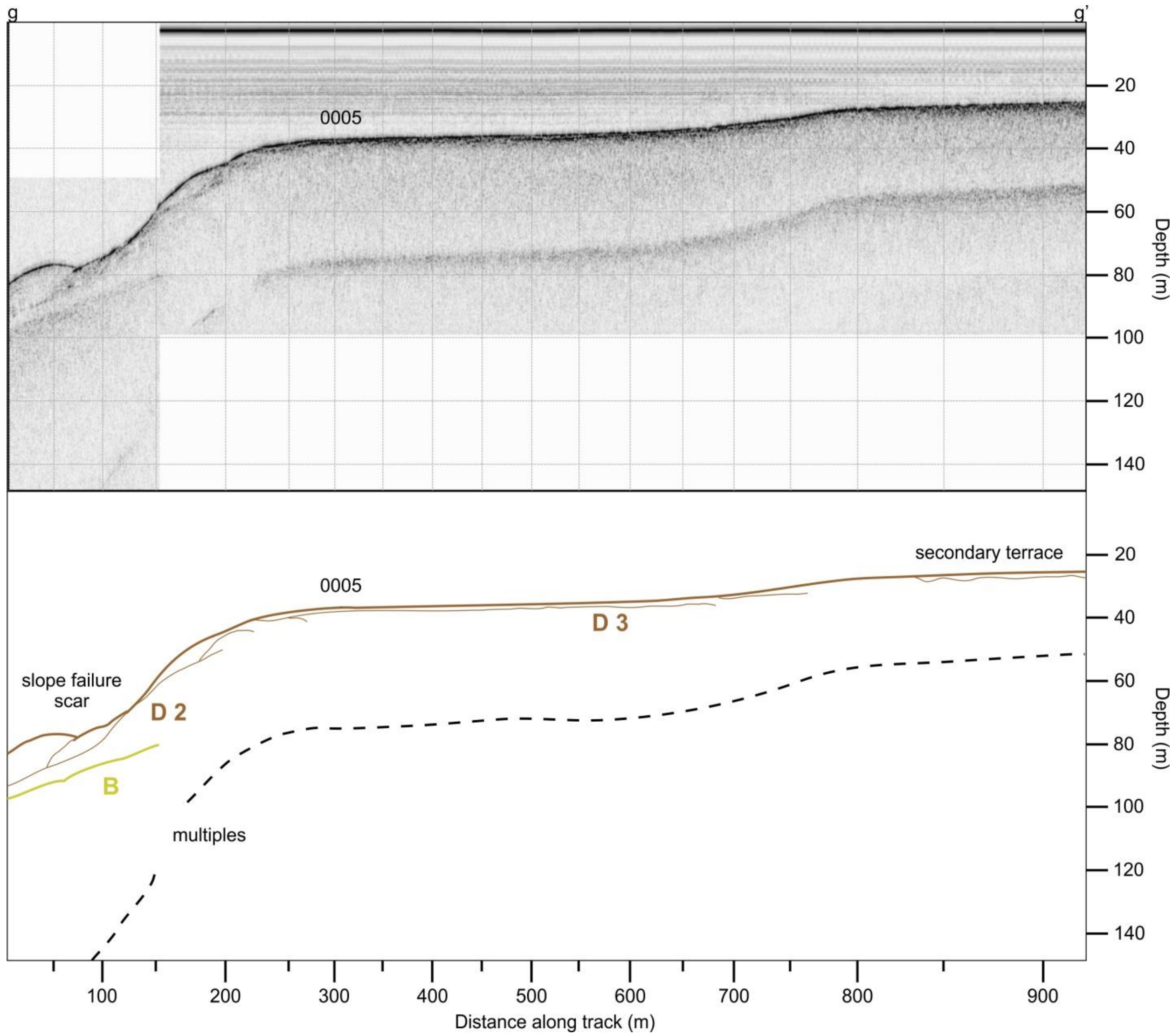

Figure B.12: Boas Fiord side-entry delta profile *g* covers part of the delta slope, and the primary and secondary terraces. (D3) delta topset beds, (D2) delta foreset beds, and (B) ice-contact sediment.

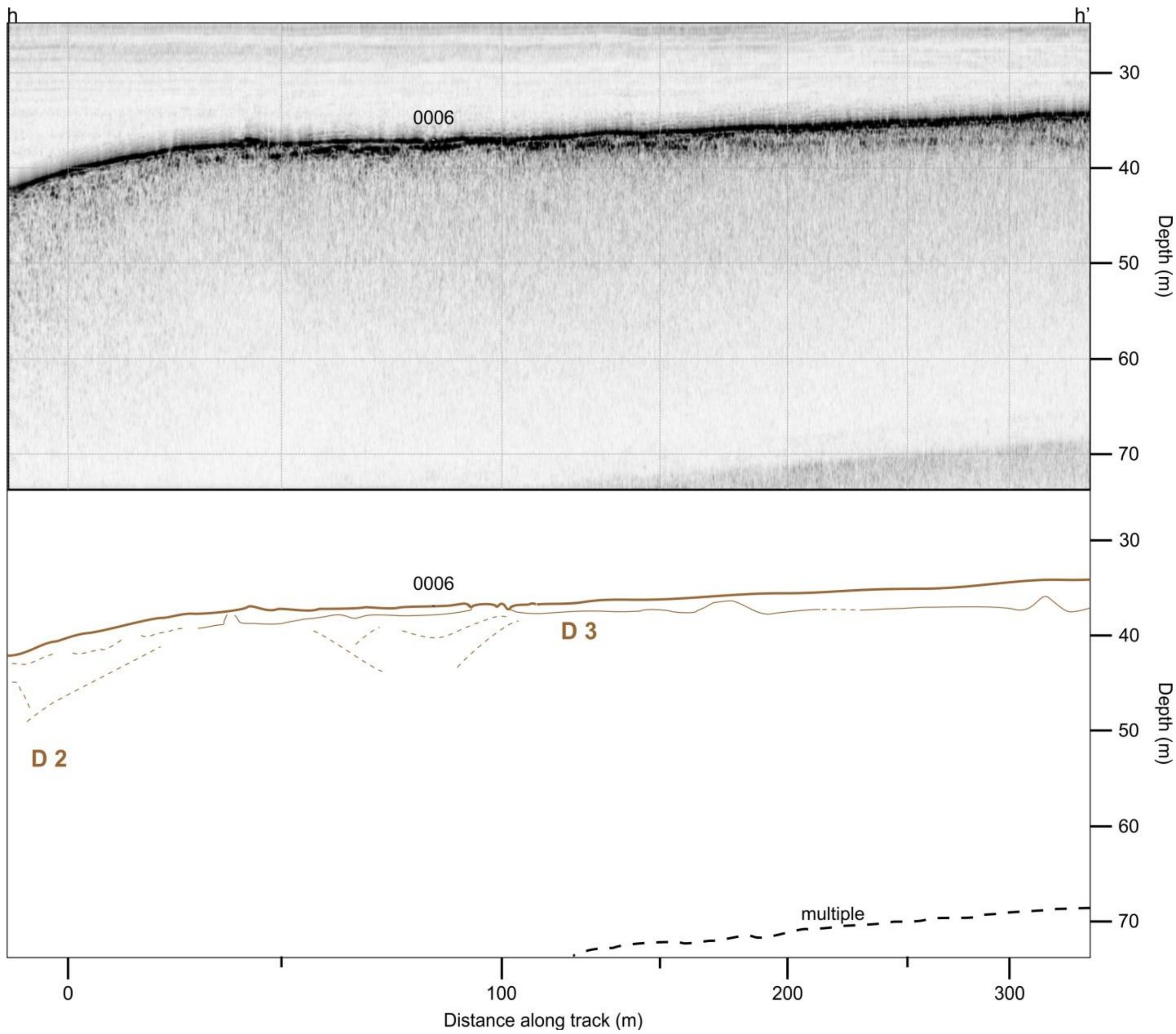

Figure B.13: Boas Fiord side-entry delta profile *h* covers a segment of the primary terrace near the edge, crossing perpendicular to profile *g*. (D3) Delta topset beds, (D2) delta foreset beds.

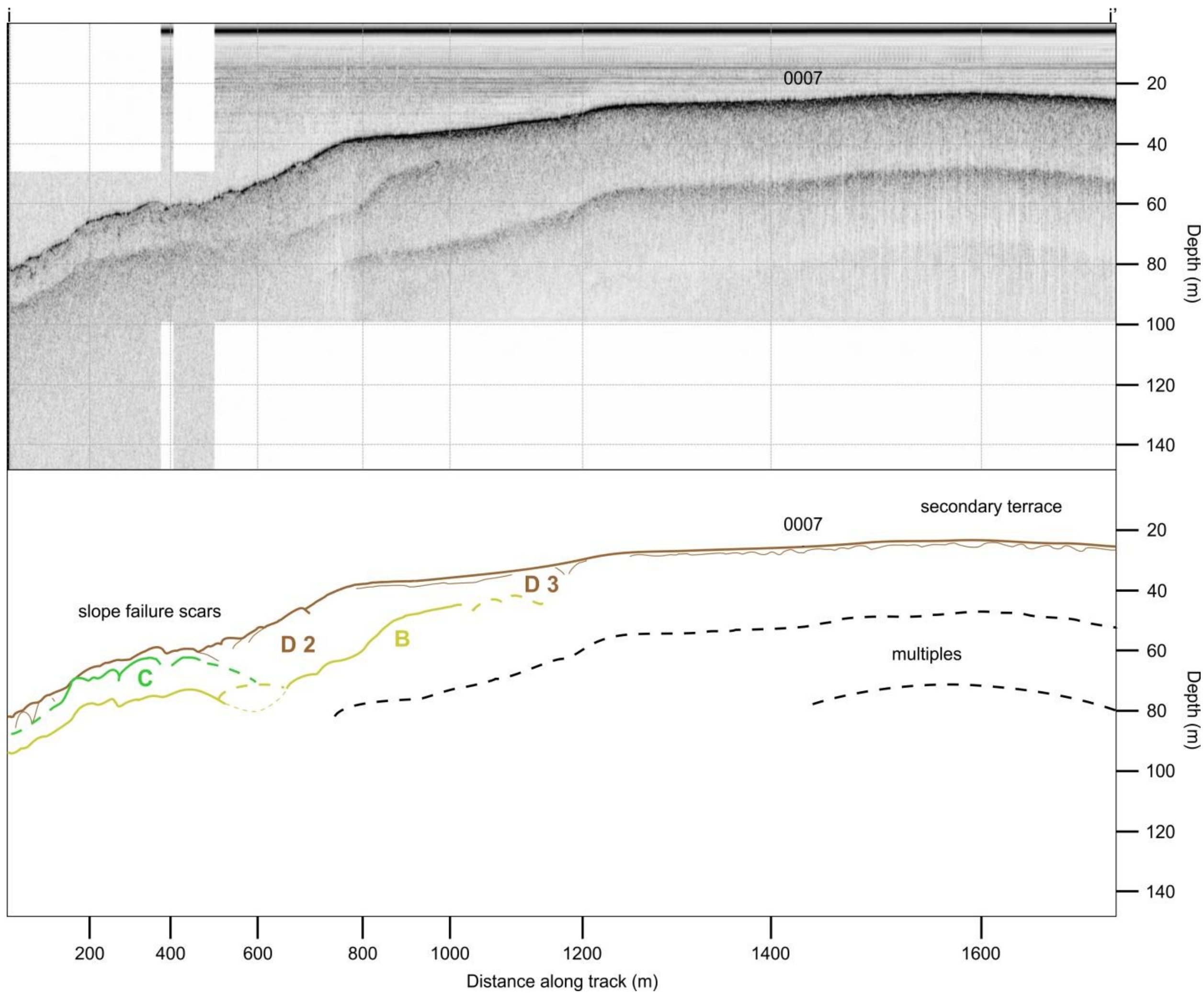

Figure B.14: Boas Fiord side-entry delta profile *i* covers the frontal plane of the northern sidewall terrace, and transects the primary and secondary terraces. (D3) Delta topset beds, (D2) delta foreset beds, (C) glaciomarine sediment, (B) ice-contact sediment.

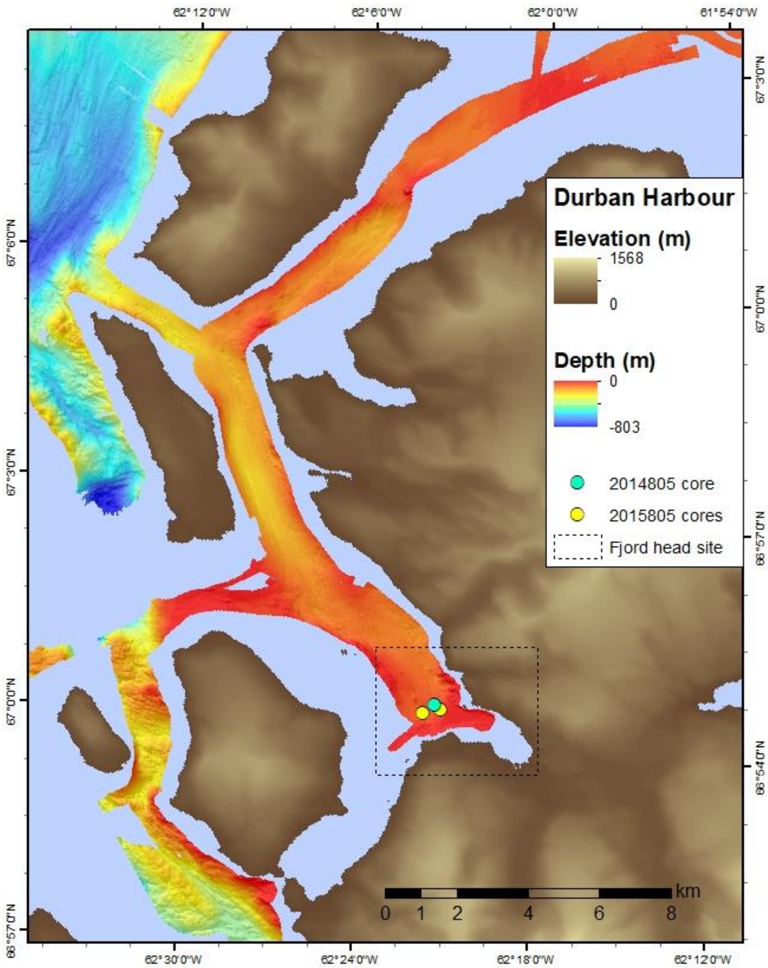

Figure B.15: Map of Durban Harbour, with the fjord-head study site and its associated coring sites indicated.

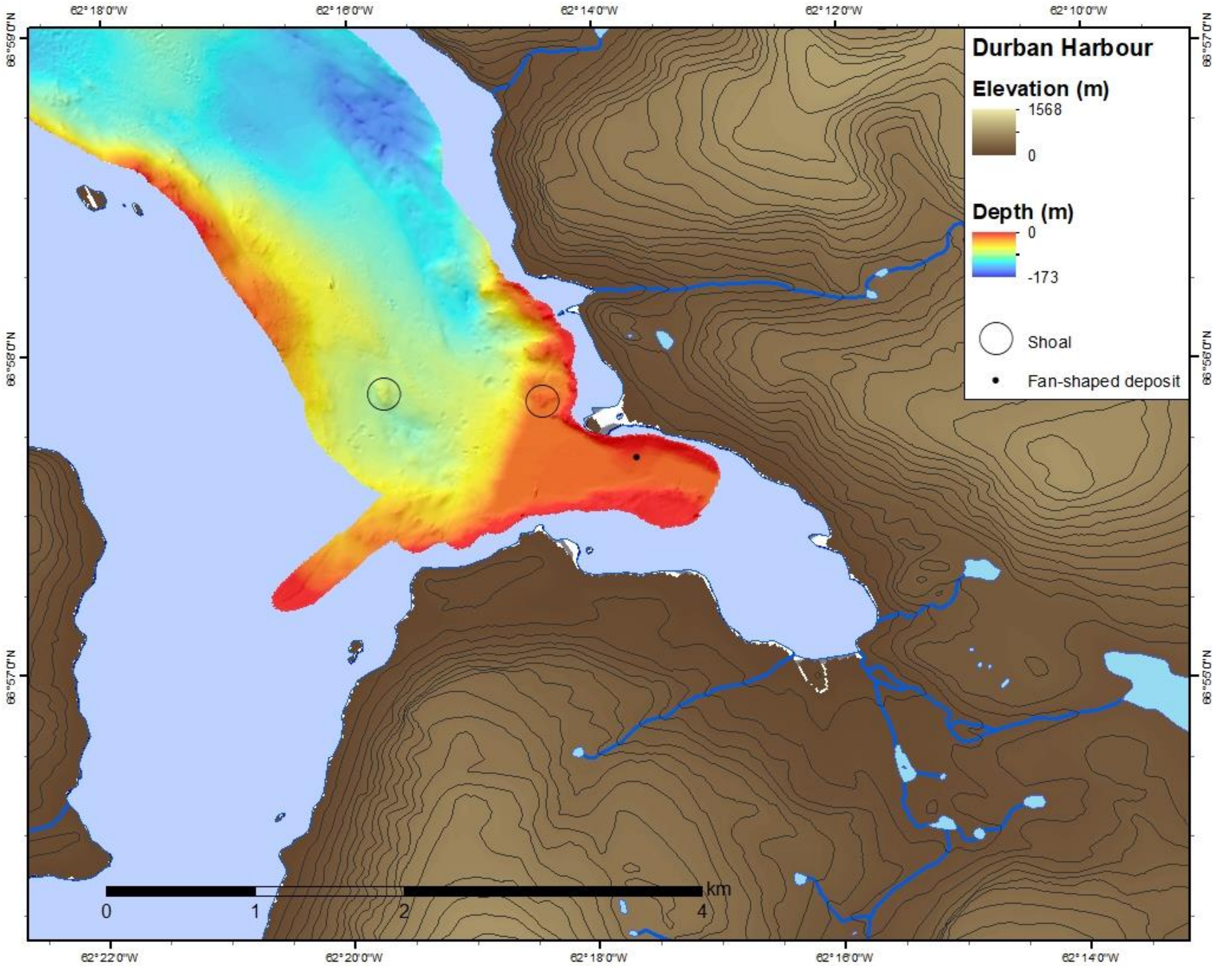

Figure B.16: Map of the submerged delta study site at the head of Durban Harbour, with some seafloor geomorphic features indicated.

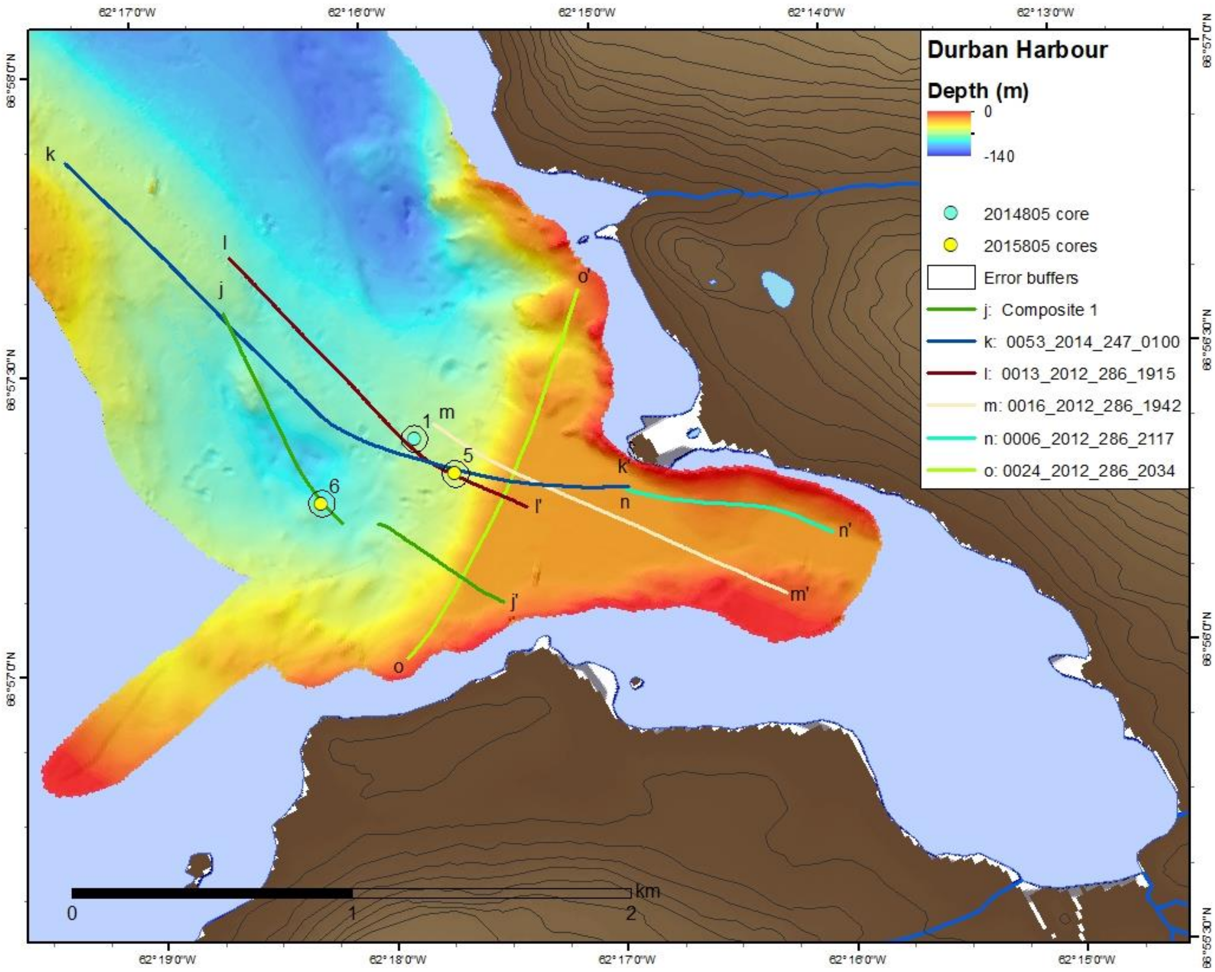

Figure B.17: Map of the submerged delta study site at the head of Durban Harbour, with the positions of the coring sites and the analyzed acoustic profiles indicated.

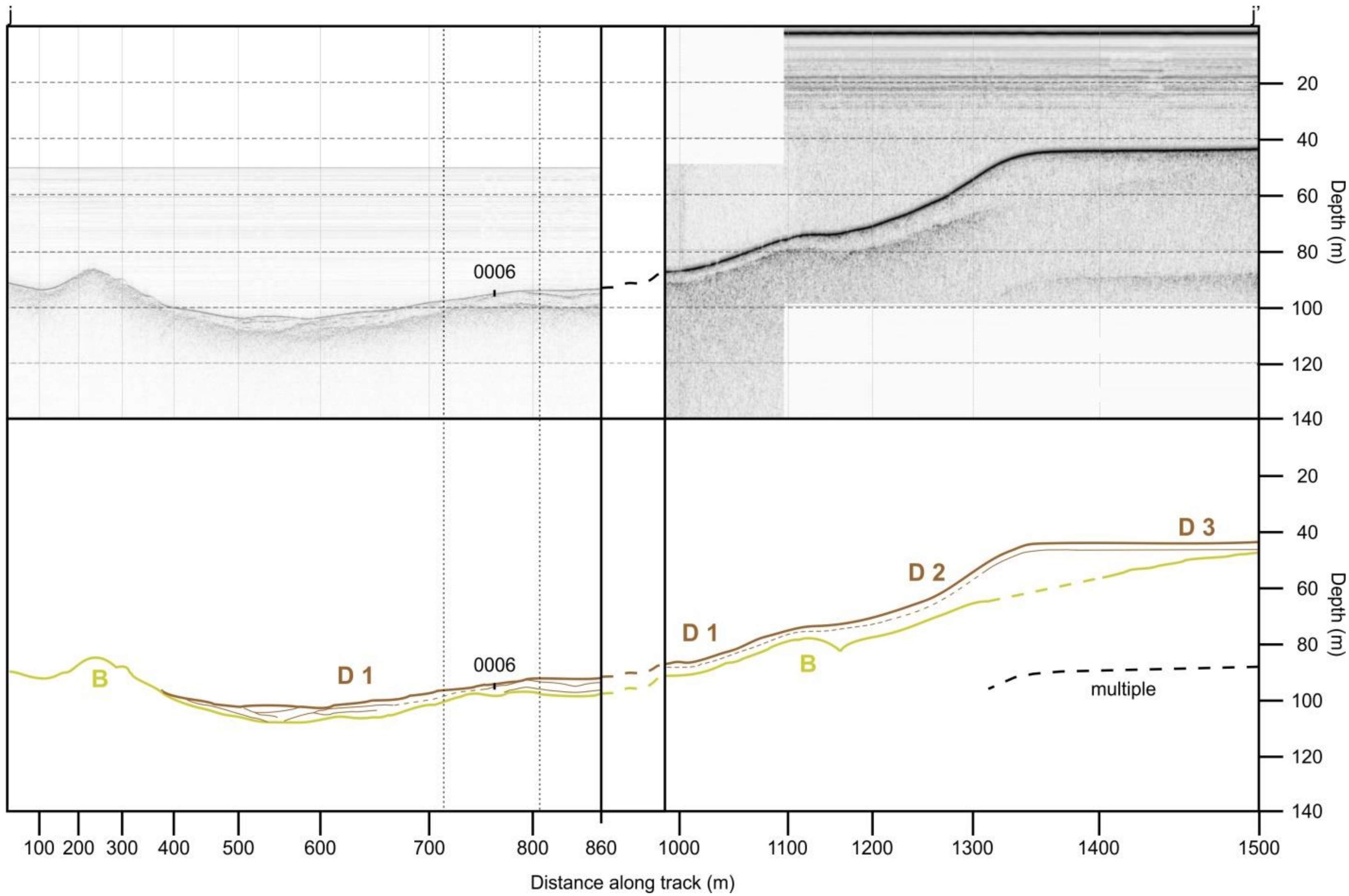

Figure B.18: Profile *j* is a composite of two separate acoustic profiles, covering the Durban Harbour prodelta and submerged delta. (D3) Delta topset beds, (D2) delta foreset beds, (D1) delta bottomset beds, (B) ice-contact sediment.

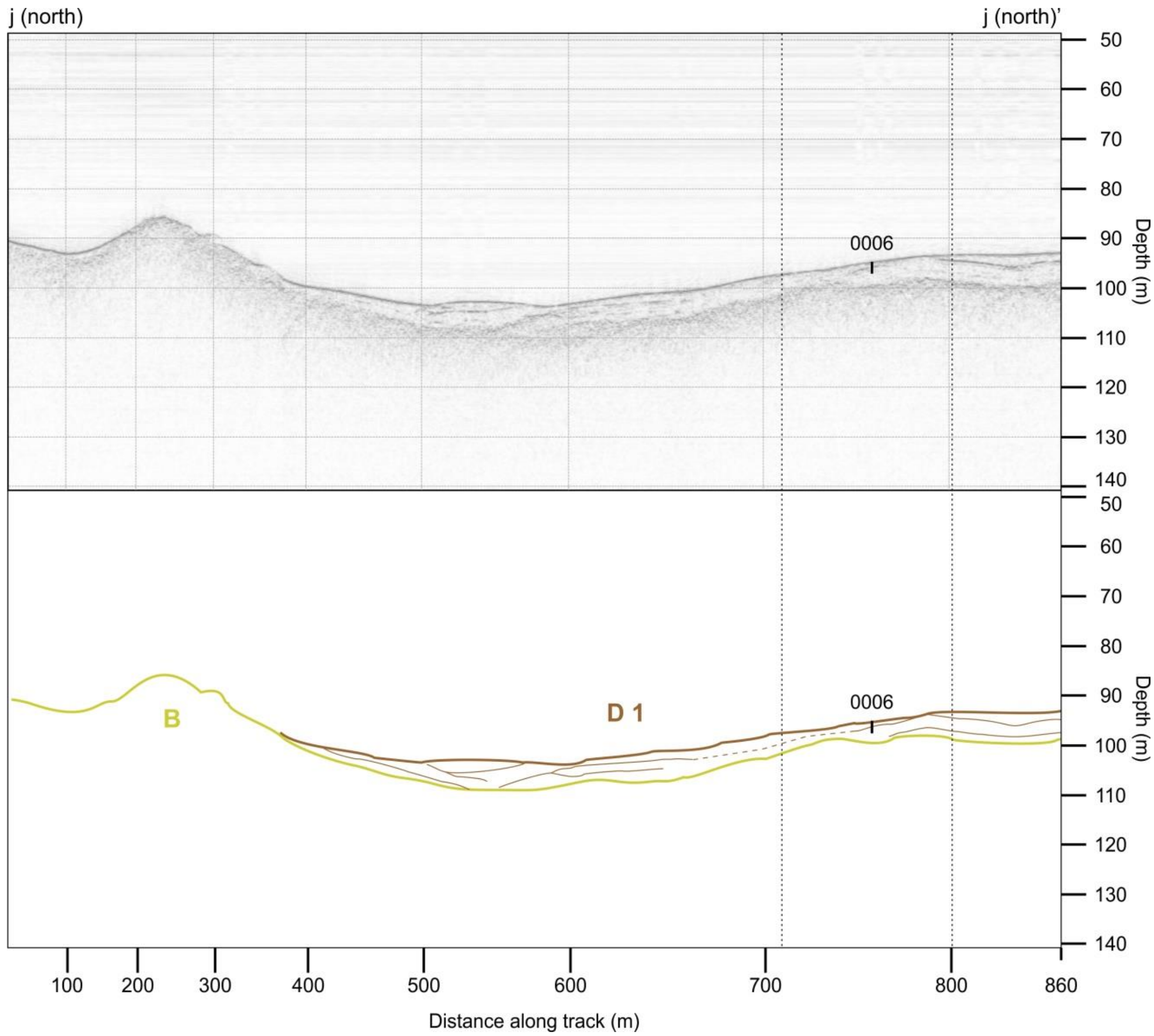

Figure B.19: The northern segment of profile *j*, which crosses only the Durban Harbour prodelta. (D1) Delta bottomset beds, (B) ice-contact sediment.

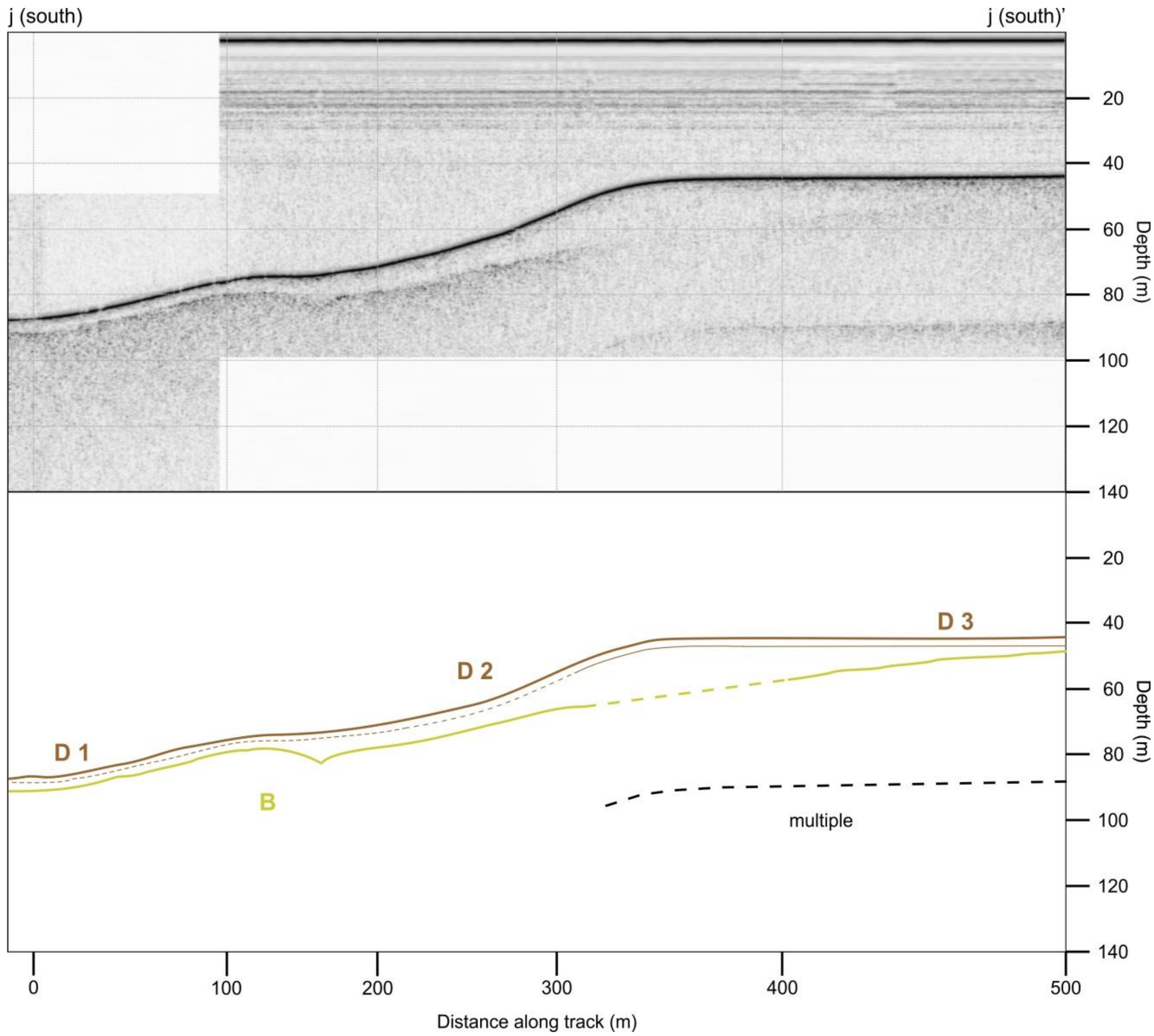

Figure B.20: The southern segment of profile *j*, which crosses only the Durban Harbour submerged delta. (D3) Delta topset beds, (D2) delta foreset beds, (D1) delta bottomset beds, (B) ice-contact sediment.

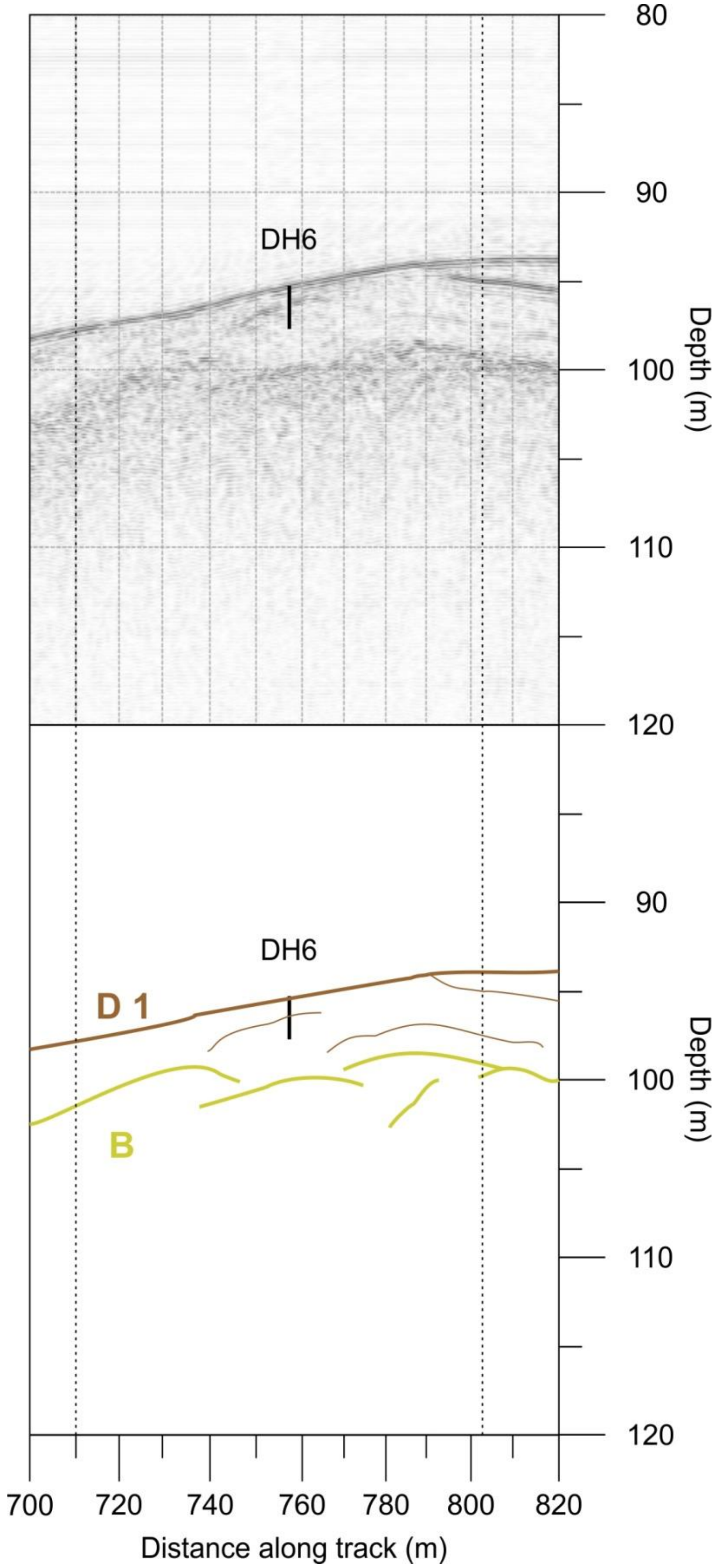

Figure B.21: Blow-up segment of profile *j* focusing on core DH6. (D1) Delta bottomset beds, (B) ice-contact sediment.

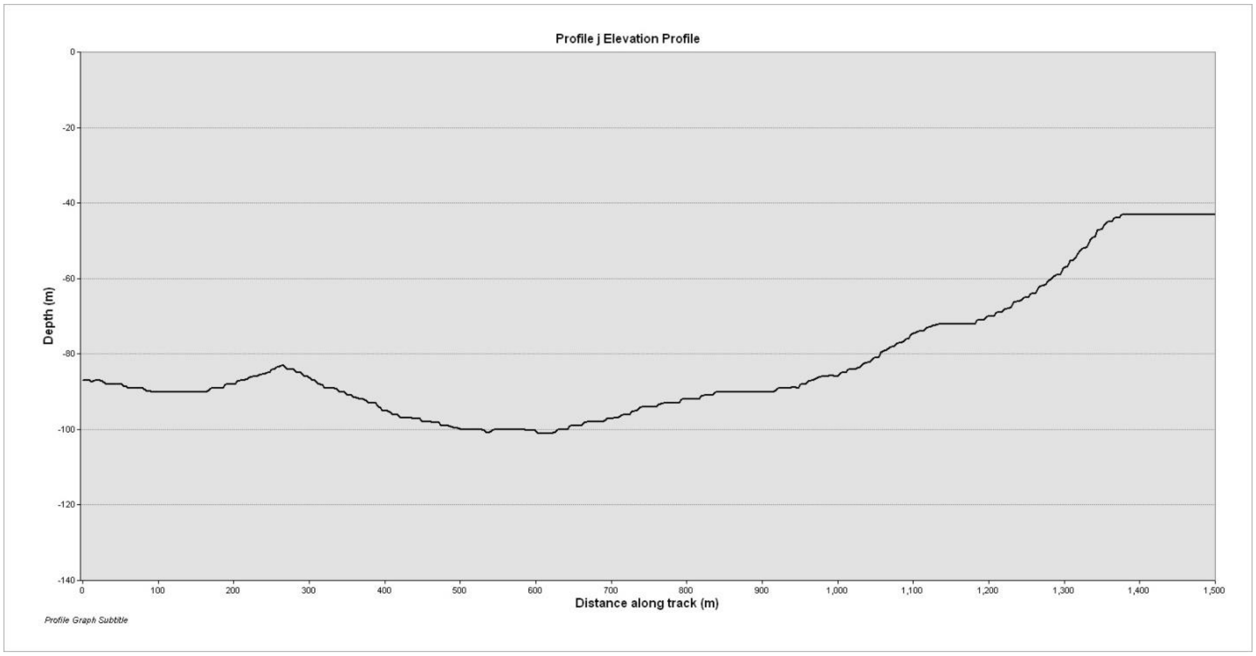

Figure B.22: Elevation data for profile *j* extracted from multibeam bathymetry, using ArcGIS. Unlike Fig.B.18, distance along the x-axis is divided into regular intervals, and thus portrays the seafloor more accurately.

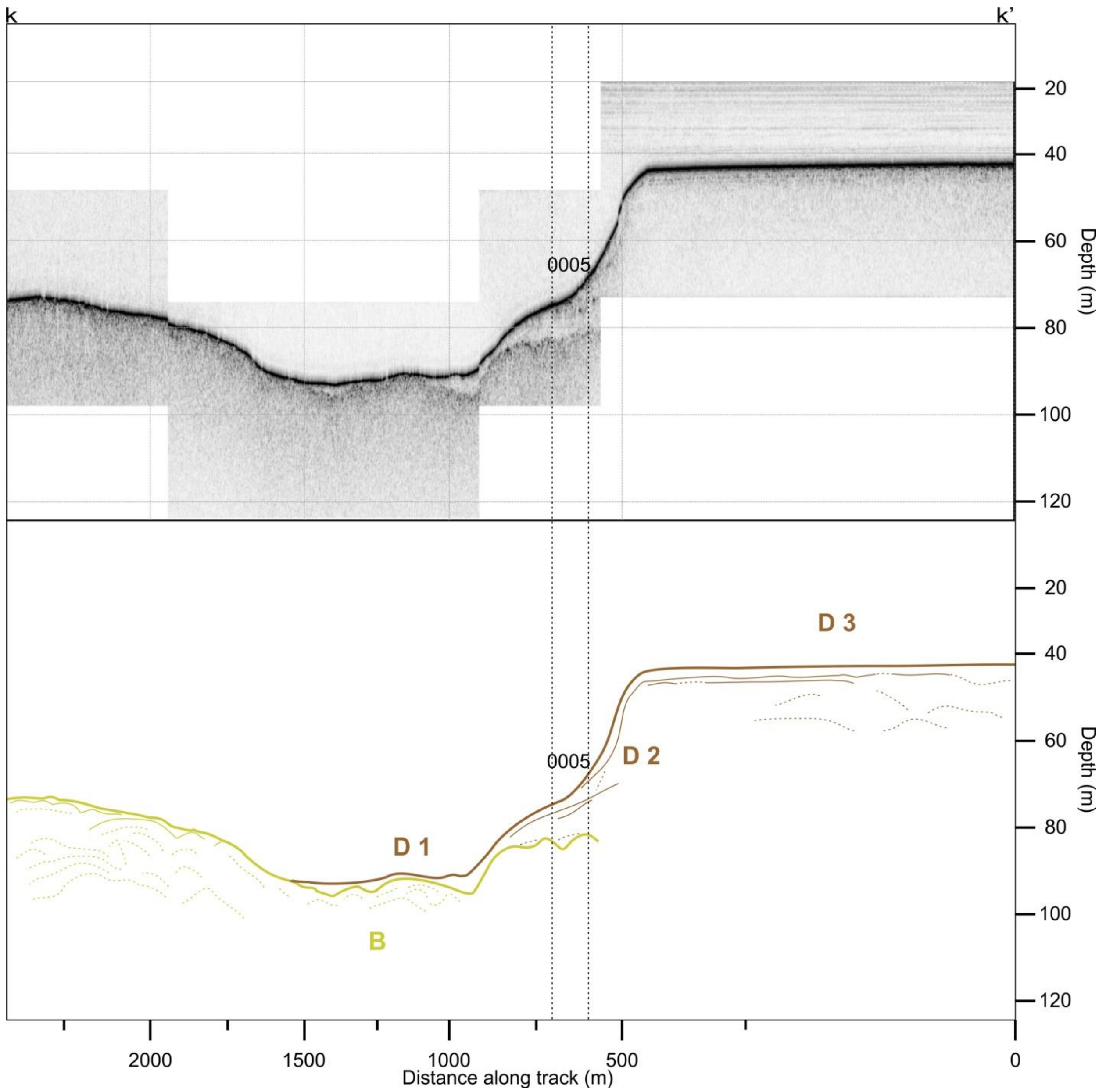

Figure B.23: Durban Harbour profile *k* covers the prodelta to delta terrace. (D3) Delta topset beds, (D2) delta foreset beds, (D1) delta bottomset beds, (B) ice-contact sediment.

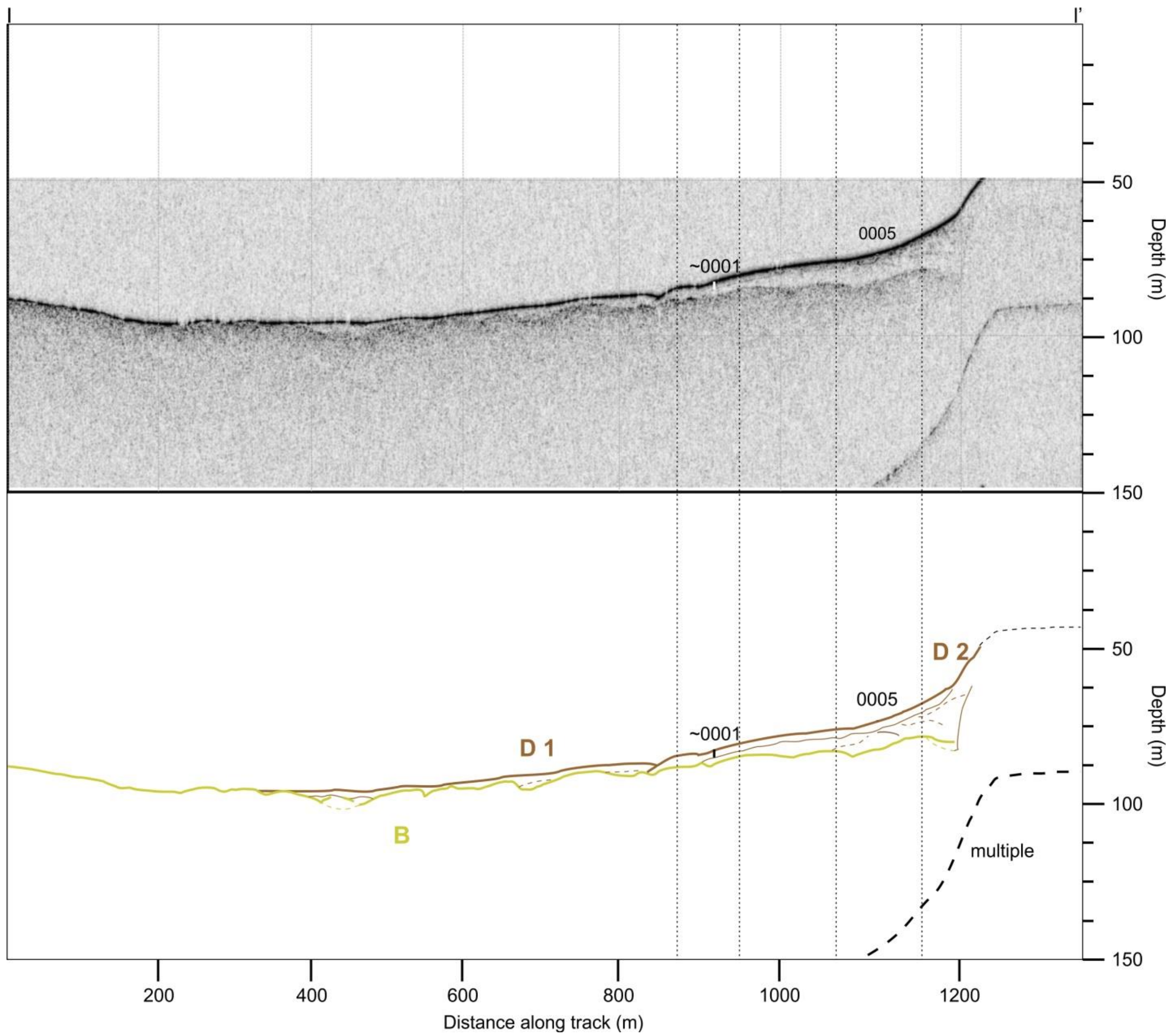

Figure B.24: Profile *l* covers the Durban Harbour prodelta area and the foot of the delta slope. (D2) Delta foreset beds, (D1) delta bottomset beds, (B) ice-contact sediment.

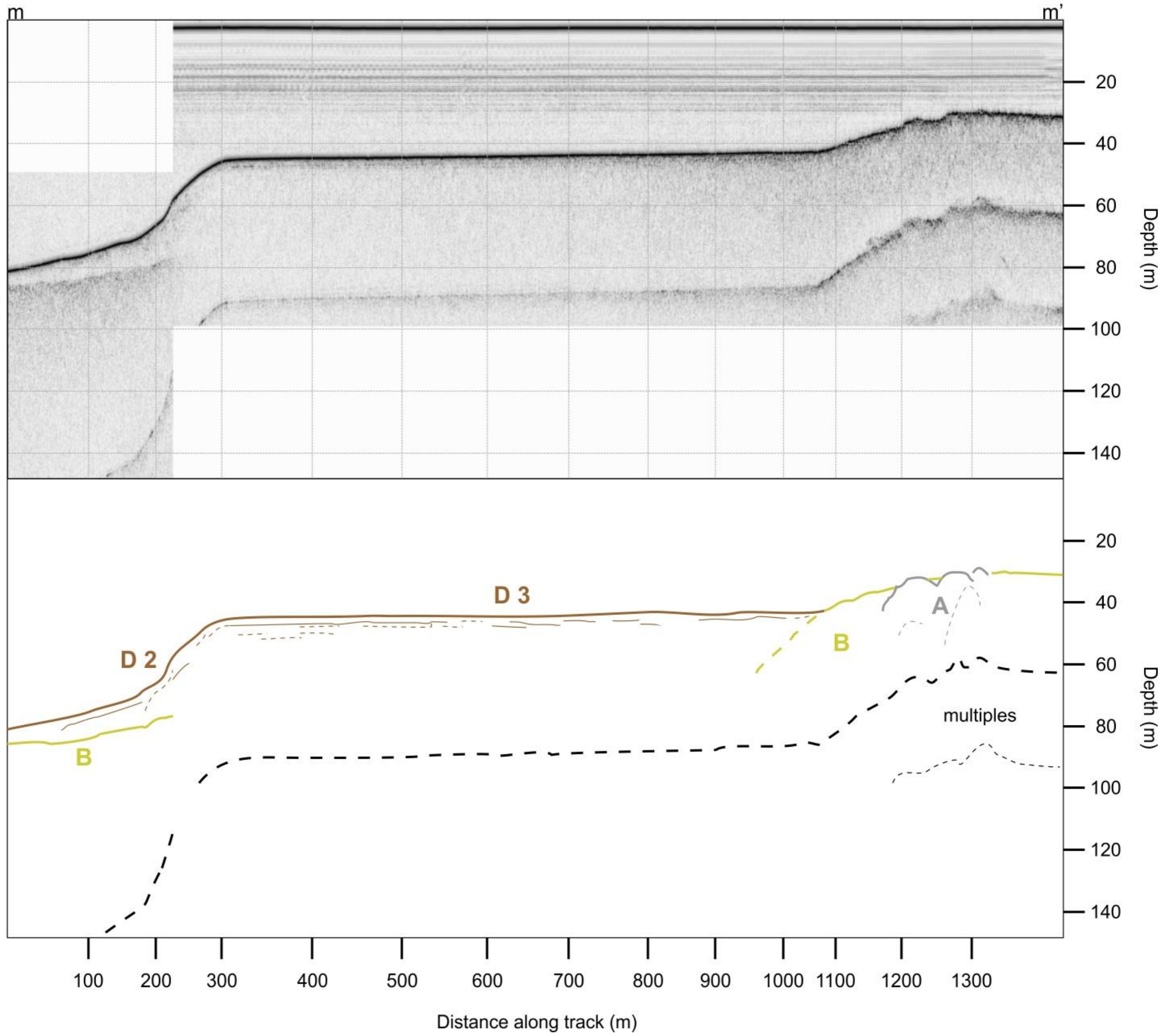

Figure B.25: Durban Harbour profile *m* crosses the submerged delta terrace from the foot of the delta slope to the foot of the western sidewall. (D3) Delta topset beds, (D2) delta foreset beds, (B) ice-contact sediment, (A) bedrock.

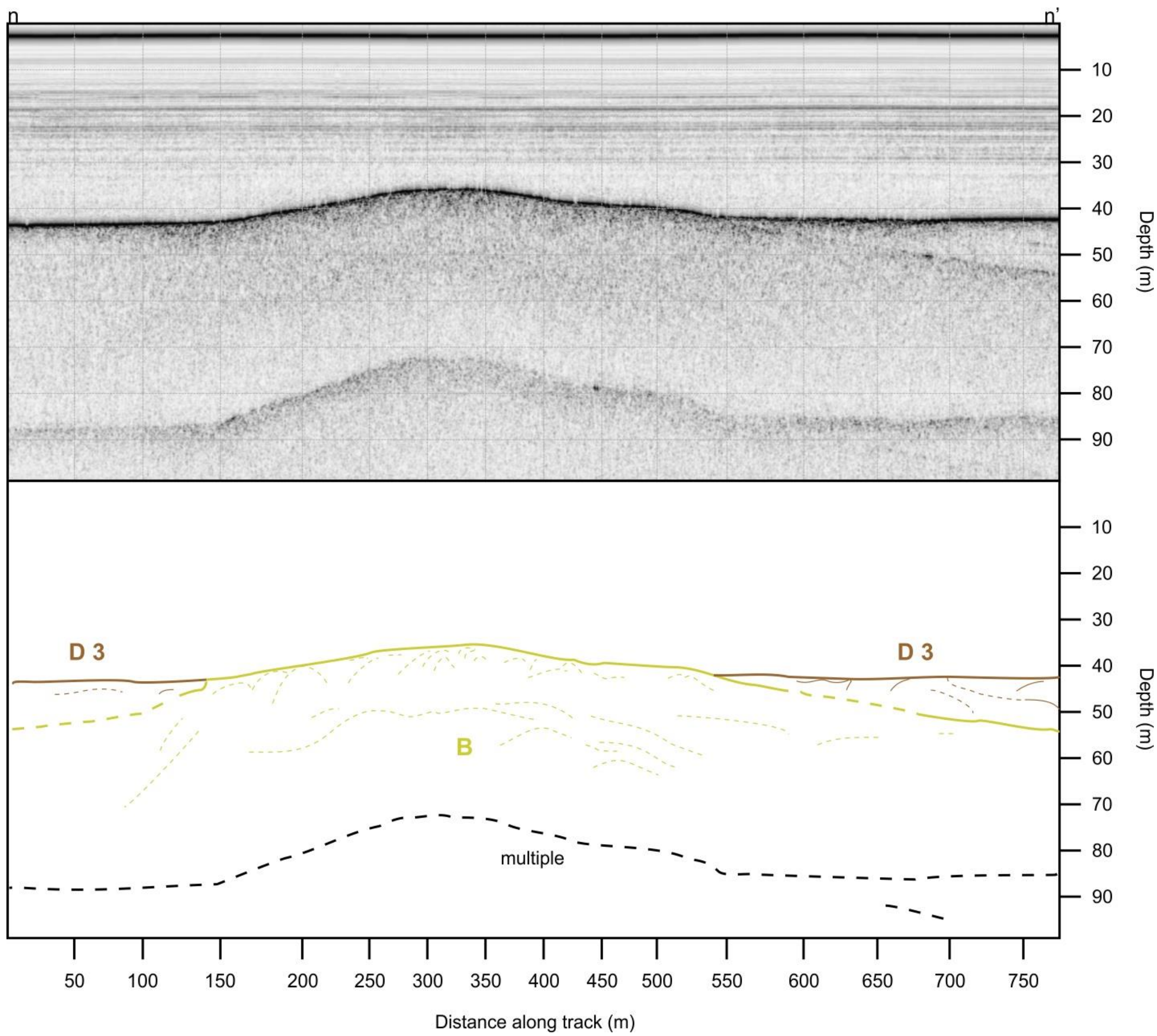

Figure B.26: Durban Harbour; profile *n* transects a fan-shaped feature on the submerged delta terrace, along the eastern sidewall. (D3) Delta topset beds, (B) ice-contact sediment.

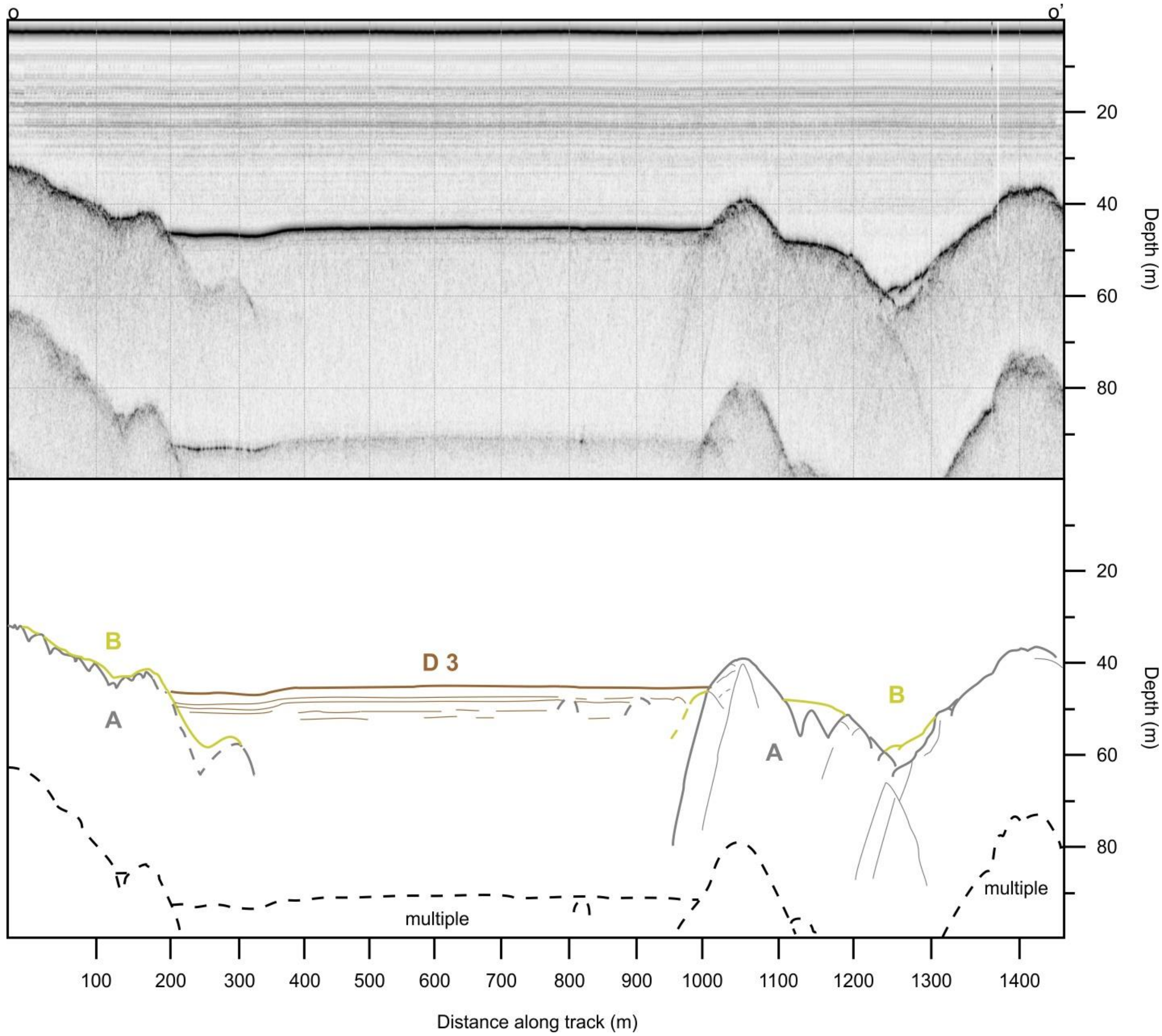

Figure B.27: Durban Harbour; profile *o* provides a frontal transect of the submerged fjord-head delta, extending from the southwest sidewall to the northeast. (D3) Delta topset bed, (B) ice-contact sediment, (A) bedrock.

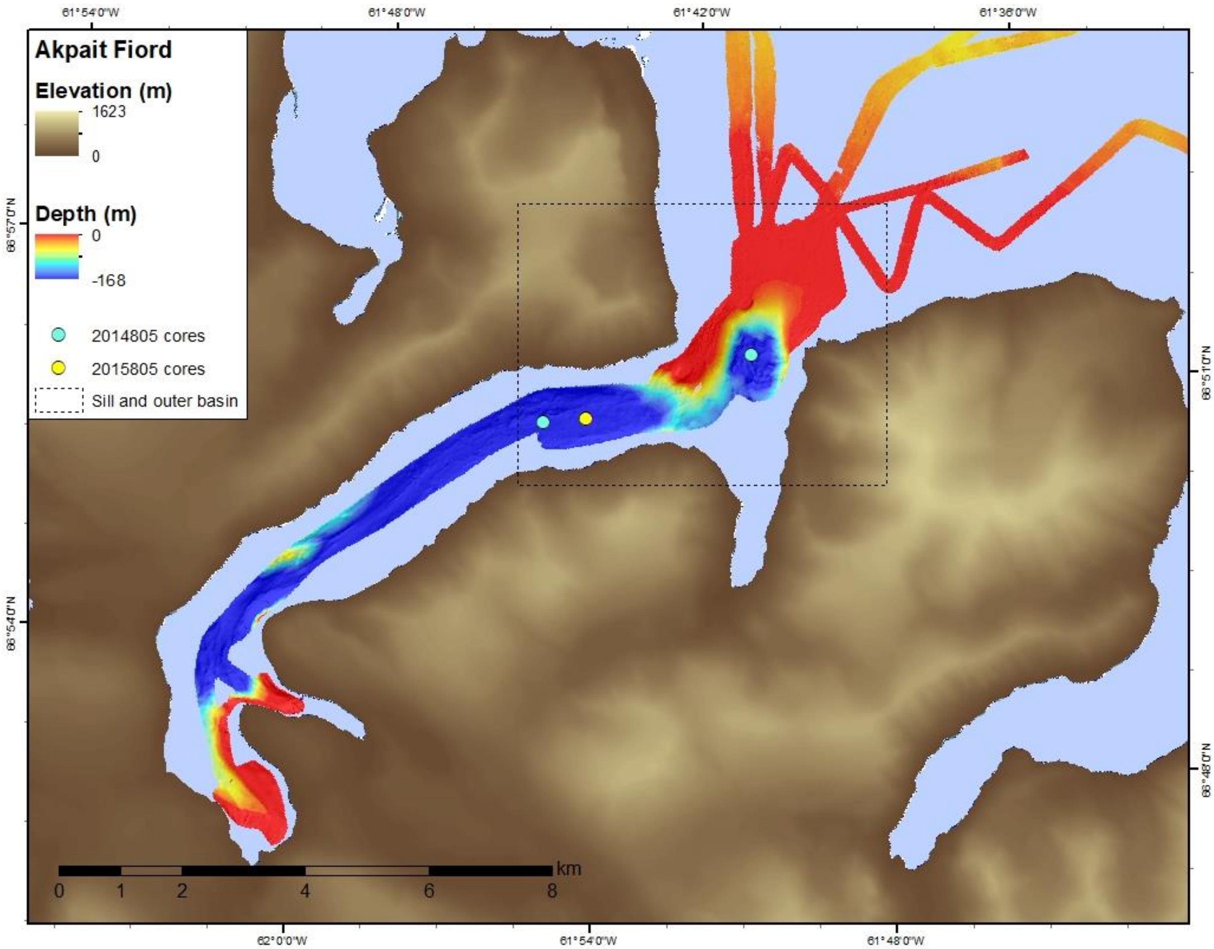

Figure B.28: Map of Akpait Fiord, with the fjord-mouth study site and its associated coring sites indicated.

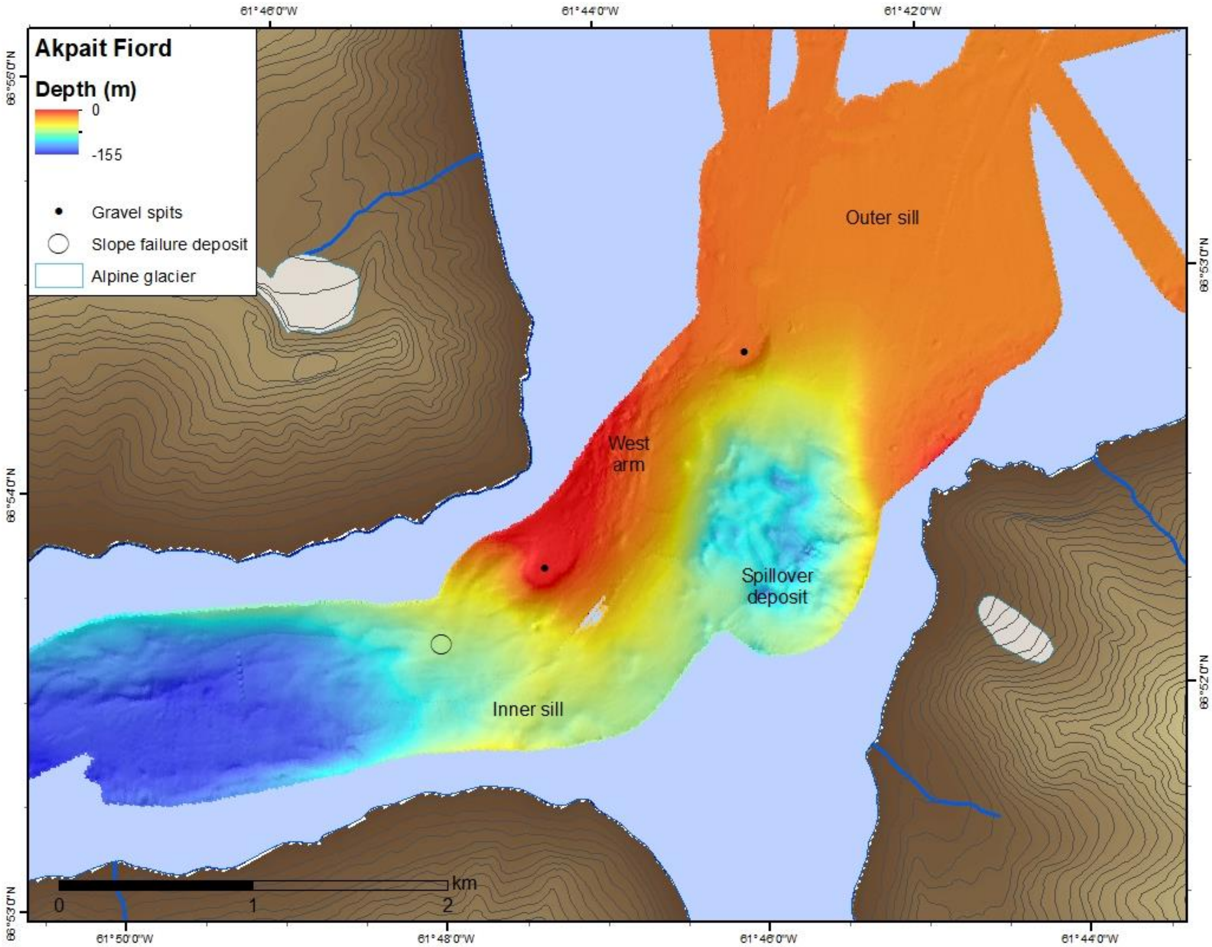

Figure B.29: Map of the fjord-mouth sill study site in Akpait Fiord, with some seafloor geomorphic features indicated.

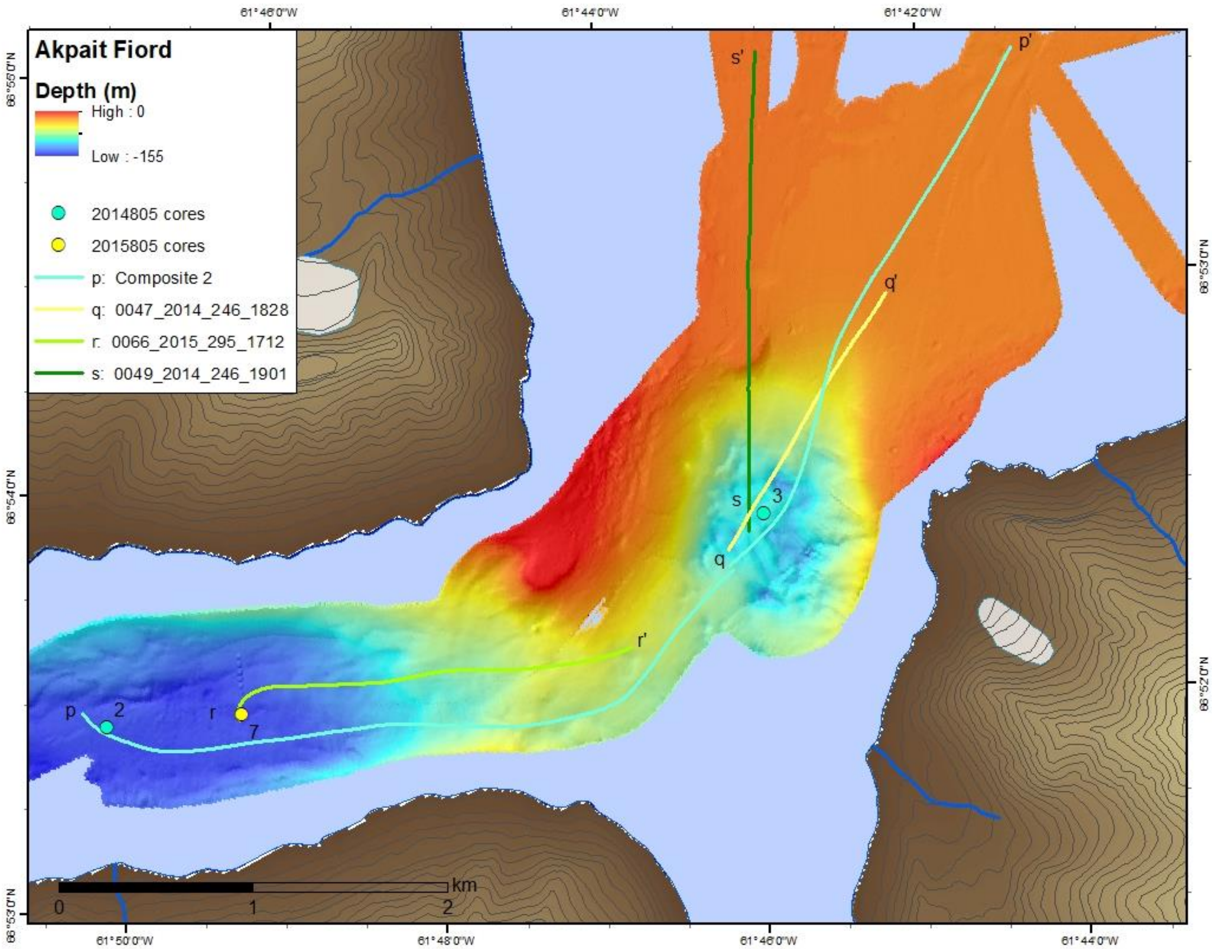

Figure B.30: Map of the fjord-mouth sill study site in Akpait Fiord, with the positions of the coring sites and the analyzed acoustic profiles indicated.

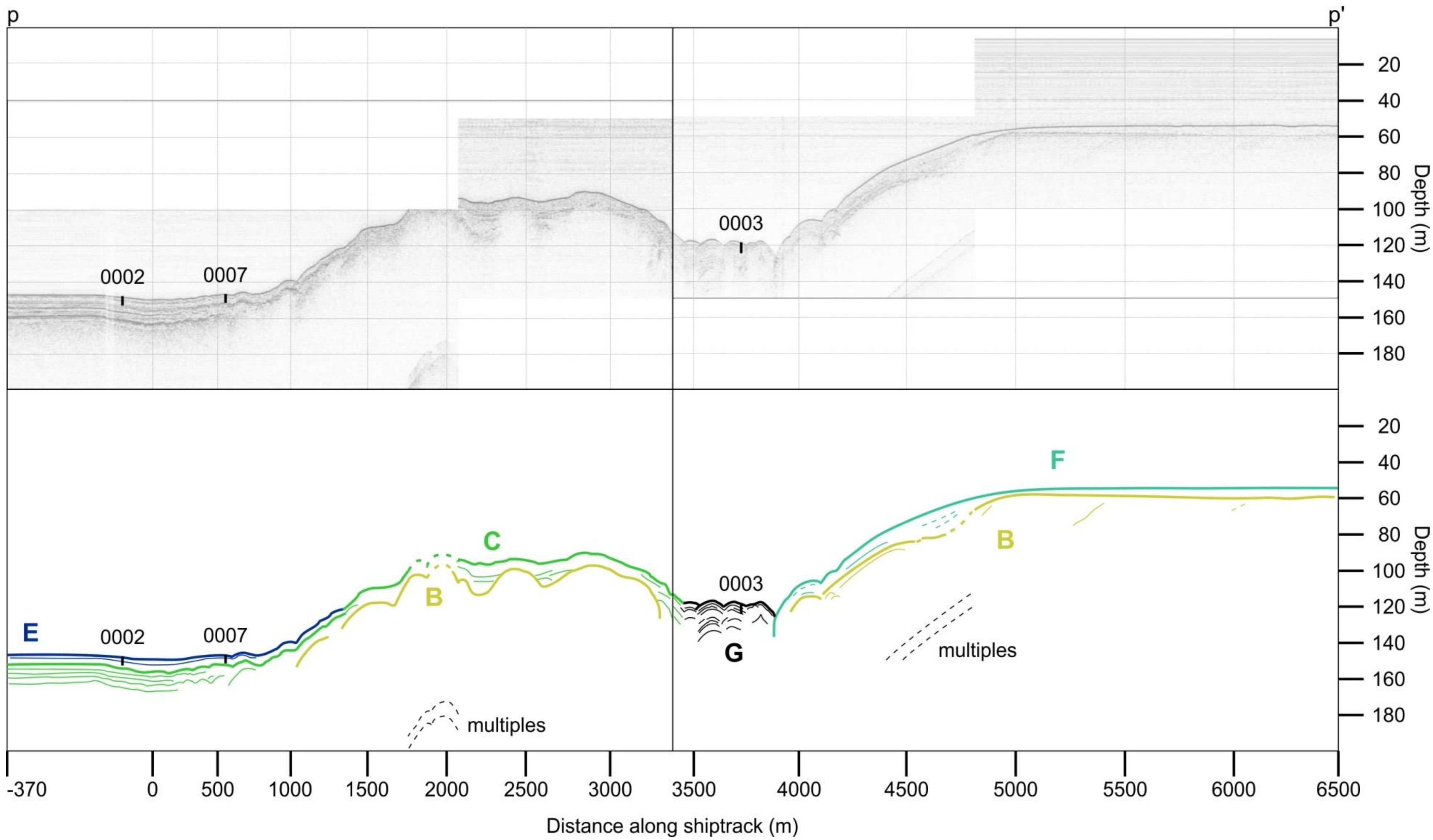

Figure B.31: Profile *p* is a composite of two separate profiles from Akpait Fiord, covering the outer area of the fjord basin, the mid-fjord sill, spillover deposit, and fjord-mouth sill. (G) Spillover deposit, (F) sill cover, (E) marine muds, (C) glaciomarine sediment, (B) ice-contact sediment.

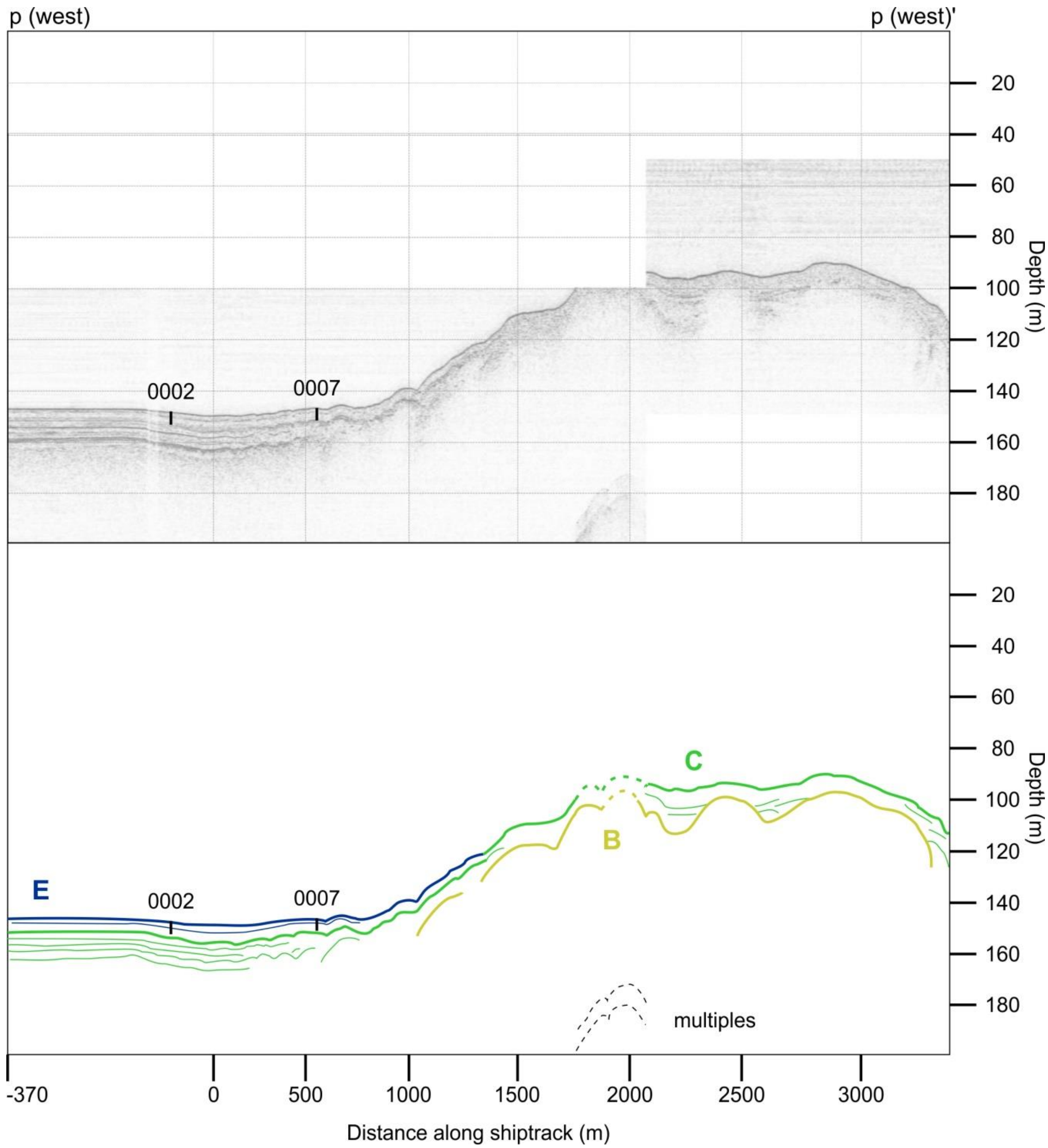

Figure B.32: The western segment of profile *p*, which crosses the Akpait Fiord basin and inner sill. (E) Marine muds, (C) glaciomarine sediment, (B) ice-contact sediment.

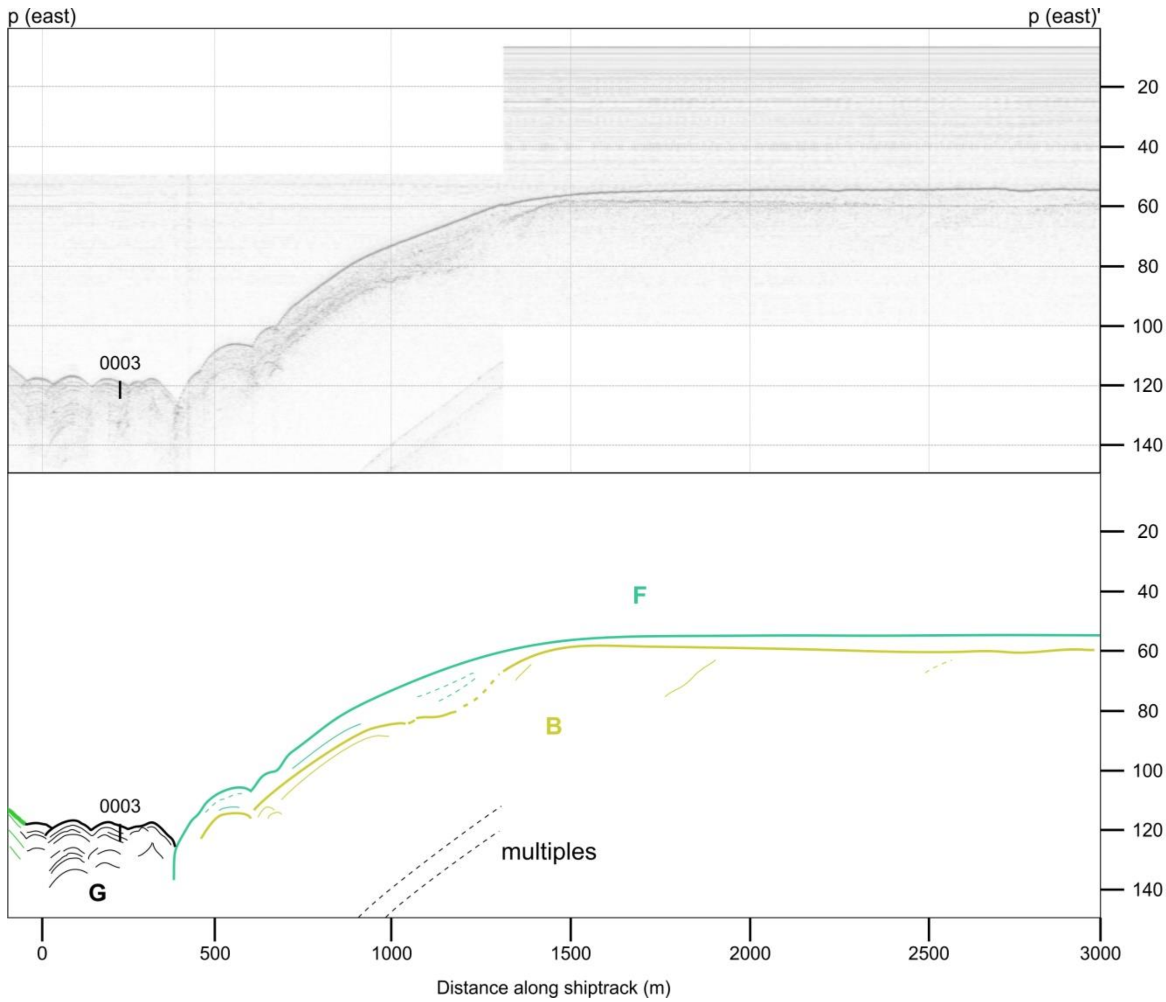

Figure B.33: The eastern segment of profile *p*, which crosses the Akpait Fiord spillover deposit and fjord-mouth sill. (G) Spillover deposit, (F) sill cover, (B) ice-contact sediment.

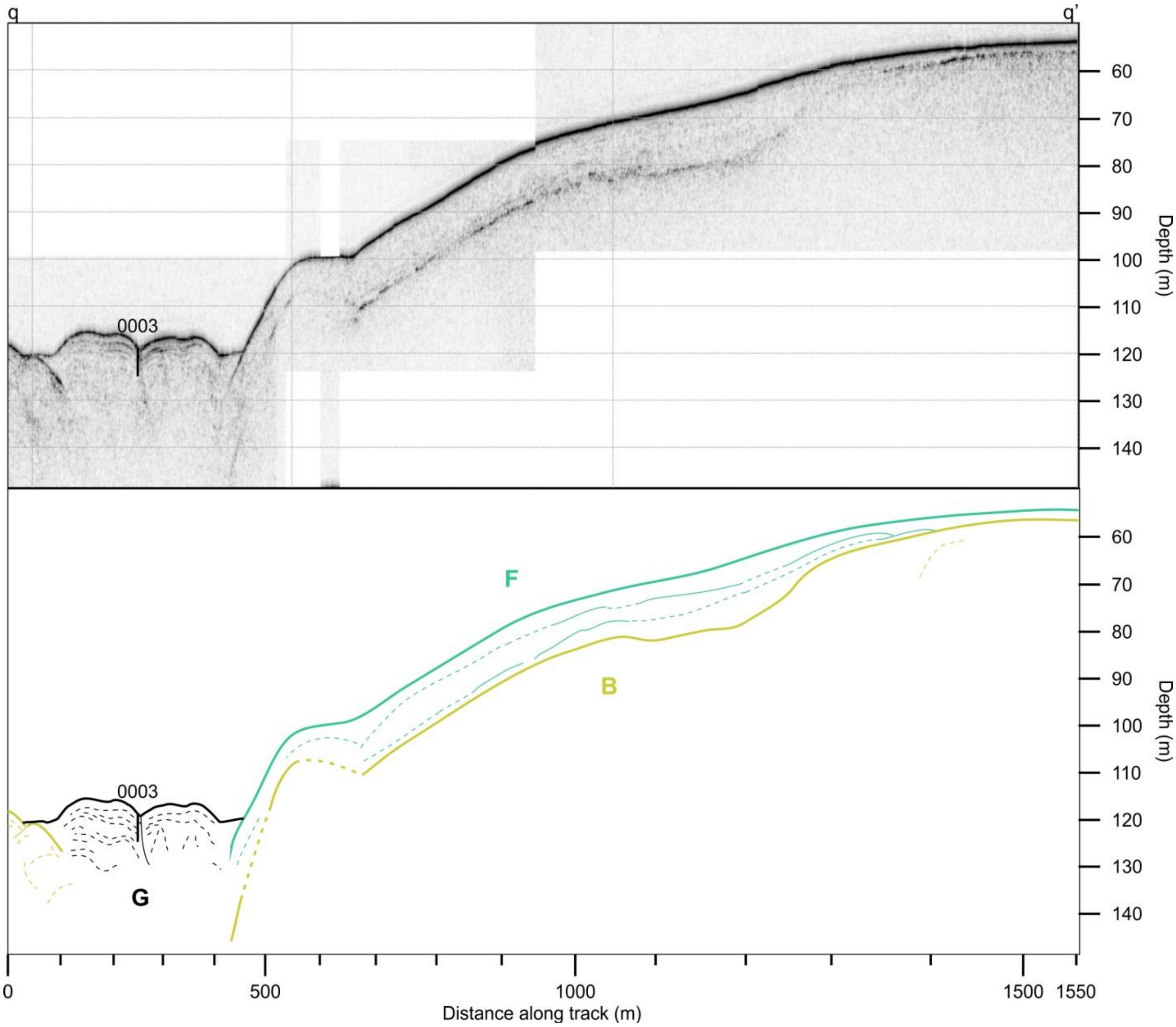

Figure B.34: Akpait Fiord profile *q* crosses the spillover deposit and inner part of the fjord-mouth sill. (G) Spillover deposit, (F) sill cover, (B) ice-contact sediment.

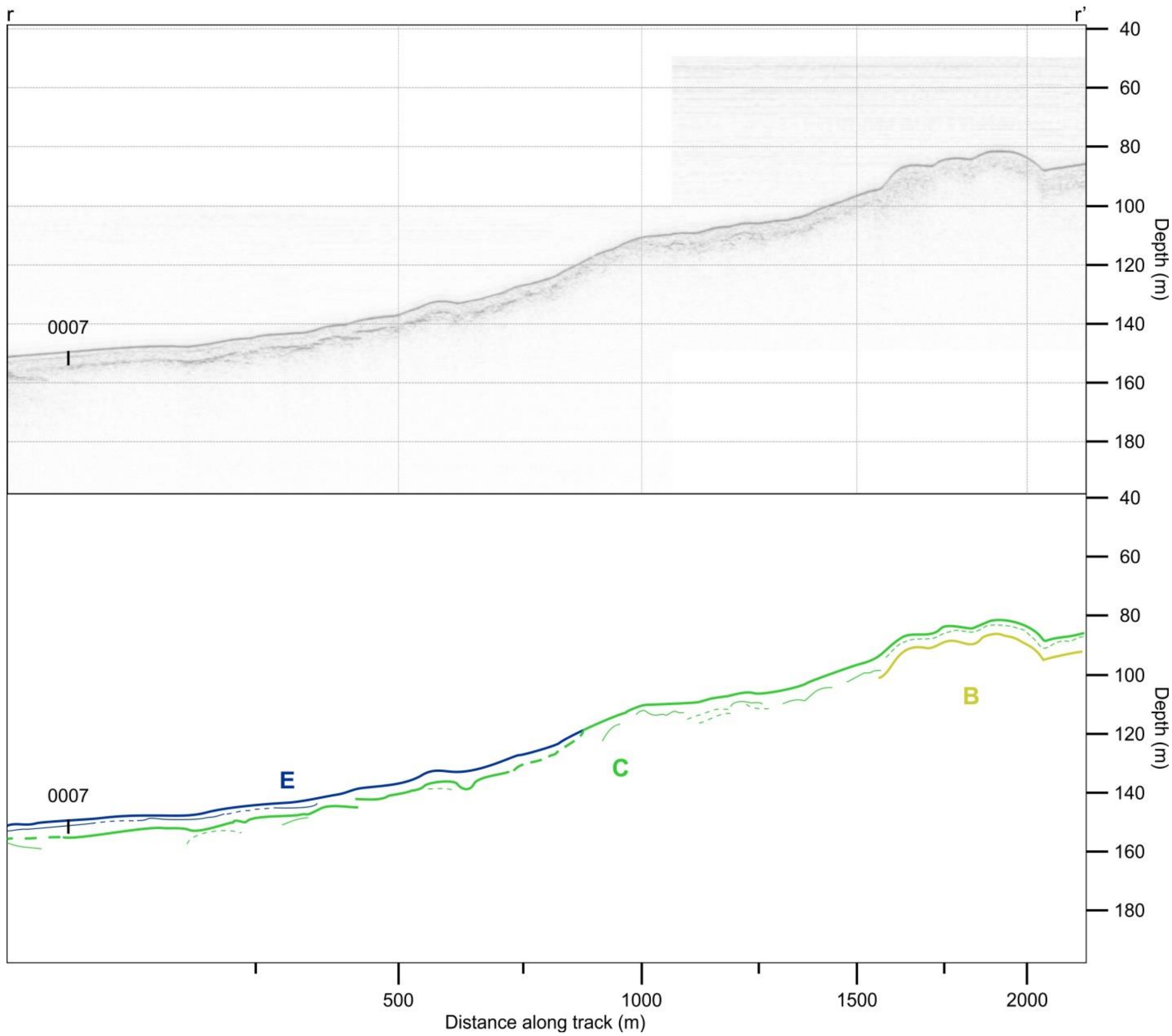

Figure B.35: Akpait Fiord profile *r* covers the outer area of the fjord basin and the slope of the mid-fjord sill. (E) Marine mud, (C) glaciomarine sediment, (B) ice-contact sediment.

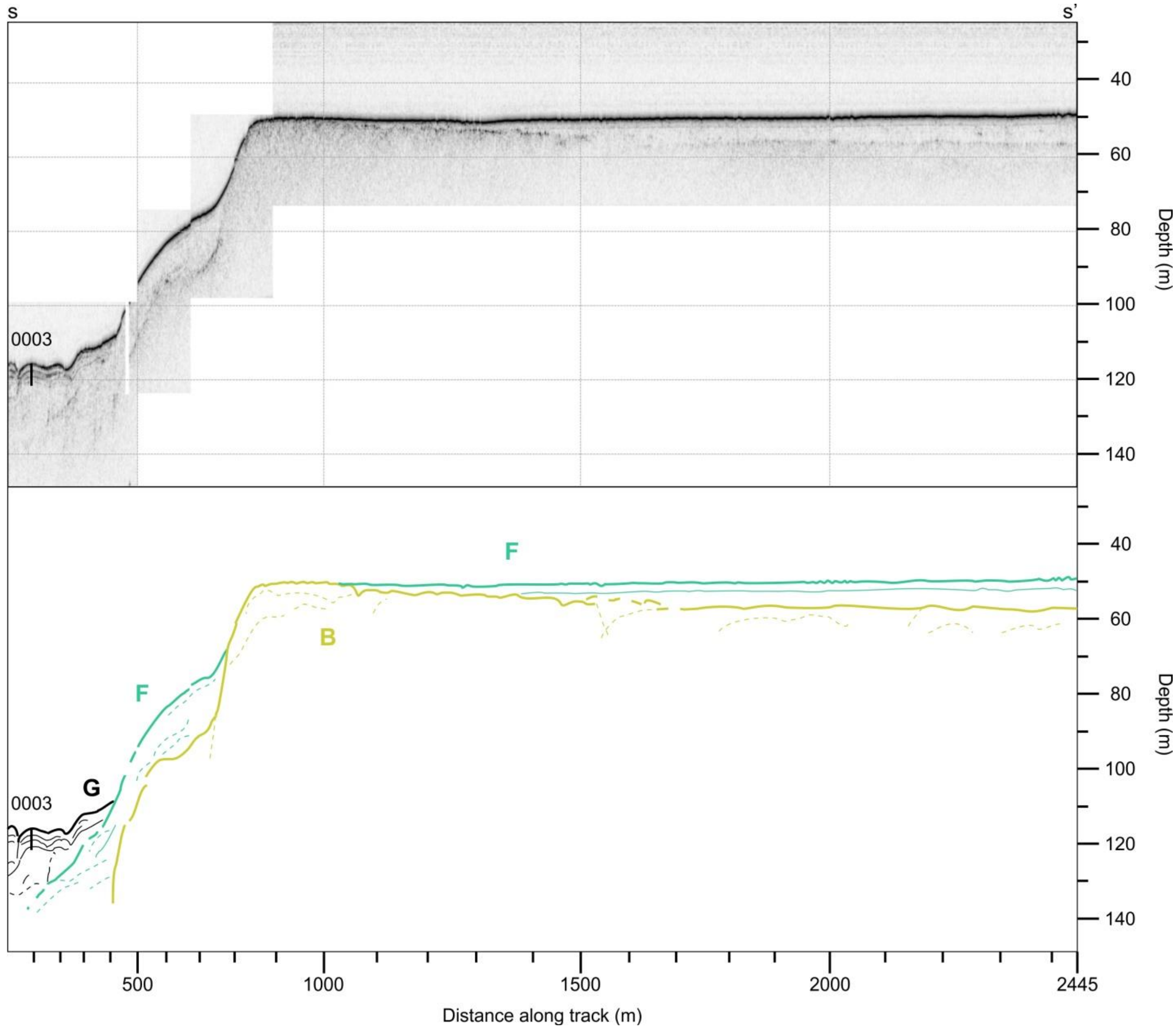

Figure B.36: Akpait Fiord profile *s* transects the spillover deposit and the fjord-mouth sill, while crossing one of the gravel spits (~900 m). (G) Spillover deposit, (F) sill cover, (B) ice-contact sediment.

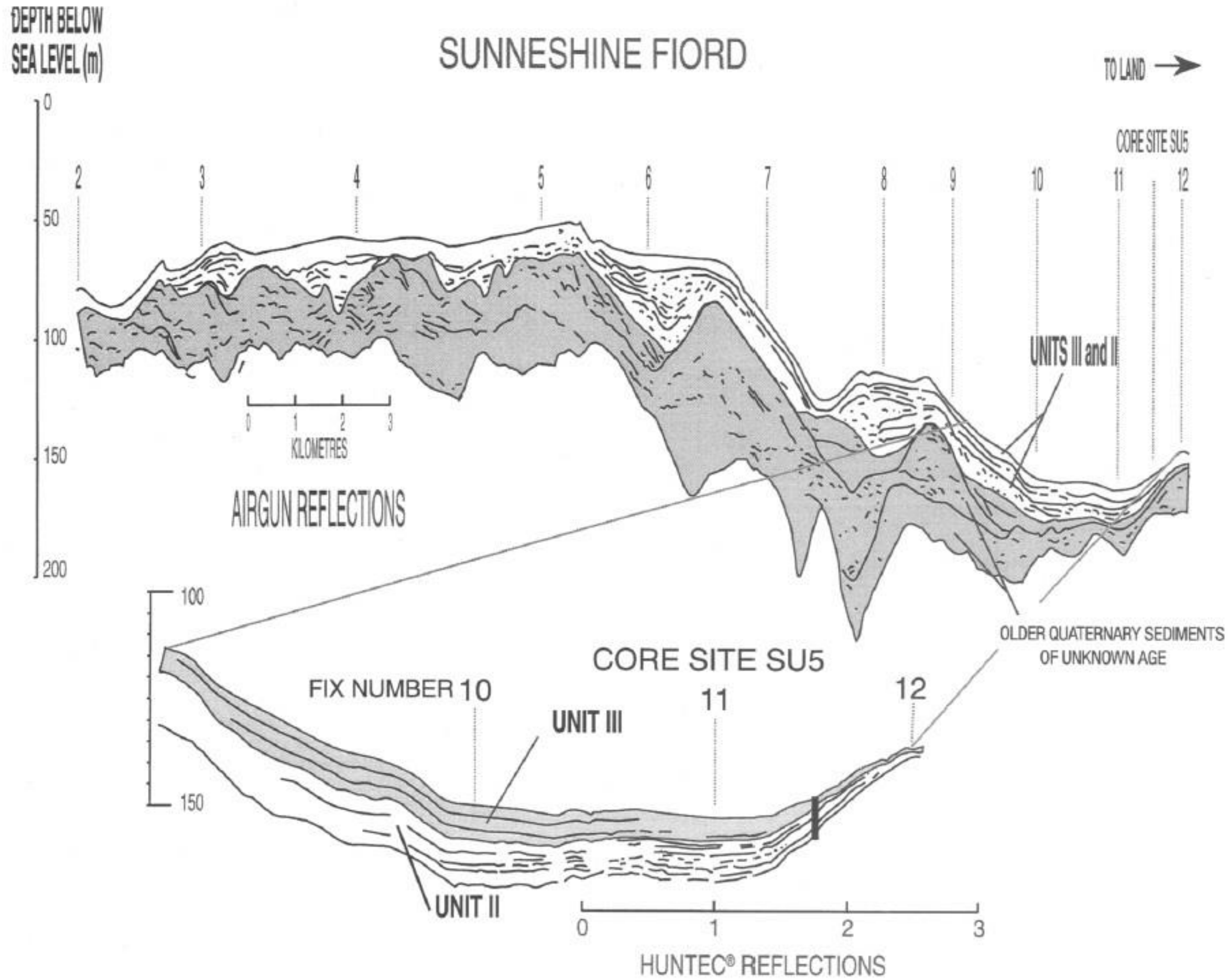

Figure B.37: Acoustic profile of Sunneshine Fiord, interpreted to contain 3 acoustic units: Quaternary sediments (Unit B, ice-contact), Unit II (Unit C, glaciomarine), and Unit I (Unit E, marine mud). From Andrews et al. (1996).

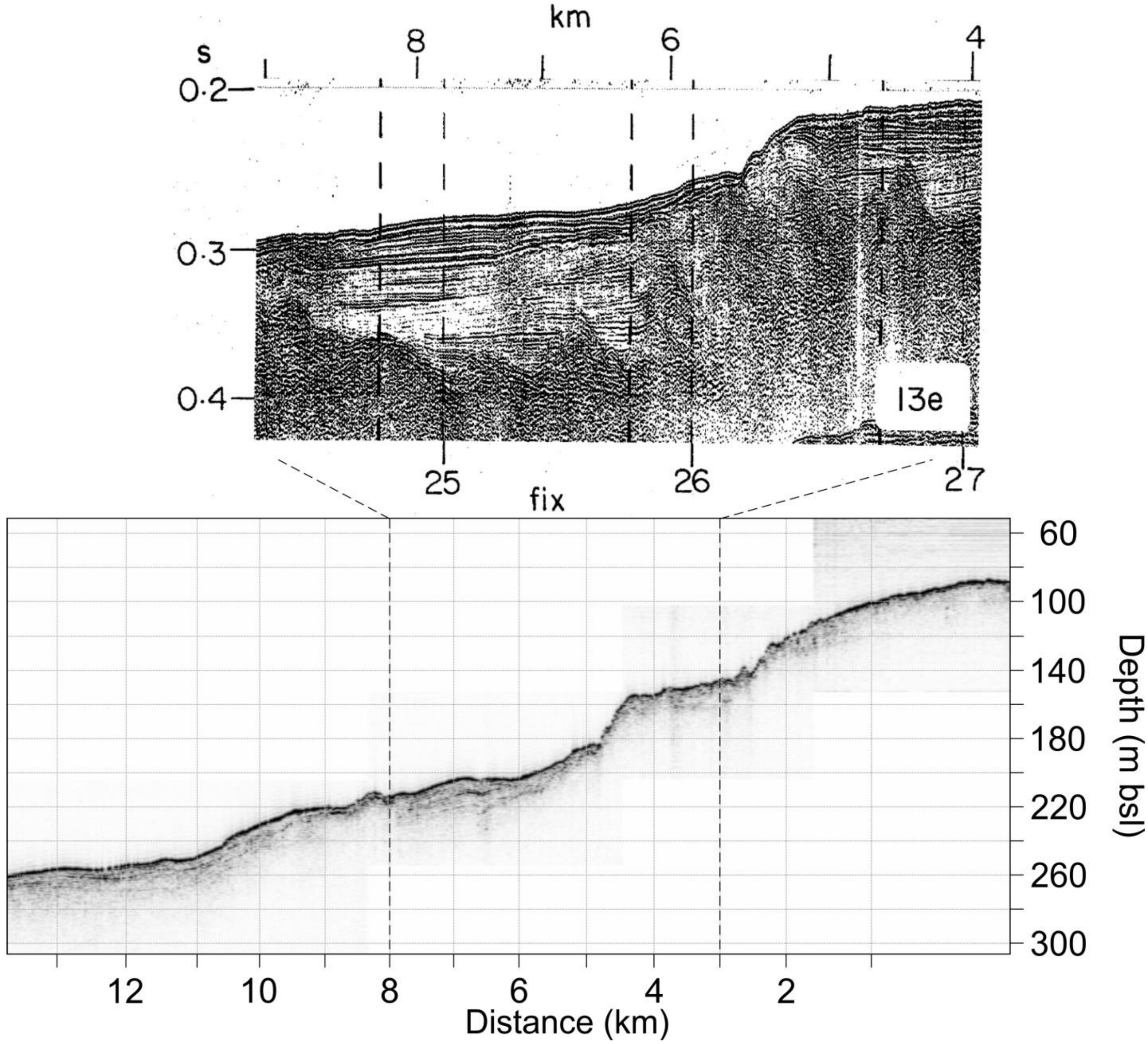

Figure B.38: Comparison of acoustic profiles for the fjord-head region of Clark Fiord, provided to illustrate how the quality of acoustic imagery differs between the earlier Huntec and more recent profiles. Top: modified from Gilbert & MacLean (1984). Bottom: from the 2011 *CCGS Amundsen* (0188_2011_294_1920)

C SEDIMENT CORES

This appendix records data on a total of 19 core samples, collected from 4 fjords along eastern Cumberland Peninsula, Baffin Island, during research cruises in 1982, 2014, and 2015 (Table C.1).

C.1 Boas Fiord

Gravity cores were collected during 2014 by the *MV Nuliajuk* at seven stations within Boas Fiord, grouped into two regions: the submerged fjord-head delta (side-terrace and delta plain), and the submerged side-entry delta at Giff's Cove. The cores from the fjord-head delta show considerably thicker fine-grained, post-submergence deposits than the side-entry delta, suggesting a more active sedimentary history.

C.1.1 Fjord-head delta (2014NULIAJUK 0001-0004)

Four gravity cores were collected from the submerged fjord-head delta: two at the eastern side-terrace and two at the delta plain. These cores range in length from 60 to 135 cm, and are interpreted from the acoustic profiles to unanimously penetrate acoustic unit E. The lithology was interpreted as predominantly clay-silt, which supports the interpretation of acoustic unit E as post-submergence marine mud. The only shell fragment subsample (2014NULIAJUK-0004 GC 103–104 cm) extracted and dated from these cores returned a calibrated date range of 820 (930) 1050 cal BP, and therefore a mean sedimentation rate range of 0.990 – 1.27 mm/yr. When these minimum and maximum sedimentation rates are extrapolated downwards to the contact with the deltaic sediments (~200 cm below the seafloor), the minimum age constraint for the submersion of the delta and the timing of the postglacial lowstand ranges about ~1570–2020 yr BP.

C.1.1.1 2014NULIAJUK-0001 GC

Lithostratigraphy: Core sample 2014NULIAJUK-0001 GC (Figs. C.1 – C.3) measures at 94 cm long. It was interpreted as predominantly silt, with a transition to clay-silt at 80 cm. An inclined ~1-cm thick clay lens crosses from 41–46 cm.

Correlation with acoustic stratigraphy: The core penetrates unit E (94 of ~200 cm; profile *b*), interpreted as post-submergence marine muds, at a position overlying the delta side-terrace.

Facies interpretation and depositional environment:The fine-grained sediments observed (clay to silt) corroborate the interpretation of acoustic unit E as post-submergence marine muds that accumulated following RSL transgression and abandonment of the delta.

C.1.1.2 2014NULIAJUK-0002 GC

Lithostratigraphy: Core sample 2014NULIAJUK-0002 GC (Figs. C.4 – C.6) measures at 76 cm long. It was interpreted as massive clay-silt, with scattered dropstones and signs of bioturbation observed.

Correlation with acoustic stratigraphy: The core shallowly penetrates unit E (76 of ~250 cm; profiles *c* and *e*), interpreted as post-submergence marine muds, at a position above the delta plain.

Facies interpretation and depositional environment:The massive clay-silt unit observed corroborates the interpretation of acoustic unit E as post-submergence marine mud, which draped the fjord-head delta at both its side-terrace and delta plain following RSL transgression.

C.1.1.3 2014NULIAJUK-0003 GC

Lithostratigraphy: Core sample 2014NULIAJUK-0003 GC (Figs. C.7 – C.9) measures at 60 cm long. It was interpreted as massive clay-silt, with scattered dropstones some and signs of bioturbation observed. Between 25 and 50 cm, the core shows signs of inclined bedding with no dropstones.

Correlation with acoustic stratigraphy: The core shallowly penetrates acoustic unit E (60 of ~400 cm; profile *c*), interpreted as post-submergence mud, at a position above the delta plain.

Facies interpretation and depositional environment: The massive clay-silt unit observed corroborates the interpretation of acoustic unit E as post-submergence marine mud. Thus, the delta plain of the fjord-head delta was draped with marine muds even towards the fjord head following sea level transgression.

C.1.1.4 2014NULIAJUK-0004 GC

Lithostratigraphy: Core sample 2014NULIAJUK-0004 GC (Figs. C.10 – C.12) measures at 135 cm long. It was interpreted as massive clay-silt, with signs of bioturbation observed.

Correlation with acoustic stratigraphy: The core penetrates unit E (135 of ~200 cm; profile *b*), which was interpreted as post-submergence marine muds. Station 2014NULIAJUK-0004 was located extremely proximal to station 2014NULIAJUK-0001, and thus the core sample penetrates a similar position above the fjord-head delta's side-terrace.

Facies interpretation and depositional environment: The massive clay-silt sediments corroborate the interpretation of acoustic unit E as post-submergence marine mud. Thus, the radiocarbon-dated subsample 103–104 cm, as extracted from the post-submergence marine mud, must postdate the submersion of the delta by RSL transgression. Logically, onset of the RSL transgression is represented by the contact between the post-submergence marine muds and the underlying deltaic sediments, at ~200 cm below the seafloor. By extrapolating the mean sedimentation rate range of 0.990–1.27 mm/yr to the depth of ~2000 mm, an age range of ~1580–2020 cal BP is estimated for the onset of RSL transgression and the minimum age constraint of the postglacial lowstand.

C.1.2 Side-entry delta (Giff's Cove)

Three gravity cores were collected from the submerged side-entry delta: two near the edge of the delta terrace and one upon the secondary terrace. These cores are significantly shorter than those from the fjord-head delta, ranging in length from 12 to 20 cm. However, similar to the fjord-head cores, they are unanimously interpreted as having predominantly clay-silt lithologies. Although acoustic unit E (post-submergence mud) is not observed on the local acoustic profiles, the lithology and length of these cores indicate that a post-submergence mud unit is present, if too thin for the resolution of the acoustic subbottom imagery. No shell fragment subsamples from these cores were submitted for radiocarbon dating, so no chronology is currently available for the side-entry delta.

C.1.2.1 2014NULIAJUK-0005 GC

Lithostratigraphy: Core sample 2014NULIAJUK-0005 GC (Figs. C.13, C.14, C.19) measures at 12 cm long, and was interpreted as faintly-bedded clay-silt with a few dropstones.

Correlation with acoustic stratigraphy: A surficial unit of post-submergence mud (unit E) was expected to drape the side-entry delta, but is not observed on the local acoustic subbottom profiles (*f* to *i*). It was hypothesized that a post-submergence mud unit may still be present, but be too thin for the acoustic subbottom imagery to resolve. The clay-silt contents of core sample 2014NULIAJUK-0005 GC support this hypothesis and indicate that post-submergence muds may be 12 cm thick at the edge of the primary terrace (core sample 2014NULIAJUK-0006 GC corroborates this). If the above hypothesis is false, then the core sample instead penetrates the upper 12 cm of unit D3, which was interpreted as the deltaic topset beds.

Facies interpretation and depositional environment: The interpreted clay-silt lithology supports the prior acoustic profile interpretation of post-submergence marine mud. In turn, the notable difference in sediment thickness indicates that fine-grained sediment deposition was less active at Giff's Cove than the fjord head. This could be due to either a scarcity of material to deposit, or a water velocity that precluded fine-grained deposition.

Giff's Cove is fed by two 3rd-order glacial stream systems, and a 1st-order stream. Both 3rd-order streams are fed by multiple valley glaciers, but also have multiple lakes (which would filter coarse sediments) and segments of braided stream morphology (which would slow water velocity) along their course. Nonetheless, the bathymetry indicates that the secondary terrace is associated with the northern 3rd-order stream system. Apparently, during reactivation and prior to submergence, this stream system was able to deposit a shallow secondary terrace of coarse material (continuous with the primary terrace on profiles *f*, *g*, and *i*). During transgression and deposition of this terrace, the sea level would have been shallow enough for wave-action to prevent fine-grained sediments from settling. However, modern subaerial signs of sedimentation are lacking in Giff's Cove. A sandur is visible on Google Earth Pro™ along the northern stream system, but only a minor delta is visible, and no minor delta observed for the southern stream system. In contrast, the submerged fjord-head delta has a thicker post-submergence unit, and is also adjacent to active modern sedimentation—a large subaerial fjord-head delta and two side-entry deltas. Thus, low sediment input appears to be the cause of the thin post-submergence marine mud unit.

Water velocity is less likely. Station 2014NULIAJUK 0005 is over 1.1 km away from the nearest modern stream mouth and local water depth is 36 m. The effects of stream current should not extend this far or this deep following RSL transgression. Similarly, while wave-action could have eroded the side-entry delta plain during transgression (profiles *f*, *g*, and *i* show the secondary terrace to be visually continuous with the primary terrace—during RSL transgression when the secondary terrace was prograding, wave action likely prevented fine sediment from accumulating and only allowed coarse sediments to settle), it should have had minimal post-submergence impact on sedimentation (be too deep for the wave-base to affect). Thus, water velocity preventing fine-grained sedimentation seems unlikely.

While anticipated to be slow, the local mean sedimentation rate could be best estimated if the subsample 6–7 cm was submitted for dating.

C.1.2.2 2014NULIAJUK-0006 GC

Lithostratigraphy: Core sample 2014NULIAJUK-0006 GC (Figs. C.15, C.16, C.19) measures at 17.5 cm long. It was interpreted as consisting of a clay-silt unit (0–12 cm) overlying a sand unit (12–17.5 cm), with angular clasts at 0–5 cm and 15–17 cm.

Correlation with acoustic stratigraphy: A surficial unit of post-submergence mud (unit E) was expected to drape the side-entry delta, but is not observed on the local acoustic subbottom profiles (*f* to *i*). It is hypothesized that a post-submergence mud unit may be present but too thin for the acoustic subbottom imagery to resolve. The clay-silt contents of core sample 2014NULIAJUK-0006 GC support this hypothesis, indicating that post-submergence muds may be 12 cm thick near the edge of the primary terrace (core sample 2014NULIAJUK-0005 GC corroborates this), with the remaining 5.5 cm corresponding to unit D3. If the above hypothesis is false, then the core sample instead penetrates the upper 17.5 cm of unit D3, which is interpreted as the deltaic topset beds.

Facies interpretation and depositional environment: The core indicates that unit E, post-submergence marine mud, is ~12 cm thick in some locations, and that the underlying deltaic topset bed is composed of sand. The thinness of the marine muds, combined with the difficulty of penetrating coarser sediments with a gravity core, is likely the reason why the three cores collected at the side-entry delta are so shallow compared to those collected from the fjord-head delta. The angular shape of the clasts indicates that they have experienced minimal erosion. Thus, the clasts were most likely deposited as ice-rafted dropstones.

C.1.2.3 2014NULIAJUK-0007 GC

Lithostratigraphy: Core sample 2014NULIAJUK-0007 GC (Figs. C.17, C.18 C.19) measures 20 cm long, and was interpreted at as massive to faintly-bedded clay-silt, with a large sub-rounded clast at 10–20 cm.

Correlation with acoustic stratigraphy: A surficial unit of post-submergence mud (unit E) is expected to drape the side-entry delta, but is not observed on the local acoustic subbottom profiles (*f* to *i*). It is hypothesized that a post-submergence mud unit may be present, but too thin for the acoustic subbottom imagery to resolve. The clay-silt content of core sample 2014NULIAJUK-0007 GC supports this hypothesis, and indicates that post-submergence muds on the secondary terrace may be 20 cm thick. If the above hypothesis is false, then the core sample instead penetrates the upper 20 cm of unit C3, which was interpreted as the deltaic topset beds.

Facies interpretation and depositional environment: The core penetrates the surface of the secondary terrace of the side-entry delta. The clay-silt sediments suggest that post-submergence marine muds are present in a thin layer (≥20 cm) that is not visible on acoustic profiles *g* and *i*. The large clast may indicate contact with the delta topset bed, or represent a dropstone. Fig. C.17 shows no deformation of sedimentary features around the clast, indicating that its tilt is *in situ*, supporting the ice-rafted dropstone interpretation. However, as the shell fragment (1–4 cm) was not extracted for radiocarbon dating, the timing of fluvial reactivation of the side-entry delta cannot currently be constrained, beyond having occurred following the onset of RSL transgression at some time during ~1580–2020 cal BP.

C.2 Durban Harbour

Piston core sampling was attempted at three stations within Durban Harbour, targeting the prodelta and delta slope region of the submerged fjord-head delta. However, the coring attempt nearest to the delta slope (2015805-0005 PC) only resulted in a 10 cm long, unsorted sample of sandy silt. The other two piston cores are 244 and 261.5 cm in length, and both are interpreted as penetrating acoustic unit D1. Lithology varies between them, but both are interpreted as predominantly clay-silt. This supports the interpretation of acoustic unit D1 as representing delta bottomset beds, with the fine-grained sediments indicating a low-velocity water environment. The one calibrated radiocarbon date retrieved from these cores (2015805-0006 PC 210–212 cm) was extracted from the delta bottomset bed sediments. Thus, representing the time when the delta was part of an active, subaerial fluvial system, and thus provides a maximum age constraint for the timing of the postglacial lowstand of ~9520–9810 cal BP.

The material recovered from the associated trigger-weight core (2015805-0006 TWC) consisted only of bagged, unsorted sediment, and thus is not discussed further here.

C.2.1 2014805-0001 PC

Lithostratigraphy: Core sample 2014805-0001 PC (Fig. C.20) measures at 261.5 cm long. The near-surface part of the core, 0–25 cm, consists of coarse-grained sediments: sand (0–10 cm) and silt-sand (15–25 cm), separated by a lens of clay-silt (10–15 cm). Below 25 cm, the core sample is interpreted as fine-grained: predominantly clay-silt (25–258 cm), interrupted by lenses of silt (197–202 and 255–258 cm). The bottom of the core (258–261.5 cm) contacts a clay unit. Small dropstones are scattered throughout its length.

Correlation with acoustic stratigraphy: The core is observed to penetrate acoustic unit D1 (261.5 of ~500 cm; profile *l*), which is interpreted as the delta bottomset bed. The core may contact the internal reflector (~300 cm below seafloor) observed on profile *l*, but should not reach the underlying unit B (ice-contact).

Facies interpretation and depositional environment: Core 2014805-0001 is located near the foot of the delta slope, and thus may represent the transition between the foreset and bottomset beds.

The abrupt transition from coarse- to fine-grained sediments at 25 cm, combined with the internal reflector observed in unit D1 (profile *l*), leads to two possible interpretations.

The more straight-forward interpretation is that the fine-grained sediments (25–261.5 cm) represent the delta bottomset beds, originally deposited in a low-energy environment, and the overlying coarse-grained sediment cap (0–25 cm) represents the progradation of the foreset beds as the delta accumulated coarse sediments.

Alternatively, the fine-grained sediment unit (25–261.5 cm) may instead represent post-submergence marine muds, while the overlying coarse-grained sediment cap (0–25 cm) represents a minor slop-failure deposit (progradational slump). Under this interpretation, the delta bottomset beds are instead represented by the D1 internal reflector, or the unit B contact line. This interpretation is suggested by the resemblance between the lithology of the fine-grained sediment unit (25–261.5 cm) and the post-submergence unit interpreted in core 2015805-0006 PC: predominant clay-silt, and even share a lens of pure silt immediately underlain by clay. However, this interpretation is unlikely, as no distinct sign of a slope-failure deposit or scar is observed on either the bathymetry or acoustic profiles (*k*, *l*, or *m*). Moreover, the x-radiography shows the silt-sand unit (15–25 cm) to have roughly horizontal bedding, while clasts in the sand unit are oriented roughly horizontal. A slope failure deposit would be expected to show significant disruption.

C.2.2 2015805-0005 PC

Lithostratigraphy: Core sample 2015805-0005 PC (no figure) was the result of a failed coring attempt, resulting in 10 cm of unsorted silt-sand with granules and shell fragments.

Correlation with acoustic stratigraphy: The sample corresponds to the surface of acoustic unit D2, interpreted as the delta foreset beds.

Chronology: Two shell fragment subsamples were extracted and combined into one vial. However, due to the mixing of the sediment during the coring attempt, they could at best provide only a rough age range for the upper 10 cm, rather than defined time intervals. Therefore, they have not yet been submitted for radiocarbon dating.

Facies interpretation and depositional environment: Silt-sand sediment corroborates the interpretation of unit D2 as the delta foreset beds. The shell fragments observed in this near-surface sample suggest previous to near-recent mollusc habitation of the unit. Moreover, the difficulty experienced by the piston core in attempting to penetrate the local sediments suggests that a thick unit of similarly coarse sediments underlies the surface. Thus, it can be inferred that the coarse sediment cap of core 2014805-0001 PC (0–25 cm) likely increases in thickness towards the delta slope.

C.2.3 2015805-0006 PC

Lithostratigraphy: Core sample 2015805-0006 PC (Fig. C.21) measures at 244 cm long. The core sample is capped by a surficial clay lens (0–2 cm). Below it, the upper-to-middle portion of the core is interpreted as predominantly clay-silt (2–67 and 84–176 cm), interrupted by a silt lens (67–69 cm) overlying a clay unit (69–84 cm). The clay-silt unit is underlain by a lens of silt-sand (176–180 cm), which then fines downwards into units of silt (180–200 cm) and clay (200–215 cm), before coarsening downward into another clay-silt unit (215–228 cm). The very bottom of the core is capped by a unit of sand containing multiple clasts (228–244 cm).

Correlation with acoustic stratigraphy: Based on profile *j*, the core is estimated to penetrate the contact lines for acoustic units E (~100 cm thick) and D1 (~400 cm thick), which were interpreted as marine muds and delta bottomset sediments, respectively. The sand-gravel unit at the base of the core indicates that acoustic unit B (glacial till) was contacted, even though this contact was not estimated for profile *j*. This demonstrates that the acoustic unit thicknesses estimated from the SegyJp2 Viewer software (Courtney, 2018) are imperfect, as a muddy sandy gravel unit suggestive of glacial till is encountered at 228 cm, while unit B is estimated to occur at ~500 cm below the seafloor.

Facies interpretation and depositional environment: Overall, the core shows an upwards-fining trend that can be grouped into two sediment packages: ice-contact (unit B) and delta bottomset bed (unit D1). The basal unit of gravel in a sand-matrix (228–244 cm) is interpreted as ice-contact glacial till, possibly representing the proglacial outwash, as gravel is unlikely to be deposited by delta progradation. The overlying package (0–228 cm), ranging in grain size from clay to silty-sand, is interpreted as the delta bottomset bed. The variations in grain size indicate the variations in stream competence expected in prodelta sedimentation: the clay-silt unit indicates the decreasing glacial outwash competence as the glacier retreats further inland, the clay unit indicates a low-energy and distal prodelta environment, and the coarsening into silt and silt-sand indicates increasing stream competence as the delta (and thus river mouth) progrades outwards.

C.3 Akpait Fiord

Piston and trigger-weight cores have been collected at three stations within Akpait Fiord. Two of these stations target the fjord basin (2014805-0002 and 2015805-0007), while one targets the spillover deposit adjacent to the fjord-mouth sill (2014805-0003).

C.3.1 Fjord basin

A total of four cores—two piston and two trigger-weight—were collected from the basin of Akpait Fiord. Station 2015805-0007 is located 0.75 km down-fjord from the earlier station 2014805-0002, and targeted the seafloor closer to the sidewall, where the strata were anticipated to be thinner, in an attempt to collect older sediments. It has been hypothesized that the local fjord-mouth sill may have been subaerial during a lower sea-level period, which would have made the fjord a former freshwater or brackish waterbody. However, none of the cores collected thus far contain evidence to support the hypothesis.

The two piston cores average ~500 cm long, while their trigger-weight cores average ~100 cm long. All four basin cores were interpreted as penetrating acoustic unit E, with core sample 2015805-0007 PC possibly contacting acoustic unit B. The lithology amongst all four basin cores is interpreted as predominantly clay-silt, supporting the interpretation of acoustic unit E as marine mud and indicating a low-velocity water environment. Moreover, core 2015805-0007 PC includes a sand unit underlain by additional marine muds, which may corroborate the interpretation of a slope-failure deposit originating from the ice-contact sill, as discussed in Appendix B.3. The six calibrated radiocarbon dates retrieved from these cores were extracted from the marine muds, and together demonstrate that the mean sedimentation rates vary across time and distance.

On profile *p*, the station 2014805-0002 and 2015805-0007 core samples are observed contacting two strong, continuous reflectors: the uppermost unit E internal reflector, and the underlying reflector which transitions from a unit E internal reflector (0002) to the unit B upper contact line (0007). The 0007 marker is also observed contacting these reflectors on profile *r*. However, profile *p* directly intersects station 0002, while profile *r* directly intersects station 0007. As a result, the acoustic unit thickness measurements from profile *p* are used for 0002, and from profile *r* for 0007. From the SegyJp2 Viewer software (Courtney, 2018), the upper reflector (uppermost unit E internal reflector) is measured to be ~1.8 m below seafloor at station 0002 and 0007, while the lower reflector (unit E to unit B transition) is ~5.1 m below seafloor at station 0002 and 0007. The near-equivalent depths for each reflector at both stations may be attributed to the sites forming a near-parallel line to the sidewalls.

C.3.1.1 2014805-0002 PC

Lithostratigraphy: Core sample 2014805-0002 PC (Fig. C.22) measures at 516.5 cm long, and was interpreted as a massive clay-silt unit with dropstones scattered throughout.

Correlation with acoustic stratigraphy: On profile *p*, the core is estimated to correspond to the highly-stratified acoustic unit E (516.5 of ~1600 cm), interpreted as marine mud. The highly-stratified appearance of the unit may be attributed to structural lamination of the fine-grained sediment (clay-silt), representing multiple layers of the same sediment rather than different units.

Facies interpretation and depositional environment: The entire core was interpreted as massive clay-silt, which corroborates the interpretation of unit E as marine mud. The fine-grained sediments indicate a low-water velocity environment, suggesting that deposition occurred via settling out in deep water. The grain size at this site correlates with Hoskin et al.'s (1987) description of grain-size along a fjord, wherein finer-grained sediments accumulate in the sill-basin. The upper chronologic interval of the core (0–237 cm) has a mean sedimentation rate range ~65–66% greater than that of the lower interval. However, the magnitudes of both rates are so small (<1 mm/yr), it is uncertain if this difference is significant.

C.3.1.2 2014805-0002 TWC

Lithostratigraphy: Core sample 2014805-0002 TWC (Fig. C.23) measures at 107 cm long. The core sample was interpreted as capped by a surficial unit of silt (0–20 cm) and underlain by a massive clay-silt unit (20–107 cm).

Correlation with acoustic stratigraphy: The trigger-weight sample corresponds to the highly-stratified acoustic unit E (107 of ~1600 cm) on profile *p*, interpreted as marine mud. The fine-grained sediments (argillaceous?) observed in the core could explain the amount the amount of stratification observed in unit E as structural laminae.

Facies interpretation and depositional environment: The trigger-weight core contains a surficial silt unit not observed in the piston core. This could be due to the spatial separation between the two core samples, or compaction of the sediment in the upper segment of the piston corer. This additional core sample further strengthens the interpretation of acoustic unit E as marine mud that settled out of suspension in the low water-velocity environment of the fjord basin.

C.3.1.3 2015805-0007 PC

Lithostratigraphy: Core sample 2015805-0007 PC (Fig. C.24) measures at 489 cm long. The sample was interpreted as predominantly clay-silt, but with multiple inclusions. The upper portion of the core includes 4 silt lenses (1 cm each) spaced out between 34–131 cm, while the middle portion includes small clay units at 255–265 and 331–338 cm. The lower portion has inclusions of coarser sediments; sand lenses occur at 358–360 and 421–425 cm, and in between them is a sand unit (378–408 cm) with transitional lenses of silt-sand immediately above (374–378 cm) and below (408–409 cm). Below these coarse inclusions, a clay unit occurs at 440–460 cm.

Correlation with acoustic stratigraphy: From profile *r*, the core is observed to penetrate acoustic unit E (489 of ~500 cm) and its uppermost internal reflector (~200 cm below the seafloor), and estimated to contact the unit B contact line. Unit E appears to correspond to the fine-grained sediments observed, supporting the marine mud interpretation. The sand unit may represent the unit B contact line. However, the return to fine-grained sediment below 408 cm indicates that the local coarse sediments are relatively thin. This may corroborate the interpreted slope-failure deposit off of the western arm of the sill, which would also explain the overlying contact lines for unit B observed on profiles *p* and *r*.

Facies interpretation and depositional environment: The predominant clay-silt sediments corroborate the interpretation of unit E as marine muds. The sand unit possibly corresponds to the unit B contact line (near the base of the core), which is continuous with the west arm of the sill and thus is interpreted to be morainal in origin (Cowan, 2015). This suggests that the sand unit (378–408 cm) represents ice-contact sediments. However, the sand unit is not observed in core

2014805-0002 PC, which is located further up-fjord and penetrates deeper and older sediment. Thus, the sand unit cannot represent a readvance deposit, as the ground moraine glacial till of the Akpait glacier would have to be also present in core 2014805-0002 PC. Moreover, the sand unit is underlain by additional fine sediments. Thus, the sand unit is interpreted as a local low-frequency high-magnitude deposition event, such as a slope failure deposit. This is supported by the signs of a slope failure observed on the bathymetry (Fig. B.29). It is unlikely that the sand unit would have been deposited by the nearest stream, based on the distance involved (1 km), and the observed lack of sediment sources. Moreover, core 2014805-0002 PC is located nearer to the same stream mouth (0.7 km) yet lacks a sand unit.

Despite their proximity, the lithology of 2015805-0007 PC is considerably more heterogeneous than 2014805-0002 PC. The former is interpreted as predominantly clay-silt, but includes multiple inclusions of coarser and finer material, while the latter is interpreted as massive clay-silt. The identification of silt and clay lenses in the clay-silt dominant core 2015805-0007 PC may be attributable to a more attentive analysis, but the distinct sand deposits require another explanation. The contrast is best attributed to the spatial separation between the cores. Core 2014805-0002 PC targeted the fjord basin and penetrated a highly stratified area of even parallel reflectors, as observed on profile *p*. Meanwhile, core 2015805-0007 PC targeted the slope of the fjord basin, penetrating an area nearer the western arm of the sill and appearing to contact a sediment horizon (unit B, ice-contact) continuous with it, as observed on profiles *p* and *r*. The surficial units of the western sill-arm were interpreted as mixed sediment, potentially due to slope failures. Thus, the position of core 2015805-0007 PC may have resulted in its contacting slope-failure deposits from the western sill-arm.

C.3.1.4 2014805-0007 TWC

Lithostratigraphy: Core sample 2014805-0007 TWC (Fig. C.25) measures at 99 cm long. The sample was interpreted as a surface unit of silt (0–9 cm) underlain by clay (9–20 cm). From 20 cm downwards, the remainder of the core is interpreted as massive clay-silt with a sand lens at 38–39 cm. Mottling was observed throughout the clay and clay-silt units, as were two sub-angular dropstones.

Correlation with acoustic stratigraphy: The trigger-weight sample corresponds to acoustic unit E (99 of ~500 cm), interpreted as marine muds. However, the sample is too short to reach the internal reflector (~200 cm; profile *r*) in unit E, so in theory the reflector should not correspond to the sand lens. However, as previously noted, the estimations of acoustic unit thickness correlate imperfectly to the core lithologies.

Facies interpretation and depositional environment: Like the upper portion of the piston core, the trigger-weight core corroborates the interpretation of unit E as marine sediment. The trigger-weight core mostly corroborates the 1st meter of the piston core, as it is made of clay, clay-silt, and silt units. However, it contains a sand lens not identified on the piston core—it may have been obscured through compaction in the piston core, or simply be a result of spatial separation. This lens could be ice-rafted material, or a small slope-failure deposit, and seems likely to have been deposited after 1620–1860 cal BP based on comparison to the piston core. As previously noted, a stream mouth is located 1 km away, but lacks any well-developed sediment sources.

C.3.2 2014805-0003 PC (spillover deposit)

Lithostratigraphy: Core sample 2014805-0003 PC (Fig. C.26) measures 603 cm long. The sample was interpreted as consisting of a surficial lens of silt-sand (0–11 cm), and then fining downwards to a silt unit (11–52 cm), and then a clay-silt unit (52–139 cm) interrupted by a sand lens (78–85 cm). Below is a thick silt-sand unit (139–290 cm) with multiple sand lenses. At 290 cm, the silt-sand unit fines downwards to silt unit (290–325 cm), and then an extensive clay-silt unit (325–603 cm) interrupted by multiple lenses of coarser sediment, ranging from silt to sand.

Correlation with acoustic stratigraphy: Profiles *p*, *q*, and *s* pass adjacent to station 2014805-0003 on either side rather than directly intersect it. Nevertheless, the core can still be identified as corresponding to the spillover deposit acoustic unit, and is estimated as penetrating the strong, near-surface reflectors and contacting the weaker underlying reflectors of the spillover deposit. The uppermost internal reflector (~200 cm below the seafloor) may correspond to the thick silt-sand unit (139–290 cm).

If the silt-sand unit was deposited by wave-action reworking of the spillover deposit as expected, then the transition away from it can suggest a RSL transgression that brought the wave base out of contact with the sill. If this is true, then the date from immediately below the surface of the unit (~1040–1260 cal BP) is the maximum constraint for this transgression. However, this is significantly more recent than either of the glacial events (Younger Dryas at 12.9–11.7 cal ka BP and Cockburn Substage at 9.5–8.5 cal ka BP) that Cowan (2015) hypothesized the delta-building postglacial lowstand to be associated with. Thus, the interpretation of the silt-sand unit of the spillover deposit as fjord-mouth sill sediment reworked by wave action, combined with the calibrated radiocarbon date of ~1040–1260 cal BP, suggests that either multiple lowstands have occurred along the coast of Cumberland Peninsula, or that only one lowstand has occurred and has been recent.

Facies interpretation and depositional environment: The coarse sediments are more prominent at this site than both stations 2014805-0002 and 2015805-0007. Although clay-silt constitutes the majority of the core, bands of coarser sediment (silt, silt-sand, and sand) are frequent throughout the core and a large silt-sand unit is prominent. The changes in grain-size are likely related to changes in the depositional environment. The fine-grain material likely represents marine muds deposited in a low-energy environment, as was interpreted for the other cores. Given the station's situation in the spillover deposit and proximity to the fjord-mouth sill, the coarser sediments were likely reworked from the sill platform. Reworking of a submerged sill via wave action would require that the RSL be low enough that the wave base could contact the sill surface. (As a whole, the silt-sand unit indicates that the local environment favoured coarse-grain sedimentation for over 500 years, which suggests that a RSL lowstand occurred—the sand lenses suggest periodic moments of intensified reworking, which in turn suggests that either RSL fluctuations occurred during said lowstand, and or low-frequency high-magnitude storm events.

C.4 Sunneshine Fiord (previous research)

The 1982 SAFE research cruise collected core samples at two stations within Sunneshine Fiord: HU82-SU1 and -SU5. Lehigh gravity core HU82-SU1 G was collected from the inner fjord, while piston and gravity cores HU82-SU5 PC and G were collected nearer to the fjord mouth. According to Andrews et al. (1996), core HU82-SU5 PC bypassed sampling the upper 1.0 m of the seabed, an omission which was addressed by stacking the SU5 G core on top and adding 1.0 m to all SU5 PC core depths. Research cruise HU-82-031 has since been relabelled as 82031, while core samples HU82-SU1 G, HU82-SU5 G, and HU82-SU5 PC have been relabelled as 82031-6213, and 82031-6216, and 82031-6221, respectively. However, the older names will be used throughout this chapter for the sake of clarity.

C.4.1 HU82-SU1 G

Lithostratigraphy: Core sample HU82-SU1 G (no figure) was described by Hein and Longstaffe (1984) as 2.4 m long and primarily composed of clay-silt, showing bioturbation and mottling along its length. Hein and Longstaffe also describe additional parameters not detailed in this appendix (shear strength, sedimentology, geotechnics, and mineralogy).

Correlation with acoustic stratigraphy: The SU1 coring site is not covered by the Sunneshine acoustic profile, but it reasonable to extrapolate that the core represents the surficial acoustic unit (Unit 1 or III; Andrews et al., 1994; 1996), which has been associated with acoustic unit E described in the current study.

Facies interpretation and depositional environment: The clay-silt unit described by Hein and Longstaffe (1984) could reasonably be interpreted as marine mud.

C.4.2 HU82-SU5 PC & G

Lithostratigraphy: Core sample HU82-SU5 PC (Fig. C.27) was initially described as 769 cm long by Cole and Blakeney (1983), but was later found to be displaced 1.0 m below the seafloor (Andrews et al., 1996; Manley & Jennings, 1996). Therefore, the core length has been updated to 869 cm, with the top 100 cm undescribed – Andrews et al. (1996) presented SU5 G as a substitute for the missing 1.0 m, but did not describe its lithology. Based on the Cole and Blakeney (1983) description, the SU5 lithology can be divided into upper and lower units at 495 cm. The upper unit (0 to 495 cm) is predominantly clay-silt, interbedded with multiple lenses of either clay or silt. The lower unit (495 to 869 cm) is predominantly clay interbedded with multiple clustered lenses of either silt-sand or sand and one instance of gravel, concentrated in between 534 to 691 cm. Bivalve shells and scattered droptstone pebbles have been reported by Andrews et al. (1985; 1994; 1996). Additionally, Andrews et al. (1996) divided core SU5 PC into three environmental facies: zone I (0 to ~303 cm), zone II (~303 to 740 cm), and zone III (740 to 869 cm). However, these environmental facies appear to be defined based on total carbonate %, and the percentages of dolomite and calcite silt and clay, rather than the total grain-size composition.

Correlation with acoustic stratigraphy: Core SU5 PC appears to penetrate the upper two acoustic units (Units E and C, associated with Units III and II), and make contact with the third (Unit B, associated with Quaternary sediment) (Fig. 3.6B) (Andrews et al., 1996). The upper and lower lithologic units described above may correspond to acoustic units E and C. However, one would expect the acoustic characters to be reversed—the coarser upper zone would be expected to appear acoustically stronger than the finer lower zone. This may be explained by the clay unit having been compacted and thus made denser than the overlying clay-silt unit. This is supported by wet and dry volume density measurements of SU5 PC, which indicate that the lower zone is denser than the upper zone (Andrews et al., 1994).

C.5 Future Research

Features resembling uncollected shell fragments can be observed in some of the radiography and photography for core 2015805-0006 PC at depths of 70, 172, and 210 cm.

C.6 References

Andrews, J.T., Osterman, L.E., Jennings, A.E., Syvitski, J.P.M., Miller, G.H., & Weiner, N. (1996). Abrupt changes in marine conditions, Sunneshine Fiord, eastern Baffin Island, NWT during the last deglacial transition: Younger Dryas and H-0 events. *Late Quaternary Palaeoceanography of the North Atlantic Margins*, Geological Society Special Publication 111: 11-27.

Google. (2021). *Google earth pro* (Version 7.3.3). https://www.google.com/earth/

Natural Resources Canada. (2017). *Expedition 82031*. [Data table]. Retrieved from http://ed.gdr.nrcan.gc.ca/cruise_detail_e.php.

Table C.1: Summary table of all 18 sediment cores included in the study.

Fjord & Position		Core	Latitude (DD)	Longitude (DD)	Core type	Length (cm)	Water depth (m)	C^{14} dates
Boas Fiord	Fjord-head delta	2014NULIAJUK-0001 GC	66.694087	-62.827428	Gravity	94	31	-
		2014NULIAJUK-0002 GC	66.67964	-62.854468	Gravity	76	29	-
		2014NULIAJUK-0003 GC	66.666221	-62.860505	Gravity	60	28	-
		2014NULIAJUK-0004 GC	66.694098	-62.827412	Gravity	135	31	Yes
	Side-entry delta	2014NULIAJUK-0005 GC	66.776107	-62.754834	Gravity	12	36	-
		2014NULIAJUK-0006 GC	66.77634	-62.754021	Gravity	17.5	36	-
		2014NULIAJUK-0007 GC	66.776629	-62.741165	Gravity	20	25	-
Durban Harbour	Prodelta	2014805-0001 PC	66.95076	-62.278863	Piston	261.5	80	-
		2014805-0006 PC	66.950367	-62.28815	Piston	244	95	Yes
		2014805-0006 TWC	66.950367	-62.28815	Trigger-weight	n/a	95	-
	Delta slope	2015805-0005 PC	66.94915	-62.277267	Piston	~10	71	-
Akpait Fiord	Fjord basin	2014805-0002 PC	66.889016	-61.824016	Piston	517	142	Yes
		2014805-0002 TWC	66.889016	-61.824016	Trigger-weight	107	142	-
		2014805-0007 PC	66.8865	-61.809333	Piston	489	147	Yes
		2014805-0007 TWC	66.8865	-61.809333	Trigger-weight	99	147	-
	Spillover deposit	2014805-0003 PC	66.882885	-61.743486	Piston	603	112	Yes
Sunneshine Fiord	Inner fjord	HU82-SU1 G	~ 66.630	~ -61.839	Gravity	240	215*	-
	Outer fjord	HU82-SU5 G	~ 66.581	~ -61.670	Gravity	232*	146	Yes
		HU82-SU5 PC	~ 66.581	~ -61.670	Piston	769**	146	Yes

*From Natural Resources Canada (2017).
** Missing the top 1 m of sediment (Andrews et al., 1996)

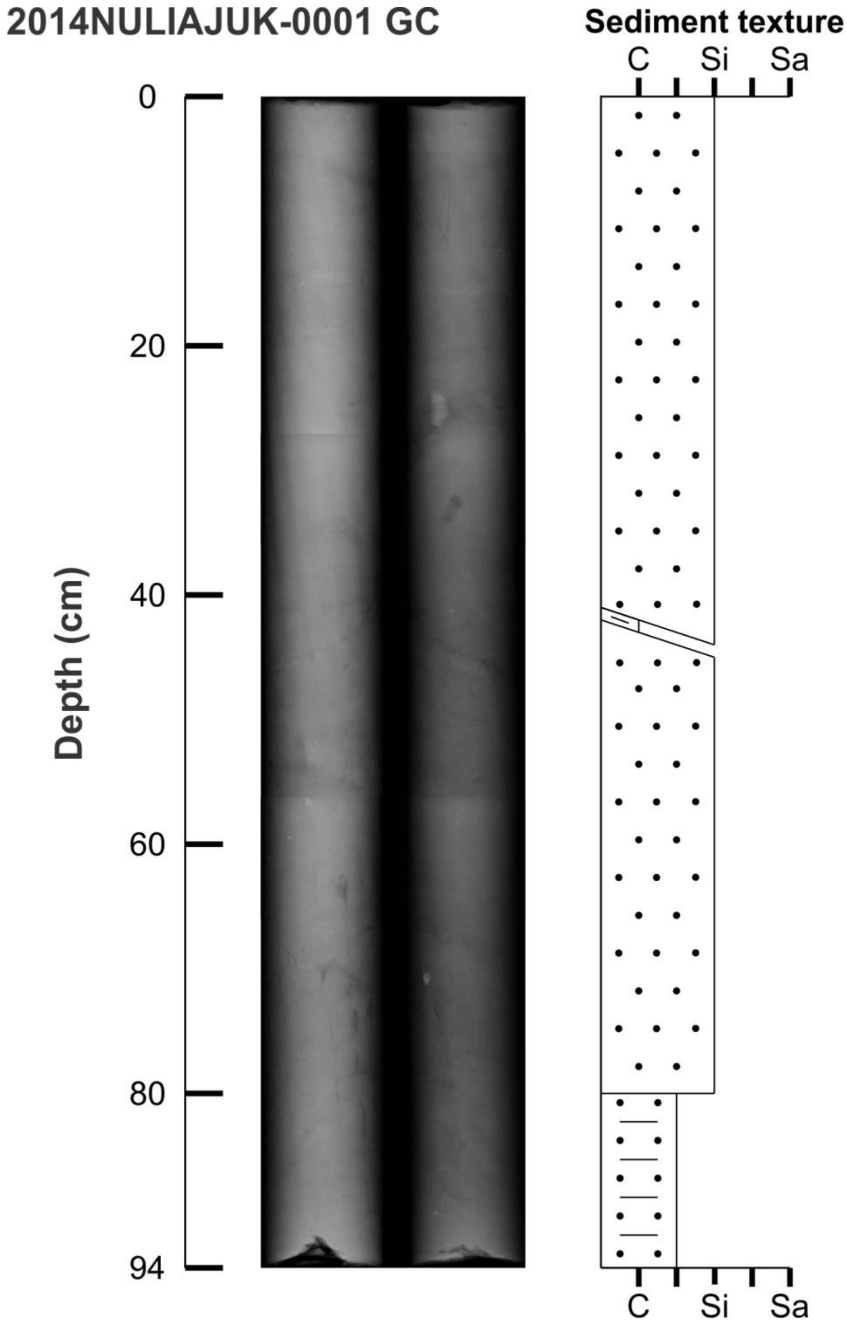

Figure C.1: Gravity core 2014NULIAJUK-0001 GC, collected from the eastern terrace of the submerged fjord-head delta in Boas Fiord.

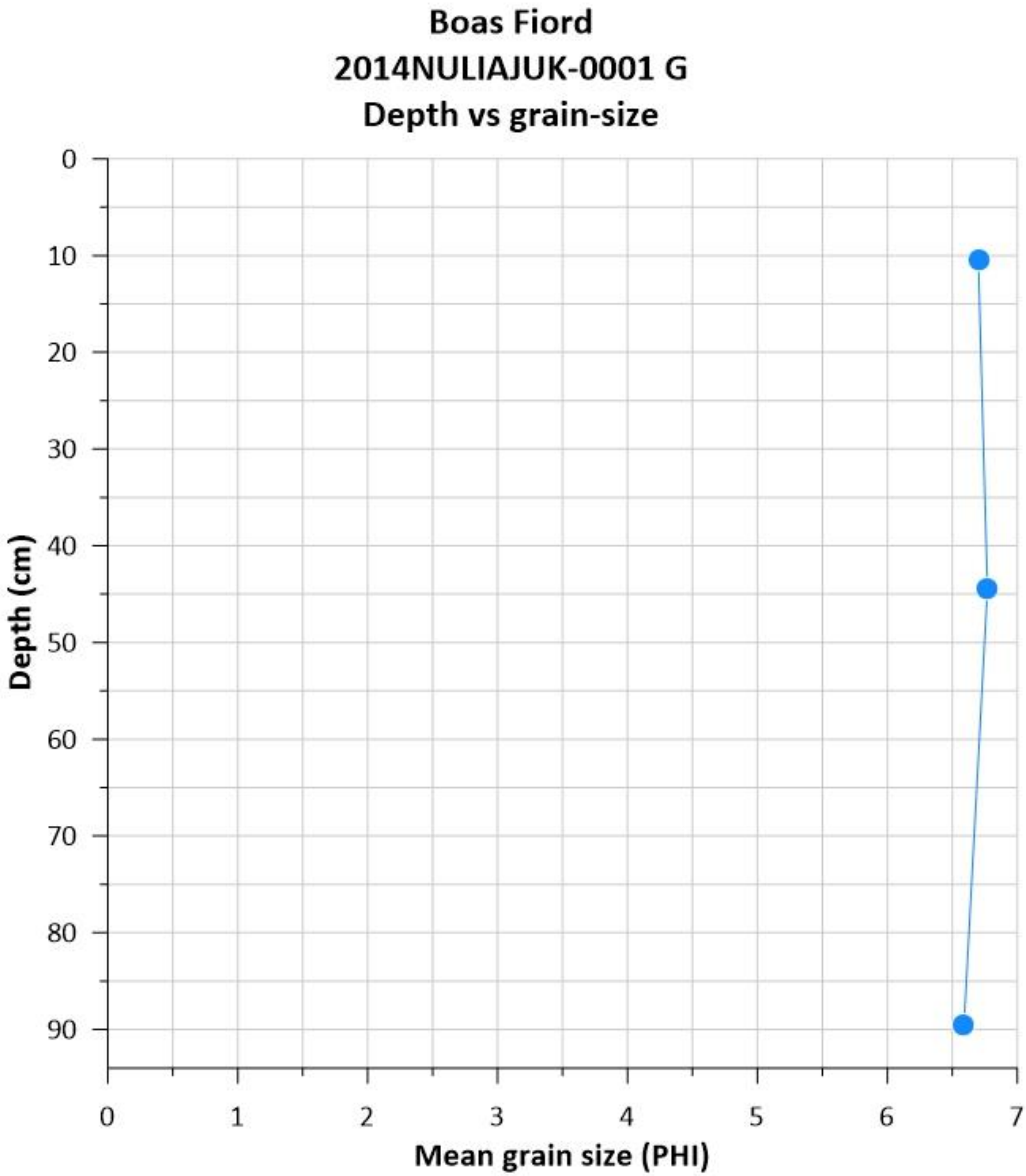

Figure C.2: Mean grain-size plot for 2014NULIAJUK-0001 GC, collected from the eastern terrace of the submerged fjord-head delta in Boas Fiord.

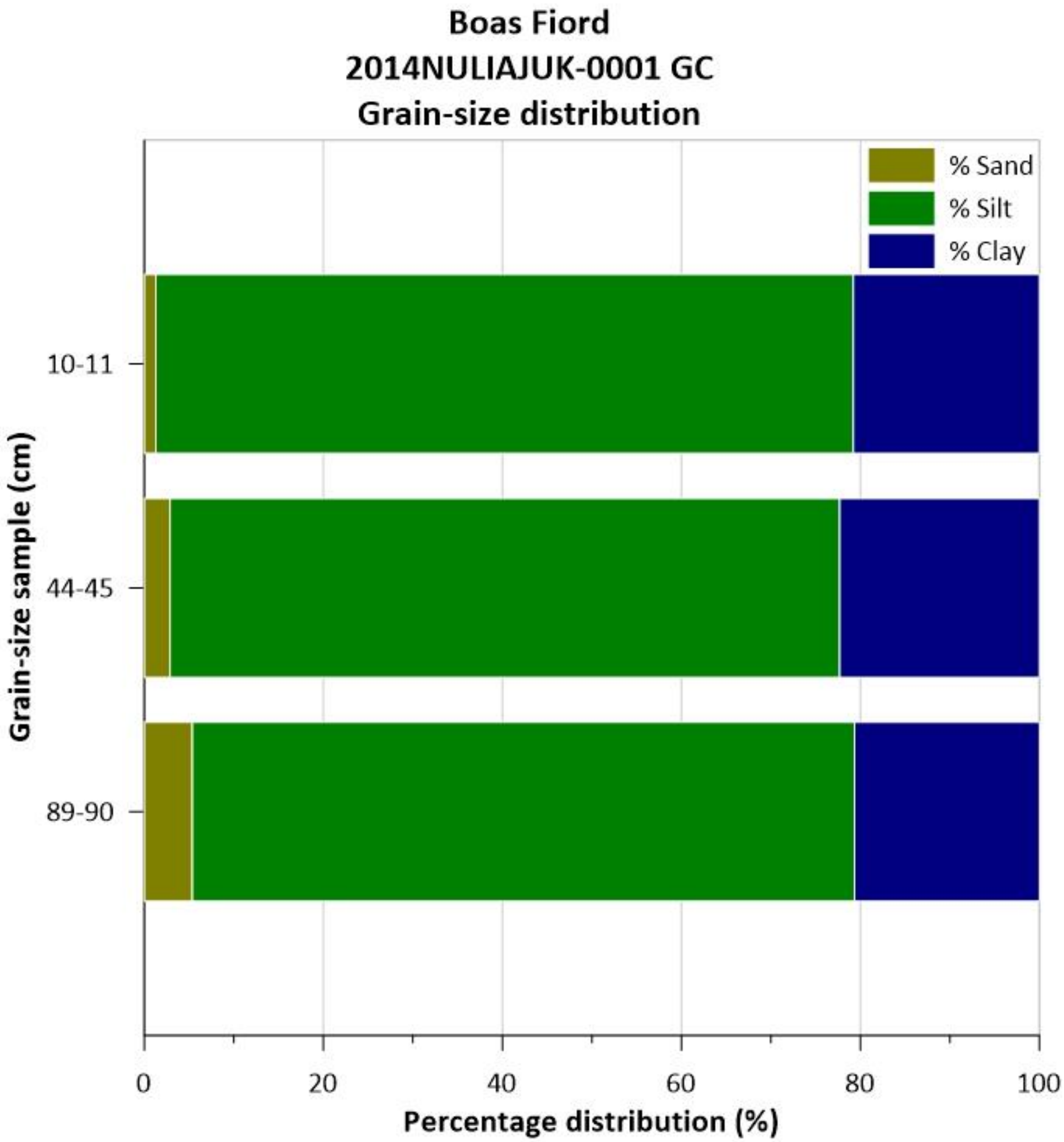

Figure C.3: Grain-size distribution for 2014NULIAJUK-0001 GC, collected from the eastern terrace of the submerged fjord-head delta in Boas Fiord.

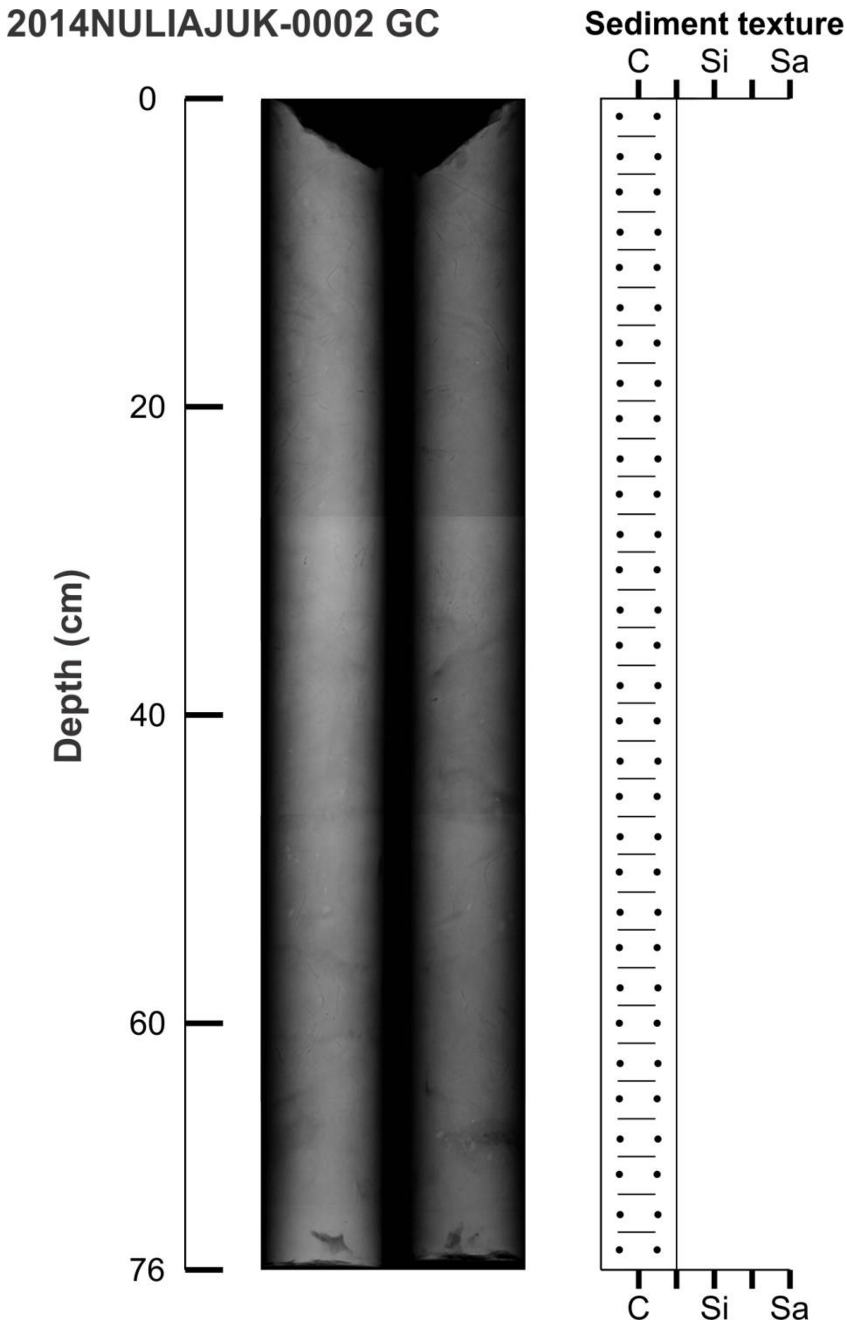

Figure C.4: Gravity core 2014NULIAJUK-0002 GC, collected from the delta plain of the submerged fjord-head delta in Boas Fiord.

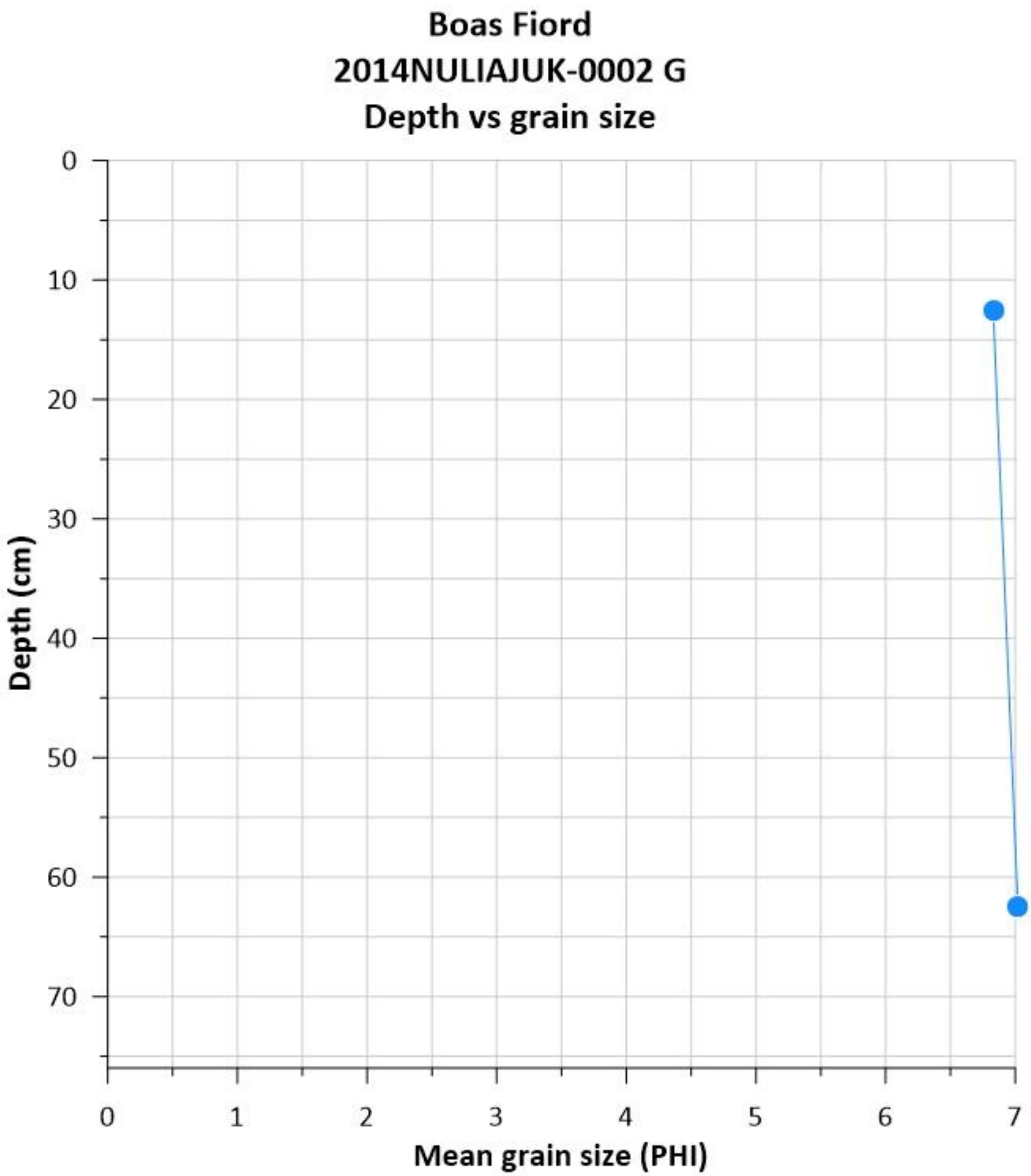

Figure C.5: Mean grain-size plot for 2014NULIAJUK-0002 GC, collected from the delta plain of the submerged fjord-head delta in Boas Fiord.

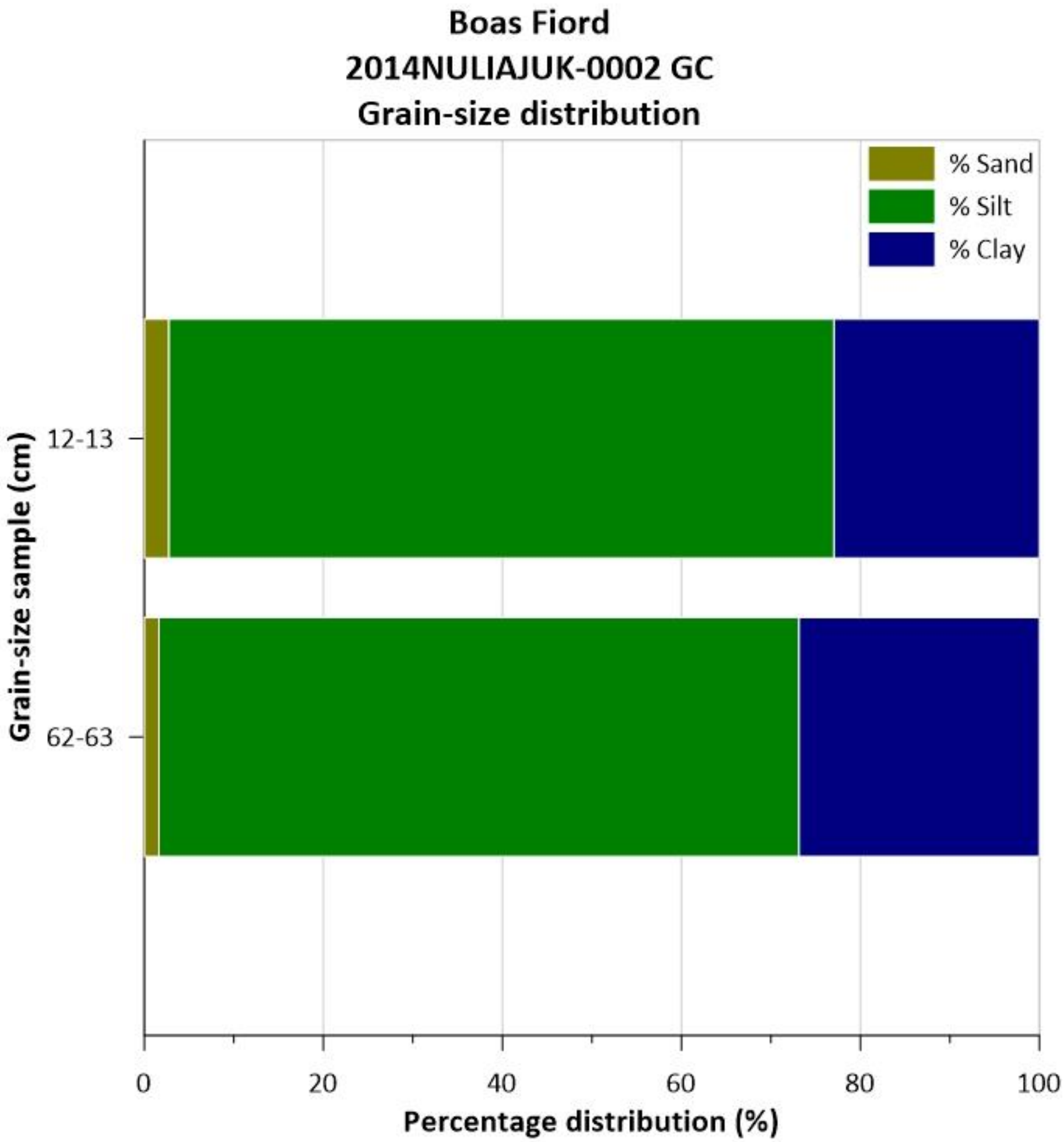

Figure C.6: Grain-size distribution for 2014NULIAJUK-0002 GC, collected from the delta plain of the submerged fjord-head delta in Boas Fiord.

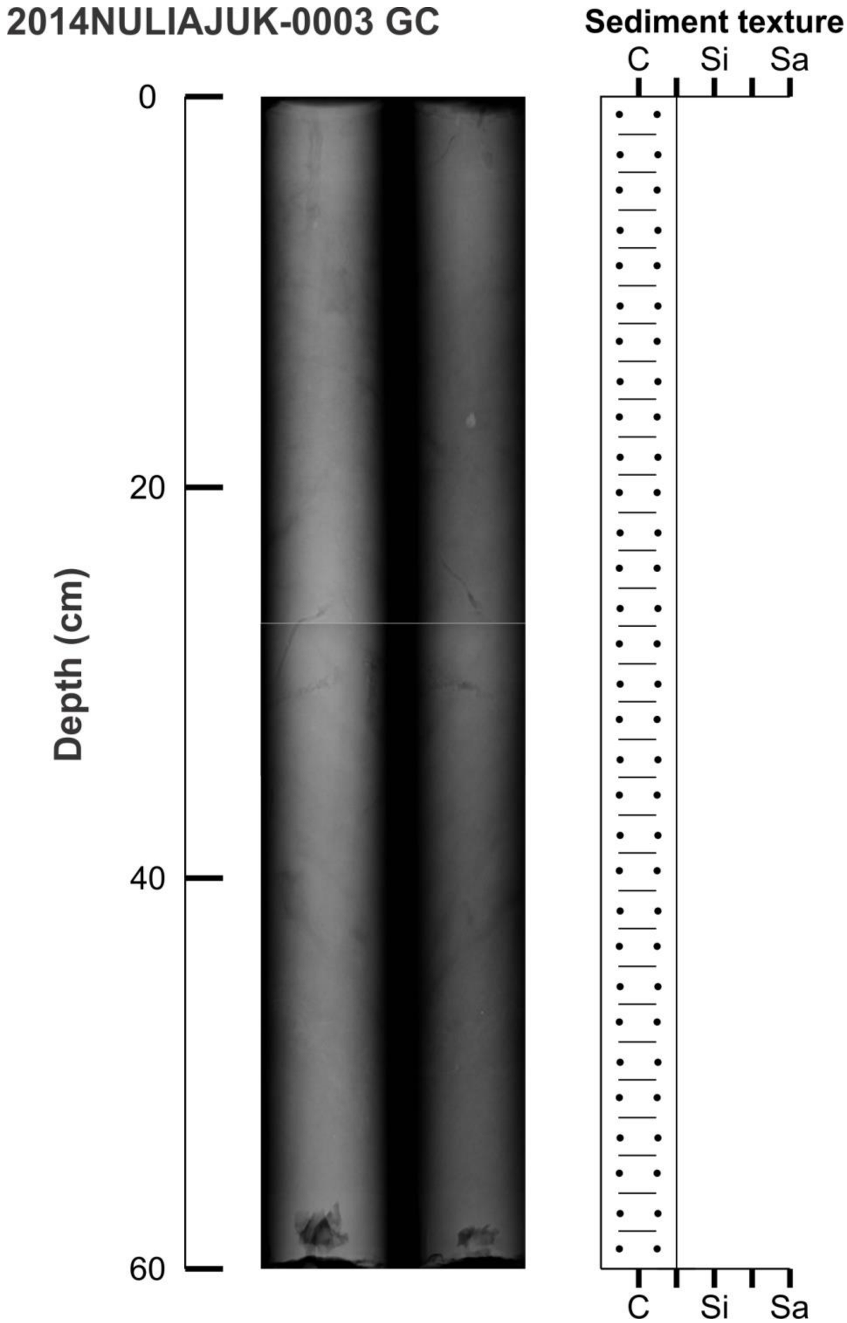

Figure C.7: Gravity core 2014NULIAJUK-0003 GC, collected from the delta plain of the submerged fjord-head delta in Boas Fiord.

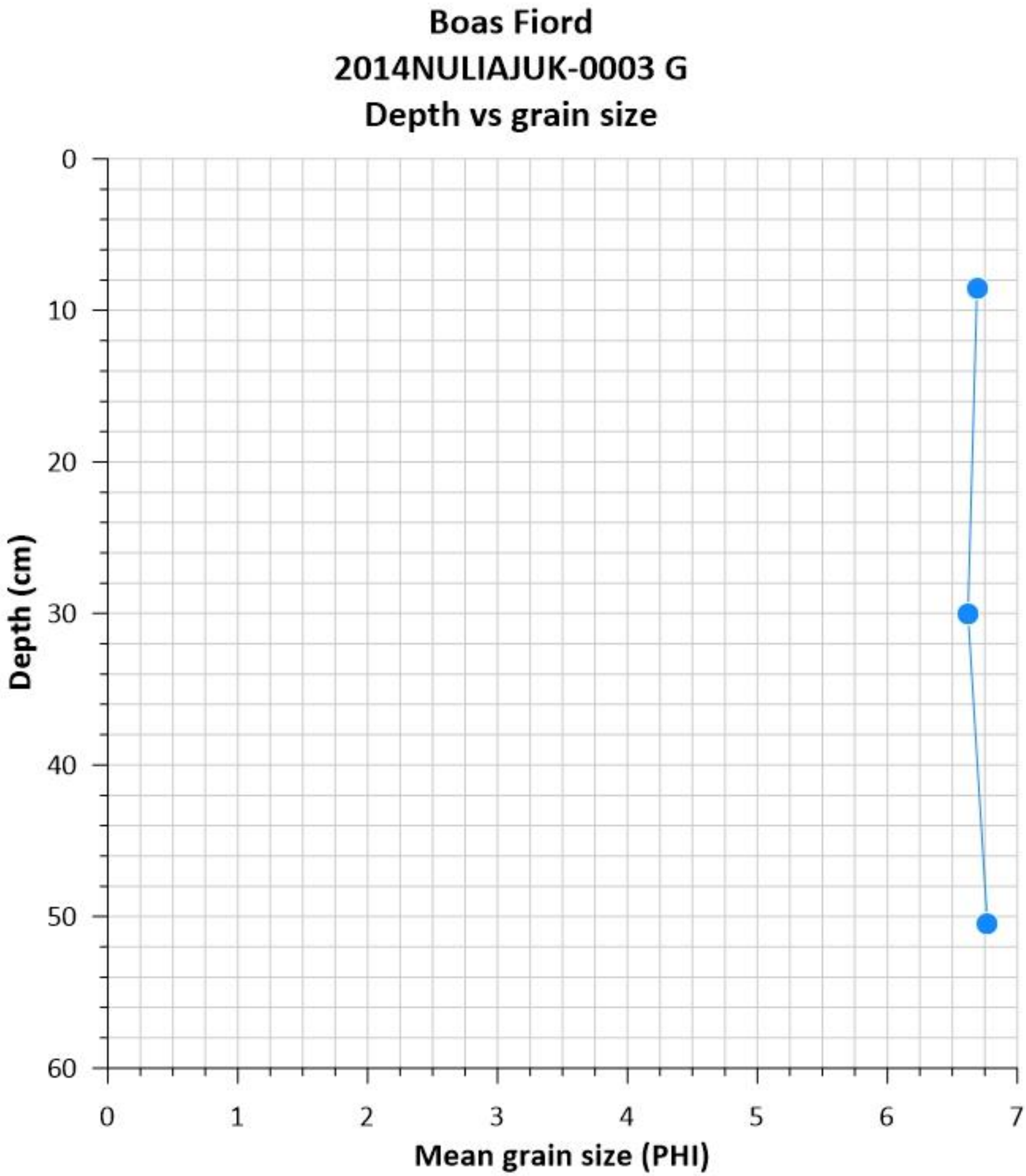

Figure C.8: Mean grain-size plot for 2014NULIAJUK-0003 GC, collected from the delta plain of the submerged fjord-head delta in Boas Fiord.

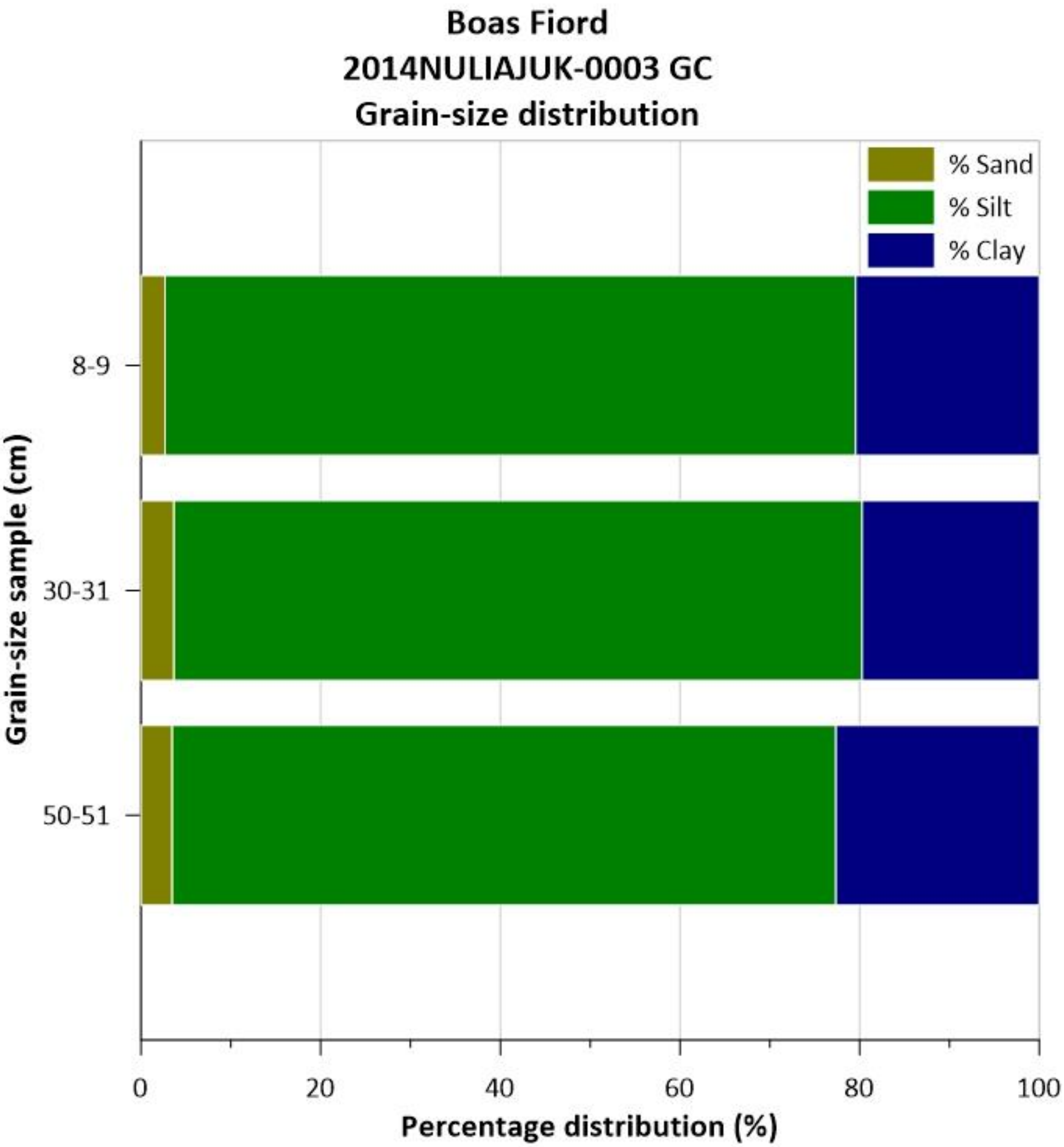

Figure C.9: Grain-size distribution for 2014NULIAJUK-0003 GC, collected from the delta plain of the submerged fjord-head delta in Boas Fiord.

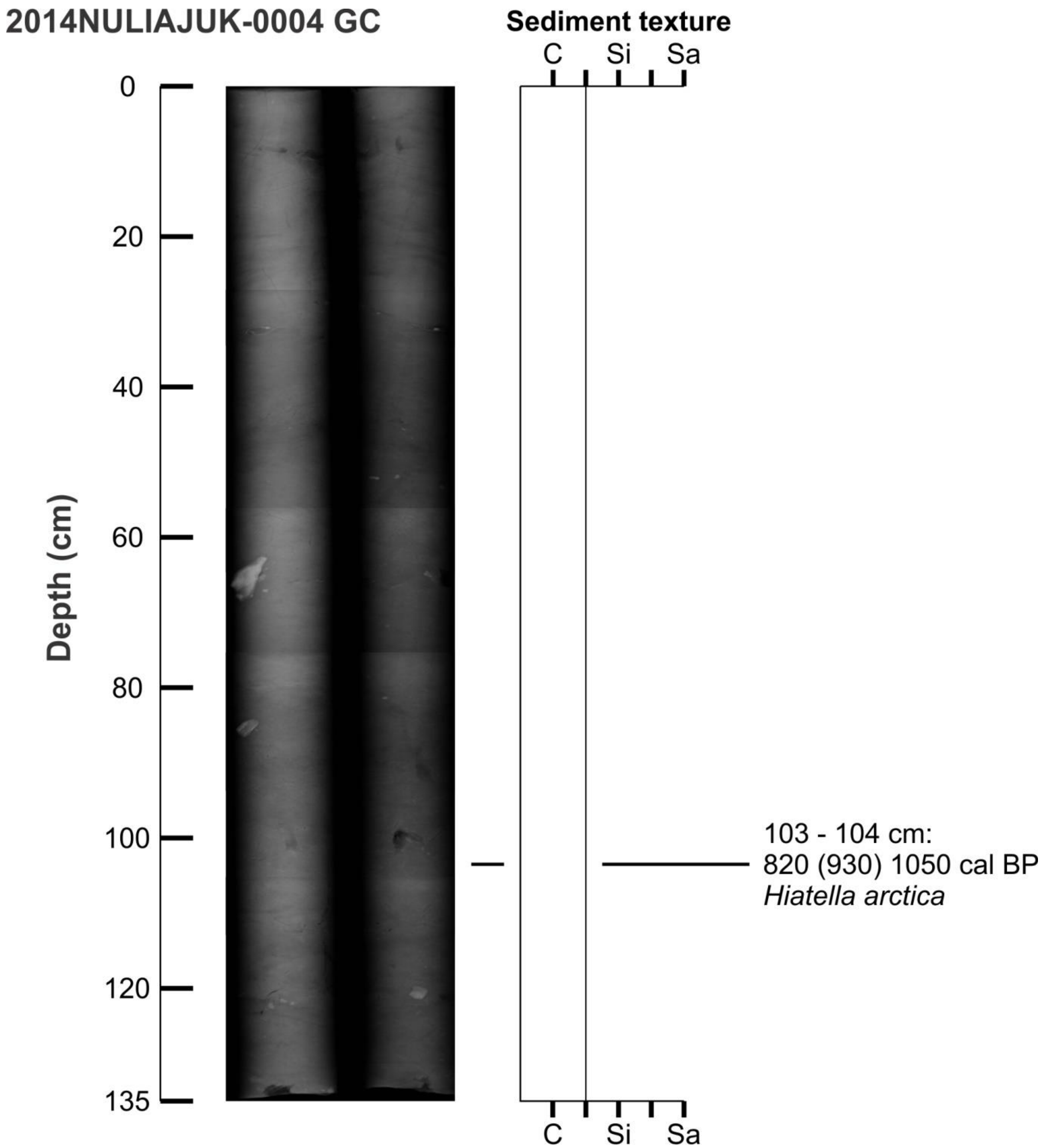

Figure C.10: Litho log of 2014NULIAJUK-0004 GC, illustrating the massive clay-silt composition and the positioning of sample 103–104 cm with its associated calibrated radiocarbon date and mean sedimentation rate.

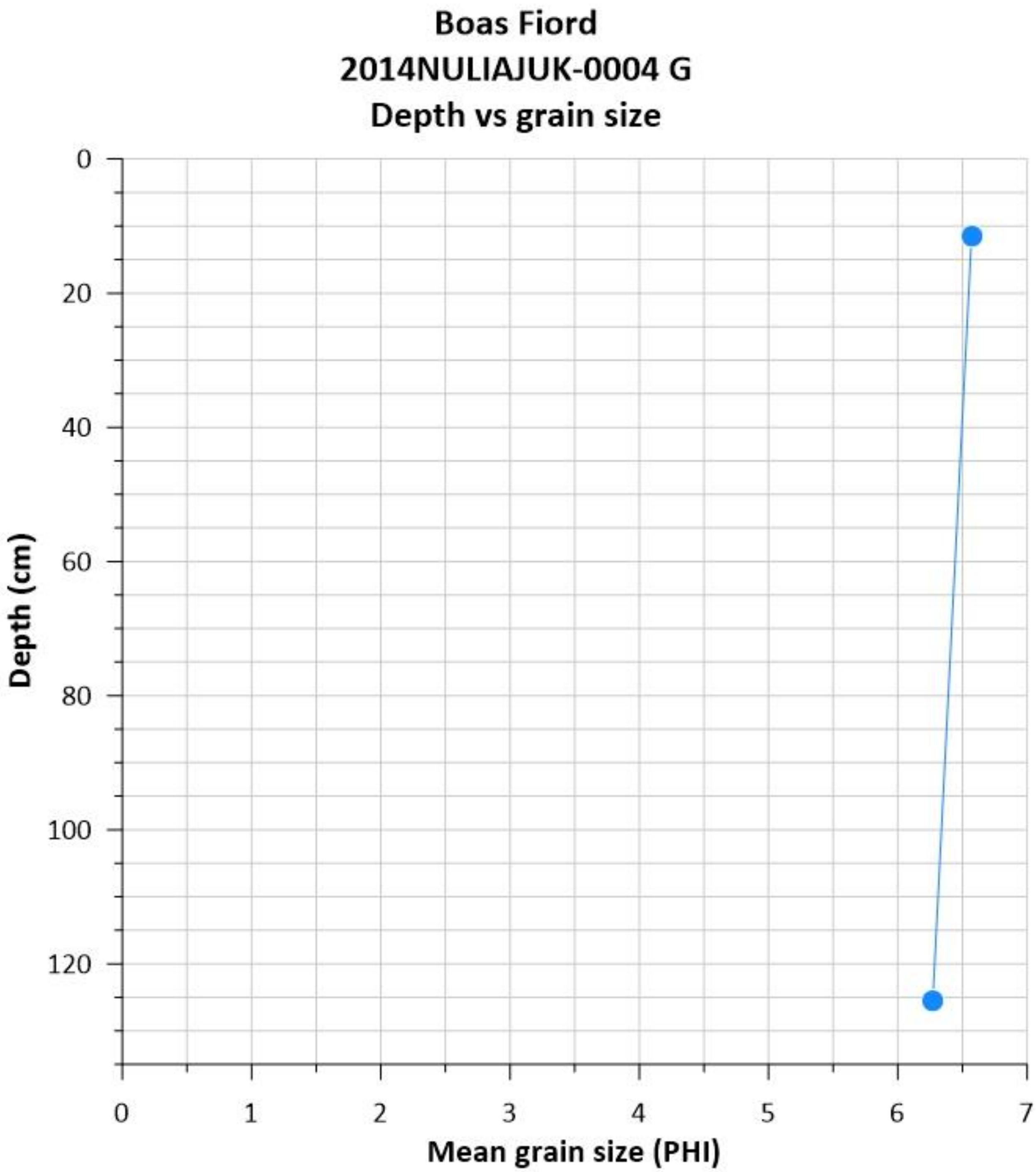

Figure C.11: Mean grain-size plot for core 2014NULIAJUK-0004 GC, collected from the eastern terrace of the submerged fjord-head delta in Boas Fiord.

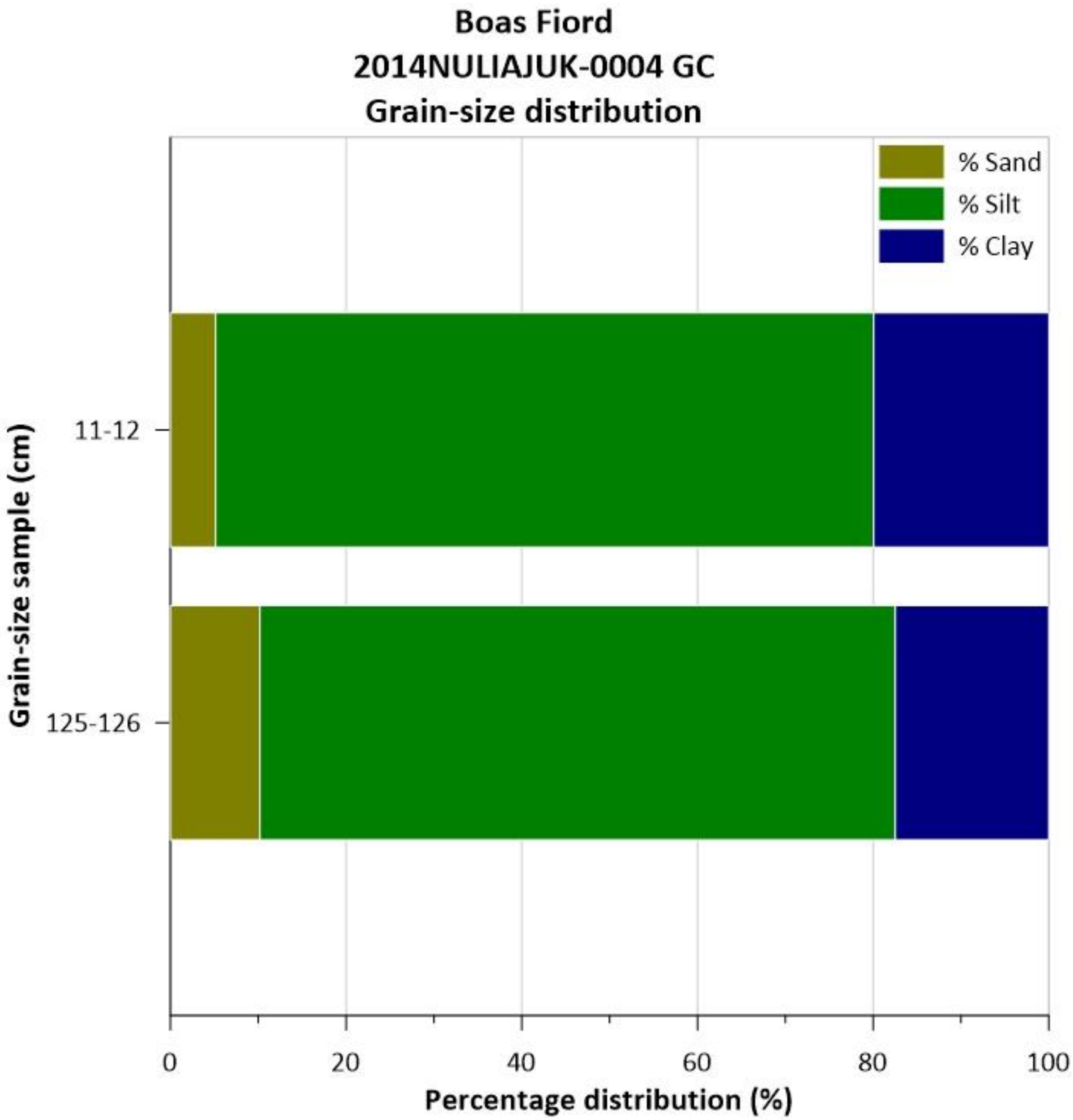

Figure C.12: Grain-size distribution for 2014NULIAJUK-0004 GC, collected from the delta plain of the submerged fjord-head delta in Boas Fiord.

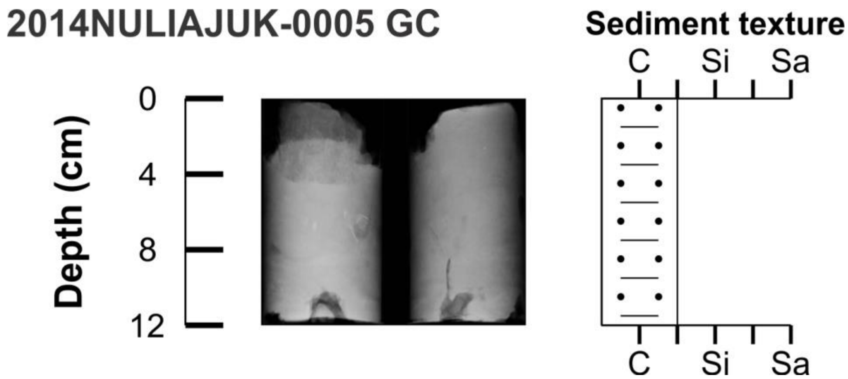

Figure C.13: Gravity core sample 2014NULIAJUK-0005 GC, collected from near the edge of the primary terrace of the submerged side-entry delta in Boas Fiord.

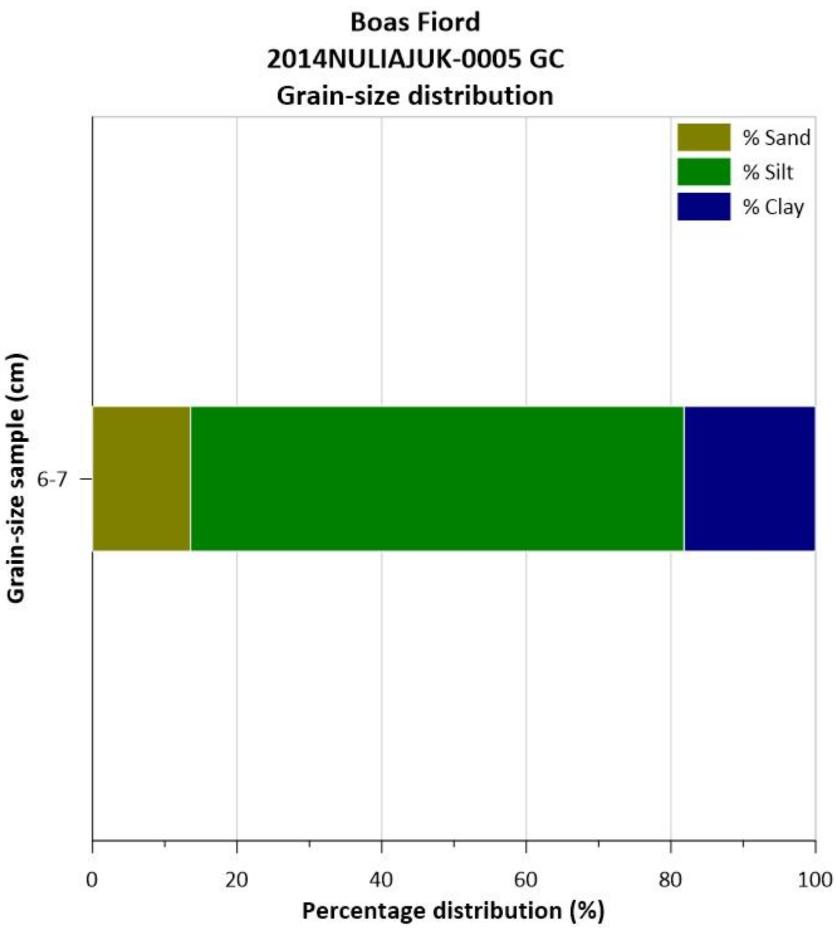

Figure C.14: Grain-size distribution for 2014NULIAJUK-0004 GC, collected from the delta plain of the submerged fjord-head delta in Boas Fiord.

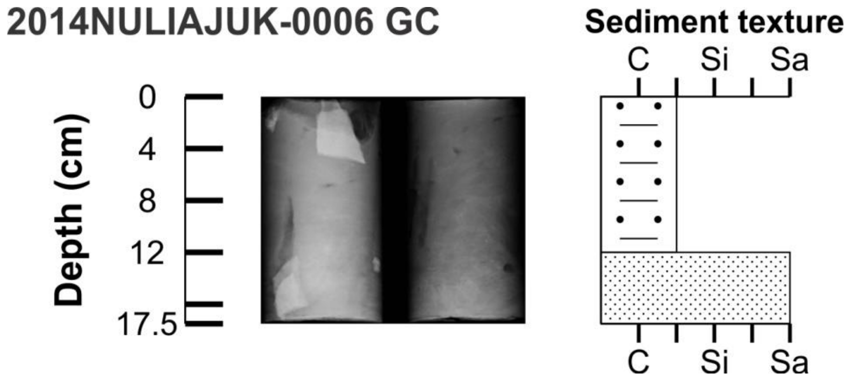

Figure C.15: Gravity core sample 2014NULIAJUK-0006 GC, collected from near the edge of the primary terrace of the submerged side-entry delta in Boas Fiord.

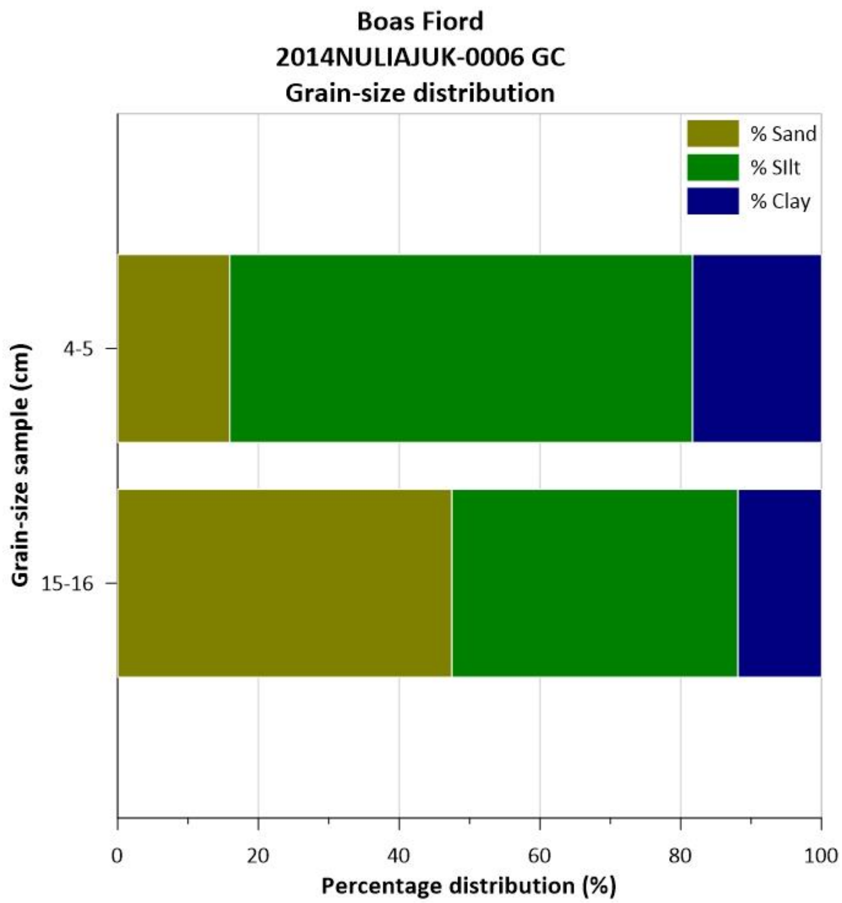

Figure C.16: Grain-size distribution for 2014NULIAJUK-0004 GC, collected from the delta plain of the submerged fjord-head delta in Boas Fiord.

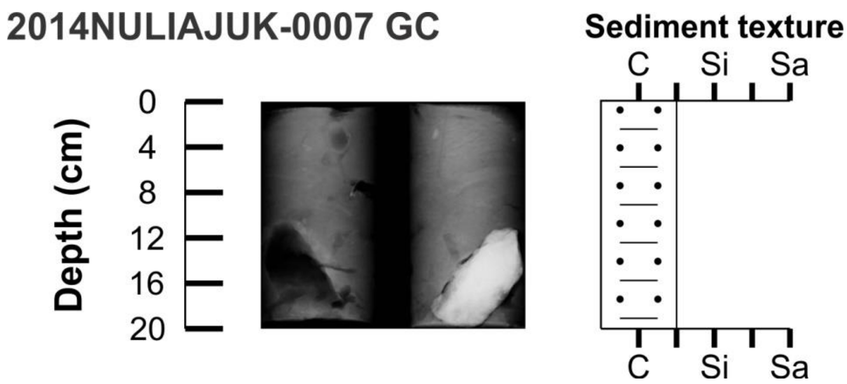

Figure C.17: Gravity core sample 2014NULIAJUK-0007 GC, collected from the secondary terrace of the submerged side-entry delta in Boas Fiord.

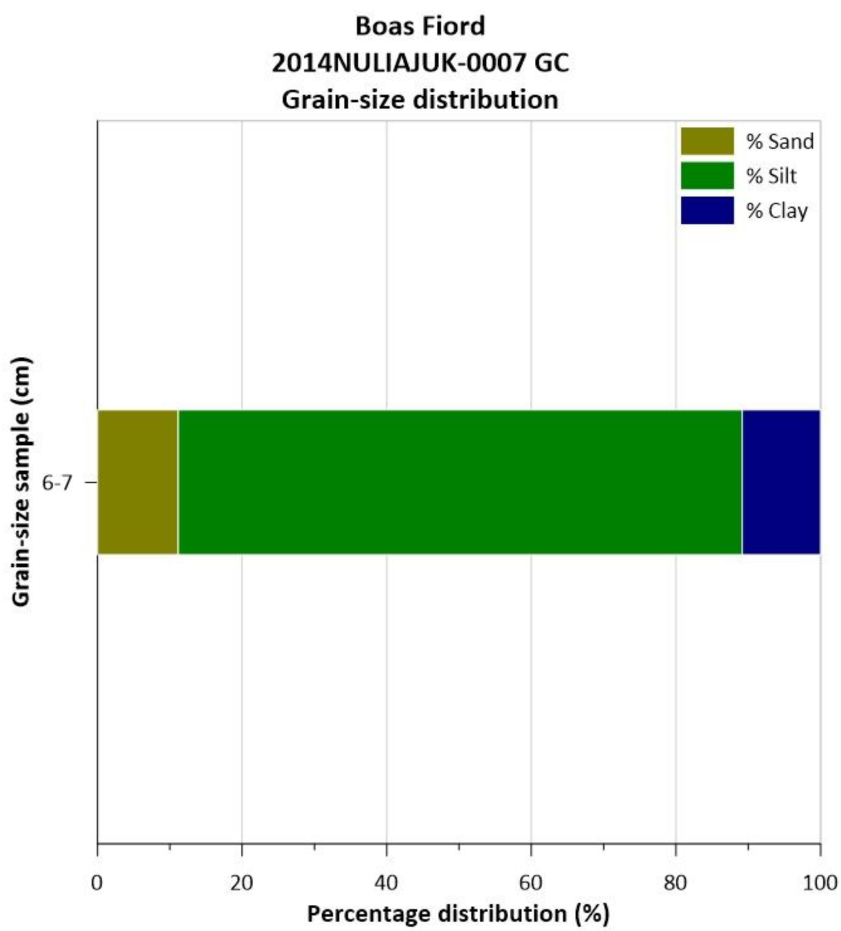

Figure C.18: Grain-size distribution for 2014NULIAJUK-0004 GC, collected from the delta plain of the submerged fjord-head delta in Boas Fiord.

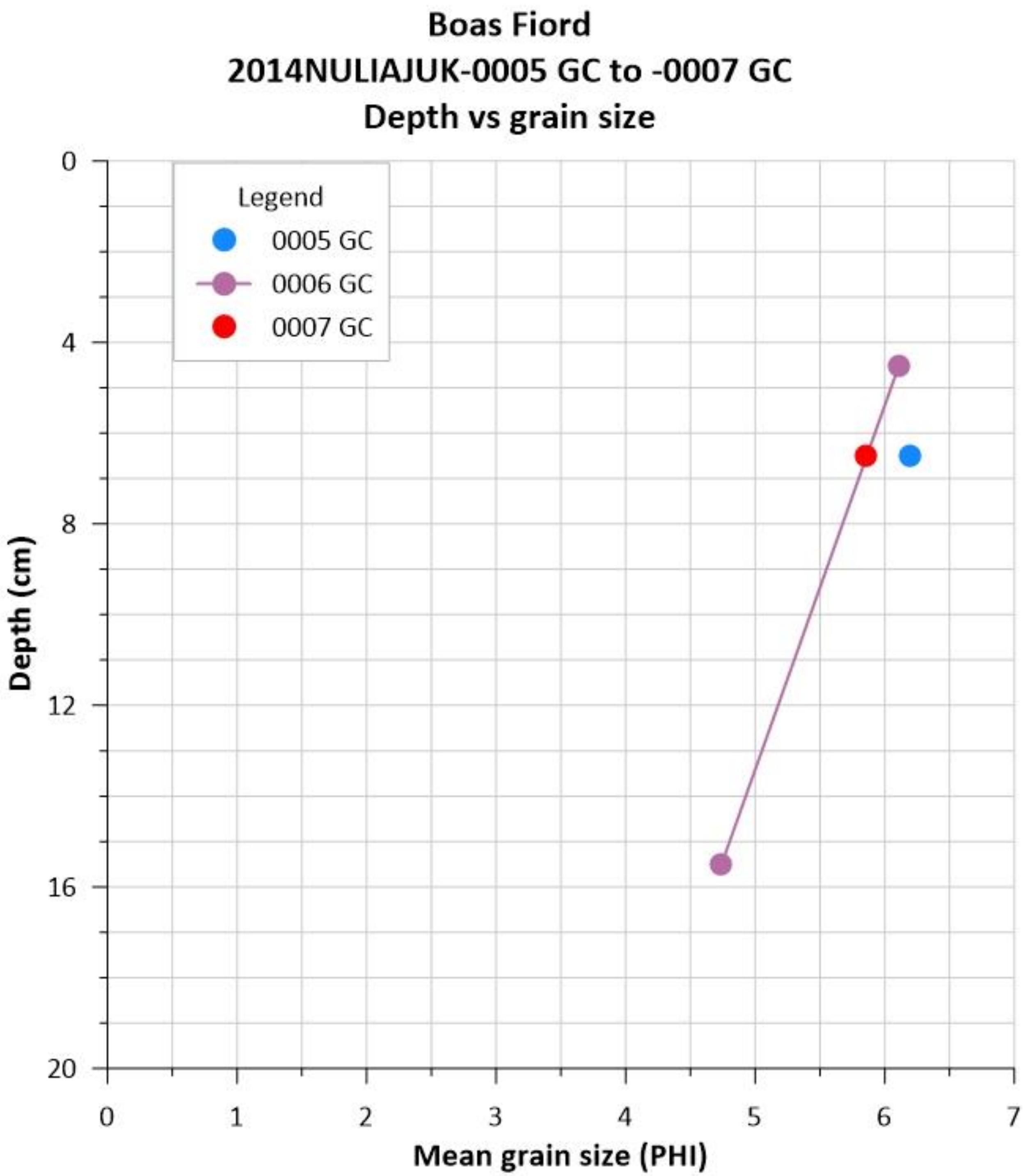

Figure C.19: Mean grain-size plot for cores 2014805-0005 to -0007 GC, collected from the submerged side-entry delta in Boas Fiord.

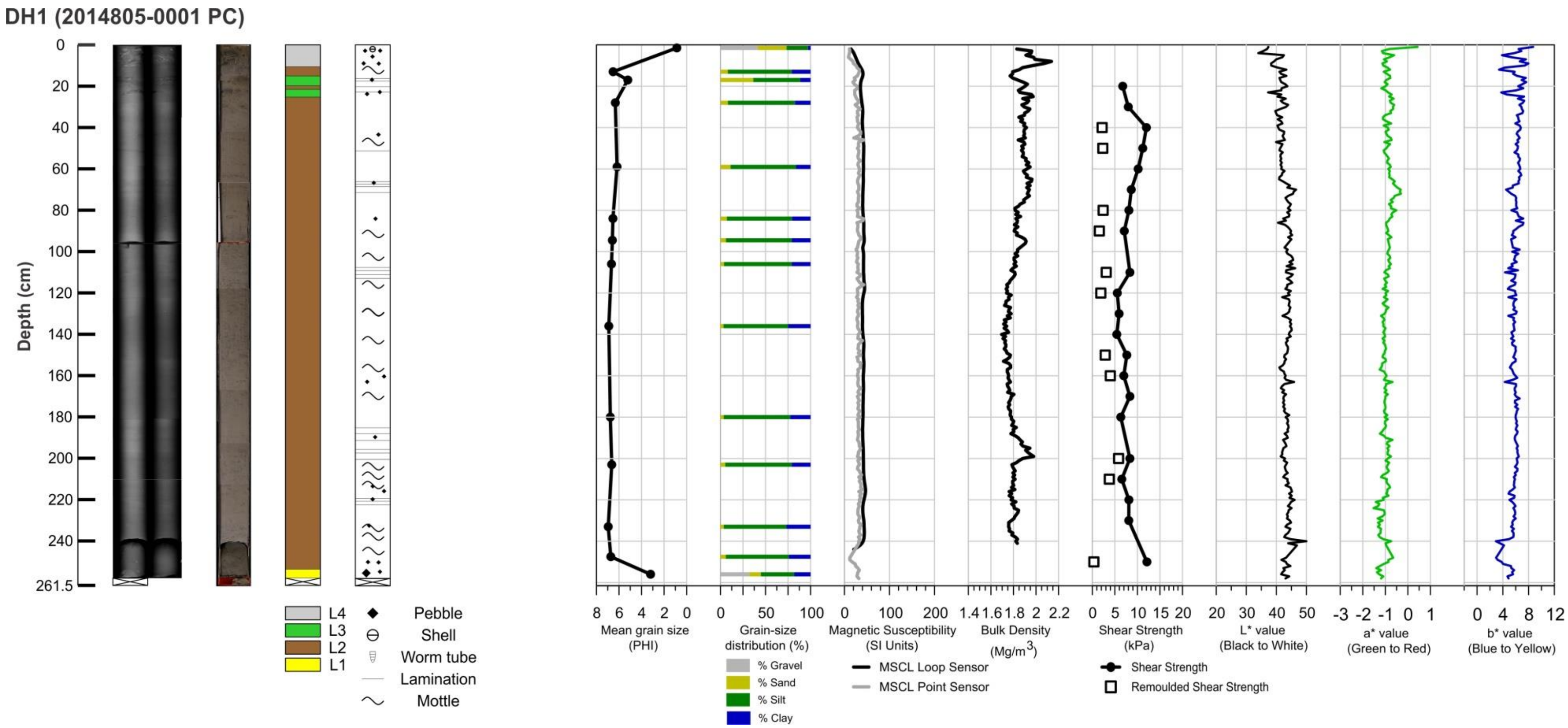

Figure C.20: Core DH1 (2014805-0001 PC), collected from the prodelta area of Durban Harbour.

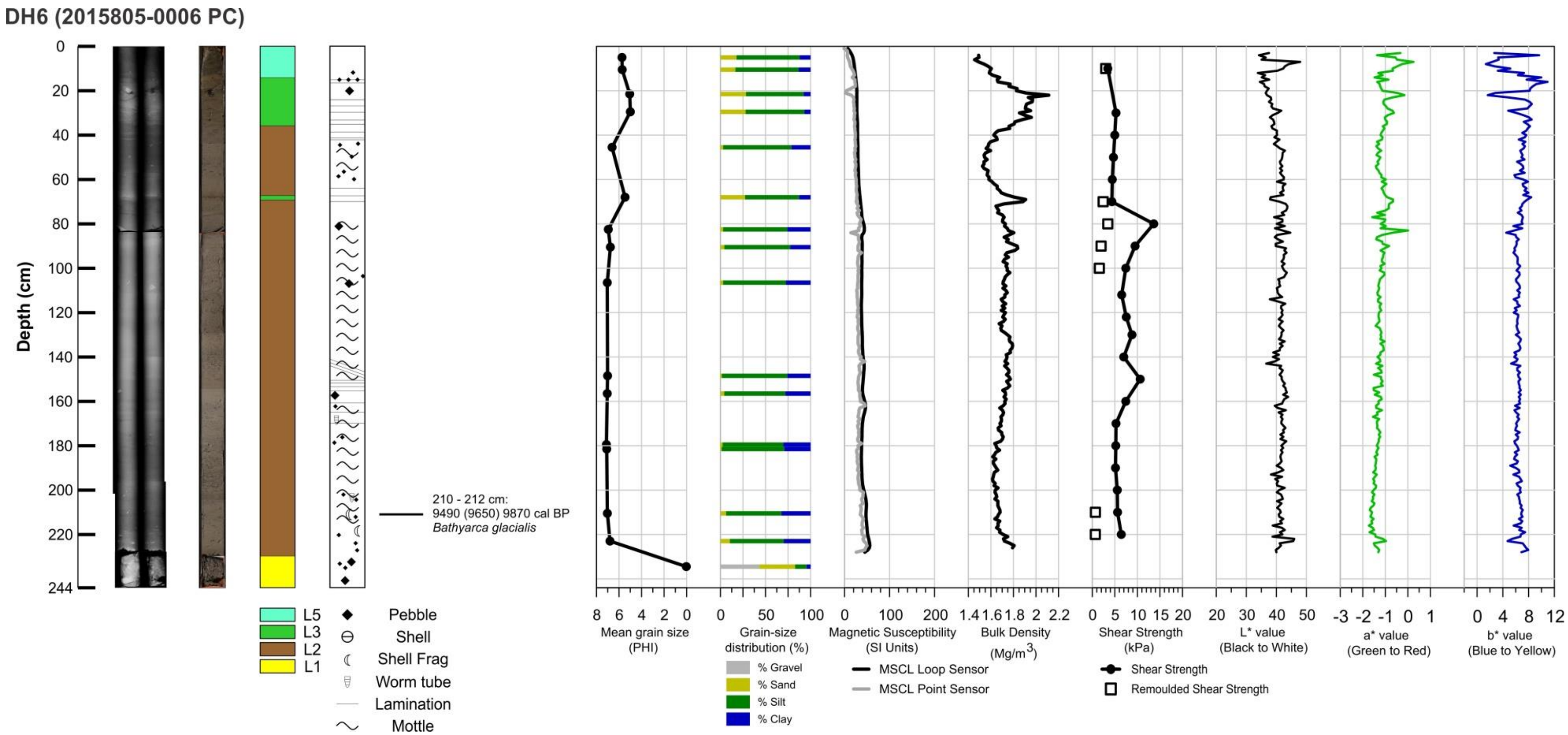

Figure C.21: Core DH6 (2015805-0006 PC), collected from the prodelta area of Durban Harbour.

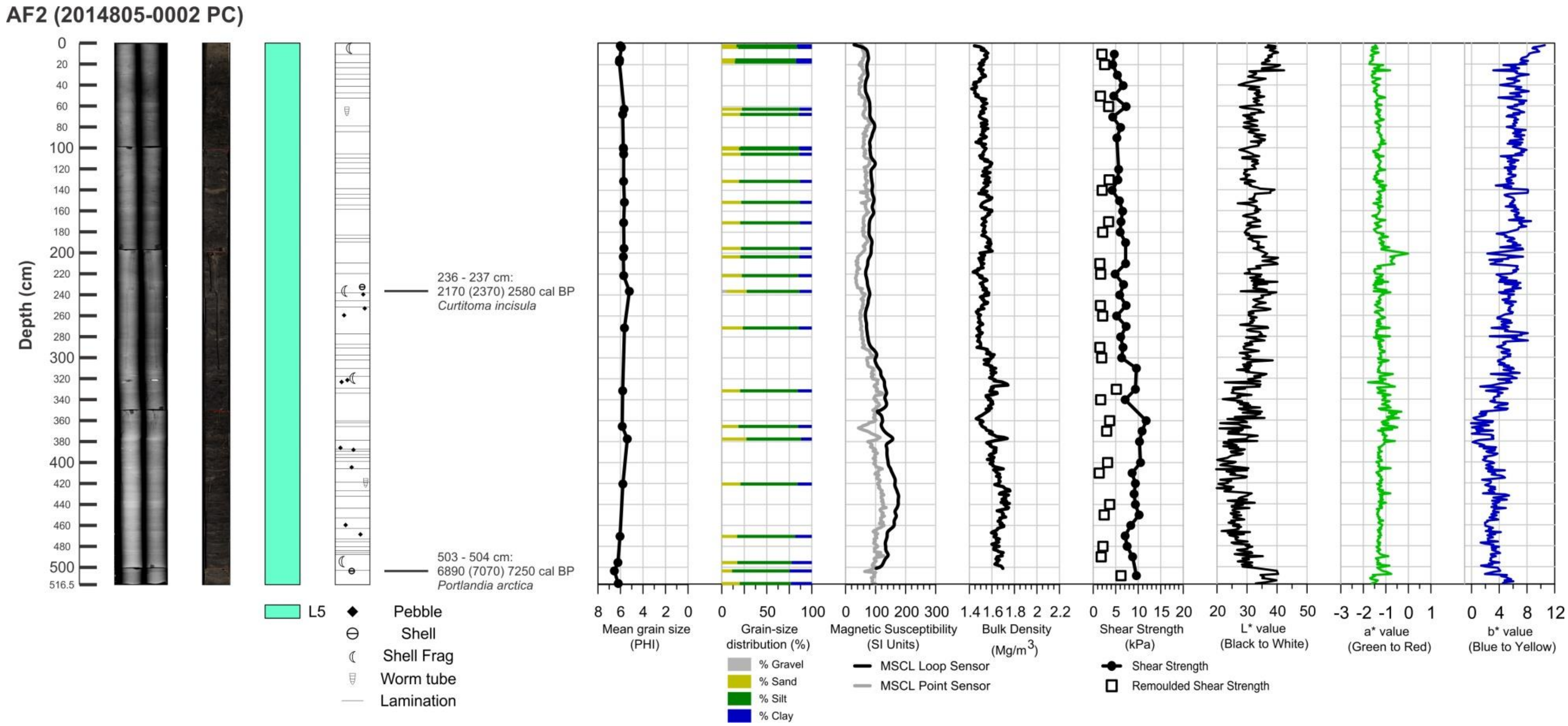

Figure C.22: Core AF2 (2014805-0002 PC), collected from the fjord basin of Akpait Fiord.

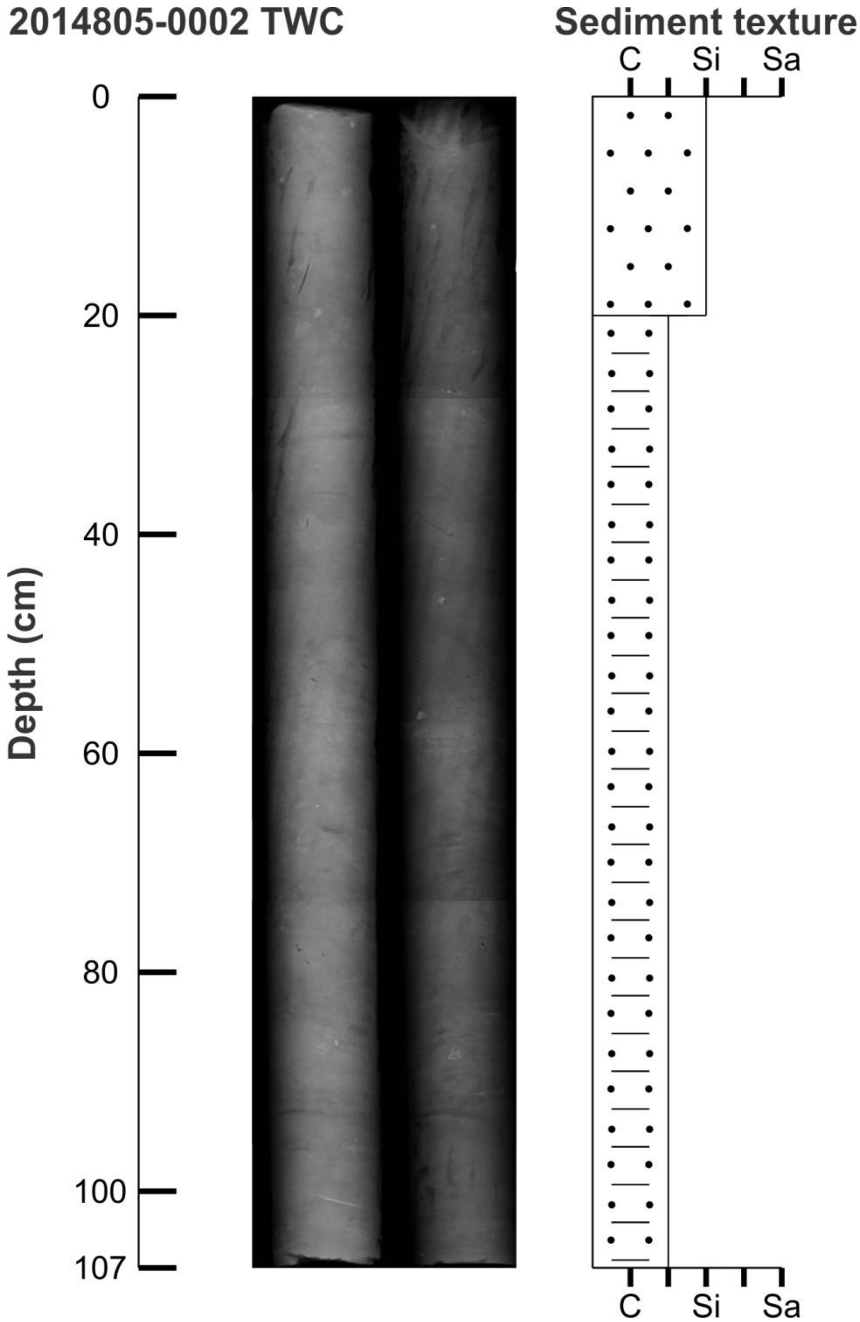

Figure C.23: Trigger-weight core sample 2014805-0002 TWC, collected from the fjord basin in Akpait Fiord.

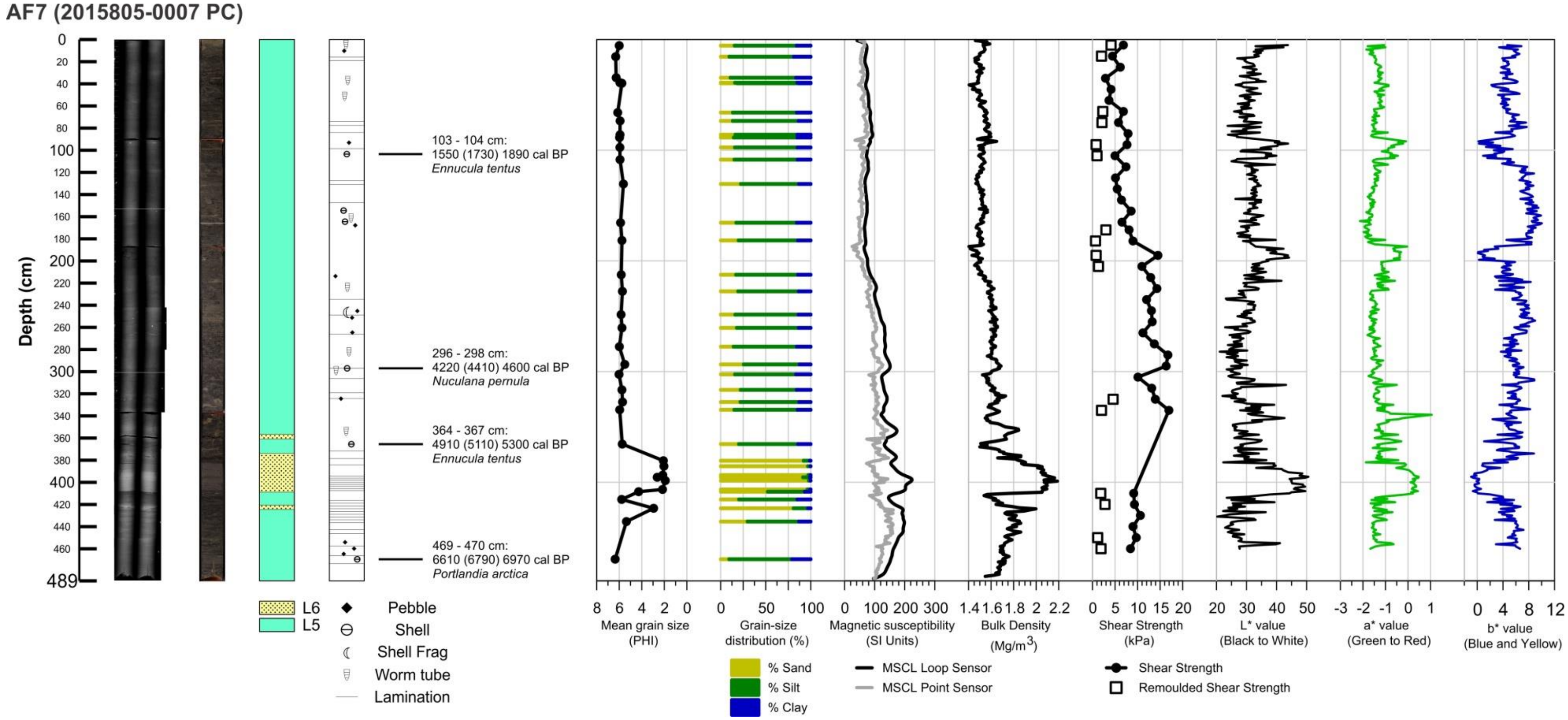

Figure C.24: Core AF7 (2015805-0007 PC), collected from the fjord basin of Akpait Fiord.

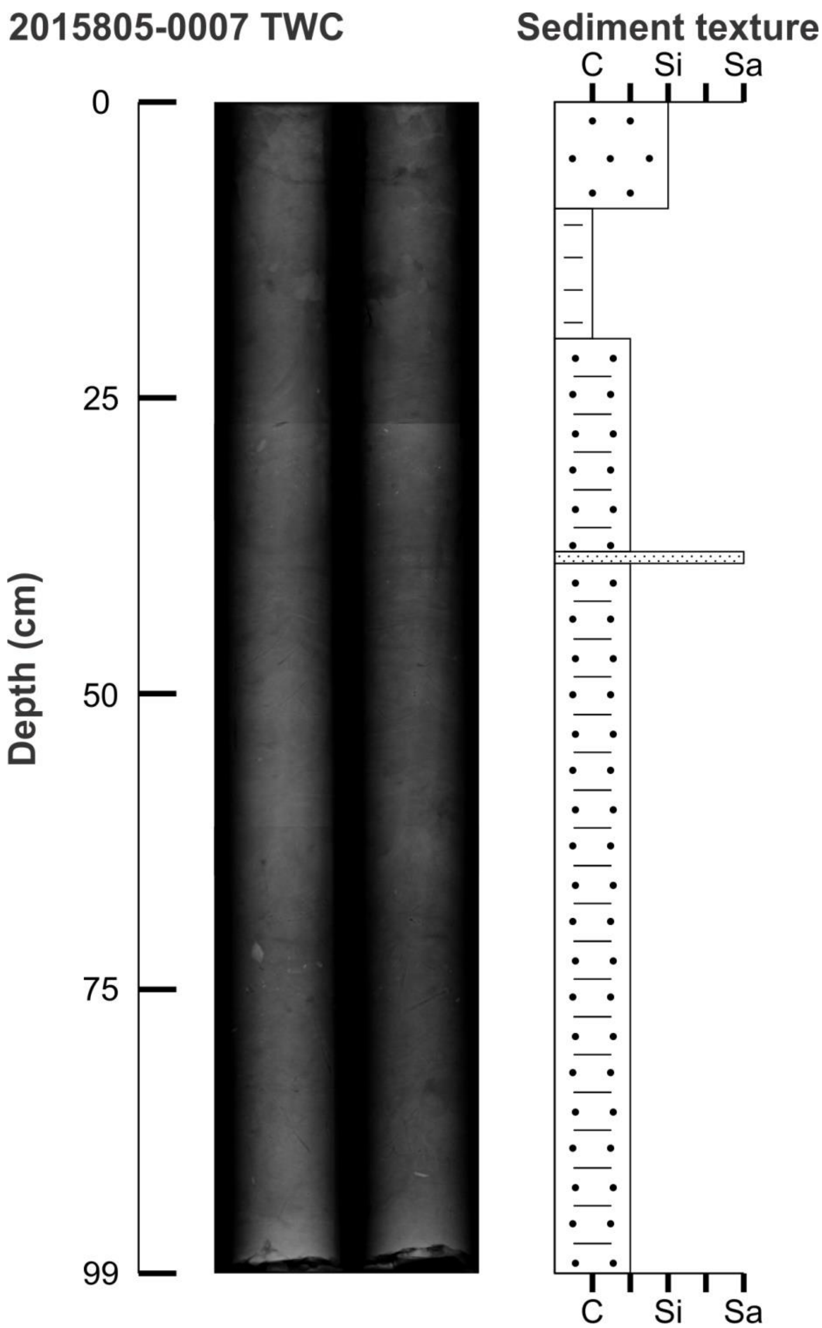

Figure C.25: Trigger-weight core sample 2015805-0007 TWC, collected from the fjord basin in Akpait Fiord.

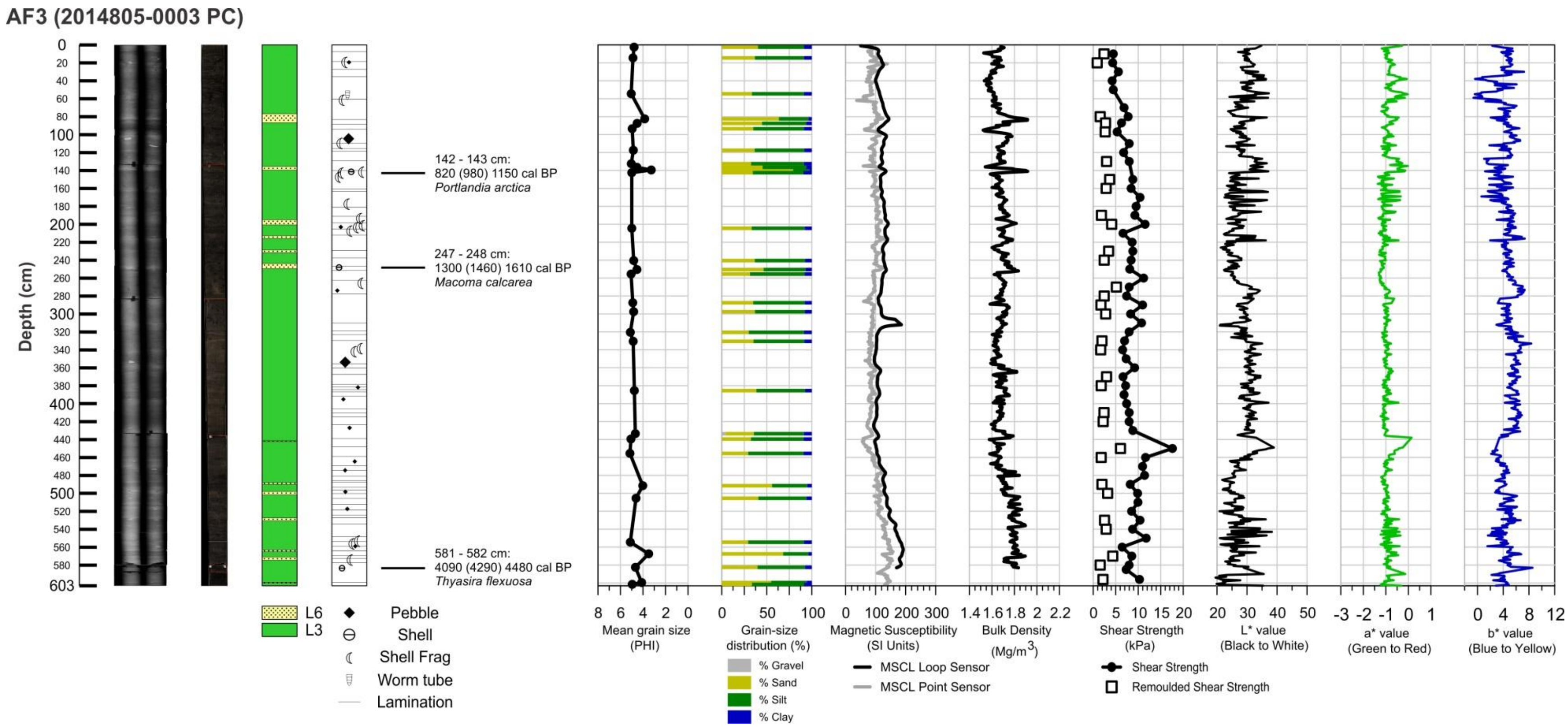

Figure C.26: Core AF3 (2014805-0003 PC), collected from the spillover deposit, adjacent to the fjord-mouth sill, of Akpait Fiord.

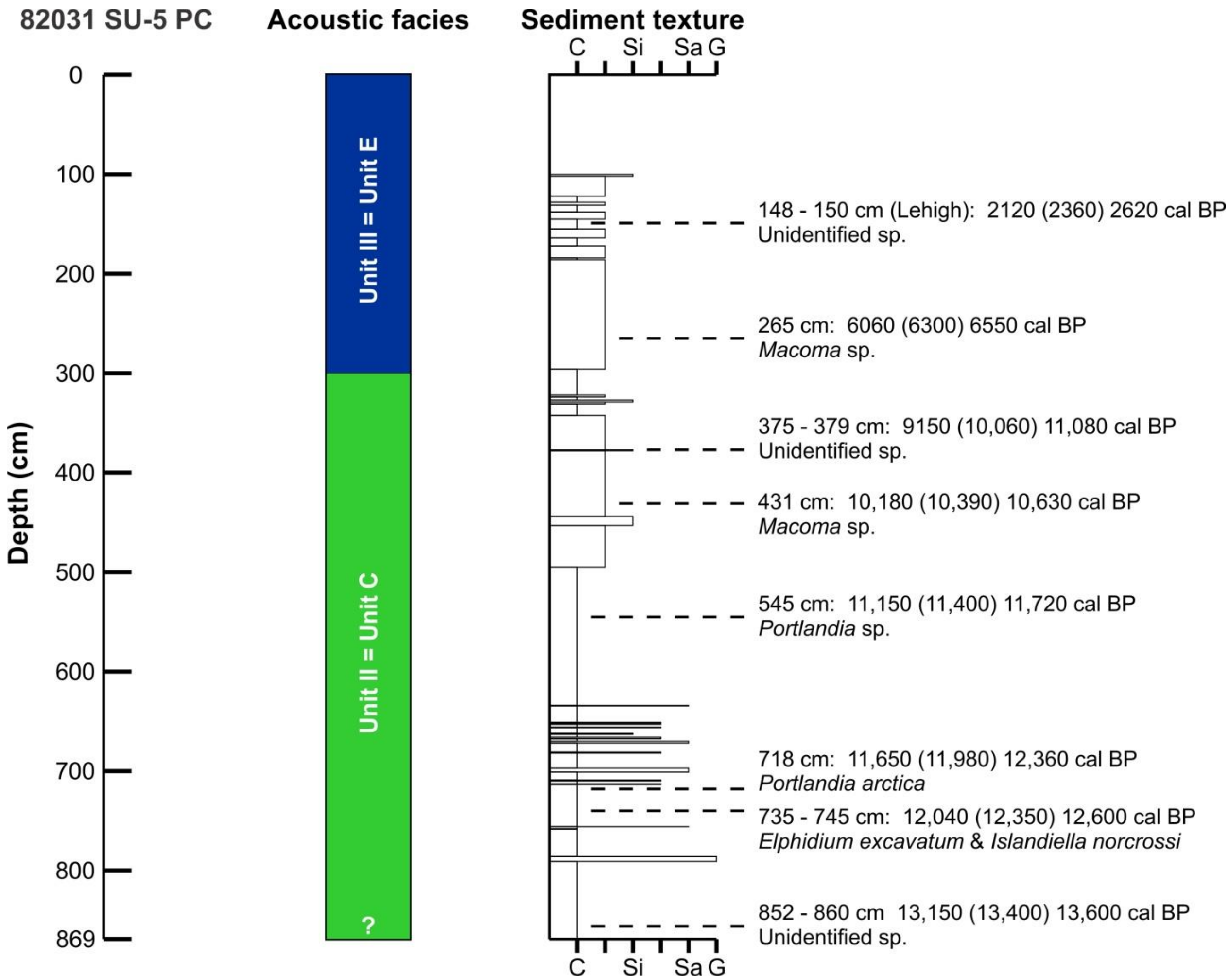

Figure C.27: Piston core sample HU82-SU5 PC, collected from outer Sunneshine Fiord.

D RADIOCARBON CHRONOLOGY

The field research conducted for this thesis yielded a total of 11 new radiocarbon dates from 3 fjords along Cumberland Peninsula: Boas Fiord, Durban Harbour, and Akpait Fiord (Tables D.1, D.2). In addition, 10 previously recorded radiocarbon dates from Sunneshine Fiord have been updated with new calibrations (Table D.8).

Boas Fiord: Subsample 2014NULIAJUK-0004 GC 103–104 cm returned an age range of 740 (910) 1060 cal BP. Based on this age range, the mean sedimentation rate is estimated to have ranged between 0.976–1.39 mm/yr for the interval of 0–104 cm. When the minimum and maximum rates are extrapolated downwards to the local unit D contact line (2000 mm below seafloor), the timing of the onset of RSL transgression, and thus the minimum age constraint for the postglacial lowstand, is estimated to occur between ~1440–2050 cal BP.

Durban Harbour: Subsample 2015805-0006 PC 210–212 cm returned an age range of 9490 (9650) 9870 cal BP, providing a maximum age constraint for the postglacial lowstand. Furthermore, based on this age range, the mean sedimentation rate is estimated to have ranged between 0.214–0.222 mm/yr for the interval of 0–211 cm. When the minimum and maximum rates are extrapolated downwards to a sand-gravel unit in core sample 2015805-0006 PC (2280 mm below seafloor; interpreted as ice-contact sediment), the onset of local deltaic bottomset sedimentation, and thus the minimum age constraint for local deglaciation, is estimated to occur between ~10250–10660 cal BP.

Akpait Fiord: A total of 9 calibrated radiocarbon age ranges were retrieved across 2 separate environments within Akpait Fiord; 6 dates from the fjord basin, and 3 from the spillover deposit.

The uppermost subsample from the fjord basin, 2015805-0007 PC 103 – 104 cm, returned an age range of 1550 (1730) 1890 cal BP, while the lowermost, 2014805-0002 PC 503 – 504 cm, returned 7040 (7220) 7390 cal BP. Estimated mean sedimentation rates for the fjord basin were found to range from 0.531 – 0.617 mm/yr to 0.874 – 1.00 mm/yr. Age ranges retrieved from the spillover deposit (2014805-0003 PC) range from 970 (1120) 1270 cal BP near the top (142 – 143 cm) to 4270 (4470) 4680 near the bottom (581 – 582 cm). The estimated mean sedimentation rates for the spillover deposit are an order of magnitude greater than in the fjord basin, ranging from 1.03 – 1.34 mm/yr to 1.28 – 6.00 mm/yr.

Sunneshine Fiord: A total of 10 calibrated radiocarbon age ranges where retrieved from cores HU82-SU5 G and PC, ranging from 2120 (2360) 2620 cal BP at the top (149 cm) to 13,150 (13,400) 13,660 cal BP at the bottom (852 – 860 cm). Some of the age ranges are so wide that the overlap with each other, so estimating mean sedimentation rates requires that some positive error values be adjusted to match the positive error of the underlying sample in order to avoid errors. A notable inflection point in the MSR curve is observed at 10.1 cal ka BP (377 cm): above, MSR ranges from 0.262 – 0.337 mm/yr to 0.570 – 0.704 mm/yr; below, from 0.230 – >0.593 mm/yr to 0.39 – 2.214 mm/yr.

Table D.1: Summary of cores and shell samples.

Core		Shell subsample (cm)					
		Observed (x-ray)		Extracted		Dated	
BF1	2014NULIAJUK-0001 GC	-		-		-	
BF2	2014NULIAJUK-0002 GCC	~2–3 (?)		-		-	
		~70 (?)		-		-	
BF3	2014NULIAJUK-0003 GC	~2–3 (?)		-		-	
BF4	2014NULIAJUK-0004 GC	8–9		8–9		-	
		32–33		32–33		-	
		103–104		103–104		103–104	
BF5	2014NULIAJUK-0005 GC	6–7		6–7		-	
BF6	2014NULIAJUK-0006 GC	-		-		-	
BF7	2014NULIAJUK-0007 GC	1–4 (?)		-		-	
DH1	2014805-0001 PC	1–3		1–3		-	
		~244–247 (?)		-		-	
DH5	2015805-0005 PC	n/a		0–10 A		-	
				0–10 B		-	
DH6	2015805-0006 PC	210–212		210–212		210–212	
		218–219		218–219		-	
AF2	2014805-0002 PC	0–2		0–2		-	
		~71–74 (?)		-		-	
		229–231		229–231		-	
		236–237		236–237		236–237	
		387–388 (?)		-		-	
		492–494		492–494		-	
		503–504		503–504		503–504	
	2014805-0002 TWC	2–3		2–3		-	
		~86–87 (?)		-		-	
		103–104		103–104		-	
AF3	2014805-0003 PC	17–19	203–204	17–19	203–204	-	-
		60–62	206–207	60–62	206–207	-	-
		108–110	247–248	108–110	247–248	-	247–248
		140–142	259–260	140–142	259–260	-	-
		142–143	~301–304	142–143	-	142–143	-
		146–147	341–342	146–147	341–342	-	-
		~165 (?)	550–552	-	550–552	-	-
		176–178	572–573	176–178	572–573	-	-
		192–193	581–582	192–193	581–582	-	581–582
AF7	2015805-0007 PC	103–104		103–104		103–104	
		154–155		154–155		-	
		164–165		164–165		-	
		246–247		246–247		-	
		296–298		296–298		296–298	
		364–367		364–367		364–367	
		469–470		469–470		469–470	
	2015805-0007 TWC	~61–62 (?)		-		-	

Table D.2: Summary table of calibrated radiocarbon dates rounded to the nearest decade, with species identified by Telka (2015; 2016).

Location	Sediment core sample	Shell subsample (cm)	Laboratory #	Conventional C^{14} data (±σ)	cal BP 2σ age range (median)	Species
Boas Fiord	2014NULIAJUK-0004 GC	103–104	UCIAMS-155824	1570 ± 20 BP	740 (910) 1060	*Hiatella arctica*
Durban Harbour	2015805-0006 PC	210–212	UCIAMS-169710	9165 ± 25 BP	9490 (9650) 9870	*Bathyarca glacialis*
Akpait Fiord	2014805-0002 PC	236–237	UCIAMS-155825	2990 ± 20 BP	2360 (2550) 2710	*Curtitoma incisula*
		503–504	UCIAMS-155826	6945 ± 25 BP	7040 (7220) 7390	*Portlandia arctica*
	2015805-0007 PC	103–104	UCIAMS-169711	2340 ± 15 BP	1550 (1730) 1890	*Ennucula tenuis*
		296–298	UCIAMS-169712	4485 ± 15 BP	4220 (4410) 4600	*Nuculana pernula*
		364–367	UCIAMS-169713	5035 ± 15 BP	4910 (5110) 5300	*E. tenuis*
		469–470	UCIAMS-169714	6560 ± 20 BP	6610 (6790) 6970	*P. arctica*
	2014805-0003 PC	142–143	UCIAMS-155827	1775 ± 20 BP	970 (1120) 1270	*P. arctica*
		247–248	UCIAMS-155828	2245 ± 20 BP	1440 (1620) 1790	*Macoma calcarea*
		581–582	UCIAMS-155829	4530 ± 20 BP	4270 (4470) 4680	*Thyasira flexuosa*

Table D.3: Summary table of all estimated mean sedimentation rates.

Fjord	Fjord area (km^2)	Drainage-basin area (km^2)	Core sample	Sediment interval (cm)	Range of mean sedimentation rates (mm/yr)	Range size (mm/yr)
Boas Fiord	116	1138	0004 GC	0–104	0.976 (1.14) 1.39	0.42
Durban Harbour	45	206	0006 PC	0–211	0.214 (0.219) 0.222	0.009
Akpait Fiord	38	247	0002 PC	0–237	0.874 (0.929) 1.00	0.13
				237– 504	0.531 (0.572) 0.617	0.086
			0007 PC	0–104	0.547 (0.599) 0.666	0.119
				104–297	0.635 (0.721) 0. 328	0.197
				297–366	0.636 (0.976) 2.22	1.59
				366–470	0.505 (0.622) 0.791	0.286
			0003 PC	0–143	1.12 (1.27) 1.47	0.35
				143–248	1.28 (2.13) 6.00	4.72
				248–582	1.03 (1.17) 1.34	0.31
Sunneshine Fiord	131	564	SU5 G	0–149	0.570 (0.633) 0.704	0.134
			SU5 PC	149–265	0.262 (0.294) 0.337	0.076
				265–377	0.245 (0.298) 0.430	0.186
				377–431	0.365 (1.66) >1.66	>1.29
				431–545	0.739 (1.13) 2.21	1.47
				545–718	1.42 (2.99) >2.99	>1.57
				718–740	0.230 (0.593) >0.593	>0.36
				740–856	0.715 (1.10) 2.12	1.41

D.1 Boas Fiord

Table D.4: Shell subsamples from Boas Fiord cores.

Core	Shell subsample
BF1	-
BF2	-
BF3	-
BF4	3 shell fragments were extracted, but only 1 was submitted for dating.
BF5	1 shell fragment was extracted (6–7 cm) but not submitted for dating.
BF6	-
BF7	1 shell visible in the x-radiography (1–4 cm) but was not extracted.

2014NULIAJUK-0004 GC

Chronology: A total of 3 shell fragment subsamples were extracted from the core, but only 1 was submitted for radiocarbon dating. Subsample 103–104 cm returned a calibrated radiocarbon date range of 740 (910) 1060 cal BP. This date range in turn indicates a mean sedimentation rate range of 0.976–1.39 mm/yr for the sediment interval of 0–104 cm (Fig D.1).

When the minimum and maximum rates are extrapolated downwards to the local unit D contact line (2000 mm below seafloor), the timing of the onset of RSL transgression, and thus the minimum age constraint for the postglacial lowstand, is estimated to occur between ~1440–2050 cal BP.

D.2 Durban Harbour

Table D.5: Shell subsamples from Durban Harbour cores.

Core	Shell subsamples
DH1	1 shell fragment extracted (1 – 3 cm), but not submitted for dating.
DH5	2 shell fragments were extracted from mixed sediment, but not submitted for dating.
DH6	2 shell fragments extracted, but only 1 was submitted for dating.

2015805-0006 PC

Chronology: A total of 2 shell fragment subsamples were extracted from the core, but only 1 was submitted for radiocarbon dating. This was subsample 210–212 cm, which returned a calibrated radiocarbon date range of 9490 (9650) 9870 cal BP. This provides a mean sedimentation rate range of 0.214–0.222 mm/yr for the interval of 0–211 cm (Fig D.2).

The radiocarbon-dated subsample 210–212 cm was extracted from the clay unit of the interpreted delta bottomset bed, and thus should date to when the submerged fjord-head delta was still part of an active fluvial system. Thus, this radiocarbon date alone provides a maximum age constraint of 9490–9870 cal BP for the timing of the postglacial lowstand. If the sand-gravel unit does represent ice-contact sediment, then by extrapolating the mean sedimentation rates (0.214–0.222

mm/yr) downwards to the unit contact at 2280 mm, an age range of ~10,250–10,660 cal BP is estimated for the onset of local deltaic bottomset sedimentation, and for the minimum age constraint of local deglaciation.

D.3 Akpait Fiord

Table D.6: Shell subsamples from Akpait Fiord cores.

Core	Shell subsamples
AF2	2 shell fragments extracted and dated.
AF2 TWC	2 shell fragments interpreted on the x-radiography, but none were dated.
AF7	4 shell fragments were extracted and dated.
AF7 TWC	-

2014805-0002 PC

Chronology: Two shell fragment subsamples were extracted from the core and submitted for radiocarbon dating. Subsample 236–237 cm returned a calibrated radiocarbon date range of 2360 (2550) 2710 cal BP, and subsample 503–504 cm returned 7040 (7220) 7390 cal BP. These two subsamples allow the core to be divided into two chronologic intervals, with mean sedimentation rate ranges of 0.874–1.00 mm/yr for the upper interval (0–237 cm) and 0.531–0.617 mm/yr for the lower interval (237–504 cm) (Fig D.3).

2014805-0007 PC

Chronology: Four shell fragment subsamples were extracted and submitted for radiocarbon dating. Subsample 103–104 cm returned a calibrated date range of 1550 (1730) 1890 cal BP, subsample 296–298 cm returned 4220 (4410) 4600 cal BP, subsample 364–367 cm returned 4910 (5110) 5300 cal BP, and subsample 469–470 cm returned 6610 (6790) 6970 cal BP. Three additional shell fragment subsamples were also extracted from the core, but were not submitted for radiocarbon dating. These four radiocarbon dates allow the core to be divided into four chronologic intervals, with mean sedimentation rate ranges of: 0.547–0.666 mm/yr for the top interval, 0.635 – 0.832 mm/yr for the upper-middle interval, 0.636–2.24 mm/yr for the lower-middle interval, and 0.505–0.791 mm/yr for the bottom interval (Fig D.4). As previously noted (Appendix B), the unit B locally shows two contact line segments, one overlying the other. The sand unit may correspond to the upper unit B contact line, which possibly represents the margin of a slope-failure deposit that occurred in between ~4910–6970 cal BP.

The mean sedimentation rates calculated for core 2015805-0007 PC are comparable to those of nearby core 2014805-0002 PC, which is expected given their proximity (0.75 km). However, whereas the mean sedimentation rate ranges of core 2014805-0002 PC increase upwards with each chronologic interval, the mean sedimentation rate ranges for core 2015805-0007 PC only increase once before switching to decrease upwards. If the interpretation of the sand unit (378–408 cm) as a slope-failure deposit is correct, then the mean sedimentation rate range of the lowermost interval (0.505–0.791 mm/yr) should be considered to be skewed upwards (large quantity of material deposited within a small timeframe). Thus, the magnitude of the switch in the trend of the mean sedimentation rate is even larger than initially appears. This discrepancy in sedimentation rate range trends between the two piston cores can likely be attributed to the difference in chronologic resolution available: 2 dates for 2014805-0002 PC, versus 4 for 2015805-0007 PC. If interpreted as a broad indication of sedimentation trends, then the contrast is surprising—the stations are far away from the fjord head (~10.9–11.7 km), with the nearest major sediment source being the fjord mouth sill. As 2015805-0007 PC is nearer to the sill it should be favoured by any reworked sediment derived from the sill via slope failure or wave action—thus, one would expect sedimentation to increase here instead of further up-fjord. While core 2014805-0002 PC is technically nearer the fjord head, another sediment source, it remains so distal while the cores are so proximal that the difference in sedimentation rate should not be significant.

2014805-0003 PC

Chronology: At least fifteen shell fragments were interpreted on the x-radiography, but only three subsamples were extracted from the core and submitted for radiocarbon dating. Subsample 142–143 cm returned a calibrated radiocarbon date range of 970 (1120) 1270 cal BP, subsample 247–248 cm returned 1440 (1620) 1790 cal BP, and subsample 581–582 cm returned 4270 (4470) 4680 cal BP (Fig D.5). These three subsamples allow the core to be divided into three chronologic intervals, with mean sedimentation rates ranging between: 1.23–1.47 mm/yr for the top interval (0–143 cm), 1.28–6.00 mm/yr for the middle interval (143–248 cm), and 1.03–1.34 mm/yr for the bottom interval (248–582 cm).

The highest range of mean sedimentation rates was estimated for the middle interval, which occurs wholly within the silt-sand unit and thus strongly indicates that at least part of the unit was deposited relatively rapidly. In contrast, the upper and lower intervals have relatively similar ranges, which suggest that both intervals were deposited under similar conditions. However, the lower interval may have a positively skewed range, as its uppermost portion overlaps with the rapidly deposited silt-sand unit.

D.4 Sunneshine Fiord

Table D.7: Shell subsamples from Sunneshine Fiord cores.

Core	Shell fragments
SU1	Hein and Longstaffe (1984) noted the presence of shell debris within the core, but none of the fragments are known to have been submitted for radiocarbon dating.
SU5	10 shell fragments were extracted and dated. However, 2 of these subsamples were dated in order to replace older ones at the same depth, for a functional total 8 dates.

HU82-SU5 PC & G

Chronology: The combined HU82-SU5 G & PC cores currently provide 10 radiocarbon dated subsamples—more than any other core discussed in the current study (Table D.8). Some subsamples were taken from identical depths (i.e., AA-0712 and CAMS-11814 from 265 cm; AA-264 and AA-13054 from 718 cm) in order to replace older dates with more precise data.

In total, eight radiocarbon dates are available from HU82-SU5 PC, ranging from 2120 (2360) 2620 cal BP near the top (148-150 cm) to 13,150 (13,400) 13,660 cal BP (852-860 cm). These eight dates allow core HU82-SU5 to be divided into eight chronologic intervals, the highest chronologic resolution for a core included in this study (Table D.9, Fig D.6). When calculated mean sedimentation rates, the age ranges of some subsamples were so wide that they overlapped. This was corrected by adjusting excessive positive error values to be equal to the positive error of the underlying sample. A notable inflection point in the MSR curve is observed at 10.1 cal ka BP (377 cm): above, MSR ranges from 0.262 – 0.337 mm/yr to 0.570 – 0.704 mm/yr; below, from 0.230 – >0.593 mm/yr to 0.39 – 2.214 mm/yr. Radiocarbon dates from organic concentrate were also listed in Andrews et al. (1989), but are excluded here in favour of more reliable shell and foraminifera subsamples.

Table D.8: Calibrated radiocarbon dates from Sunneshine Fiord. The topmost subsample was retrieved from HU82-SU5 G, while all underlying subsamples are from HU82-SU5 PC with their depths corrected for a missing 1.0 m (Andrews et al., 1996).

Sample #	Depth (cm)	Conventional ^{14}C data (yr BP)	Rounded cal BP 2σ age range (median)	Species
CAMS-13511 [2]	149	2840 ± 60	2120 (2360) 2620	Bivalve
AA-0712 [1]	265	5600 ± 330	4940 (5740) 6470	Bivalve
CAMS-11814 [2]	265	6120 ± 80	6060 (6300) 6550	*Macoma* sp.
AA-0412 [1]	377	9450 ± 360	9150 (10 060) 11 080	Bivalve
CAMS-11815 [2]	431	9710 ± 60	10 180 (10 390) 10 630	*Macoma* sp.
AA-13053 [2]	545	10 430 ± 80	11 150 (11 400) 11 720	*Macoma* sp.
AA-0264 [1]	718	10 490 ± 450	10 290 (11 500) 12 650	Bivalve
AA-13054 [2]	718	10 805 ± 80	11 650 (11 980) 12 360	*Portlandia arctica*
CAMS-17398 [2, 3]	735-745	11 060 ± 70	12 040 (12 350) 12 600	*Elphidium excavatum forma clavata, Islandiella norcrossi*
AA-13052 [2, 3]	852-860	12 125 ± 90	13 150 (13 400) 13 660	Foraminifera

[1] Andrews et al. (1989b)
[2] Manley & Jennings (1996)
[3] These dates were taken from foraminifera, but are treated the same as the dated shell samples.

Table D.9: Mean sedimentation rates for Sunneshine Fiord from station HU82-SU5.

Interval	Depth range (cm)*	Top age range Bottom age range (cal BP)	Depth interval (cm)	Min time interval Max time interval (yr)	Range of mean sedimentation rates (mm/yr)
1	0–149	0 2120–2620	149	2116 26150	0.570 – 0.704
2	149–265	2120–2620 6060–6550	116	3440 4432	0.262 – 0.337
3	265–377	6060–6550 9150–11 080	112	2602 4575	0.245 – 0.430
4	377–431	9150–11 080 10 180–10 630	54	0 1480	0.365 – >1.66
5	431–545	10 180–10 630 11 150–11 720	114	515 1480	0.739 – 2.21
6	545–718	11 150–11 720 11 650–12 360	173	0 1217	1.42 – >2.99
7	718–740	11 650–12 360 12 040–12 600	22	0 958	0.230 – >0.593
8	740–856	12 040–12 600 13 150–13 660	116	547 1622	0.715– 2.12

As can be observed, the older dates from Andrews et al. (1989b) have considerably wider error ranges than those from Manly and Jennings (1996). Two depths (265 and 718 cm) have been redated – according to Manly and Jennings, this was intentionally done to replace the date with a narrow error range. Presumably, the same logic can be applied to the 265 cm subsample as well.

Facies interpretation and depositional environment: The sand units may represent traction current deposits or local debris flows (Andrews et al., 1985; 1994; 1996). Andrews et al. (1994) interpreted SU5 PC to represent two zones (above and below ~220 cm): a lower Late Pleistocene zone characterized by a strong fjord-shelf interaction, and an upper Holocene zone dominated by local fjord-drainage processes. Andrews et al. (1996) linked abrupt changes in carbonate to glacier readvance. Core HU82-SU5 PC has also been previously studied in terms of multiple additional parameters (biotic, mass physical, mineralogical, geotechnical, and paleomagnetic) and properties (sediment bulk density, moisture content, total organic carbon weight percentage, grain-size spectra, weight percentage total carbonate, and silt- and clay-sized mineral species, and foraminifera and pollen) (Andrews et al., 1994; 1996).

The mean sedimentation rate changes significantly in between intervals 3 and 4, decreasing by an order of magnitude after ~10 cal ka BP. Earlier studies have previously noted this change for SU5 PC and other sediment cores, and attributed it to the final phase of glacial retreat for the northeast LIS and its outlet glaciers (Andrews et al., 1985; Andrews, 1987; Andrews et al., 1989a).

D.5 References

Andrews, J.T., Jull, A.J.T., Donahue, D.J., Short, S.K., & Osterman, L.E. (1985). Sedimentation rates in Baffin Island fiord cores from comparative radiocarbon dates. *Canadian Journal of Earth Sciences,* 22: 1827-1834.

Andrews, J.T. (1987). Late Quaternary marine sediment accumulation in fiord-shelf-deep-sea transects, Baffin Island to Baffin Bay. *Quaternary Science Reviews,* 6: 231-243.

Andrews, J.T., Geisdóttir, Á., & Jennings, A.E. (1989a). Late Quaternary spatial and temporal changes in clay- and silt-size mineral assemblages of fiord and shelf cores, western Baffin Bay, northwest North Atlantic. *Continental Shelf Research*, 9(5): 445-463.

Andrews, J.T., Laymon, C.A., & Briggs, W.M. (1989b). Radiocarbon date list III: Labrador and northern Quebec, Canada and radiocarbon date list VI: Baffin Island, N.W.T., Canada. *INSTAAR Occasional Paper No. 46*, University of Colorado, Boulder.

Andrews, J.T., Syvitski, J.P., Osterman, L.E., Williams, K.M., Mode, W.N., Kravitz, J.E. & Locke, W.W. III. (1994). *Quaternary geology of Sunneshine Fiord (Baffin Island).* Geological Survey of Canada, Open File 3004. doi:10.4095/195129

Andrews, J.T., Osterman, L.E., Jennings, A.E., Syvitski, J.P.M., Miller, G.H., & Weiner, N. (1996). Abrupt changes in marine conditions, Sunneshine Fiord, eastern Baffin Island, NWT during the last deglacial transition: Younger Dryas and H-0 events. *Late Quaternary Palaeoceanography of the North Atlantic Margins,* Geological Society Special Publication 111: 11-27.

Hein, F.J. & Longstaffe, F.J. (1984). Geotechnical sedimentology and mineralogical investigations in Arctic fjords. In J.P.M. Syvitski & C.P. Blakeney (Compilers), *Sedimentology of Arctic Fjords Experiment: HU 82-031 Data Report, Volume 1* (GSC Open File 960). doi: 10.4095/129793

Manley, W.F. & Jennings, A.E. (1996). Radiocarbon date list VIII: Eastern Canadian Arctic, Labrador, northern Quebec, East Greenland Shelf, Iceland Shelf, and Antarctica. *INSTAAR Occasional Paper No. 50*, University of Colorado, Boulder.

Telka, A. (2015). *Expedition 2014805 Baffin Island shell dating report*. Paleotec Services.

Telka, A. (2016). *Expedition 2014805 Baffin Island shell dating report*. Paleotec Services.

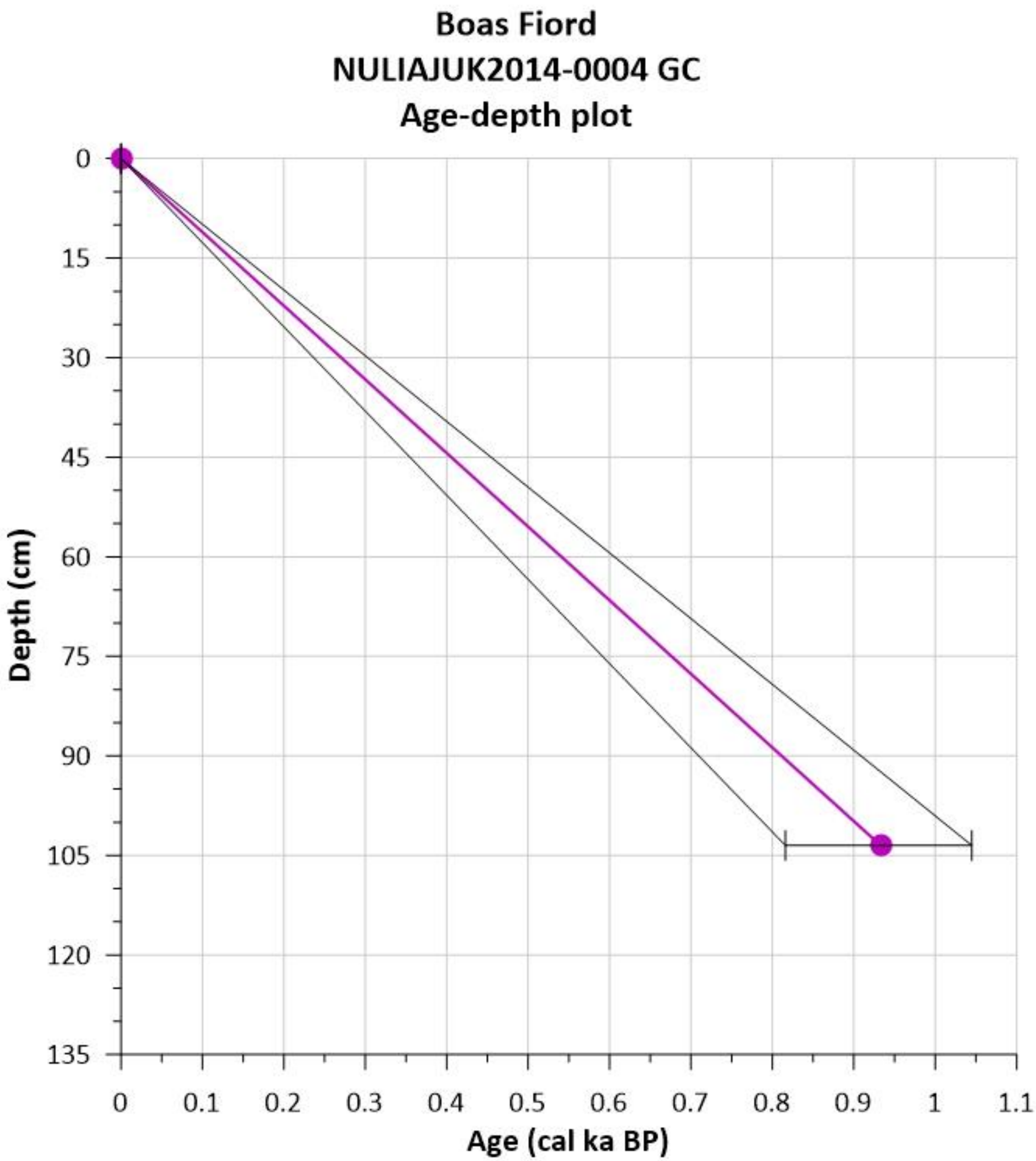

Figure D.1: Mean sedimentation rates for core 2014NULIAJUK-0004 GC, collected from the eastern terrace of the submerged fjord-head delta in Boas Fiord.

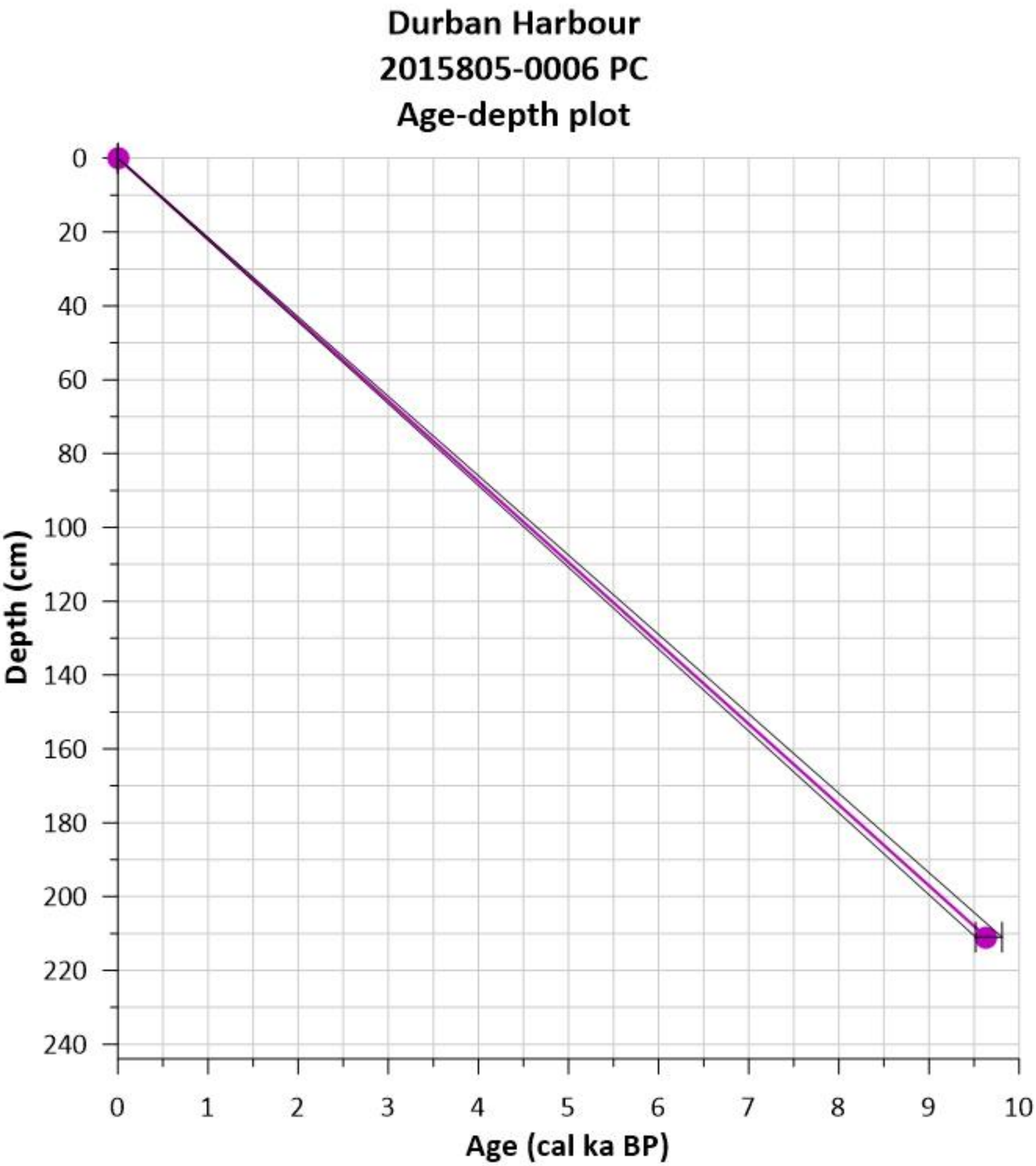

Figure D.2: Mean sedimentation rates for core sample 2015805-0006 PC, from the head of Durban Harbour.

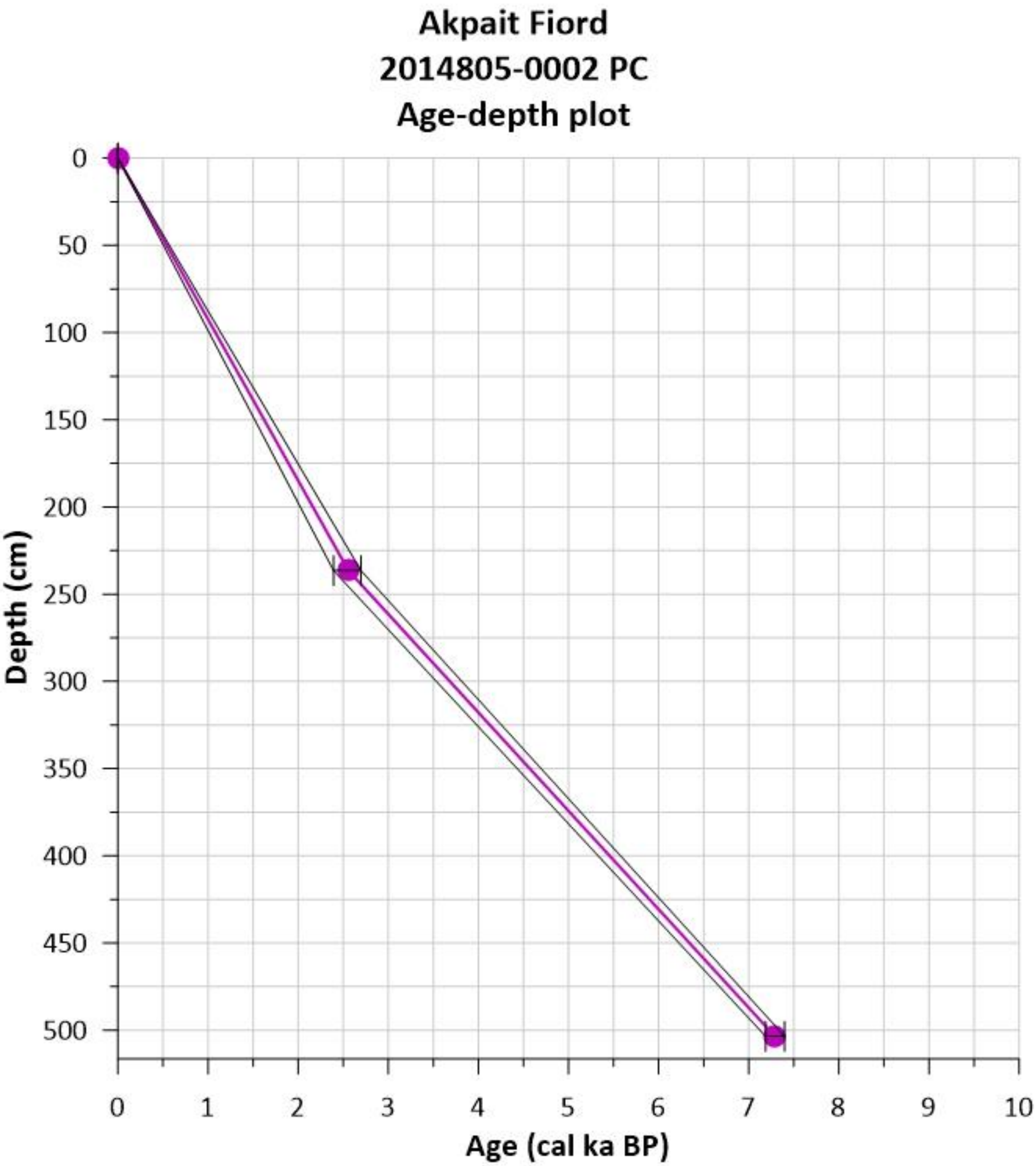

Figure D.3: Mean sedimentation rates for core sample 2014805-0002 PC, from the basin of Akpait Fiord.

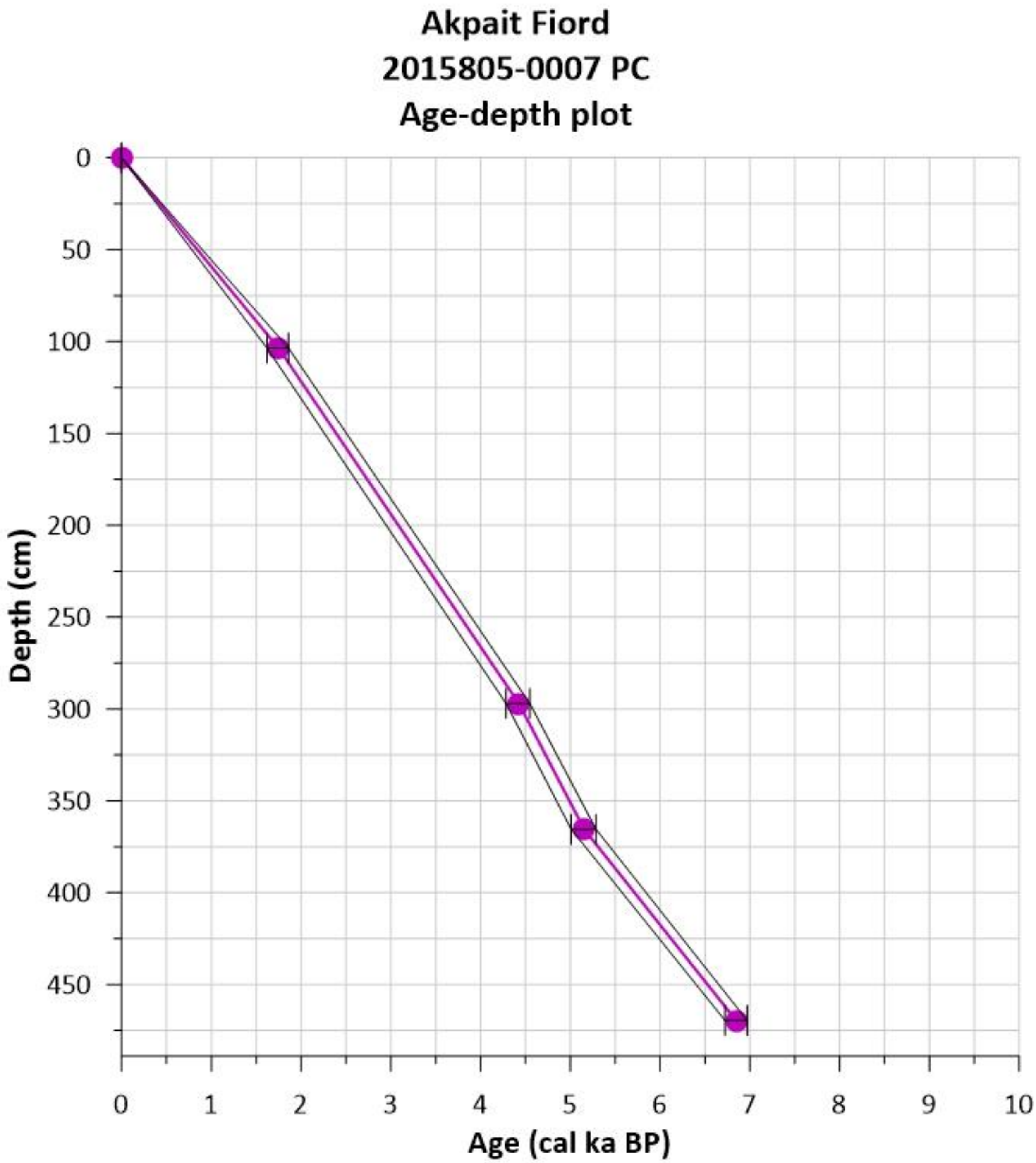

Figure D.4: Mean sedimentation rates for core sample 2015805-0007 PC, from the basin of Akpait Fiord

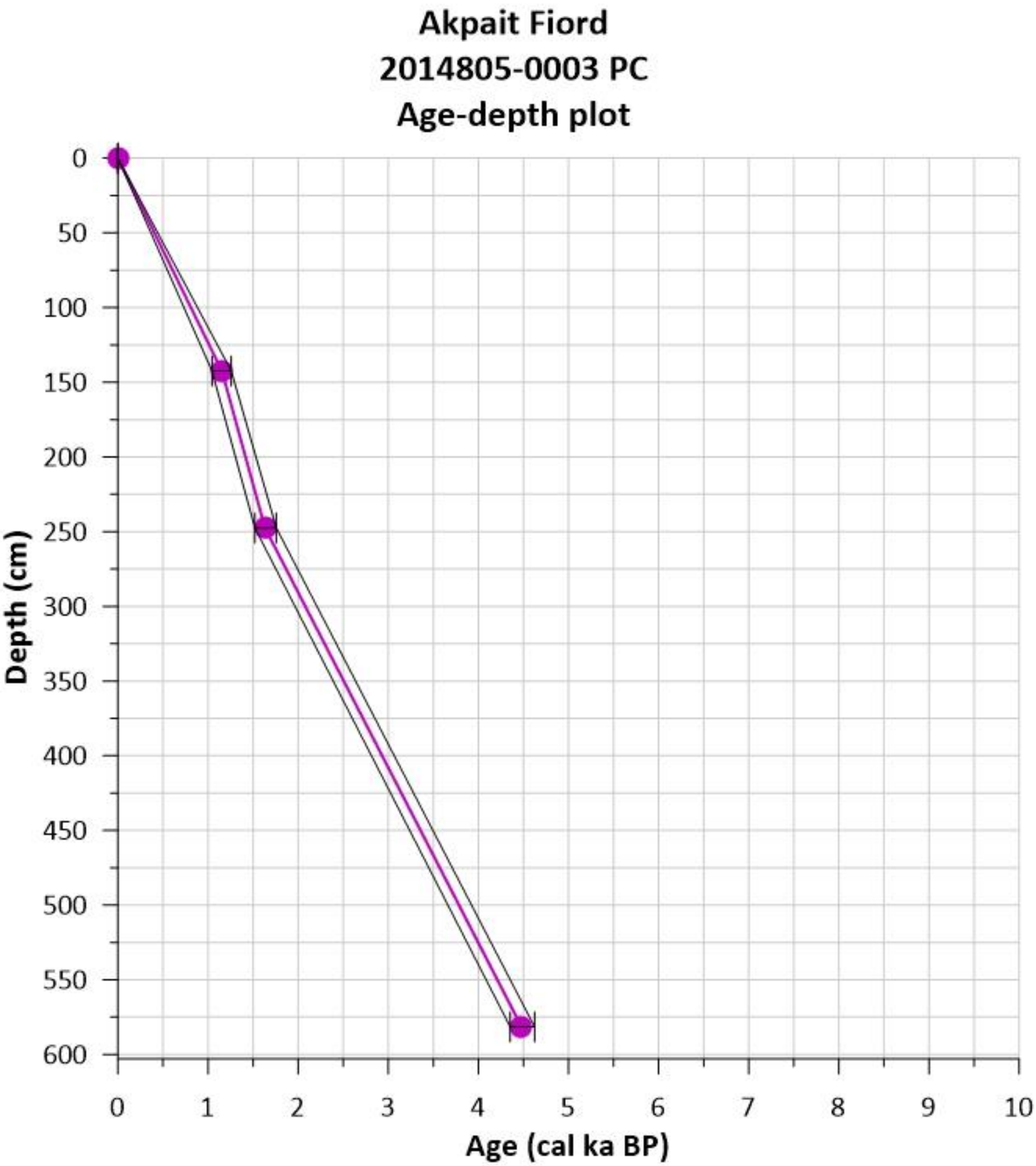

Figure D.5: Mean sedimentation rates for core sample 2014805-0003 PC, from the spillover deposit near the mouth of Akpait Fiord.

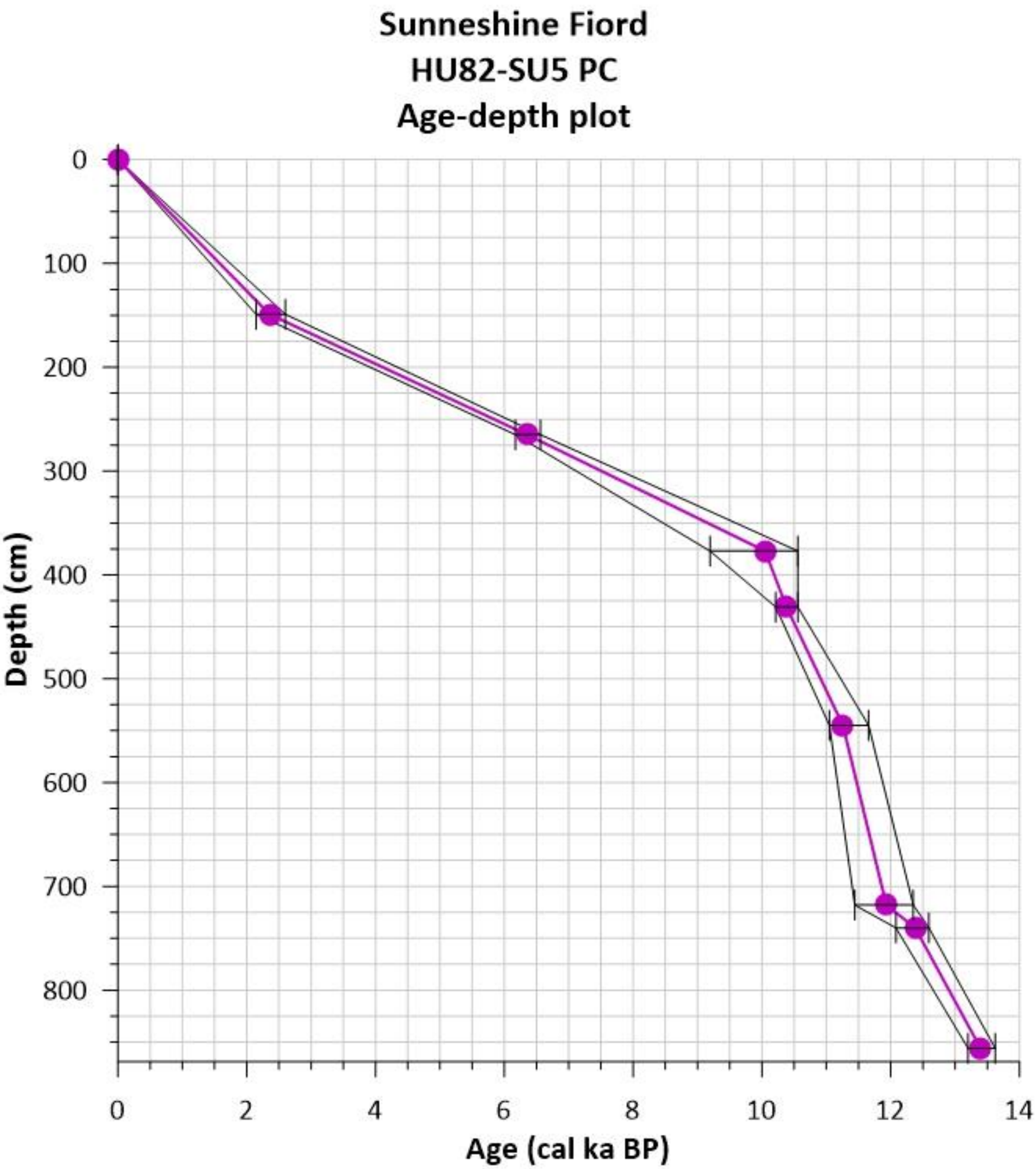

Figure D.6: Mean sedimentation rates for core sample HU82-SU5, from the basin of Sunneshine Fiord.